Fluorescence and active site engineering studies of copper-containing oxidoreductases

Dorota Natalia Kostrz

A Thesis Submitted for the Degree of Doctor of Philosophy

March 2014

Institute for Cell and Molecular Biosciences

Newcastle University

Declaration

I certify that this thesis contains my own work, except where acknowledged, and that no part of this work has been submitted in support of an application for other qualifications at this or any other institution.

Abstract

Copper-containing proteins are involved in a wide range of biological processes mainly *via* oxidation and reduction reactions. The oxidation state of these proteins can be monitored *via* Förster resonance energy transfer (FRET) between a covalently attached fluorescent dye and the protein's redox active centre. Consequently, changes in absorbance upon reduction or oxidation of the protein can be related to changes in the fluorescence intensity and lifetime. This FRET-based approach has been applied to study the catalytic activity of the copper-containing blue nitrite reductase (bNiR) from *Alcaligenes xylosoxidans* at the single molecule level by means of scanning confocal microscopy combined with fluorescence lifetime imaging (FLIM). bNiR catalyzes the reduction of nitrite to nitric oxide during denitrification. The active centre of bNiR consists of a type 1 (T1) Cu site, which acts as the initial port of entry for electrons, and a type 2 (T2) Cu site, where nitrite reduction occurs. Detailed analysis of single molecules of immobilized, fluorescently labeled bNiR has allowed two populations of molecules to be identified that turn over with different catalytic rates. Previous studies of the catalytic mechanism of copper-containing NiRs distinguished two possible reaction pathways. The single molecule results imply these occur as a consequence of heterogeneity in the enzyme population.

Fluorescent labeling of laccases, which catalyze the oxidation of a range of substrates coupled to the four electron reduction of O_2, with fluorescent dyes was investigated for their potential use in the development of a FRET-based biosensor. A novel expression system for the *Trametes versicolor* laccase Lcc1 in *Schizophyllum commune* was developed. The recombinant protein is similar to another native laccase (Laccase A) from *T. versicolor* and both exhibit significantly higher catalytic efficiency with phenolic compounds than the bacterial small laccase (SLAC) from *Streptomyces coelicolor*. Regardless, preliminary data indicate involvement of a tyrosyl radical in the catalytic activity of fungal laccases, similar to what is observed in SLAC.

bNiR and SLAC are trimers, with each monomer consisting of two cupredoxin-like domains. The structure of the catalytic site and the location of a T1 Cu site are different in these two enzymes. A crystal structure provides detailed insight into why an attempt to introduce the SLAC active site into bNiR was unsuccessful. Attempts to introduce T1 Cu sites into the cupredoxin-like domains of bNiR and SLAC, which normally lack this site, resulted in the introduction of a tetragonal thiolate-containing T2 Cu site.

Acknowledgements

I would like to thank my supervisor, Prof. Christopher Dennison, for providing me with the opportunity to join his group. I am very grateful for all, patience, guidance and support that he has given me during my PhD, especially when writing this thesis. I would also like to thank all of the lab members, both past and present that have helped me with this project. In particular I am grateful to Dr. Shilpa Aggarwal, Dr. Adriana Badarau and Dr. Stephen Allen for their daily support, many invaluable advices and helpful discussions throughout the project. Thanks also go to Dr. Abdelnasser El Ghazouani and Semeli Platsaki for their encouragement.

I would like to thank Dr. Katsuko Sato, Rafal Zur and Dr. Isabelle Salard for their work on bNiR, Lcc1 and T1D azNiR proteins. Dr. Arnaud Baslé is acknowledged for data collection and processing for the LacNiR crystal structure. Thanks to Dr. Joe Gray and Bob Liddell from Pinnacle for analysis of proteins by mass spectrometry. I am also thankful to Dr. Julian Rutherford for his continuous interest in my work, his help and very useful suggestions with setting up a fungal over-expression system for Lcc1. I would like to thank Dr. Timothy Cheek and Dr. Jun-yong Huang for their help and advice over the years. Thanks to Dr. Randall Goldsmith and Prof. W.E. Moerner (Stanford University, USA) for fruitful collaboration on the ABEL-trapped bNiR molecules. Thanks also go to Dr. Jessica van Wonderen and Prof. Fraser MacMillan (University of East Anglia, Norwich, UK) for PELDOR studies and to Dr. Sachiko Yanagisawa (University of Hyogo, Japan) for RR studies on the bNiR and SLAC variants.

Thanks to all the members of the EdRox Research and Training network for many useful suggestions and productive exchange of ideas during the network's meetings. I am very grateful to Prof. Gerard Canters and Prof. Thijs Aartsma for hosting me at Leiden University. I am deeply thankful to Dr. Leandro Tabares for introducing me to the world of single molecule studies, teaching me and ensuring that I will never loose my faith in the project whenever things were not working at all. I would like to acknowledge Dr. Abdulmohsen Elmalk for facilitating my understanding of confocal microscopy and his never-ending patience during long-hours measurements. Thank you for your help and friendship. Thanks also go to Dr. Armand Tepper, whose help was invaluable in measurements of Laccase A. I would like to thank Dr. Gerhild Zauner, Dr. Alessio Andreoni and Dr. Michał Siwek for their help and the time we spent together throughout my stay in Leiden. Dr. Razvan Stan is acknowledged for AFM data collection and processing for the immobilized bNiR. I am very grateful to Dr. Karin Scholtmeijer for

hosting me at Utrecht University and introduction to the world of *Schizophyllum commune*. Your help was fundamental in development of the over-expression system for Lcc1.

I would also like to acknowledge all my friends outside the lab, particularly Micol, Susana, Vitoria, Tiago, Stefano and Staszek for making my stay in Newcastle so much more enjoyable. I want to acknowledge Lola and Piotrek for motivating me when it was the most important and listening to all my thesis-related complaints.

I am deeply indebted to my family for supporting me during this PhD and simply believing in me. *Mamo i Tato, dziekuję z całego serca za Waszą miłość i wsparcie*. Special thanks go to André for his constant support and encouragement. Your patience and love gave me strength and motivation whenever I needed it. Thank you for following me to Newcastle and enjoying this time with me.

This work was funded by the European Commission under the 6th Framework Programme (FP6).

Abbreviations, acronyms and units

A	absorbance
ET	electron transfer
F	fluorescence
FRET	Förster resonance energy transfer
LMCT	ligand to metal charge transfer
MBD	metal-binding domain
MBS	metal-binding site
MCO	Multicopper oxidase
S(Cys)-T2 Cu	thiolate-ligated type 2 copper
T1 Cu	type 1 copper
T1.5 Cu	type 1.5 copper
T2 Cu	type 2 copper
T2/T3 Cu	trinuclear copper cluster
T3 Cu	type 3 copper
WT	wild type
ε	extinction coefficient ($M^{-1}cm^{-1}$)
λ	wavelength

Measurements and techniques

AAS	atomic absorption spectroscopy
ABEL	anti-Brownian electrokinetic
AFM	atomic force microscopy
CD	circular dichroism
EPR	electron paramagnetic resonance
FLIM	fluorescence lifetime imaging microscopy
MALDI-MS	matrix assisted laser desorption ionization mass spectrometry
MCD	magnetic circular dichroism
MW	molecular weight
MW^{app}	apparent molecular weight
MWCO	molecular weight cut off
OD	optical density
PCR	polymerase chain reaction

PELDOR	pulsed electron-electron double resonance
SDS-PAGE	sodium dodecyl sulphate polyacrylamide gel electrophoresis
SR	switching ratio
TCSPC	time-correlated single photon counting
UV-Vis	ultraviolet-visible

Units

nanokatal×mL^{-1} nkat×mL^{-1}	10^{-9} mol×s^{-1}×mL^{-1}
ppm	parts per million
rpm	revolutions per minute
RT	room temperature
v/v	volume per volume
w/v	weight per volume

Selected chemicals and media

ABTS	2,2'-azinobis-3-ethylthiazoline-6-sulfonat
APTS	3-aminopropyl-trimethoxysilane
BV	1,1'-dibenzyl-4,4'-bipyridinium dichloride; benzyl viologen
CM	complete medium
DEAE	diethylaminoethyl
DTT	dithiothreitol
2,6-DMP	2,6-dimethylphenol
EDTA	ethylenediaminetetraacetic acid
Hepes	4-(2-Hydroxyethyl)piperazine-1-ethanesulfonic acid
IPTG	isopropyl β-D-1-thiogalactopyranoside
LB	Luria-Bertani medium
Mes	2-(N-morpholino)ethanesulphonic acid
MM	minimal medium
MPTS	3-mercaptopropyl-trimethoxysilane
NHS	N-hydroxysuccinimide
PES	phenazine ethosulfate
SP	sulfopropyl

TB	terrific broth
TES	triethoxysilane
Tris	tris(hydroxymethyl)aminoethane
TCEP	tris(2-carboxyethyl)phosphine hydrochloride
2×YT	2×yeast extract and tryptone medium

Selected proteins

AO	Ascorbate oxidase
Ami	Amicyanin
Az	Azurin
A99H mgSLAC *	Ala99 to His variant of mgSLAC
A99H nirSLAC *	Ala99 to His variant of nirSLAC
BCO	Two-domain MCO from *Nitrosomonas europaea*
bNiR	"Blue" nitrite reductase from *Alcaligenes xylosoxidans*
Cp	Ceruloplasmin
Fet3p	Yeast multicopper ferroxidase from *Saccharomyces cerevisiae*
gdcLAC	Two-domain MCO from *Arthrobacter* sp. fb24
gdcSLAC	SLAC variant whose 1st domain loop is replaced with the T1 Cu-binding loop of gdcLAC
gNiR	"Green" nitrite reductase from *Alcaligenes faecalis S*-6
Laccase A	Native (isolated) fungal laccase from *Trametes versiolor*
LacNiR	Asp92 to His, Ala131 to His, Ile251 to His and Leu298 to His variant of bNiR
Lcc1	Recombinant fungal laccase from *T. versicolor*
Lcc1_cMYC	Lcc1 variant with C-terminal cMYC tag
mgLAC	Two-domain MCO from metagenome database
mgSLAC	SLAC variant whose 1st domain loop is replaced with the T1 Cu-binding loop of mgLAC
nirSLAC	SLAC variant whose 1st domain loop is replaced with the T1 Cu-binding loop of bNiR
NusA_Lcc1	Recombinant Lcc1 fused N-terminally with N-utilization substance A
Paz	Pseudoazurin
Pc	Plastocyanin

SLAC	Bacterial, two-domain (small) laccase from *Streptomyces coelicolor*. Also referred to as $SLAC_{truncated}$
$SLAC_{long}$	SLAC from *S. coelicolor* containing TAT-leader sequence
$SLAC_{truncated}$	$SLAC_{long}$ variant lacking the N-terminal 44 residues
STC	Stellacyanin
tSLAC *	Asp157 to Cys, Gly168 to His and Leu173 to Met variant of SLAC
TvL1KYA	Native fungal laccase from *T. versicolor* (pdb code: 1KYA)
TvL1GYC	Native fungal laccase from *T. versicolor* (pdb code: 1GYC)
T1D azNiR	T1 Cu site depleted, Cys130 to Ser variant of bNiR whose 2nd domain loop is replaced with the T1 Cu-binding loop of Az
T1D A99H nirSLAC *	T1 Cu site depleted, Cys288 to Ser variant of A99H nirSLAC
T1D_lcc1_cMYC	T1 Cu site depleted, Cys452 to Ser variant of Lcc1_cMYC
T1D mgSLAC *	T1 Cu site depleted, Cys288 to Ser variant of mgSLAC
T1D nirSLAC *	T1 Cu site depleted, Cys288 to Ser variant of nirSLAC
T1D SLAC *	T1 Cu site depleted, Cys288 to Ser variant of SLAC
T1D tSLAC *	T1 Cu site depleted, Cys288 to Ser variant of
T1D T246H azNiR	Thr246 to His variant of T1D azNiR
T1D qNiR	T1 Cu site depleted, Cys130 to Ser variant of qNiR
T1D qSLAC *	T1 Cu site depleted, Cys288 to Ser variant of qSLAC
qNiR	Asn299 to Cys, Glu304 to His, Ala310 to Met and Thr246 to His variant of bNiR
qSLAC *	Ala99 to His variant of tSLAC
Δ252G_LacNiR	Gly252 depleted variant of LacNiR

* Numbering of $SLAC_{long}$

Amino acids and nucleic acids

Alanine	Ala	A	Methionine	Met	M
Cysteine	Cys	C	Asparagine	Asn	N
Aspartic acid	Asp	D	Proline	Pro	P
Glutamic acid	Glu	E	Glutamine	Gln	Q
Phenylalanine	Phe	F	Arginine	Arg	R
Glycine	Gly	G	Serine	Ser	S
Histidine	His	H	Threonine	Thr	T

Isoleucine	Ile	I	Valine	Val	V
Lysine	Lys	K	Tryptophan	Trp	W
Leucine	Leu	L	Tyrosine	Tyr	Y

Adenine	A	Guanine	G
Cytosine	C	Thymine	T

Table of contents

CHAPTER 1

Introduction

1.1 Introduction

In nature, oxidation and reduction reactions are essential for vital processes such as photosynthesis, respiration, redox homeostasis, and antioxidant defense mechanisms [1]. Many of the proteins that are involved in these reactions rely on the presence of redox active metal cofactors: most commonly iron (Fe) and copper (Cu). Both metals are transition elements, with more than one stable and biologically accessible oxidation state. The biological functions of these metals relate to their ability to convert between these oxidation states in oxidation-reduction processes. The bioavailability of iron and copper has changed over the geological history of the Earth [2]. While iron (as Fe(II)) was favored in the anaerobic Earth, the oxygenation by early photosynthetic organisms promoted the use of copper, particularly in systems that mediate oxygen (O_2) chemistry [2].

Copper is one of the most important trace elements found in living organisms, with functions ranging from the influence on specific gene expression [3] to serving as a cofactor for multiple proteins. However, free copper is highly toxic to living cells (particularly at high concentrations [4]), and therefore, the uptake, transport and incorporation of the metal into the copper requiring proteins within the cell are tightly regulated [5 - 8]. Cu-binding proteins account for up to 1 % of the total cellular proteome [9]. The metabolic roles of these proteins fall into four major categories including electron transfer (ET) reactions (for example azurin, Az) [1, 10 - 12], O_2 binding, transfer and activation (as in tyrosinase, Ty, and hemocyanin, Hc) [12, 13], transport or storage of metal itself (for example metallochaperones, which transport copper to their specific target proteins [5] and metallothioneins, which are cysteine-rich polypeptides with high affinity for Cu(I) [14]) and catalysis. Cu sites in proteins can exhibit oxidase activity by oxidation of substrates, which is coupled to either two or four electron reduction of O_2 (in amine oxidases, CuAOs [15], galactose oxidases, GOs [16] and multicopper oxidases, MCOs [17]), oxygenase activity by incorporating one oxygen atom from O_2 (in peptidylglycine α-hydroxylating monoxygenase, PHM [18], particulate methane monooxygenase, pMMO [19, 20] and ammonia monooxyganese, AMO [21]), act as reductases (for example in nitrite reductases, NiRs [22]), and can also participate in superoxide scavenging (copper/zinc superoxide dismutase, Cu/Zn-SOD) [23].

1.2 Copper coordination chemistry and copper sites in proteins

The ground state of Cu has a $3d^{10}4s^1$ valence electronic configuration. The Cu(I) oxidation state occurs through the loss of the 4s electron ($3d^{10}$), whilst Cu(II) has a singly occupied d orbital ($3d^9$) [24]. Cu(I) is a soft Lewis acid and prefers to bind to soft ligands such as those containing sulfur donor atoms (Cys or Met), whereas Cu(II) as a hard Lewis acid preferentially binds to harder ligands containing nitrogen (His) and oxygen (Asp or Glu) donor atoms [2]. Depending on coordination number, Cu(I) predominantly forms tetrahedral and trigonal planar complexes, whilst Cu(II) prefers tetragonal geometries, including square planar and axially elongated octahedral [25, 26]. The latter geometry of Cu(II) occurs due to the partial occupancy of degenerate d orbitals. The resulting instability is overcome *via* Jahn-Teller distortion that removes the orbital degeneracy through a reduction in symmetry by forming an axially distorted octahedron [24].

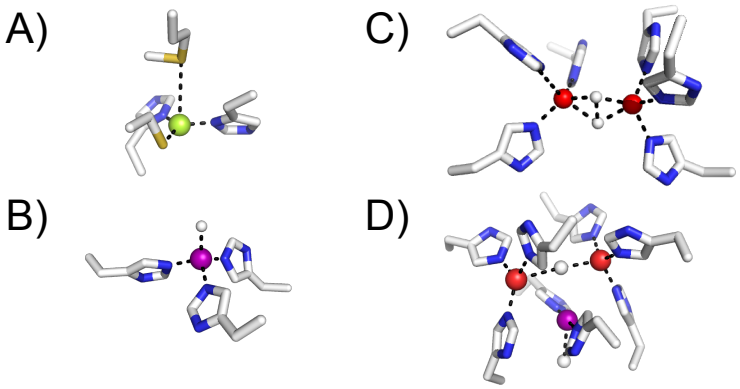

Figure 1.1 Some examples of Cu sites in proteins. (A) Type 1 (T1) Cu site of small laccase (SLAC) from *Streptomyces coelicolor* (pdb file: 3KW8 [27]), (B) type 2 (T2) Cu site of blue NiR (bNiR) from *Alcaligenes xylosoxidans* (pdb file: 1OE1 [28]), (C) type 3 (T3) Cu site of Ty from *Streptomyces castaneoglobisporus* (pdb file: 1WX2 [29]) and (D) trinuclear (T2/T3) Cu cluster from SLAC (pdb file: 3KW8 [27]). The T1, T2 and T3 Cus are shown as green, purple and red spheres, respectively, whilst O_2^{2-}/OH^-/H_2O ligands are shown as small white spheres.

The active sites of many Cu-containing proteins exhibit distinct spectral properties as compared to those of inorganic copper complexes [10, 11, 26, 30]. These properties reflect the geometric and electronic structures that are imposed on the Cu ion by the protein coordination environment. Historically, based on their

spectroscopic properties, Cu sites in proteins were classified as either type 1 (T1, "blue" or "green"), type 2 (T2, "normal") or type 3 (T3) [31]. In some cases T2 and T3 Cus form a trinuclear cluster (TNC) also referred to as a T2/T3 or T4 Cu site [10]. This original classification has been extended as novel Cu sites are discovered including the "red" Cu in nitrosocyanin [32], the binuclear "purple" Cu_A, for example in cytochrome *c* oxidase [33, 34] and the tetranuclear Cu_Z in nitrous oxide reductase (that also has a Cu_A site) [35]. Cu sites have also been created by protein engineering, including type zero [36], type 1.5 [37] and "yellow" thiolate-containing T2 (S(Cys)-T2) Cu [37, 38] (for more details see Chapter 4).

1.2.1 *The mononuclear T1 Cu site*

T1 Cu sites (Figure 1.1.A) carry out ET in a wide variety of biological systems [10, 11, 39, 40, 41]. The site consists of a single Cu ion protected by a protein envelope, which is commonly referred to as a cupredoxin fold [40, 41]. The cupredoxin fold consists of eight β-strands arranged into two β-sheets forming a Greek key β-barrel [42, 43]. Cupredoxins can occur as either single domain proteins, such as Az [42] and plastocyanin (Pc) [44], or as components (cupredoxin-like metal-binding domains, MBDs) of larger enzymes, such as NiRs [28] and MCOs, including laccases [27, 45 - 48], ascorbate oxidase (AO) [49], Fet3p [50] and ceruloplasmin (Cp) [51]. The metal ion at the T1 Cu site of cupredoxins is bound to the protein by two Cu-N(His) bonds and a short Cu-S(Cys) bond [26, 39, 52]. Additionally, weaker interactions either from Met (for example in Pc [44]), Gln (in stellacyanin, STL [53]), and Met and a carbonyl oxygen from the protein's backbone (in Az [42]) can be present. In some T1 Cu-containing proteins, a non-coordinating Val (in the plantocyanin (PLN) from tomato [54]), Leu (in PLN from lily [55], Cp [51] and Fet3p [50]) and Phe (fungal laccases [48]) occupy the axial position. Therefore, the geometry of a T1 Cu site varies from trigonal planar (as in fungal laccases [48]) *via* distorted tetrahedral (as in Pc [44]) to trigonal bipyramidal (as in Az [42]).

The reduction potential (E_m) of a T1 Cu site can vary from 190 (in STL) to > 1000 mV (in Cp) versus the normal hydrogen electrode [39, 40]. The single domain cupredoxins have E_m values ranging from 190 to 370 mV [40], except for rusticyanin, which has an E_m value of 670 mV [23]. The E_m of the T1 Cu sites of MCOs covers a wide range of values, with the three-coordinate T1 Cu sites of fungal laccases having E_ms of ~ 790 mV [40]. The residue in the axial position of a T1 Cu site is considered as

one of the factors influencing E_m, as the T1 Cu sites containing Phe or Leu in the axial position show typically higher E_m values than those containing Met. However, other factors such as hydrogen bonding [56], site hydrophobicity [57] and electrostatics [58] have been suggested to play an important role in modulation of the E_m value. Lu *et al.* demonstrated the additive nature of these effects by tuning the E_m of Az from *Pseudomonas aeruginosa* in the range of 80 to > 700 mV range [59]. The highest E_m among T1 Cu sites has that of Cp (with non-coordinating Leu in the axial position) [60] but it has been hypothesized that this site stays permanently reduced [60]. The replacement of the T1 Cu axial Leu with Met resulted in a silent mutation, which failed to modify either the spectroscopic or catalytic properties of Cp [61].

T1 Cu(II) sites show unusual spectroscopic properties as a consequence of their coordination geometry compared to those of normal tetragonal Cu(II) complexes [26]. In the visible region of its absorption spectrum a T1 Cu(II) site has an intense ($\varepsilon \sim 2000$ - 6000 $M^{-1}cm^{-1}$), low-energy S(Cys)$\pi \rightarrow$Cu(II) $d_{x^2-y^2}$ ligand to metal charge transfer (LMCT) transition centered at ~ 600 nm and a weak, high energy S(Cys)$\sigma \rightarrow$Cu(II) $d_{x^2-y^2}$ LMCT band at ~ 450 nm [10, 26, 39, 40, 52]. The electron paramagnetic resonance (EPR) spectrum of a T1 Cu(II) site has a small hyperfine coupling constant in the g_z region (A_z), typically < 95×10^4 cm^{-1} [26]. This unique visible spectrum and small A_z value are attributed to the highly covalent Cu(II)-S(Cys) bond (the unpaired electron is strongly delocalized onto the Cys ligand, hence reducing its interaction with the nuclear spin on the Cu ion) [10, 26, 60, 61].

The relative intensities of the two LMCT bands in the visible spectrum and the separation between g_x and g_y in the EPR spectrum of a T1 Cu(II) site vary [40, 62]. The classic "blue" T1 Cu sites (for example in Pc and bNiR from *A. xylosoxidans*) have lower absorbance at ~ 450 nm in their visible spectra and an axial EPR signal (similar g_x and g_y values). Upon tetragonal distortion of the ligand field (LF) of a "blue" T1 Cu site, the intensity of the LMCT band at ~ 600 nm decreases, whilst that at ~ 450 nm increases, resulting in a "green" T1 Cu site (for example the perturbed T1 Cu site in green NiR from *Rhodobacter sphaeroides*) [10, 26, 52, 60, 61]. Concomitantly, the separation between g_x and g_y increases giving rise to a rhombic EPR signal [40, 62]. The half-occupied Cu(II) $d_{x^2-y^2}$ orbital is oriented perpendicular to the long Cu(II)-S(Met) bond and close to the plane of the short S(Cys) and two N(His) ligands. The lobes of the Cu(II) $3d_{x^2-y^2}$ orbital in a "blue" T1 Cu bisect the Cu-S(Cys) 3p orbital giving highly covalent π overlap with the S(Cys) ligand (in square planar Cu(II)

complexes the $3d_{x^2-y^2}$ orbital is oriented towards a ligand's 3p orbital allowing for (ligand)σ→Cu(II) $d_{x^2-y^2}$ LMCT) [10, 26, 60, 63]. The spectral changes of a "green" T1 Cu site are attributed to rotation of the Cu(II) $d_{x^2-y^2}$ orbital and a shift from π to σ bonding with the S(Cys) ligand, and therefore, a weakening of the Cu(II)-S(Cys) bond that leads to strengthening of the axial Cu(II)-S(Met) interaction [10, 52, 60, 61]. Interestingly, the relative intensities of the two LMCT bands of the perturbed T1 Cu site of green NiR are temperature dependent, indicating thermodynamic equilibrium between "green" and "blue" T1 Cu sites [60, 61].

1.2.2 *The mononuclear T2 Cu site*

Mononuclear T2 Cu sites are found in a range of proteins including Cu/Zn-SOD, PHM, dopamine β-hydroxylase (DβM), NiRs, CuAOs and GOs [26, 64]. In MCOs, a T2 Cu site contributes to the T2/T3 Cu cluster (see below) [63]. The T2 Cu ion is usually coordinated by imidazole side chains of His residues, but Tyr (in GO [65]) and Met (in PHM [18]) can also be present. T2 Cu sites can have a range of geometries including square planar (as in Zn/Cu-SOD [66]), tetrahedral (as in NiRs [28], Figure 1.1.B) and square pyramidal (as in GO [65] and CuAO [67]). T2 Cu sites are typically catalytic and the substrate binds to the Cu ion in place of the exogenous ligand (such as H_2O and OH^- [22, 64]). T2 Cu can catalyze a range of reactions including the disproportionation of superoxide (Cu/Zn-SOD [23]), reduce NO_2^- to NO (NiRs [22], see Chapter 2) and have oxidase (as part of a T2/T3 Cu cluster in MCOs [17], see Chapter 3) and oxygenase (in PHM, which hydroxylates the C^α atom of a terminal Gly residue in the amidation of peptide hormones, neuropeptides and antimicrobials, and DβM that converts dopamine to norepinephrine [18]) activities.

The spectral features of a T2 Cu(II) site are similar to those of normal tetragonal Cu(II) inorganic complexes [26]. Due to the absence of a thiolate ligand, the absorption spectrum of this site does not show any distinct features in the visible region. The T2 Cu(II) site exhibits an EPR signal with an A_z value of ~ (150 - 250) × 10^4 cm^{-1} [26] and several weak LF transitions in the magnetic circular dichroism (MCD) spectrum [68, 69].

1.2.3 *The binuclear T3 Cu site*

Binuclear T3 Cu sites (Figure 1.1.C) are found in proteins such as Hc [70], Ty [29] and catechol oxidase (CatOx) [71]. In Hc, the site reversibly binds O_2 facilitating storage and transport, whilst it participates in the hydroxylation of monophenolic substrates in Ty and the oxidation of catechol substrates (*ortho*-diphenols) in both Ty and CatOx [13, 29, 70, 71]. The binuclear T3 Cu site is composed of two Cu ions, both coordinated by three His ligands in a trigonal planar geometry [29, 70, 71]. The metal ions are strongly coupled through a bridging ligand, such as O_2^{2-} and OH^- [3, 26, 30]. Molecular O_2 binds to the reduced and colourless T3 Cu(I)s yielding two forms of oxygenated species that exhibit different spectral features [12, 13, 26, 30, 72 - 76]. The peroxide-bound Cu(II)-O_2^{2-}-Cu(II) *oxy* form, in which O_2 is bound in a side-on geometry (Figure 1.1.C) is characterized by $O_2^{2-}\rightarrow$Cu(II) $d_{x^2-y^2}$ LMCT transition bands at ~ 350 nm ($\varepsilon \sim 20000\ M^{-1}cm^{-1}$) and ~ 550 nm ($\varepsilon \sim 1000\ M^{-1}cm^{-1}$). The *met* Cu(II)-Cu(II) species, in which the T3 Cus are OH^--bridged, show a weak $OH^-\rightarrow$Cu(II) $d_{x^2-y^2}$ LMCT transition band at ~ 330 - 360 nm. Both forms of T3 Cu(II) site do not give rise to an EPR signal and spectral features in the MCD spectrum owing to strong antiferromagnetic coupling mediated by a bridging ligand [12, 13, 26, 77].

1.2.4 *The trinuclear T2/T3 Cu cluster*

Trinuclear T2/T3 Cu cluster consists of a T2 Cu ion and a T3 Cu pair (Figure 1.1.D), and is found in MCOs, which catalyze substrate oxidation coupled to the four-electron reduction of O_2 to H_2O (the reactivity of the T2/T3 Cu cluster in laccases is discussed in detail in Chapter 3) [30, 63]. In the resting enzyme, the T3 Cu(II)s are coupled through a bridging OH^- ligand [12, 26, 63]. Therefore, each T3 Cu is four-coordinated (three His and OH^- ligands) in a distorted tetrahedral geometry [27, 48 - 51, 63]. The T2 Cu is three-coordinated (two His and OH^- ligands) in a trigonal planar geometry.

Similar to the binuclear T3 Cu site, the T3 Cu(II)s in the T2/T3 Cu cluster are EPR and MCD silent due to strong antiferromagnetic coupling of the T3 Cu(II) pair bridged by an OH^- ion [26]. The site demonstrates a bridging OH^- to Cu(II) LMCT band at ~ 330 nm ($\varepsilon \sim 4000\ M^{-1}cm^{-1}$) [39] and several LF transitions in the circular dichroism (CD) spectrum [77]. The T2 Cu(II) is not bridged to the T3 Cus and, therefore, shows an EPR signal and LF transitions in the MCD spectrum, similar to those observed for the mononuclear T2 Cu(II) [26, 77].

1.3 Structural relationship between copper-containing proteins

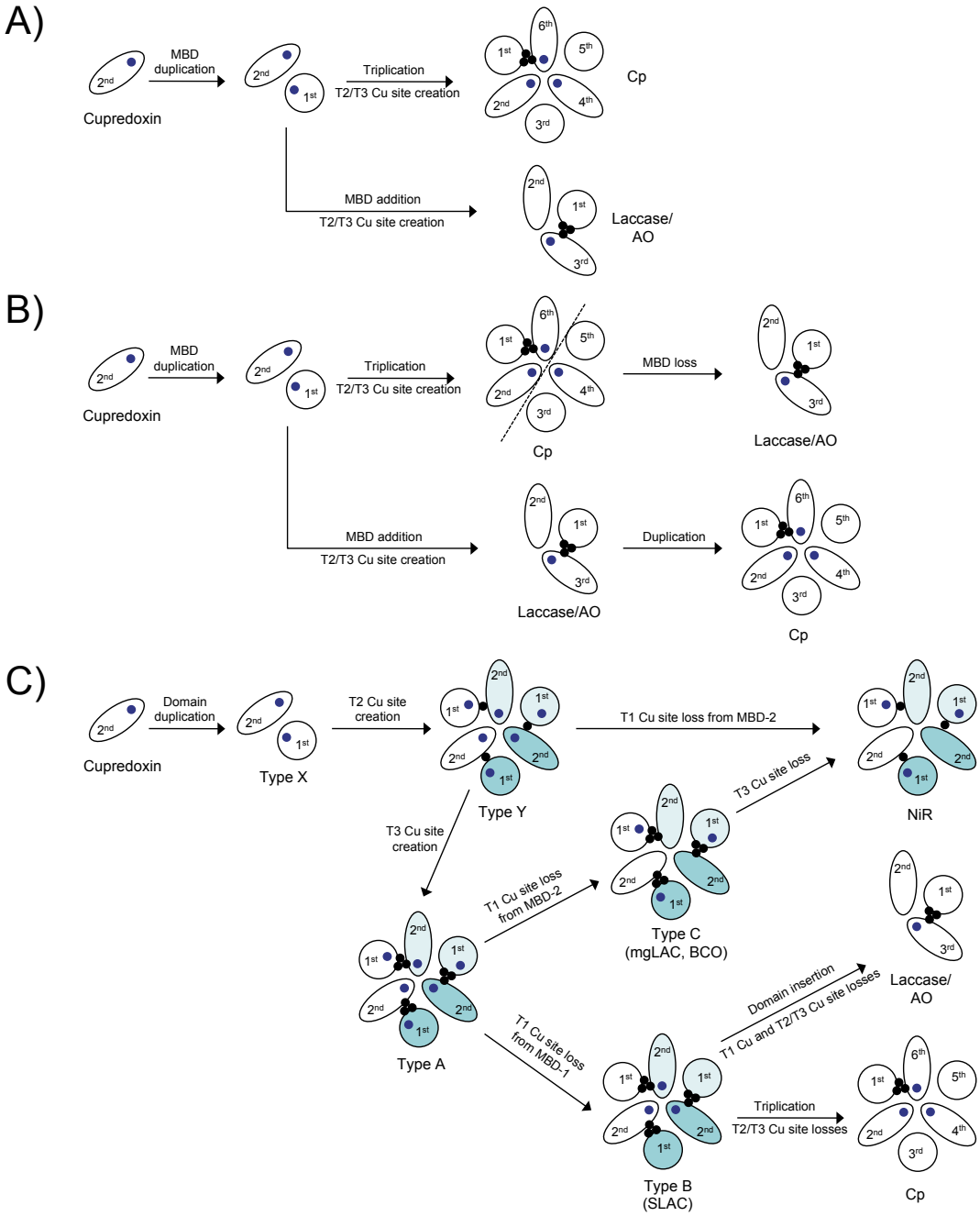

Figure 1.2 Schematic representations of MBDs and Cu ions organization in Cu-containing proteins and their hypothetical ancestors as proposed by (A) Ryden and Hunt [78], (B) Murphy *et al.* [79] and (C) Nakamura *et al.* [80]. Blue represents the two-domain monomer of trimeric proteins. The T1 Cu and IDCB (the T2 Cu and T2/T3 Cu cluster) sites are shown as blue and black dots, respectively.

Multi-domain Cu-containing proteins consist of two (for example NiRs [28] and two-domain laccases [27, 45 - 47]), three (for example AO [49], and three-domain laccases

[48]) or six (for example Cp [51]) MBDs. Only some of these MBDs bind a T1 Cu, some are involved in inter-domain Cu-binding (IDCB) sites, and some do not bind metal at all. Several NiRs with an additional MBD have been found and a crystal structure of a hexameric NiR (tightly associated dimer of trimers, with each monomer consisting of three MBDs) is available [81]. However, the function of this additional MBD is as yet unknown.

Genome sequence analyses combined with structural and spectroscopic data suggest that the multiplication of a MBD followed by creation of the IDCB and substrate-binding sites led to the formation of multi-domain Cu-binding proteins. Several duplicated cupredoxins such as dicyanin from tomato (NCBI accession no. Q9M510; containing two T1 Cu sites, one in each MBD), dinodulin from *Arabidopsis thaliana*, (NCBI accession no. Q9MAK3, Q9LFI4 and Q9M135; lacking T1 Cu sites) and hDN from *Halobacterium* sp. NRC-1 (NCBI accession no. Q9HPH3; containing only one T1 Cu site), have been identified [80, 82]. However, Nakamura *et al*. suggested that the duplication of cupredoxins to form these proteins were separate events from the one that led to the creation of multi-domain Cu-binding proteins [80]. Ryden and Hunt [78] proposed that a pair of MBDs from the initial duplication of a cupredoxin domain was duplicated twice more to create a six-domain form such as Cp, whereas three-domain MCOs were formed by a single addition of an MBD to a two-domain protein (Figure 1.2.A). Based on the similarities between the proteins' structure and function of their IDCB sites, Murphy *et al.* [79] proposed (Figure 1.2.B) that either triplication of a two-domain protein, which led to the formation of Cp, was followed by the loss of three MBDs to form a three-domain MCOs, or that duplication of a three-domain MCO led to the formation of Cp.

Nakamura *et al.* hypothesized [80, 83] the presence of three types of trimeric, two-domain MCOs (type A, B and C) as common ancestors in the formation of three- and six-domain Cu-binding proteins (Figure 1.2.C). The difference between the type A, B and C intermediates is the distribution of T1 Cu sites. The type A MCOs contain a T1 Cu site in each MBD, and are considered the precursors to the type B and type C MCOs, which contain T1 Cu sites in the second (MBD-2) and the first (MBD-1) MBD, respectively (Figure 1.2.C). Trimeric NiRs evolved either from the type C MCOs with concomitant loss of the T3 Cus, or from the type Y ancestor (an analogue to the type A MCO containing a T2 Cu instead of a T2/T3 cluster) with concomitant loss of a T1 Cu site in MBD-2 (Figure 1.2.C). Deposition of several crystal structures of trimeric two-domain MCOs, such as mgLAC obtained from metagenome database [45], SLAC

[27, 47] and the blue copper oxidase (BCO) from *Nitrosomonas europaea* [46], supports the evolutionary scheme presented in Figure 1.2.C. However, Nakamura *et al.* did not identify sequences of any type Y proteins in genome databases [80], and although the sequences of three type A proteins were identified [80], no crystal structures are available.

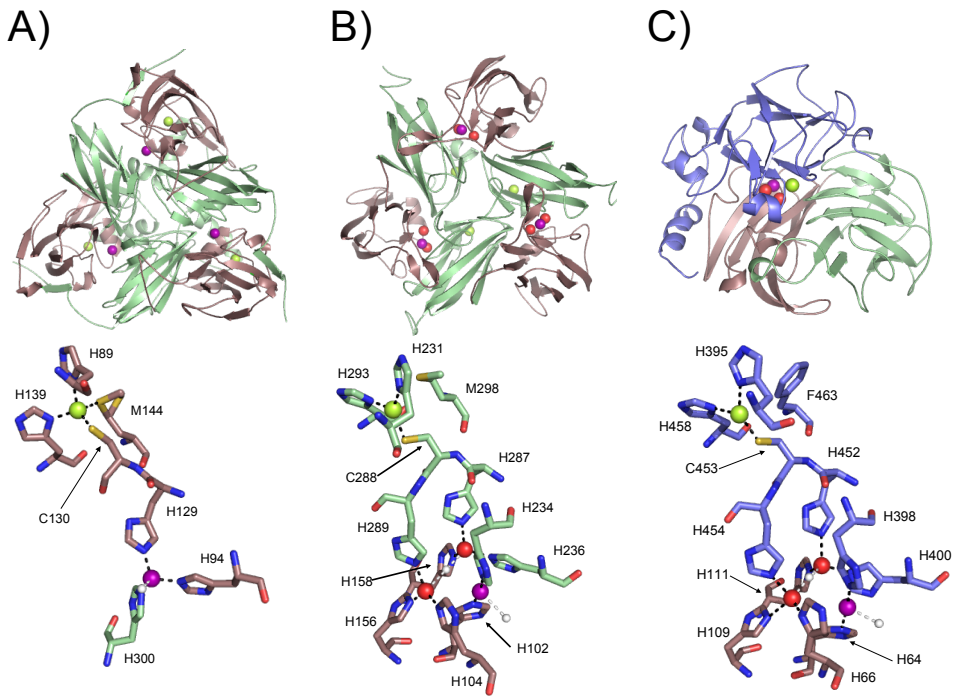

Figure 1.3 Cartoon representations of the overall structures (top) and the active sites (bottom) of (A) bNiR (pdb file: 1OE1 [8]) and (B) SLAC (pdb file: 3KW8 [27]) and (C) laccase from *Trametes versicolor* (pdb file: 1KYA [48]). MBD-1, MBD-2 and MBD-3 are coloured pink, green and blue. The T1, T2 and T3 Cus are shown as green, purple and red spheres, respectively, whilst OH^- and H_2O ligands are small white spheres.

The core domains of characterized two-domain MCOs and NiRs are well conserved (Figure 1.3), with only minor structural differences [27, 28, 45 - 47]. In NiRs (Figure 1.3.A) [28], mgLAC [45] and BCO [46] (latter two enzymes are the type C MCOs), the T1 Cu site is located in MBD-1, whilst in SLAC (Figure 1.3.B) [27, 47] it is located in MBD-2 (type B MCO). The IDCB site of two-domain MCOs and NiRs is located at the interface between MBD-1 and MBD-2 of two adjacent monomers, whilst in three-domain MCOs (Figure 1.3.C) it is at the interface between MBD-1 and MBD-3 [27, 28, 45 - 49]. The three-dimensional structure of the IDCB sites and their adjacent T1 Cu site (~ 13 Å away) is similar to some extend, in MCOs and NiRs. In NiRs, the

T1 Cu and the IDCB sites are connected by a Cys(T1 Cu)-His(T2 Cu) motif (Figure 1.3.A), whilst in MCOs by a His(T3 Cu)-Cys(T1Cu)-His(T3 Cu) (Figure 1.3.B and 1.3.C). The potential T1 Cu sites in the remaining MBDs (MBD-1 for SLAC and MBD-2 for NiRs, mgLAC and BCO) are missing, mainly due to the substitution of the potentially Cu-ligating Cys residue to either Asp, Asn or Glu (more details can be found in Chapter 4).

1.4 The FluoRox principle

1.4.1 *General introduction to fluorescence*

Luminescence is a phenomenon occurring when a molecular system absorbs light and dissipates the energy through the emission of a photon [84]. The mechanism of luminescence is usually described by means of Jablonski diagram (Figure 1.4) that illustrates the processes that occur between the absorption and emission of light by a molecule. The singlet ground, first and second electronic states are depicted by S_0, S_1 and S_2, respectively, whilst the first triplet state is T_1. Each of these states carries a series of vibrational energy levels, denoted by 0, 1, 2 and 3 (Figure 1.4).

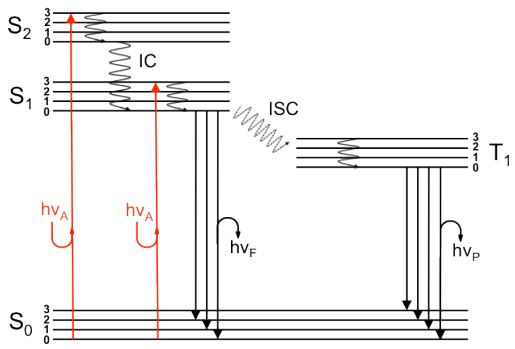

Figure 1.4 Jablonski diagram as adapted from [84], describing the electronic states of a luminescent molecule that are involved in luminescence. S_0 is a ground electronic state, whilst S_1 and S_2 are first and second singlet excited electronic states and T_1 is the first triplet state. $h\nu_A$ indicates absorbed photons ($S_0 \rightarrow S_1$ and $S_0 \rightarrow S_2$ transitions), whilst $h\nu_F$ and $h\nu_P$ are the photons emitted in fluorescence ($S_1 \rightarrow S_0$ transitions) and phosphorescence ($T_1 \rightarrow S_0$ transitions), respectively. Wiggly arrows represent non-radiative energy dissipation. IC and ISC are internal conversion and intersystem crossing, respectively.

Depending on the nature of the excited state from which the emission occurs, luminescence is divided into fluorescence and phosphorescence (Figure 1.4). Fluorescence (10^{-8} s timescale) generally occurs from a thermally equilibrated excited state, which is the lowest vibrational level of S_1. Therefore, following light absorption ($S_0 \rightarrow S_1$ and $S_0 \rightarrow S_2$ transitions, 10^{-15} s timescale), a fluorophore in the excited states relaxes to the lowest vibrational level in a process called internal conversion (IC, 10^{-12} s timescale) prior to decay from S_1 to S_0 [84]. Typically, this return occurs to a higher excited vibrational level of S_0, which then quickly reaches thermal equilibrium (10^{-12} s timescale). Alternatively, the molecules in the S_1 state undergo a spin conversion to the T_1 in a process called intersystem crossing (ISC) [84]. The $T_1 \rightarrow S_0$ transition is forbidden, and thus, the rate constants for triplet emission are smaller than those for fluorescence (10^3 to 1 and 10^8 s^{-1}, respectively), resulting in phosphorescence lifetimes ranging from 10^{-3} to 1 s [84]. The presence of heavy atoms such as bromine and iodine facilitates ISC and therefore, enhances phosphorescence quantum yields (number of emitted photons relative to the number of absorbed photons).

The same fluorescence emission spectrum is generally independent of an excitation wavelength (Kasha-Vavilov rule) due to the strong overlap among numerous vibrational levels (of nearly equal energy) of S_1 and rapid relaxation (10^{-12} s) to the lowest vibrational level of S_1 [84, 85]. Exceptions exist, such as molecules emitting from the S_2 level, but such emissions are generally not observed in biological molecules [84]. The fluorescence spectrum of a system is typically a mirror image of the absorption spectrum of the $S_0 \rightarrow S_1$ transition, but photon emission occurs at lower energies (longer wavelengths) than excitation. This red shift, also called the Stokes shift, is caused by the relaxation, mainly by thermal equilibration, of the excess vibrational energy. The fluorescence parameters that are typically measured for the biophysical and biochemical characterization of molecules are the fluorescence quantum yield, fluorescence intensity as a function of wavelength, fluorescence lifetime (average time that a molecule spends in the excited state prior to return to the S_0 level) and fluorescence polarization [84].

The main fluorescent probes used in biochemistry are classified as intrinsic (natural) and extrinsic fluorophores, and fluorescence indicators [84]. Intrinsic fluorophores include among others the indole group of Trp, oxidized flavins, reduced nicotinamide adenine dinucleotide (NADH), pyridoxal phosphate and chlorophyll. Extrinsic fluorophores, including fluorescent proteins such as GFP and YFP, and commercially available organic molecules such as rhodamine- (for example ATTO 532)

and cyanine- (for example Cy5) based dyes are used when the molecule of interest is not fluorescent or the intrinsic fluorescence is either inadequate or insufficient. Fluorescence indicators are fluorophores whose spectral features are sensitive to a substance of interest (such as metal ions, O_2 or pH) [84]. Although relatively few copper-selective fluorescent probes have been reported, their use has enabled the detection and visualization of intracellular copper present in living cells [86 - 90]. For example the Cu(II)-selective Phen Green FL fluorescent probe has been used to study binding of metal to the full-length Alzheimer's amyloid-β peptide [86] and to investigate the mechanism of Cu(II) uptake by different types of hepatopancreas epithelial cells and mitochondria [87, 88].

1.4.2 *Förster Resonance Energy Transfer*

Förster Resonance Energy Transfer (FRET) is a radiation-less energy transfer resulting from long-range dipole-dipole interactions between a donor molecule (D) in the excited electronic state and an acceptor molecule (A) in the ground electronic state [84]. FRET is widely used in biology and biochemistry as a sensitive method for measuring distances within or between molecules [91, 92]. The conditions required for FRET to occur are: sufficient spectral overlap between the emission spectrum of D and the absorption spectrum of A, a D to A distance of 20 to 90 Å [84], and optimal relative orientation of the transition dipoles of D and A.

The dependence of FRET efficiency of energy transfer (E) on the D to A distance (r) is given by Equation 1.1 [84]:

$$E = \frac{R_0^6}{R_0^6 + r^6} \qquad \text{(Equation 1.1),}$$

where R_0 is the Förster distance, which is the distance at which E is 50 %. R_0 is dependent on the spectral properties of D and A, and their relative orientation, as described by Equation 1.2 [84]:

$$R_0 = 0.211\left(\kappa^2 n^{-4} Q_D J(\lambda)\right)^{1/6} \qquad \text{(Equation 1.2),}$$

in which κ^2 describes the relative orientation in space of the transition dipoles of D and A, n is the refractive index of the medium, Q_D is the quantum yield of D and $J(\lambda)$ is the

spectral overlap integral, which expresses the degree of spectral overlap between the emission of D and the absorption of A as a function of wavelength, λ. *J(λ)* is defined as [84]:

$$J(\lambda) = \frac{\int_0^\infty F_D(\lambda)\varepsilon_A(\lambda)\lambda^4 d\lambda}{\int_0^\infty F_D(\lambda)d\lambda} \qquad \text{(Equation 1.3)},$$

where F_D is the fluorescence intensity of D and ε_A is the extinction coefficient of A as a function of λ. In case of a fixed D-A distance, E can be expressed in terms of fluorescence intensities (Equation 1.4) or lifetimes (Equation 1.5) [84]:

$$E = 1 - \frac{F_{DA}}{F_D} \qquad \text{(Equation 1.4)},$$

$$E = 1 - \frac{\tau_{DA}}{\tau_D} \qquad \text{(Equation 1.5)},$$

where F_{DA} and τ_{DA} are the fluorescence intensity and lifetime respectively of D in the presence of A, whilst F_D and τ_D are the fluorescence intensity and lifetime respectively of D in the absence of A.

1.4.3 *FRET as a reporter of the oxidation state of metalloproteins*

The FluoRox principle is a FRET-based approach that relies on the use of a surface-conjugated fluorescent dye molecules acting as the FRET donor and the redox-active cofactor of a protein or enzyme acting as the FRET acceptor (Figure 1.5.A). The use of a fluorescent label whose emission spectrum overlaps with the absorption spectrum of the cofactor in one of its oxidation states results in partial quenching of the label's fluorescence by that state. Upon changing the oxidation state of the cofactor the spectral overlap, and the R_0 value of the D-A pair, changes (Figure 1.5.B). Therefore, fluctuations in the oxidation state of the cofactor are reflected in changes in fluorescence intensity (Figure 1.5.C). This FRET-based approach provides increased sensitivity compared to absorbance and electrochemical measurements of oxidation state changes, making FluoRox particularly attractive for biosensing applications [93 - 96] and single molecule investigations (as in Chapter 2) [97 - 99].

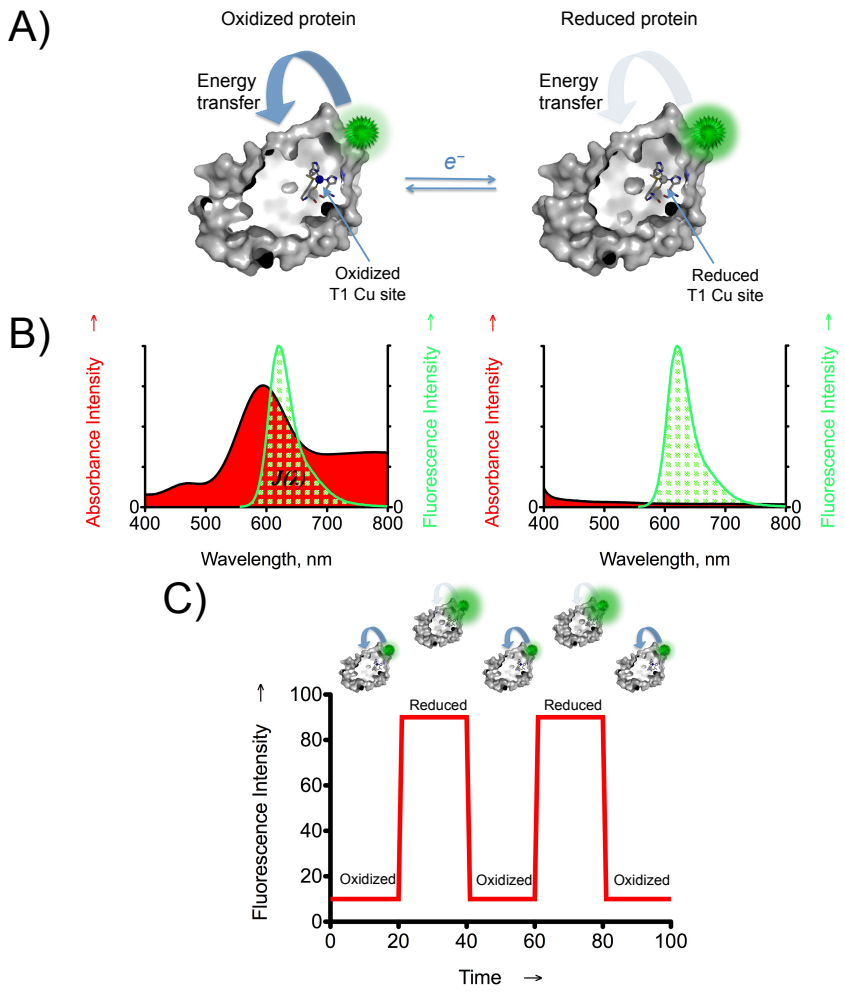

Figure 1.5 (A) Schematic depiction of the FluoRox principle, (B) spectral overlap (***J(λ)***) between absorption (red) of a T1 Cu-containing protein and emission (green) of a fluorescent label, and (C) fluorescence intensity changes upon oxidation and reduction of labeled protein. Left and right panels in (A) and (B) correspond to the Cu(II) and Cu(I) forms of the protein, respectively. The fluorescent label is shown as a green star, whilst the oxidized and reduced states of the T1 Cu are blue and gray spheres, respectively.

The strong absorbencies at ~ 330 and ~ 600 nm of oxidized T3 (and also T2/T3) and T1 Cu-containing proteins (Section 1.2), which are absent in the reduced forms, make them particularly amenable to the FluoRox approach (Figure 1.5, scheme for the T1 Cu-containing protein). The fluorescence of a surface-attached fluorescent label (whose spectrum overlaps with ~ 600 nm absorbance of the T1 Cu(II) site) is quenched owing to FRET between the label and the T1 Cu(II) site, and thus the fluorescence intensity is low (Figure 1.5.C). Upon reduction, no FRET occurs and the fluorescence intensity of the label is much higher (Figure 1.5.C). The absorbance at ~ 330 nm of

oxidized T3 and T2/T3 Cu sites overlaps with the emission of Trp residues (intrinsic fluorescence in proteins typically occurs between ~ 308 to 355 nm [100]). This intrinsic fluorescence is quenched as a result of FRET between the Trp residues and the T3 and T2/T3 Cu(II) sites resulting in low intensity of Trp emission [101, 102]. Upon reduction, no FRET occurs and higher intensity of Trp fluorescence is detected. Intrinsic fluorescence is therefore a sensitive reporter for O_2 bound to the T3 Cu center and, thus, the T3 Cu and T2/T3 Cu-containing enzymes can be used for O_2 biosensing [93, 103, 104].

1.5 Aims of the thesis

The first aim of this research was to apply a FRET-based approach (FluoRox) to study the catalytic mechanism of bNiR from *A. xylosoxidans* at the single molecule level (work in collaboration with Leiden University, Chapter 2). The enzyme mechanism is controversial and therefore the single molecule approach was anticipated to provide a better understanding of this.

The second objective was to develop an efficient over-expression system for the high-potential fungal laccase Lcc1 from *T. versicolor* (work in collaboration with Utrecht University) and comparison of this enzyme with native Laccase A from *T. versicolor* and low-potential bacterial SLAC from *S. coelicolor*. Potential application of these laccases in development of a laccase-based FluoRox biosensor was investigated (Chapter 3).

The third aim was to explore whether it was possible to modify the cupredoxin-like domains of bNiR and SLAC, which normally lack a T1 Cu site, to introduce metal-binding site (Chapter 4). Additionally, owing to the high structural similarity between trimeric NiRs and two-domain MCOs, the possibility to transform the T2 Cu site of bNiR into a T2/T3 Cu cluster using protein engineering was tested (Chapter 4).

1.6 References

1) Holm R.H., Kennephohl P., Solomon E.I., 1996, Chem. Rev., 96, 2239-2314

2) Frausto da Silva J.J.R., Wiliams R.J.P., 2001, The Biological Chemistry of the Elements, Oxford University Press

3) Rademacher C., Masepohl B., 2012, Microbiology, 158, 2451-2464

4) Halliwell B., Gutteridge J.M., 1984, Biochem. J., 219, 1-14

5) Robinson N.J., Winge D.R., 2010, Annu. Rev. Biochem., 79, 537-562

6) Rae T.D., Schmidt P.J., Pufahl R.A., Culotta V.C., O'Halloran T.V., 1999, Science, 284, 805-805

7) Huffman D.L., O'Halloran T.V., 2001, Annu. Rev. Biochem., 70, 677-701

8) Rosenzweig A.C., 2001, Acc. Chem. Res., 34, 119-128

9) Andreini C., Banci L., Bertini I., Rosato A., 2008, J. Proteome Res., 7, 209-216

10) Solomon E.I., Szilagyi R.K., George S.D., Basumallick L., 2004, Chem. Rev., 104, 419-458

11) Solomon E.I., Randall D.W., Glaser T., 2000, Coord. Chem. Rev., 200-202, 595-632

12) Solomon E.I., Lowery M.D., 1993, Science, 259, 1575-1581

13) Solomon E.I., Chen P., Metz M., Lee S.K., Palmer A.E., 2001, Angew. Chem. Int. Ed., 40, 4570-4590

14) Blindauer C.A., Leszczyszyn O.I., 2010, Nat. Prod. Rep., 27, 720-41

15) Dawkes H.C., Phillips S.E.V., 2001, Curr. Opin. Struct. Biol., 11, 666-673

16) Whittaker J.W., 2005, Arch. Biochem. Biophys., 433, 227-239

17) Solomon E.I., Augustine A.J., Yoon J., 2008, Dalton Trans., 30, 3921-3932

18) Klinman J.P., 2005, J. Biol. Chem., 281, 3013-3016

19) Lieberman R.L., Rosenzweig A.C., 2004, Crit. Rev. Biochem. Mol. Biol., 39, 146-164

20) Culpepper M.A., Rosenzweig A.C., 2012, Crit. Rev. Biochem. Mol. Biol., 47, 483-492

21) Arp D.J., Sayavedra L.A., Hommes N.G., 2002, Arch. Microbiol., 178, 250-255

22) Merkle A.C., Lehnert N., 2012, Dalton Trans., 41, 3355-3368

23) Culotta V.C., Yang M., O'Halloran T.V., 2006, Biochim. Biophys. Acta, 1763, 747-758

24) Kettle S.F.A., 1998, Physical Inorganic Chemistry: A Coordination Chemistry Approach, Oxford University Press

25) Gray H.B., Malmström B.G., Williams R.J.P., 2000, J. Biol. Inorg. Chem, 5, 551-559

26) Yoon J., Solomon E.I., 2009, High Resolution EPR, Biological Magnetic Resonance, 28, 471-504, Springer, New York, USA

27) Skálová T., Dušková J., Hašek J., Stěpánková A., Koval T., Østergaard L.H., Dohnálek J., 2011, Acta Crystallogr. Sect. F Struct. Biol. Cryst. Commun., 67, 27-32

28) Ellis M.J., Dodd F.E., Sawers G., Eady R.R., Hasnain S.S., 2002, J. Mol. Biol., 328, 429-438

29) Matoba Y., Kumagai T., Yamamoto A., Yoshitsu H., Sugiyama M., 2006, J. Biol. Chem., 281, 8981-8990

30) Solomon E.I., Sundaram U.M., Machonkin T.E., 1996, Chem. Rev., 96, 2563-2606

31) Malkin R., Malmström B.G., 1970, Adv. Enzymol., 33, 177-244

32) Lieberman R.L., Arciero D.M., Hooper A.B., Rosenzweig A.C., 2001, Biochemistry, 40, 5674-5681

33) Iwata S., Ostermeier C., Ludwig B., Michel H., 1995, Nature, 376, 660-669

34) Tsukihara T., Aoyama H., Yamashita E., Tomizaki T., Yamaguchi H., Shinzawa-Itoh K., Nakashima R., Yaono R., Yoshikawa S., 1995, Science, 269, 1069-1074

35) Brown K., Tegoni M., Prudêncio M., Pereira A.S., Besson S., Moura J.J., Moura I., Cambillau C., 2000, Nat. Struct. Biol., 7, 191-195

36) Lancaster K.M., DeBeer George .S., Yokoyama K., Richards J.H., Gray H.B., 2009, Nat. Chem., 1, 711-715

37) Canters G.W., Gilardi G., 1993, FEBS Lett., 325(1-2), 39-48

38) Van Amsterdam I.M.C., Ubbink M., van den Bosch M., Rotsaert F., Sanders-Loehr J., Canters G.W., 2002, J. Biol. Chem., 46, 44121-44130

39) Sakurai T., Kataoka K., 2007, Cell Mol. Life Sci., 64, 2642-2656

40) Dennison C., 2005, Coord. Chem. Rev., 249, 3025-3054

41) Adman E.T., 1991, Curr. Opin. Struct. Biol., 1, 895-904

42) Nar H., Messerschmidt A., Huber R., van de Kamp M., Canters G.W., 1991, J. Mol. Biol., 221, 765-772

43) Choi M., Davidson V.L., 2011, Metallomics, 3, 140-151

44) Guss J.M., Bartunik H.D., Freeman H.C., 1992, Acta Crystallogr. B., 48, 790-811

45) Komori H., Miyazaki K., Higuchi Y., 2009, FEBS Lett., 583, 1189-1195

46) Lawton T.J., Sayavedra-Soto L.A., Arp D.J., Rosenzweig A.C., 2009, J. Biol. Chem., 284, 10174-10180

47) Skálová T., Dohnálek J., Østergaard L.H., Østergaard P.R., Kolenko P., Dusková J., Stepánková A., Hasek J., 2009, J. Mol. Biol., 385, 1165-1178

48) Bertrand T., Jolivalt C., Briozzo P., Caminade E., Joly N., Madzak C., Mougin C., 2002, Biochemistry, 41, 7325-7333

49) Messerschmidt A., Ladenstein R., Huber R., Bolognesi M., Avigliano L., Petruzzelli R., Rossi A., Finazzi-Agró A., 1992, J. Mol. Biol., 224, 179-205

50) Taylor A.B., Stoj C.S., Ziegler L., Kosman D.J., Hart P.J., 2005, Proc. Natl. Acad. Sci. USA, 102, 15459-15464

51) Bento I., Peixoto C., Zaitsev V.N., Lindley P.F., 2007, Acta Crystallogr. D Biol. Crystallogr., 63, 240-248

52) Solomon E.I., 2006, Inorg. Chem., 45, 8012-8025

53) Hart P.J., Nersissian A.M., Herrmann R.G., Nalbandyan R.M., Valentine J.S., Eisenberg D., 1996, Protein Sci., 5, 2175-2183

54) Dennison C., Harrison M.D., Lawle A.T., 2003, Biochem. J., 371, 377-383

55) Kim S., Mollet J.C., Dong J., Zhang K., Park S.Y., Lord E.M., 2003, Proc. Natl. Acad. Sci. USA, 100, 16125-16130

56) Donaire A., Jiménez B., Fernández C.O., Pierattelli R., Niizeki T., Moratal J.M., Hall J.F., Kohzuma T., Hasnain S.S., Vila A.J., 2002, J. Am. Chem. Soc., 124, 13698-13708

57) Yanagisawa S., Banfield M.J., Dennison C., 2006, Biochemistry, 45, 8812-8822

58) Battistuzzi G., Borsari M., Loschi L., Menziani M.C., De Rienzo F., Sola M., 2001, Biochemistry, 40, 6422-6430

59) Marshall N.M., Gerner D.K., Wilson T.D., Gao Y.G., Robinson H., Nigels M.J., Lu Y., 2009, Nature, 462, 113-116

60) Solomon E.I., Hadt R.G., 2011, Coord. Chem. Rev., 255, 774-789

61) Ghosh S., Xie X., Dey A., Sun Y., Scholes C.P., Solomon E.I., 2009, Proc. Natl. Acad. Sci. USA, 106, 4969-4974

62) Sato K., Dennison C., 2006, Chem. Eur., J., 12, 6647-6659

63) Kosman D.J., 2010, J. Biol. Inorg. Chem., 15, 15-28

64) MacPherson I.S., Murphy M.E.P., 2007, Cell Mol. Life Sci., 64, 2887-2899

65) Ito N., Philips S.E.V., Stevens C., Ogel Z.B., McPherson M.J., Keen J.N., Yadav K.D.S., Knowles P.F., 1992, Faraday Discuss., 93, 75-84

66) Tainer J.A., Getzoff E.D., Beem K.M., Richardson J.S., Richardson D.C., 1982, J. Mol. Biol., 160, 181-217

67) Wilmot C.M., Hajdu J., McPherson M.J., Knowles P.F., Phillips S.E., 1999, Science, 286, 1724-1728

68) Zhekova H. R., Seth M., Ziegler T., 2010, J. Phys. Chem. A, 114, 6308-6321

69) LaCroix L.B., Shadle S.E., Wang Y., Averill B.A., Hedman B., Hodgson K.O., Solomon E.I., 1996, J. Am. Chem. Soc., 118, 7755-7768

70) Magnus K.A., Hazes B., Ton-That H., Bonaventura C., Bonaventura J., Hol W.G., 1994, Proteins, 19, 302-309

71) Hakulinen N., Gasparetti C., Kaljunen H., Kruus K., Rouvinen J., 2013, J. Biol. Inorg. Chem., 18, 917-929

72) Hepp A.F., Himmelwright R.S., Eickman N.C., Solomon E.I., 1979, Biochem. Biophys. Res. Commun., 89, 1050-1057

73) Jolley R.L. Jr., Evans L.H., Makino N., Mason H.S., 1974, J. Biol. Chem., 249, 335-345

74) Schoot Uiterkamp A.J., Evans L.H., Jolley R.L., Mason H.S., 1976, Biochim. Biophys. Acta, 453, 200-204

75) Himmelwright R.S., Eickman N.C, LuBien C.D., Solomon E.I., Lerch K., 1980, J. Am. Chem. Soc., 102, 7339-7344

76) Eickman N.C., Himmelwright R.S., Solomon E.I., 1979, Proc. Natl. Acad. Sci. USA, 76, 2094-2098

77) Machonkin T.E., Quintanar L., Palmer A.E., Hasset R., Severance S., Kosman D.J., Solomon E.I., 2001, J. Am. Chem. Soc., 123, 5507-5517

78) Ryden l.G., Hunt L.T., 1993, J. Mol. Evol., 36, 41-66

79) Murphy M.E., Lindley P.F., Adman E.T., 1997, Protein Sci., 6, 761-770

80) Nakamura K., Kawabata T., Yura K., Go N., 2003, FEBS Lett., 553, 239-244

81) Nojiri M., Xie Y., Inoue T., Yamamoto T., Matsumara H., Kataoka K., Deligeer, Yamaguci K., Kai Y., Suzuki S., 2007, Proc. Natl. Acad. Sci. USA, 104, 4315-4320

82) Nersissian A.M., Shipp E.L., 2002, Adv. Protein Chem., 60, 271-340

83) Nakamura K., Go N., 2005, Cell Mol. Life Sci., 62, 2050-2066

84) Lakowicz J.R., 2006, Principles of Fluorescence Spectroscopy, Springer Science, New York, USA

85) Kasha M., 1950, Discuss. Faraday Soc., 9, 14-19

86) Tõugu V., Karafin A., Palumaa P., 2008, J. Neurochem., 104, 1249-1259

87) Chavez-Crooker P., Garrido N., Ahearn G.A., 2001, J. Exp. Biol., 204, 1433-1444

88) Chavez-Crooker P., Garrido N., Ahearn G.A., 2002, J. Exp. Biol., 205, 405-413

89) Qi J., Han M.S., Chang Y.C., Tung C.H., 2011, Bioconjug. Chem., 22, 1758-1762

90) Yin S., Leen V., Van Snick S., Boens N., Dehaen W., 2010, Chem. Commun. (Camb.), 46, 6329-6331

91) Stryer L., 1978, Annu. Rev. Biochem., 47, 819-846

92) Selvin P.R., 2000, Nat. Struct. Biol., 7, 730-734

93) Strianese M., Zauner G., Tepper A.W., Bubacco L., Breukink E., Aartsma T.J., Canters G.W., Tabares L.C., 2009, Anal. Biochem., 385, 242-248

94) Strianese M., De Martino F., Pavone V., Lombardi A., Canters G.W., Pellecchia C., 2010, J. Inorg. Biochem., 104, 619-624

95) Gustiananda M., Andreoni A., Tabares L.C., Tepper A.W., Fortunato L., Aartsma T.J., Canters G.W., 2012, Biosens. Bioelectron., 31, 419-425

96) Strianese M., Zauner G., Tabares L.C., Tepper A.W., De Martino F., Pellecchia C., Aartsma T.J., Canters G.W., 2013, Chemistry, doi: 10.1002/chem.201201876

97) Schmauder R., Librizzi F., Canters G.W., Schmidt T., Aartsma T.J., 2005, ChemPhysChem., 6, 1381-1386

98) Kuznetsova S., Zauner G., Aartsma T.J., Engelkamp H., Hatzakis N., Rowan A.E., Nolte R.J.M., Christianen P.C.M., Canters G.W., 2008, Proc. Natl. Acad. Sci. USA, 105, 3250-3255

99) Goldsmith R.H., Tabares L.C., Kostrz D., Dennison C., Aartsma T.J., Canters G.W., Moerner W.E., 2011, Proc. Natl. Acad. Sci. USA, 108, 17269-17274*)*

100) Vivian J.T., Callis P.R., 2001, Biophys. J., 80, 2093-2109

101) Tepper A.W., Bubacco L., Canters G.W., 2004, J. Biol. Chem., 279, 13425-13434

102) Tepper A.W., Aartsma T.J., Canters G.W., 2011, Faraday Discuss., 148, 161-171

103) Zauner G., Strianese M., Bubacco L., Aartsma T.J., Tepper A.W.J.W., Canters G.W., 2008, Inorg. Chim. Acta., 361, 1116-1121

104) Zauner G., Lonardi E., Bubacco L., Aartsma T.J., Canters G.W., Tepper A.W., 2007, Chemistry, 13, 7085-7090

CHAPTER 2

Studies on the mechanism of nitrite reductase from *Alcaligenes xylosoxidans* at the single molecule level [a]

[a] Sections of the work presented in this chapter have been published as the following articles:

1) Tabares L.C., Kostrz D., Elmalk A., Andreoni A., Dennison C., Aartsma T.J., Canters G.W., 2011, Chem. Eur. J., 17, 12015-12019, *Fluorescence lifetime analysis of nitrite reductase from Alcaligenes xylosoxidans at the single-molecule level reveals the enzyme mechanism* (also published in 2012 in A. Andreoni's PhD thesis "Shedding light on biological redox processes - single molecule studies of Cu-containing oxidoreductases")

2) Goldsmith R.H., Tabares L.C., Kostrz D., Dennison C., Aartsma T.J., Canters G.W., Moerner W.E., 2011, Proc. Natl. Acad. Sci. USA, 108, 17269-17274, *Redox cycling and kinetic analysis of single molecule of solution-phase nitrite reductase*

2.1 Introduction

2.1.1 *Nitrite reductases in dissimilatory denitrification*

Dissimilatory denitrification (Figure 2.1) is a complex, four-step anaerobic process analogous to aerobic respiration. In this process protons are transferred from the cytoplasm to the periplasm of a cell during reduction of nitrate (NO_3^-) to dinitrogen (N_2) to support adenosine triphosphate (ATP) synthesis [1 - 5]. Aerobic respiration is more energetically preferred, thus denitrification occurs only in oxygen-deprived environment and when sufficient quantities of NO_3^- are present. Microorganisms capable of denitrification are distributed mainly among bacteria, but also archaea [2].

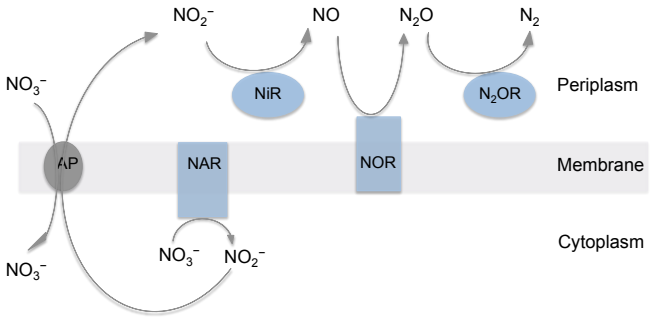

Figure 2.1 Schematic arrangement of dissimilatory denitrification in Gram-negative bacteria adapted from [1]. Nitrate reductase is depicted as NAR; nitrite reductase as NiR; nitric oxide reductase as NOR and nitrous oxide reductase as N_2OR. AP is a postulated nitrate/nitrite antiporter.

The enzymes, nitrate reductase (NAR), nitrite reductase (NiR), nitric oxide reductase (NOR) and nitrous oxide reductase (N_2OR) are required to facilitate the sequential reduction of NO_3^- to N_2. In Gram-negative bacteria, NAR is located at the cytoplasmic membrane, with its active site directed towards the cytoplasmic side. The product of the two-electron reduction of NO_3^-, nitrite (NO_2^-), is transported to the periplasm, where it is further reduced to nitric oxide (NO) by the soluble NiR. NOR is a membrane-bound protein localized in the cytoplasm that releases its product, nitrous oxide (N_2O), back into the periplasmic space, where a soluble enzyme, N_2OR converts it to N_2.

NiR catalyses the one-electron reduction of NO_2^- to NO ($NO_2^- + e^- + 2H^+ \rightleftharpoons NO + H_2O$) [1, 2]. This reaction is bidirectional and at alkaline pH the catalytic rate of the reverse reaction is higher than that of the forward reaction [6]. Two distinct classes

of NiR are distinguished, those utilizing heme iron (cd_1) as the prosthetic group and those containing copper (Cu) ions, the type 1 (T1 Cu) and the type 2 (T2 Cu) [2, 7]. Copper-containing NiRs (CuNiRs) have been isolated from a number of bacterial sources, including *Alcaligenes faecalis S*-6 (referred herein as "green" NiR, gNiR) [8], *Alcaligenes cycloclastes* [9], *Alcaligenes xylosoxidans* (referred herein as "blue" NiR, bNiR) [10], *Pseudomonas aureofaciens* [11], *Rhodobacter sphaeriodes* [12], *Pseudomonas chlororaphis* [13] and *Hyphomicrobium denitrificans* (HdNiR) [14].

Majority of CuNiRs are trimeric, with each monomer consisting of two cupredoxin-like domains (Chapter 1.3) [15]. These enzymes have been shown to exhibit high structural similarity with two-domain laccases (see Chapters 1.3 and 4) [16]. Trimeric CuNiRs contain one T1 Cu and one T2 Cu per monomer, and subtle differences at a T1 Cu(II) centre result in these proteins being either green or blue (Chapter 1.2.1) [17 - 22]. The T1 Cu site plays a crucial role in electron transfer (ET) and serves as an initial port of entry of electrons from putative physiological donors such as azurin (Az), pseudoazurin (Paz) or cytochrome c_{551} [8, 23 - 27]. The electrons are subsequently transferred to the T2 Cu site, in which NO_2^- is bound and reduced [28, 29]. Several models of the complex formed by bNiR and Az have been proposed [27, 30, 31] but only complexes of gNiR with Paz [32, 33] and bNiR with cytochrome c_{551} [34] have been determined.

2.1.2 *The CuNiR from Alcaligenes xylosoxidans*

bNiR from *A. xylosoxidans* that is analyzed in this study is a homotrimeric, blue CuNiR. Several crystal structures reveal that the T1 Cu site is buried ~ 7 Å beneath the protein surface in the first domain of each monomer, with the T2 Cu site located at the interface between two monomers [35, 36]. The T1 Cu of bNiR (Figure 2.2.A) is coordinated by His89, His139, Cys130 and Met144 in a distorted tetrahedral geometry. The axial ligand to the T1 Cu, Met144, shows a degree of flexibility, reflected by two distinct conformations [36]. In the resting state, the T2 Cu is coordinated by His94, His129, His300 and a H_2O or OH^- ligand in a tetrahedral geometry (Figure 2.2.A). All three His ligands remain in the same orientation on removal of the T2 Cu ion [37]. Within the same monomer, the two Cu centers are connected by the 12.6 Å covalent bridge, which consists of the T1 Cu-coordinating Cys130 and the T2 Cu-coordinating His129. It has been suggested that this covalent bridge provides the ET pathway from the T1 Cu to the substrate-binding T2 Cu center [38].

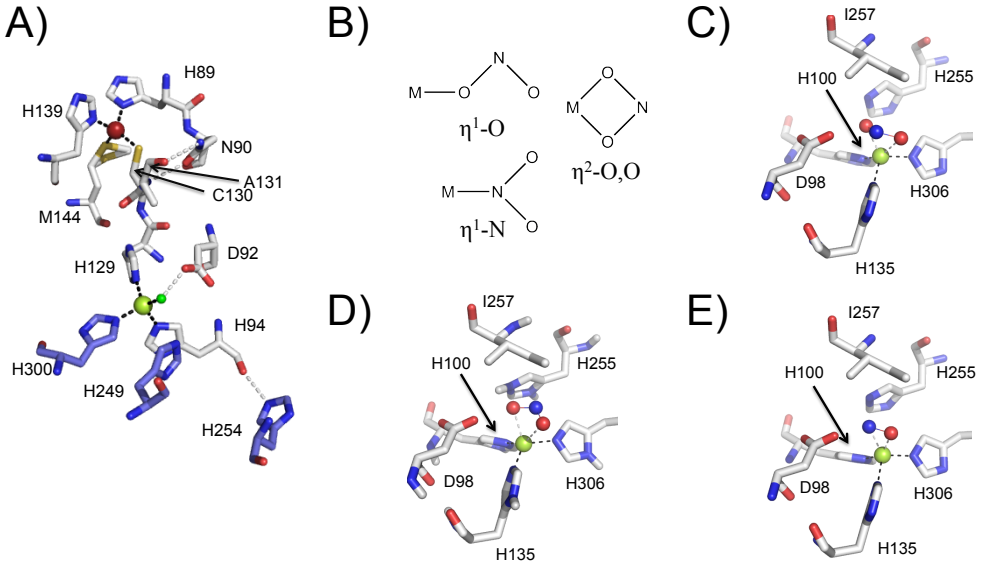

Figure 2.2 (A) Structure of the active site of bNiR (pdb file: 1OE1 [36]) including the residues involved in the electron and putative proton transfer pathways. His249, His254 and His300, which are depicted in blue, are from the adjacent monomer. (B) Different modes (η^2-O,O, η^1-O and η^1-N) of binding NO_2^- to Cu ion [42], where **M**, **O** and **N** are Cu, oxygen and nitrogen atoms, respectively. Crystal structures of gNiR showing (C) the T2 Cu(II)−NO_2^- complex (pdb file: 1SJM [39]), (D) the T2 Cu(I)−NO_2^- complex (pdb file: 1AS8 [40]) and (E) the T2 Cu(I)−NO complex (pdb file: 1SNR [39]). The T1 and T2 Cus are large red and yellow spheres, respectively. Water molecule is small green, while oxygen and nitrogen from NO_2^- (or NO) are small red and blue spheres, respectively. The images were generated using PyMol [41].

Within the active site pocket, a number of residues are considered relevant for catalysis of bNiR, in particular Asp92, His249 and Ile251 [40, 43]. Asp92 and His249 are conserved among CuNiRs and are responsible for holding an H_2O/OH^- ligand in place, positioning NO_2^- and reaction intermediates, and proton donation during catalytic turnover [36, 44]. Ile251 is proposed to help position NO_2^- within the active site [40, 43]. Recently, it has been demonstrated that ET from the T1 Cu to T2 Cu is tightly coupled to protons transfer [45 - 48]. Two distinct proton channels, which are conserved among CuNiRs have been identified [36, 49 - 51]. One of these connects Asp92 at the T2 Cu site to the protein surface *via* His254, which is proposed to regulate the proton flow [50], whilst the second connects Asp92 to the surface *via* Ala131, Asn90 and Asn107 and several molecule waters [49]. Although those channels were identified at low (4.6) and high (8.5) pH, respectively, a crystal structure determined at pH 6.5 shows the presence of both networks [36].

2.1.3 *Binding modes of NO_2^- and NO*

The geometry of substrate binding to the T2 Cu of CuNiRs was characterized in detail by structural studies. A number of gNiR crystal structures in the presence of NO_2^- show large variations in the T2 Cu(II)−NO_2^- complex [35, 37, 39, 43, 52]. Typically, NO_2^- is bound asymmetrically through both oxygen atoms (bidentate coordination, η^2-O,O, Figure 2.2.B) with T2 Cu(II)−O_1 longer (2.19 to 2.4 Å) than T2 Cu(II)−O_2 (1.98 to 2.2 Å), where O_1 of NO_2^- corresponds to the oxygen atom closest to Asp98 (gNiR numbering, Figure 2.2.C) [5, 39, 40, 52]. A wide range of dihedral angles between the planes created by the O−N−O and O−Cu−O atoms has also been observed [5, 39, 40, 52]. A hydrogen bond is found between the O_1 of NO_2^- and the Asp98 side chain, which is suggested to be involved in NO_2^- turnover. His255 and Ile257 (gNiR numbering) do not seem to change their conformation upon substrate binding [40, 43]. In the T2 Cu(I)−NO_2^- complex (Figure 2.2.D), NO_2^- binds more weakly to the T2 Cu (crystals with lower occupancy of NO_2^- bound to the T2 Cu) but also in asymmetrical way, with T2 Cu(I)−O_1 and T2 Cu(I)−O_2 distances in a range from 2.4 to 2.7 Å and 2.2 to 2.3 Å, respectively [5, 40]. The space restrictions imposed by the side chain of Ile257 together with hydrogen bonding between NO_2^- and Asp98 limits the possibility of NO_2^- binding in the T2 Cu(I)−NO_2^- complex through nitrogen atom (monodentate coordination η^1-N, Figure 2.2.B). The solvent around Asp98 at the T2 Cu(I)−NO_2^- appears to be less ordered than is found at the T2 Cu(II)−NO_2^- [40, 50]. Structures of gNiR containing the T2 Cu(II)−NO_2^- show additional (five) solvent molecules in the active site compared to gNiR containing T2 Cu(I)−NO_2^- (two molecules) [40, 50]. Figure 2.2.E shows NO (the product of NO_2^- reduction) bound to the T2 Cu(I) site of gNiR with a side-on geometry (Cu−N−O angle of 71°) and almost equal Cu−N_{NO} and Cu−O_{NO} distanced [39, 52]. Interactions with the bulky Ile257 and hydrogen bonding between NO and the Asp98 side chain result in side-on binding of NO within the active site [53].

Several model compounds of intermediates in the catalytic cycle of CuNiRs have been synthesized and extensively studied [3, 5]. Different modes of binding of NO_2^- have been identified for Cu(II)−NO_2^- including bidentate η^2-O,O, and monodentate η^1-O and η^1-N [42, 54 - 58] (Figure 2.2.B). Most of the Cu(I)−NO_2^- model complexes shows η^1-N bound nitrite, in disagreement to what is observed in CuNiR crystal structures [59 - 61]. In addition, a number of model complexes with unknown structures but capable of nitrite reduction have been published [55, 62 - 64]. Despite multiple possibilities in the way of binding (end-on linear, end-on bent and side-on) the

only structurally characterized Cu(II)−NO model complex [65] contains N-bound, end-on bent NO with a Cu−N−O angle of 121° and Cu−N_{NO} length comparable to that observed in the Cu(I)−NO CuNiR crystal structure [39]. All structurally characterized Cu(I)−NO model complexes show end-on NO with Cu−N−O angles ranging from 168 to 176° [66 - 68].

2.1.4 *Proposed mechanisms for NO_2^- reduction by CuNiRs*

Despite intense studies, the exact order of events of NO_2^- reduction by CuNiR is still under debate [3, 5, 51, 69 - 71]. The dispute over the mechanism revolves around whether NO_2^- binds to the T2 Cu site only after it has received an electron from the T1 Cu site (the "reduction first" mechanism) [1, 28, 29, 31, 34, 35], or whether an electron is transferred only after binding of the substrate ("substrate-binding first" mechanism) [37, 40, 69, 71 - 76]. However, most evidence now favor the theory proposed by Wijma *et al.* [70, 77], that the enzyme operates according to a "random sequential" mechanism in which either pathway is possible and the predominant route depends on parameters such as pH and NO_2^- concentration.

The "reduction first" reaction mechanism (Figure 2.3.A) was proposed by Hulse and Averill and resembles the mechanism of cd_1 NiRs, in which the T2 Cu(II) is reduced to Cu(I) before NO_2^- binding occurs [1, 78, 79]. NO_2^- displaces a water molecule at the T2 Cu site and a cuprous nitrosyl (Cu(I)−NO^+) and its resonance form (Cu(II)−$NO^\bullet$) are generated *via* N-bound Cu(I)−NO_2^- complex. The cycle is completed with the release of NO from unstable Cu(II)−$NO^\bullet$ complex. The observed 10-fold tighter binding of NO_2^- to the reduced rather than the oxidized protein (determined at pH 7.5) further supported enzyme reduction preceding the binding of NO_2^- [80].

The "substrate-binding first" ordered reaction mechanism (Figure 2.3.B) was primarily proposed by Adman and coworkers [37, 40] and favored by groups of Suzuki [24, 74], Hasnain [52, 69] and Murphy [76]. The concept of an ordered mechanism has been extensively investigated by computational [71, 81], kinetic, spectroscopic, site-directed mutagenesis and structural studies [36, 44, 69, 72 - 74]. It describes the ET from the T1 Cu(I) site to the T2 Cu(II) site, which is triggered by substrate binding to the T2 Cu site. NO_2^- binds to the T2 Cu(II) *via* its oxygen atoms and forms a η^2−O,O T2 Cu(II)−NO_2^- intermediate. Once NO_2^- is bound, the T2 Cu is reduced to form the T2 Cu(I)−NO_2^- complex, leading to a quick release of NO and formation of the T2 Cu(II)−H_2O complex. Differently to the "reduction first" mechanism, the η^1−N

T2 Cu(I)−NO_2^- intermediate is not formed. It is assumed that the information about NO_2^- binding at the T2 Cu is sent to the T1 Cu site through the so-called substrate "sensor loop" (consisting of His89, Asp92 and His94, bNiR numbering), thereby triggering ET [36, 44, 50, 69, 73]. Further support for this mechanism is provided by combined crystallographic and single-crystal spectroscopic studies, which showed that ET could only be detected when NO_2^- was bound to the T2 Cu site [72]. In contrary, pulse radiolysis results at pH 7.0 show that ET occurs without NO_2^-, with the rate sharply decreasing upon substrate binding [82 - 85]. In the presence of NO_2^-, the pH dependence of this ET rates matches that of enzyme activity however, in the absence of substrate, the rate is not influenced by pH [79].

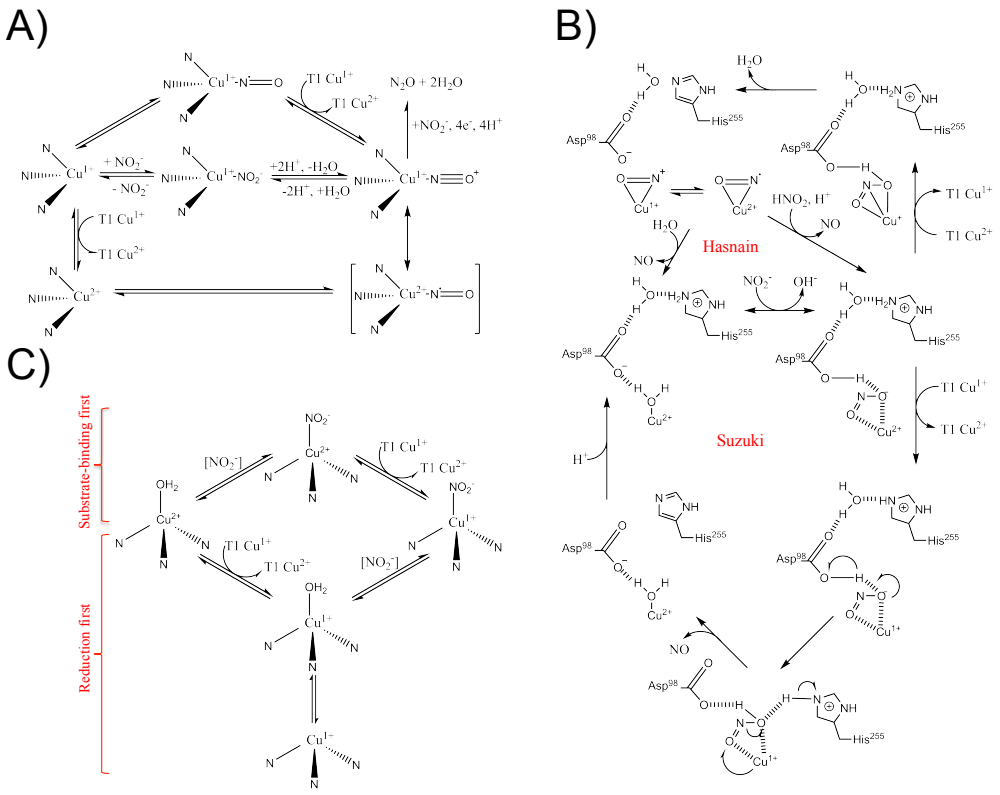

Figure 2.3 Schemes of catalytic mechanism of CuNiRs proposed by the groups of (A) Averill ("reduction first" mechanism) [1], (B) Suzuki and Hasnain ("substrate-binding first" mechanism) [52, 74] and (C) Canters ("random sequential" mechanism) [70]. Figures taken from [5] and [70].

Activity assays and electrochemical measurements on gNiR suggest that the enzyme can operate using both pathways in a "random sequential" mechanism (Figure 2.3.C). The velocity of the ET between the T1 Cu and T2 Cu depends on the ligand coordinated at the T2 Cu site and decreases in the order: H_2O > NO_2^- > OH^-

[70]. In addition, it has been shown that the binding of substrate does not effect the midpoint potential of the T1 Cu site, thus excluding the cooperativity between the two sites during the catalytic cycle that is postulated in the "ordered" mechanism [77]. Random sequential mechanism received further support from electrochemical [86] and single molecule studies on gNiR [87], and from Scrutton and coworkers [45, 47], who postulated the possible existence of two substrate-binding sites or two different substrate-binding affinities for bNiR.

2.1.5 *Single molecule studies*

Biochemical research uses a range of tools, including X-ray crystallography, UV-Vis, circular dichroism, electron paramagnetic resonance (EPR), resonance Raman (RR), NMR, X-ray absorption, fluorescence spectroscopy and many more to investigate structure and function of proteins. These techniques are used for so-called "in bulk" investigations, in which the properties of ensemble of molecules is sampled at the same time and averaged. Recent advances in single molecule spectroscopy allow for manipulation of individual molecules and study their behavior in the course of a chemical reaction. The ability to resolve microscopic catalytic states during turnover and observe their subsequent conversion provides unique information that is normally hidden in ensemble experiments due to averaging. The groups of Xie, Rigler, De Schryver, and others have shown that the intensity time traces of single molecules contain detailed information about enzyme dynamics by providing novel evidence for static and dynamic heterogeneity, and have enabled the observation of transient intermediates and the determination of microscopic rate constants for catalytic cycles [88 - 92].

Single molecule fluorescence data can be collected using an inverted confocal microscope (Figure 2.4.A). Typically, the sample is mounted on a precisely moving piezoelectrical scanning (translation) stage that allows for sub-micrometer movements. Using this scanning stage, the sample is moved across the confocal volume. Pulsed laser light at particular wavelength is reflected on a dichroic mirror and is focused by an objective on a glass slide coated with sample. Fluorescence is collected by the same objective, transmitted by the dichroic mirror and imaged onto a pinhole oriented in front of the detector, e.g. a single-photon avalanche photodiode. To generate fluorescence lifetime imaging microscopy (FLIM) images, the signal from the detector is fed into a Time-Correlated Single Photon Counting (TCSPC) unit, which allows for the repetitive

precisely timed registration of single photons using the excitation pulse as the timing reference [93, 94].

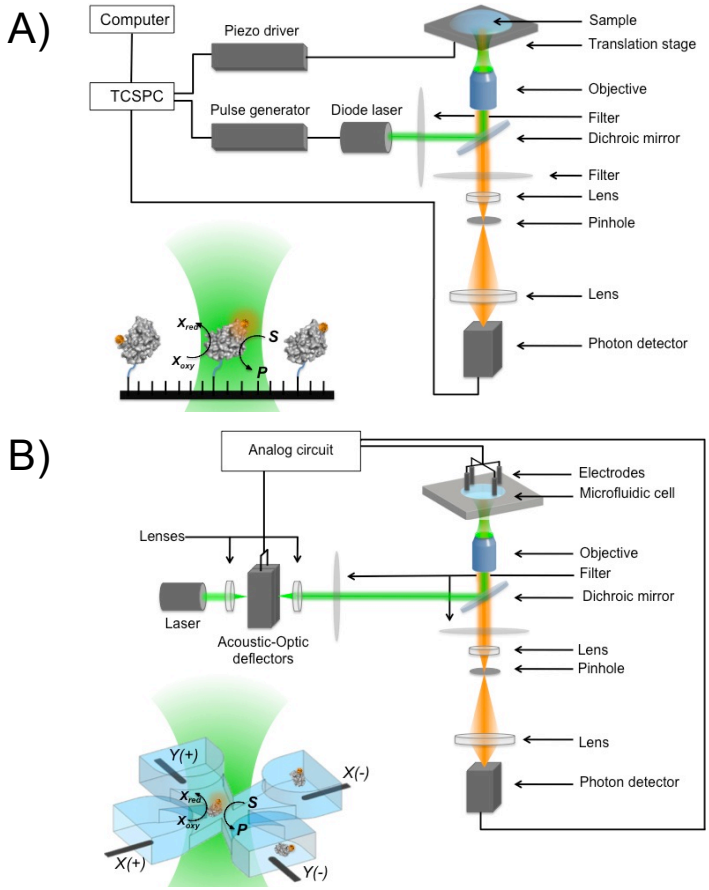

Figure 2.4 Experimental setups for single molecule measurements using (A) a confocal scanning microscope and (B) an anti-Brownian electrokinetic (ABEL) trap [95]. The insets: schematic overview on (A) an immobilized fluorescently labeled protein and (B) microfluidic cell of an ABEL trap with fluorescently labeled protein in the confocal beam under turnover conditions. The green and orange paths are an excitation and emission beams, respectively. The electron donor in its oxidized and reduced states is depicted as $\boldsymbol{X_{oxy}}$ and $\boldsymbol{X_{red}}$, respectively. The reaction substrate and product are depicted as ***S*** and ***P***, respectively.

Activity measurements of single enzymes require the observation of multiple turnovers for several seconds or more. The observation window is several orders of magnitude longer than the typical diffusion time of solution-phase molecules through confocal volume, and therefore molecules are typically immobilized on a solid support (Figure 2.4.A) [88 - 90, 96]. A fundamental problem with this approach is to avoid perturbations to the system resulting from protein immobilization. In most cases,

measured properties of the freely diffusing and immobilized biomolecules tend to show good agreement [88, 90, 97]. However, immobilization is suspected of contributing to observed enzyme behavioral heterogeneity [91, 98 - 100]. Recently, an alternative way for prolonged solution-phase measurements without protein immobilization but *via* a specialized microfluidic trapping device has been developed [95, 101]. The anti-Brownian electrokinetic (ABEL) trap (Figure 2.4.B) estimates the position of fluorescent molecule in real time using a laser spot revolving in a circular pattern (at 40 kHz). This laser spot is phase-locked in an analogue circuit to a feedback force that is gated by photon detection and applied *via* two orthogonal pairs of electrodes to cancel Brownian displacements of the molecule. The molecule is therefore held near the center of the trap that enables prolonged solution-phase measurements. This ABEL trap has been successfully applied in a number of studies, including conformational dynamics of single photosynthetic antenna proteins and ATP binding stoichiometry of the multi-subunit chaperonin [102].

One of the common methods of determining the oxidation state of cofactor of metalloproteins is *via* its optical absorption spectrum. Recently, a new method for sensing the changes in protein absorption spectra, and therefore in the oxidation state of cofactor, based on fluorescence by means of Förster Resonance Energy Transfer (FRET) have been developed (FluoRox principle, for details see Chapter 1.4.3) [103, 104]. This approach relies on FRET from a surface-conjugated fluorescent dye (FRET donor) to the cofactor of the protein or enzyme (FRET acceptor). In the present work, the T1 Cu(II) site of bNiR possesses a strong absorption band at approximately 600 nm (see Chapter 1.2.1), which disappears upon reduction [22]. The emission spectrum of a surface-conjugated fluorescent dye overlaps with the absorption spectrum of the T1 Cu(II) site what results in partial quenching of the label's fluorescence when the protein is in its oxidized state. Therefore, fluctuations in the oxidation state of the T1 Cu site during turnover are reflected in changes in fluorescence intensity. It has been shown that the occurrence of FRET between the donor and acceptor also influences the fluorescence lifetime of the donor. Therefore, both intensity and fluorescence lifetime time traces may be used to reveal related information about enzyme kinetics [105 - 107]. Although lifetime measurements are not sensitive to instrument-derived or photo-physically induced variations in intensity, the intensity-based technique has the advantage that fewer photons are needed to obtain useful data [108]. FluoRox approach has been successfully applied in biosensor development [109 - 112] and studies of the electrochemical behavior of metalloproteins [86, 113 - 115]. Additionally, this approach

was used for single molecule studies on gNiR [87], in which the fluorescence intensity distributions in time traces of immobilized single molecules during NO_2^- turnover were analyzed by means of autocorrelation analysis. The approach was based on the pioneer single molecule fluorescence spectroscopy studies on cholesterol oxidase [85], but did not require an intrinsically fluorescent enzyme.

2.2 Scope of the chapter

The aim of the research described in this chapter is to study the catalytic mechanism of bNiR at the single molecule level, using a FRET-based approach. This research deals with the development of a new method for data collection and analysis of individual fluorescently labeled bNiR molecules using scanning confocal fluorescence microscopy combined with FLIM of the sample. M87C bNiR and K329C bNiR, with surface-exposed Cys residues introduced have been prepared to allow labeling with fluorescent dyes and protein immobilization. The Cys variants are characterized and labeled with fluorescent ATTO 532 and ATTO 647N maleimide labels. To determine the optimal approach for immobilization of labeled enzymes on a glass surface, several methods are described. FLIM images are collected from an area of the sample containing immobilized enzyme molecules, which is scanned in steps and the fluorescence is collected for few milliseconds between the steps. The analysis of FLIM images provides the information about the oxidation state of the molecules at each sampling point, which is then transformed into information on behavior of a single molecule and gives a new insight into the catalytic mechanism of immobilized enzyme. The results are compared to those from single molecule solution-phase measurements using the ABEL trap.

2.3 Materials and methods

2.3.1 *Site-directed mutagenesis*

The M87C and K329C variants of bNiR from *A. xylosoxidans* were created using QuickChange mutagenesis (Stratagene) as described in Chapter 5.7.2. The plasmid pET22b-bNiR [22] was used as a template along with the following pairs of primers: 5'–CAACCCGGCCACCAACGCCTGCCCGCACAACGTCGACTTCC–3' (forward) and 5'−GGAAGTCGACGTTGTGCGGGCAGGCGTTGGTGGCCGGGTTG−3'

(reverse), 5'–CTGATGAAGCAGATCTGCGCGCCCGCGCCGATTCC–3' (forward) and 5'–GGAATCGGCGCGGGCGCGCAGATCTGCTTCATCAG−3' (reverse) for M87C bNiR and K329C bNiR, respectively. The sequences of both strands of the mutated plasmids (pET22b-bNiRM87C and pET22b-bNiRK329C) were verified.

2.3.2 *Over-expression, isolation and purification of wild type, M87C and K329C bNiR*

Wild type (WT), M87C and K329C variants were over-expressed in *Escherichia coli* BL21 (DE3), isolated and purified as described in Chapter 5.10.3 [22]. Purity was confirmed by sodium dodecyl sulfate polyacrylamide gel electrophoresis (SDS-PAGE, 12.5 % gel) and the protein concentrations were determined using an extinction coefficient (ε) of 5200 $M^{-1}cm^{-1}$ at 594 nm [22]. Purified Az from *Pseudomonas aeruginosa* was kindly provided by Prof. C. Dennison.

2.3.3 *Determination of proteins' apparent molecular weight by gel-filtration*

The apparent molecular weight (MW^{app}) of proteins was determined, as described in Chapter 5.13.4, using a HiLoad Superdex 200 16/60 (GE Healthcare) gel-filtration column in 20 mM tris(hydroxymethyl)aminomethane (Tris) pH 7.5 containing 200 mM NaCl [22].

2.3.4 *Determination of proteins' molecular weight by mass spectrometry*

The molecular weight (MW) of proteins was determined as described in Chapter 5.12.1 by matrix-assisted laser desorption ionization time-of-flight mass spectrometry, MALDI-TOF-MS [22]. MALDI-TOF-MS was also performed on a K329C bNiR sample that had been incubated with 300 equivalents of tris(2-carboxyethyl)phosphine hydrochloride (TCEP) for 1 h at room temperature (RT) prior to measurements.

2.3.5 *Activity assay for nitrite reduction by WT, M87C and K329C bNiR*

The catalytic activity of WT bNiR and the variants was determined as previously described [70]. Measurements were performed in 50 mM phosphate pH 7.0 at 21 °C following the rate of oxidation of dithionite-reduced 1,1'-dibenzyl-4,4'-bipyridinium dichloride (benzyl viologen, BV). The reaction mixture was prepared in an anaerobic

chamber (Belle Technology, $[O_2]$ << 2 ppm) in a 3 mL sealed cuvette, and routinely contained 200 μM BV, 100 μM dithionite and $NaNO_2$ (7 - 400 μM). The reaction was started by the addition of enzyme (1.0 - 3.7 nM final concentration), and the oxidation of BV was measured from the absorbance decrease at 603 nm (ε_{603} = 14500 $M^{-1}cm^{-1}$), with the data corrected for any baseline drift. The kinetic parameters, K_M and k_{cat} were obtained from fitting of the initial velocities for each substrate concentration to the nonlinear Michaelis-Menten equation (Equation 2.1).

$$v_0 = \frac{d[P]}{dt} = \frac{v_{max}[S]}{K_M + [S]} = k_{cat}[E]\frac{[S]}{K_M + [S]} \qquad \text{(Equation 2.1),}$$

where v_0 is the initial velocity of the reaction, v_{max} is the maximal velocity of the reaction, [P] is the product concentration, [S] the substrate concentration, and [E] is enzyme concentration.

2.3.6 *UV-Vis spectroscopy*

UV-Vis spectra were acquired with a Perkin Elmer λ 35 spectrophotometer at RT as described in Chapter 5.12.2.

2.3.7 *Continuous wave electron paramagnetic resonance spectroscopy*

Continuous wave (cw), X-band (9.48 GHz) EPR spectra of oxidized WT, M87C and K329C bNiR were acquired at ~ 80 K with a Bruker EMX EPR spectrometer equipped with an ESR900 cryostat (Oxford Instruments) as described in Chapter 5.12.5.

2.3.8 *Fluorescence spectroscopy*

Fluorescence spectra and time course measurements were performed on a Cary Eclipse Fluorescence Spectrophotometer (Varian Inc., Agilent Technologies), as described in Chapter 5.12.6. ATTO 647N and ATTO 532 labeled proteins were excited at 630 and 520 nm, respectively, and the emission was measured at 657 and 550 nm, respectively. The protein samples were prepared in 50 mM phosphate pH 7.5 at 20 °C.

2.3.9 *Protein labeling with fluorescent dyes*

The proteins were labeled using modified versions of published protocols [105, 106] as described in Chapter 5.11. Structure of ATTO 532 label (ATTO-TEC GmbH) is shown in Appendix A, whereas structure of ATTO 647N (ATTO-TEC GmbH) is not available. WT protein was labeled at the surface-exposed amine groups (including N-terminus), whilst K329C bNiR was labeled at the free thiol group of the introduced Cys residue. M87C bNiR was labeled either at the free thiol group (for 'in bulk' measurements) or at the amine groups (for protein immobilization studies). Prior to labeling with ATTO 532 or ATTO 647N N-hydroxysuccinimide (NHS) ester, WT and M87C bNiR were exchanged into 100 mM 4-(2-hydroxyethyl) piperazine-1-ethanesulfonic acid (Hepes) pH 8.3, and then incubated with 0.25 equivalents of appropriate dye for 30 min at 4 °C. Prior to labeling with ATTO 647N maleimide, M87C bNiR was exchanged into 100 mM phosphate pH 7.5, and then incubated with 0.5 equivalents of a dye for 1 h at 4 °C in 100 mM phosphate pH 7.5. Prior to labeling, K329C bNiR was incubated for 2 h at 4 °C with 25-equivalents of TCEP and desalted on a Superdex 200 10/300 GL column (GE Healthcare) equilibrated in 20 mM Tris pH 7.5 containing 200 mM NaCl. Following this procedure, which removed some of the glutathione bound to Cys329, the protein was exchanged into 100 mM phosphate pH 7.5 and incubated with an excess (in this case the exact amount of dye used was less important as the labeling ratio was dependent upon the amount of glutathione that had been removed from Cys329) of ATTO 647N maleimide for 1 h at 4 °C.

The excess of unlabeled dye was removed by desalting on a PD10 column (GE Healthcare) and the labeling ratios (DOL) were determined according to the manufacturer's protocol as described in Chapter 5.11. To observe the activity of only one monomer in the trimer a low DOL was maintained of ~ 11 % for the WT and M87C bNiR and ~ 13 % for the K329C variant.

2.3.10 *'In bulk' fluorescence spectroscopy measurements and determination of the fluorescence switching ratios*

Labeled proteins were routinely reduced with sodium ascorbate containing phenazine ethosulfate (PES) (stock solution of 1 M ascorbate plus 50 μM PES) and oxidized with potassium ferricyanide (0.5 M stock solution). Enzyme turnover was studied by addition of 250, 500, 1000 and 5000 μM $NaNO_2$.

Alternatively, the proteins were reduced with dithionite-reduced Az. Prior to reaction, Az was incubated in an anaerobic chamber with 5-equivalents of sodium dithionite for 30 min at RT, after which the reductant was removed by ultrafiltration (Vivaspin, 3 kDa cut off). The reaction mixture was prepared anaerobically and consisted of 145 nM of WT bNiR and the variants (28 - 36 nM of ATTO 647N labeled enzyme) in 50 mM phosphate pH 7.5. The reaction was initiated by the addition of 15 μM of anaerobic dithionite-reduced Az. Enzyme turnover was studied by addition of 66, 265, 530 and 5300 μM of anaerobic $NaNO_2$. The switching ratio (*SR*) is defined as described in Chapter 5.12.6.

2.3.11 *Protein immobilization via 1-11-bis-maleimidotetraethyleneglycol linker on a silanised glass slide*

ATTO 532 labeled WT and M87C bNiR were immobilized on a surface modified glass slide (MENZEL GLÄSER Nr. 1, Gerhard Menzel GmbH) using previously described, modified, methods [87]. Prior to protein immobilization, the glass slides were sonicated sequentially for 30 min in acetone and 10 % NaOH (twice), and stored in methanol. Between the sonication steps the glass slides were rinsed and sonicated for 5 min in deionised water. The glass slides were nitrogen-dried and ozone-cleaned (UVP PR-100 UV-ozone photoreactor) for 1 hour on each side immediately prior to silanisation. To generate a hydrophobic layer the glass slides were sonicated for 30 min in a mixture of 10 % triethoxysilane (TES) and 0.1 % 3-mercaptopropyl-trimethoxysilane (MPTS) in toluene, rinsed with toluene and dried with nitrogen. To generate a hydrophilic surface, the glass slides were treated with a mixture of 10 % 3-aminopropyl-trimethoxysilane (APTS) and 0.1 % MPTS in toluene.

N-terminally ATTO 532 labeled M87C bNiR was conjugated *via* the thiol group of Cys87 with the linker 1-11-bis-maleimidotetraethyleneglycol ($BM(PEO)_3$). Prior to deposition on a modified glass slide, typically, 50 - 100 pM of the labeled protein was incubated with 50-equivalents of the linker in 0.1 M phosphate pH 7.5 for approximately 1.5 h on ice. The unbound linker was removed using a Centrispin-10 size-exclusion chromatography spin column (Princeton Separations, Adelphia). Since an excess of linker was used the protein can have two or three linkers attached, and as these are bi-functional either dimerization or aggregation can occur. However, the protein conjugates were not further purified to separate the various species. The

modified protein was deposited on a modified glass slide and incubated overnight at 4 °C. Any unbound protein was removed with 0.1 M phosphate pH 7.5.

2.3.12 *Protein immobilization via biotin/streptavidin interactions on a silanised glass slide*

ATTO 647N labeled K329C bNiR was immobilized on a surface modified glass slide using a previously described, modified, method [116]. Prior to protein immobilization, the glass slides were cleaned and modified as described in Section 2.3.11. To generate a hydrophilic surface, the glass slides were sonicated with a 10 % APTS in toluene, rinsed with toluene and dried with nitrogen. Surface-modified glass slides were incubated overnight at 4 °C with NHS ester-modified polyethylene glycol (PEG) polymers (10 % methyl-PEG-NHS (MW 2000) and 0.1 % biotin-PEG-NHS (MW 3400), Laysan Bio) in 0.1 M sodium bicarbonate pH 8.3. The incubation mixture was washed away with deionised water and the glass slides were incubated for 10 min with 0.2 mg/mL streptavidin (Pierce) in 0.1 M phosphate pH 7.5. Any unbound streptavidin was washed away with 0.1 M phosphate pH 7.5.

Cys329 ATTO 647N labeled K329C bNiR was conjugated *via* exposed amine groups with an NHS-PEG-biotin linker (conjugation *via* maleimide-PEG-biotin (MW 3400) linker was not successful). Prior to deposition on a modified glass slide, the NHS-PEG-biotin linker was added in excess (50-equivalents) to the labeled protein (300 pM in 0.1 M phosphate pH 7.5), followed by incubation for approximately 1.5 h on ice before the unbound linker was removed using a Centrispin-10 size-exclusion chromatography spin column. Since a biotin group (for reaction with streptavidin) is present at one of the ends of the linker, the possibility of proteins aggregating *via* the linker is eliminated. Protein conjugates were not further purified to separate the various species that could form. The modified protein was deposited on a modified glass slide and incubated for 10 min at RT. Any unbound protein was removed with 0.1 M phosphate pH 7.5.

2.3.13 *Protein immobilization in a layer of agarose gel*

ATTO 647N labeled K329C bNiR was immobilized on a glass slide in high purity agarose IV (Sigma) with a gelling point of 36 ± 1.5 °C using a previously described procedure [117] with some modifications. Prior to agarose deposition, the glass slides

were incubated overnight in 10 % TritonX-100 and sonicated sequentially for 30 min in 10 % TritonX-100, acetone, 3 M KOH and methanol. Between these sonication steps the glass slides were rinsed and sonicated for 5 min in deionised water. Subsequently, the glass slides were incubated for 15 min in a 3:1 mixture of hydrochloric acid and nitric acid, sonicated for an additional 30 min, extensively rinsed with deionised water and spin-dried at 6000 rpm for 25 s. The agarose (1 %) was melted in 0.1 M phosphate pH 7.5 and cooled to ~ 50 °C. ATTO 647N labeled K329C bNiR was added to give a final concentration of labeled protein of 300 pM. Bovine liver catalase (final concentration of 100 μg/mL) was added to the agarose to remove hydrogen peroxide that is produced by the slow reaction of reduced NiR with O_2 and leads to the inactivation of enzyme [118]. ATTO 647N labeled K329C bNiR-containing agarose was spin-coated onto a cleaned glass slide at 2000 rpm for 10 s yielding a thin layer of gel. The coated glass slide was immediately put into a holder and covered with 1 mL of buffer containing 100 μg/mL bovine liver catalase in 0.1 M phosphate pH 7.5 or 0.1 M ammonium acetate pH 5.0 or 0.1 M sodium borate pH 9.0, as indicated in experiment.

2.3.14 *Single molecule setup for FLIM measurements*

Single molecule fluorescence measurements were performed with a home-built scanning confocal microscope with TCSPC capabilities that was built by Dr. Abdulmohsen Elmalk and optimized by Dr. Leandro C. Tabares. Excitation was achieved with a pulsed picosecond diode laser (PDL 800-B, PicoQuant GmbH) emitting at 639 nm with a 40 MHz repetition rate. The excitation beam was coupled into a single-mode fibre, passed through a narrow band clean-up filter (LD01-640/8-25, Semrock) and reflected by a dichroic mirror (Z 532/633 M) to a high numerical aperture (NA) oil objective (100×oil, NA 1.4, Zeiss) and onto the sample surface. The power density at the sample was 0.5-1 kW/cm^2. The emitted fluorescence was filtered with an emission filter (D 675/50 M) and imaged onto the active area of a single photon counting avalanche photodiode (Perkin-Elmer SPCM-AQR-14) using a +4.5 mm achromatic lens. Data acquisition was performed using a TimeHarp 200 TCSPC PC-board (PicoQuant, GmbH) working in the Time-Tagged Time-Resolved Mode (Benda, 2005 311). Samples were mounted onto a Physik Instrumente P-517 nanopositioner. The control of the equipment and data acquisition was performed using a SymPho Time software (PicoQuant, GmbH).

2.3.15 *Sample preparation for FLIM measurements and data collection*

Agarose-immobilized ATTO 647N labeled K329C bNiR was reduced using 10 mM sodium ascorbate and 100 nM PES and oxidized using either 1.5 mM potassium ferricyanide or 5 mM $NaNO_2$. Enzyme turnover was studied in the presence of 10 mM sodium ascorbate, 100 nM PES and $NaNO_2$ (5 μM - 5 mM). Although the diffusion of chemicals through the thin agarose layer is very fast, a minimum of 10 minutes was allowed for equilibration. A fresh sample was used for each condition and measured for no more than one hour before discarding.

FLIM images were taken by scanning a 15×15 μm area of the immobilized sample, with a step size of 75 nm and a dwell time of 4 ms per point. The samples were scanned row by row from the top to the bottom and from left to the right. To determine the fluorescence lifetimes of the reduced and oxidized states, a decay histogram of the photons collected over the whole image was constructed. Deconvolution with the instrumental response function (IRF) and a fit to a single and double exponential decay was carried out using the SymPhoTime software (PicoQuant GmbH).

2.3.16 *FLIM data analysis*

To generate the FLIM images the fluorescence decay observed for each pixel was fit to a double exponential decay with fluorescence decay times (τ), τ_1 and τ_2, fixed (τ_1 = 1.1 ns and τ_2 = 3.7 ns), and using the maximum likelihood algorithm as implemented by a SymPhoTime software. Each pixel was false coloured either blue or red depending on whether the resulting average lifetime was smaller or larger than 2.5 ns, respectively. Pixels with signal strength of less than 10 photons were discarded to reduce the noise. A minimum of six FLIM images (15×15 μm) from at least two independent measurements and containing an average of 50 spots per image were analyzed for each condition.

To obtain the time-averaged degree of oxidation, P_{ox}, for a spot, a circular area around the center of the spot with a 15 pixel diameter (1.125 μm) was selected. P_{ox} and P_{red} values were calculated using Equations 2.2 and 2.3, respectively.

$$P_{OX} = \frac{\sum_{i=1}^{n} p_{i,blue}}{\sum_{i=1}^{n} p_{i,blue} + \sum_{j=1}^{m} p_{j,red}} \quad \text{(Equation 2.2)}$$

$$P_{RED} = 1 - P_{OX} = \frac{\sum_{j=1}^{m} p_{j,red}}{\sum_{i=1}^{n} p_{i,blue} + \sum_{j=1}^{m} p_{j,red}} \quad \text{(Equation 2.3)}$$

where, $p_{i,red}$ and $p_{j,blue}$ are the *i*-th and *j*-th red and blue pixel, respectively. *n* and *m* are the total number of blue and red pixels in a single spot, respectively.

The total numbers of spots used for the histograms were: 357, 274, 298, 340 and 388 for turnover conditions at 5, 50, 500, 1000 and 5000 μM NO_2^- concentration, and 308, 289 and 269 in buffer (in the absence of reductant, oxidant and substrate), reduced and oxidized conditions, respectively. P_{ox} histograms were fit to a double Gaussian distribution except for the completely reduced and oxidized samples that were fit to a single Gaussian. Waiting time histograms were constructed as follows. The rows of pixels of a 15 pixel diameter spot represent a window with a 4 ms time resolution varying in length from 20 to 60 ms (12 - 52 ms for 12 pixel diameter spot). The times that the enzyme molecule stayed in the reduced (τ_{on}) and the oxidized (τ_{off}) states were collected into two histograms and fit to single exponentials allowed exponential time constants, τ_{red} and τ_{ox} to be extracted.

2.4 Results

2.4.1 *Protein purification and characterization*

WT bNiR and the variants were pure, giving apparent single bands on SDS-PAGE gels at ~ 35 kDa. The elution volumes of the M87C and K329C bNiR variants (74.0 and 73.9 ml) on the gel-filtration column correspond to an MW^{app} of 113.2 and 114.3 kDa respectively (Table 2.1), indicative of the proteins being stable trimers in solution, which is also the case for WT protein (elution volume of 73.8 ml corresponding to an MW^{app} of 115.2 kDa). MALDI-TOF-MS gives MWs of 36653.3 Da for the monomer of WT bNiR (Table 2.1), which is close to the theoretical value (36654.8 Da). The experimental MWs for the M87C and K329C variants are 36638.7 and 36928.0 Da,

respectively. The MW of M87C bNiR is within 12.0 Da of the expected value (theoretical MW of 36626.7 Da), whilst the MW for K329C bNiR monomer is 298.2 Da heavier than the theoretical value (36629.8 Da). This mass difference indicates that a small molecule, most likely glutathione (MW = 307.3 Da), attaches to the mutated protein *via* the introduced Cys residue during over-expression in the cytosol of *E. coli*. Consistent with this, K329C bNiR reduced with TCEP gives an MW of 36618.4 Da, which is within 11.4 Da of the expected value.

The UV-Vis spectra of WT bNiR and the M87C and K329C variants (Figure 2.5.A) are very similar and are dominated by an intense S(Cys)$\pi \rightarrow$Cu(II) $d_{x^2-y^2}$ ligand to metal charge transfer (LMCT) transition band from the T1 Cu(II) site at 594 nm [22], which is absent in the reduced form. The relative absorbance at 280 and 594 nm (A_{280}/A_{594} ratio) of WT bNiR and the variants is ~ 11 for the fully oxidized forms (Table 2.2). Contribution of the T2 Cu site to the absorption spectra in the visible region is negligible [119]. Differently to bNiR, gNiR, which was previously studied at the single molecule level, exhibits much weaker LMCT absorption band at ~ 600 nm, but more pronounced at ~ 460 nm, responsible for green colour of the protein (Figure 2.5.B). The EPR spectra of WT bNiR and the M87C and K329C variants are comparable (Figure 2.5.C and Table 2.2), indicating that the structures of the T1 Cu and the T2 Cu sites in the Cys variants are very similar to those in WT protein. Removal of glutathione from K329C bNiR did not influence the spectral properties of the variant (data not shown).

The kinetic parameters of NO_2^- reduction by WT bNiR and the M87C and K329C variants were determined in 50 mM phosphate pH 7.0 with dithionite-reduced BV as an electron donor (Figure 2.5.D), and the values are listed in Table 2.2. An obtained K_M of 32 μM and k_{cat} of 378 s^{-1} of WT bNiR are in good agreement with previously published results for native bNiR [74]. The affinities (K_M) towards NO_2^- of M87C and K329C variants are comparable to that of WT bNiR, but k_{cat} value of M87C bNiR (k_{cat} of 279 s^{-1}) is significantly lower to those of WT and K329C bNiR (k_{cat} of 373 s^{-1}).

2.4.2 *Protein fluorescent labeling*

The emission spectra of ATTO 647N and ATTO 532 show significant overlap with the LMCT absorption band at 594 nm of the T1 Cu(II) site of WT bNiR and the variants. Therefore, the fluorescence intensity of the label attached to the protein's surface is

partially quenched as a result of a FRET process from the fluorescent donor to the T1 Cu(II) site, which acts as an acceptor. The FLIM measurements were performed using the ATTO 647N label, as a compromise for several considerations. On one hand, too small spectral overlap lowers the *SR*, thus the contrast between the oxidized and reduced state's intensities and lifetimes is reduced. However, a large spectral overlap between the emission band of this label and the absorption band of the T1 Cu(II) site (resulting in a high quenching efficiency) hampers the intensity and lifetime determination in the oxidized state due to the lack of photons.

The maleimide active groups of fluorescent dyes allow more specific (in terms of dye positioning) labeling to a surface exposed thiol group (provided by a Cys residue), compared to that of NHS active groups, which react with the surface-exposed amine groups [104, 120]. Previous single molecule studies on the catalytic mechanism of CuNiR were performed using the amine group-labeled ATTO 655 L93C gNiR, whilst engineered Cys93 was used for protein immobilization [87]. This engineered Cys93 corresponds to Met87 in bNiR and the distances between Met87 and the T1 Cu sites within the trimer are 8, 45 and 47 Å, all estimated from the crystal structure (pdb file: 1OE1, [36]). The corresponding distances in the second variant, K329C bNiR, between Cys329 and the T1 Cu sites are 18, 54 and 58 Å.

The amine group-labeled ATTO 647N WT bNiR shows almost 2-fold higher *SR* than amine group-labeled ATTO 655 L93C gNiR (0.84 and 0.49 [87], respectively, Figure 2.6.A, i). The *SR* of Cys329-labeled ATTO 647N K329C bNiR (Figure 2.6.A, ii) is very similar to that of ATTO 647N labeled WT bNiR (0.86 and 0.84, respectively) but lower than that of Cys87-labeled ATTO 647N M87C bNiR (0.95, data not shown). The *SR* is higher, probably due to the shorter distance between the label and the T1 Cu site in the monomer of M87C bNiR (~ 8 Å). When dithionite-reduced Az is used as electron donor, the *SRs* are lower than those obtained with an artificial electron donor (ascorbate/PES mixture). The *SRs* of ATTO 647N labeled WT bNiR (Figure 2.6.B, i) and ATTO 647N labeled K329C bNiR (Figure 2.6.B, ii) are almost identical (0.71 and 0.70, respectively), whilst the *SR* of ATTO 647N labeled M87C bNiR is very low (0.12, data not shown), indicative of labeled protein not being reduced with a protein electron donor, such as Az.

2.4.3 *Strategies for immobilization of labeled proteins*

The schematic overview of the different strategies used for immobilization of labeled WT bNiR and the variants is shown in Figure 2.7, whilst the fluorescence images from confocal microscope are shown in Figure 2.8. Initially, ATTO 532 labeled M87C bNiR was immobilized *via* a homo bis-functional linker on both hydrophilic (APTS/MPTS coated) and hydrophobic (TES/MPTS-coated) glass slides (Figure 2.7.A) using the modified protocol optimized for ATTO 655 L93C gNiR [87]. In the absence of a linker the labeled protein was found to react non-specifically with the hydrophobic (Figure 2.8.A, i, upper panel) but not with the hydrophilic surface (Figure 2.8.A, ii, upper panel). This surface-protein interaction was also observed using tapping mode atomic force microscopy (AFM). Distinct AFM features resembling aggregates were observed, also when ATTO 532 labeled M87C bNiR was immobilized *via* linker on the hydrophilic glass slide (data not shown, measurements performed by Dr. Razvan Stan, Leiden University).

To prevent non-specific protein interactions, the hydrophilic glass slide was coated with an additional layer of a PEG-based blunt linker. ATTO 647N labeled K329C bNiR was immobilized on the hydrophilic, PEG-coated glass surface *via* biotin/streptavidin interactions using an NHS-PEG-biotin linker to the protein's surface exposed amine groups (Figure 2.7.B). Additionally, the high affinity of the biotin/streptavidin interaction increases the efficiency of the immobilization process. Although the labeled protein could be successfully immobilized (Figure 2.8.B, bottom panel), the results were less reliable as the streptavidin that was used for the experiments was either fluorescent or contaminated (Figure 2.8.B, upper panel).

ATTO 647N labeled K329C bNiR was successfully trapped in a high purity, low-gelling point, 1 % agarose gel (Figure 2.7.C). This method of immobilization is the least intrusive, but the protein has to be stable at elevated temperatures, higher than the gelling point of agarose. The melting temperature (T_m) of CuNiRs is ~ 100 °C [121] and ATTO 647N labeled K329 bNiR was found equally active before and after incubation for 10 min at 50 °C (data not shown). The immobilization procedure is simple, resulting in high-quality images (Figure 2.8.C). The molecules of ATTO 647N labeled K329C bNiR are not mobile within the agarose gel and the diffusion of chemicals does not seem to be restricted.

2.4.4 *Single molecule lifetime imaging of ATTO 647N labeled K329C bNiR*

FLIM images of agarose-trapped single molecules of ATTO 647N labeled K329C bNiR were recorded at pH 7.5 in buffer (fresh sample without reductant or oxidant present), under oxidizing (in the presence of 5 mM NO_2^-), reducing (in the presence of ascorbate and PES), and turnover (in the presence of five different concentration of NO_2^-, varying from 5 μM to 5 mM) conditions. Figure 2.9 shows a 15×15 μm area of a glass slide with ATTO 647N labeled K329C bNiR (300 pM) immobilized in an agarose gel as observed under a fluorescence microscope at RT. The size of the spots is slightly larger (≈ 600 nm, full width at half maximum, FWHM) than the diffraction limit (≈ 300 nm FWHM). Bleaching was occasionally observed, which appears to happen as a single step event, in which intensity is reduced to background level, meaning that each spot corresponds to a singly labeled K329C bNiR molecule. The fluorescence intensities and lifetimes could be correlated for individual ATTO 647N K329C bNiR molecules for prolonged periods of time (Figure 2.10). The correlograms indicate that either the fluorescence intensity (number of photons per ms) or lifetime (ns) can be used to distinguish between the reduced and oxidized states when using thresholds (yellow dashed line in Figure 2.10) of 15 photons per ms for the intensity and 2.5 ns for the lifetime.

Figure 2.11 shows examples of fluorescence decay curves obtained by creating histograms of all the photon arrival times collected during a 15×15 μm image scan (such as Figure 2.9.B) together with the histograms of pixel-averaged lifetimes observed for the ensemble of pixels in the same area. The fluorescence decay of oxidized and reduced ATTO 647N labeled K329C bNiR averaged to τ_1 = 1.1 ± 0.1 ns and τ_2 = 3.7 ± 0.1 ns, respectively, whilst these values obtained from the Gaussian distribution fit of the histograms of pixel-averaged lifetimes per pixel amount to 1.5 ns and 3.7 ns, respectively. For ATTO 647N labeled K329C bNiR under turnover conditions a sum of two exponentials (or two Gaussians) was needed to obtain a satisfactory fit, which demonstrates that the sample contained a mixture of reduced and oxidized enzyme molecules. The *SR* calculated from the decay times corresponds to a FRET efficiency of 0.70 ± 0.01, which is in a good agreement with the "in bulk" value of 0.86 (Figure 2.6).

Figures 2.9.C and 2.12 show FLIM images of a 15×15 μm scanned area in which the fluorescence decay observed for each pixel was fit to a double exponential decay with fixed τ_1 of 1.1 ns and τ_2 of 3.7 ns, and falsely coloured in red and blue.

Pixels for which the observed lifetime is longer than 2.5 ns (red) are assigned to the reduced state of the T1 Cu site, whilst pixels for which the observed lifetime is shorter than 2.5 ns (blue) are assigned to the oxidized state. Under reducing (inset, Figure 2.12.A, i) and oxidizing (inset, Figure 2.12.A, iii) conditions, the enzyme molecules are overwhelmingly in the reduced and oxidized state, respectively. Under turnover conditions (inset, Figure 2.12.A, ii) the spots consist of a mixture of red and blue pixels, which clearly indicates that the oxidation state of the T1 Cu site of ATTO 647N labeled K329C bNiR alternates over time between the reduced and oxidized states during scanning of a particular spot.

Changing the threshold for the observed fluorescence lifetime from 2.5 to 2.3 or 2.7 ns modified the assignment of oxidized and reduced pixels in less than 10 % of cases. To address the possibility of under-estimation of pixels, in which the T1 Cu site is oxidized, the background intensity level was compared to the number of photons across randomly selected spots (Figure 2.12.B). A threshold of 10 photons per pixel, which was used for the analysis, provides good discrimination between the background and signal, even at the edges of the spot.

2.4.5 *Time-averaged degree of oxidation of ATTO 647N labeled K329C bNiR*

The histograms of the time-averaged degree of oxidation of single spots, P_{ox} (which describes the fraction of time that a single molecule is in the oxidized form during the scan of a single spot), for few hundreds spots at pH 7.5 as a function of NO_2^- concentration are shown in Figure 2.13. Under reducing and oxidizing conditions (Figure 2.13.A; ii, viii) the distribution centers at P_{ox} values close to 0 and 1, respectively, whilst without reductant or oxidant present (Figure 2.13.A; i), two concomitant distributions are observed, one centered close to 0 and second close to 1. Under turnover conditions (Figure 2.13.A; iii - vii) a much broader distribution of P_{ox} values is observed and can be fit to two populations: one (labeled **A**) remains centered close to $P_{ox} = 0$, and the other (labeled **B**) progressively moves towards larger values of P_{ox} as the concentration of substrate (NO_2^-) increases (Figure 2.13.A and B). The width of the distributions, particularly for population **B**, increases considerably as the NO_2^- concentration increases. At the same time, the fraction of molecules in population **A** decreases with respect to population **B** (Figure 2.13.C). The weighted mean of P_{ox} values of the populations **A** and **B** for the different turnover conditions match the degree

of oxidation encountered for “in bulk” measurements under the same conditions (Figure 2.14).

Preliminary experiments show that ATTO 647N labeled K329C bNiR molecules belong either to the population **A** or **B** (Figure 2.15), with the transitions between the two populations occurring, but at a relatively infrequent rate. Additionally, experiments carried out at low (5.0) and high (9.0) pH showed that the population distribution for samples measured under turnover conditions are significantly affected by pH (Figure 2.16). At higher pH, the distribution centers close to 0 indicating that population **A** is more dominant than **B** and most of the molecules are in the reduced state. Population **B** increases at the expense of population **A** on moving towards lower pH.

2.4.6 *Time-dependent behavior of ATTO 647N labeled K329C bNiR*

To obtain information about the time-dependent behavior of single molecules, the waiting time distributions of the populations **A** and **B** were extracted. The schematic overview of histogram creation and data analysis is shown in Figure 2.17, whilst the histograms are shown in Figure 2.18. A 4 ms-binned (“ON”/”OFF”) time trace was created from each spot of population **A** and **B** of ATTO 647N labeled K329C bNiR (Figure 2.17.D). The occurrences of dwell times in the upper, τ_{on} (T1 Cu reduced), and in the lower, τ_{off} (T1 Cu oxidized), state were plotted and these waiting times histograms (Figures 2.17.E and 2.18) were fit to single exponential decays. Obtained τ_{red} and τ_{ox} lifetime values for the reduced and oxidized states of the enzyme, respectively, are summarized in Figure 2.19. During turnover, molecules in population **A** stay in the reduced state for approximately 20 to 30 ms, whereas for molecules in population **B** this period is approximately 10 ms (Figure 2.19, circles). The time that molecules from population **A** and **B** stay in the oxidized state amounts to a few ms (Figure 2.19, triangles). In buffer, in which a mixture of oxidized and reduced molecules are present and some switching of the T1 Cu site can be observed due to internal ET between the T1 and T2 Cu sites, the molecules in population **A** spend a longer time in the reduced form, whereas the opposite happens for population **B** (Figure 2.19).

The effect of the dwell time per pixels and time resolution on the accuracy in which τ_{red} and τ_{ox} can be determined was analyzed using a series of simulated “ON”/”OFF” time traces (for more information see Appendix B). The biggest deviation of the experimental τ_{red} from the theoretical τ_{red} is seen only when the latter is much

shorter then the dwell time per pixel (“bin size”, 1 or 4 ms) or much larger than the time windows used for the analysis (typically 20 - 60 ms). Additionally, the effect of the spot shape on the waiting time results was investigated using different shapes for the selected area of the same spot (Appendix B). Analysis of the whole spot, a rectangular area (5×15 pixels) or a square (7×7 pixels) produced similar trends in τ_{red} and τ_{ox}.

Protein	MW, Da		Δ $MW_{theo-exp}$, Da	V_e, mL	MW^{app}, kDa [c]
	Theoretical mass [a, b]	Experimental mass [b]			
WT bNiR	36654.8	36653.3	1.5	73.8	115.2
M87C bNiR	36626.7	36638.7	12.0	74.0	113.2
K329C bNiR	36629.8	36928.0, 36618.4 [d]	298.2 11.4	73.9	114.3

[a] MW including the N-terminal Met residue. [b] MW corresponds to the monomeric form of the protein. [c] MW^{app} corresponds to the trimeric form of the protein. [d] The experimental MWs correspond to the K329C bNiR reduced with TCEP.

Table 2.1 MALDI-TOF-MS the gel-filtration data for WT, M87C and K329C bNiR.

Properties	Protein		
	WT bNiR	M87C bNiR	K329C bNiR
	UV-Vis [a]		
$\lambda_{1,max}$, nm	~ 470	~ 470	~ 470
$\lambda_{2,max}$, nm	594	594	594
$\varepsilon_{max\ (1)}$, $M^{-1}cm^{-1}$	1040 [b]	1040	1040
$\varepsilon_{max\ (2)}$, $M^{-1}cm^{-1}$	5200 [b]	5200	5200
$A_{280}/A_{max(2)}$	~ 11	~ 11	~ 11
	T1 Cu (T2 Cu) EPR parameters [c]		
g_x	2.038 (2.017)	2.038 (2.017)	2.038 (2.017)
g_y	2.058 (2.122)	2.058 (2.119)	2.058 (2.122)
g_z	2.221 (2.372)	2.221 (2.359)	2.221 (2.359)
A_z, 10^{-4} cm^{-1}	10.3 (0)	10.3 (0)	10.3 (0)
A_z, 10^{-4} cm^{-1}	8.3 (0)	8.3 (0)	8.3 (0)
A_z, 10^{-4} cm^{-1}	66 (110)	66 (110)	66 (110)
	ATTO 647N labeled WT, M87C and K329C bNiR [d]		
SR, with ascorbate/PES	0.84	0.95	0.86
SR, with dithionite reduced Az	0.71	0.12	0.71
	Activity with $NaNO_2$ [e]		
K_M, μM	32 ± 1	30 ± 4	36 ± 1
k_{cat}, s^{-1}	387 ± 2	279 ± 8	373 ± 1
k_{cat}/K_M, $s^{-1}\mu M^{-1}$	12.1 ± 0.3	9.3 ± 0.9	10.4 ± 0.3

[a] In 20 mM MES pH 6.0 at RT. [b] Taken from [22]. [c] In 24 mM Tris pH 7.5 plus 40 % glycerol at ~ 80 K. [d] In 50 mM phosphate pH 7.0 at 20 °C. [e] In 50 mM phosphate pH 7.0 at 21 °C with 200 μM dithionite-reduced BV as electron donor.

Table 2.2 Comparison of spectral properties of WT, M87C and K329C bNiR and kinetic parameters for NO_2^- reduction.

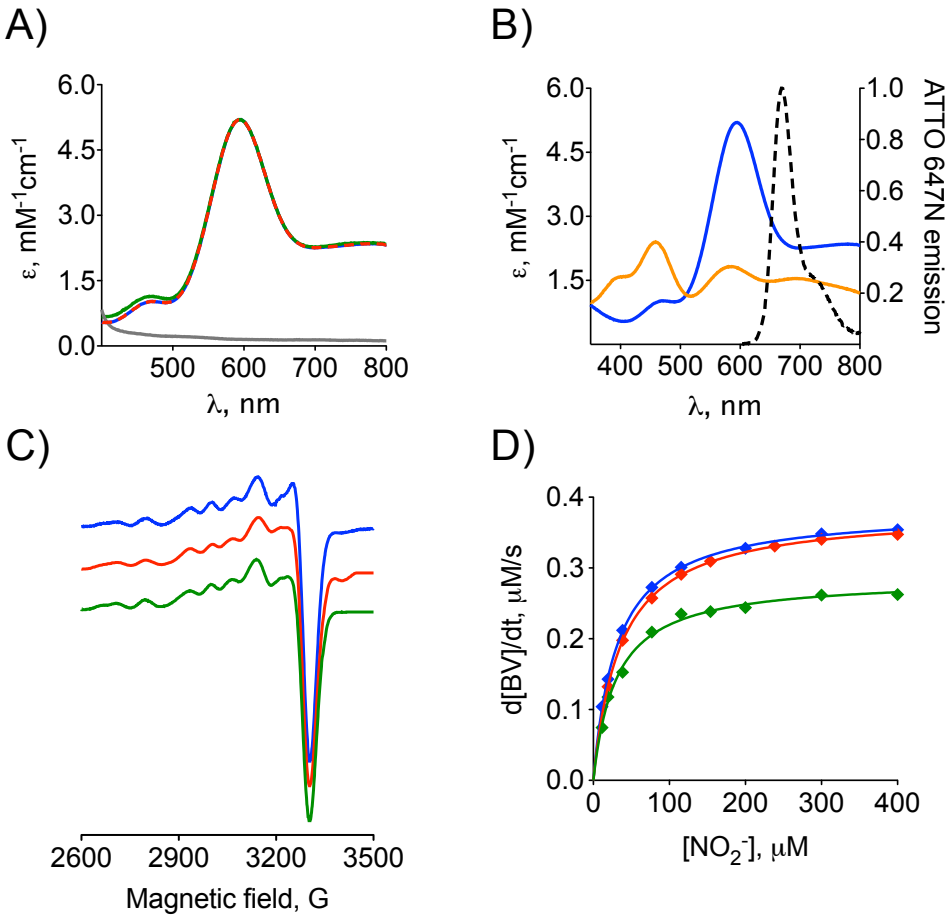

Figure 2.5 (A) Absorption spectra of oxidized WT (▬), M87C (▬) and K329C (▬) bNiR and reduced WT bNiR (▬) in 20 mM MES pH 6.0 at RT. The optical spectra of the species coincide. (B) Absorption spectra of oxidized WT bNiR (▬) and WT gNiR (▬) with the emission spectrum of ATTO 647N dye (▬). (C) EPR spectra of oxidized WT (▬), M87C (▬) and K329C (▬) bNiR in 24 mM Tris pH 7.6 (40 % glycerol) at ~ 80 K. (D) The Michaelis-Menten plots of WT (◆), M87C (◆) and K329C (◆) bNiR (each of 1.0 nM final concentration) activity with $NaNO_2$ using an artificial electron donor (BV) in 50 mM phosphate pH 7.0 at 21 °C.

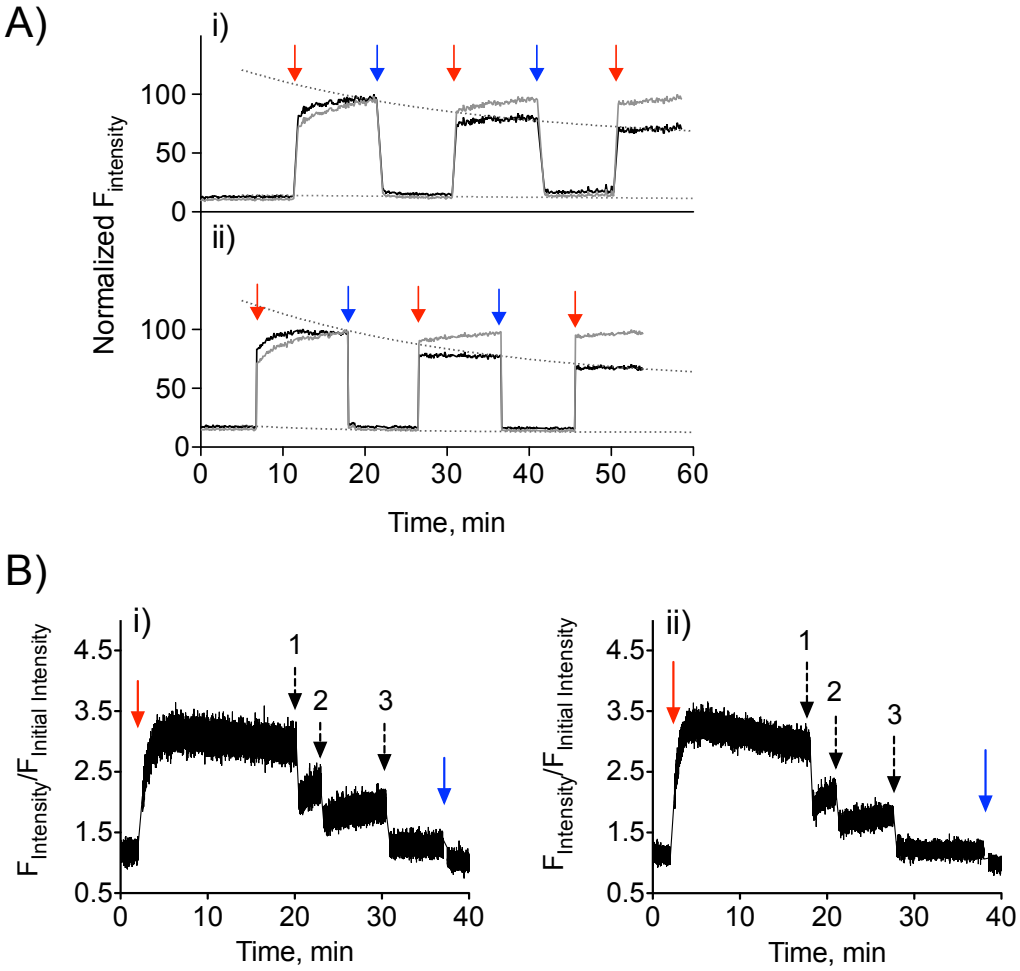

Figure 2.6 Fluorescence intensity changes of ATTO 647N labeled WT (i) and K329C bNiR (ii) reduced with (A) an excess of sodium ascorbate with PES and (B) 15 µM dithionite-reduced Az. (A) The concentrations of labeled enzymes are (i) 31 nM and (ii) 48 nM, and (i) 30 nM and (ii) 28 nM for (A) and (B), respectively. The addition of reductant, oxidant (potassium ferricyanide) and $NaNO_2$ (1: 66 µM, 2: 265 µM and 3: 5300 µM) is indicated with red, blue and black arrows, respectively. The fluorescence intensity was followed at 657 nm using an excitation wavelength of 630 nm (▬). ATTO 647N bleaching-corrected experimental traces (▬) in (A) were obtained by constructing the exponential bleaching curves (▪▪▪▪) that run through the experimental points at 21, 41 and 58 min (i), and 18, 36 and 54 min (ii). In the similar way the low intensity parts of experimental traces were corrected for bleaching.

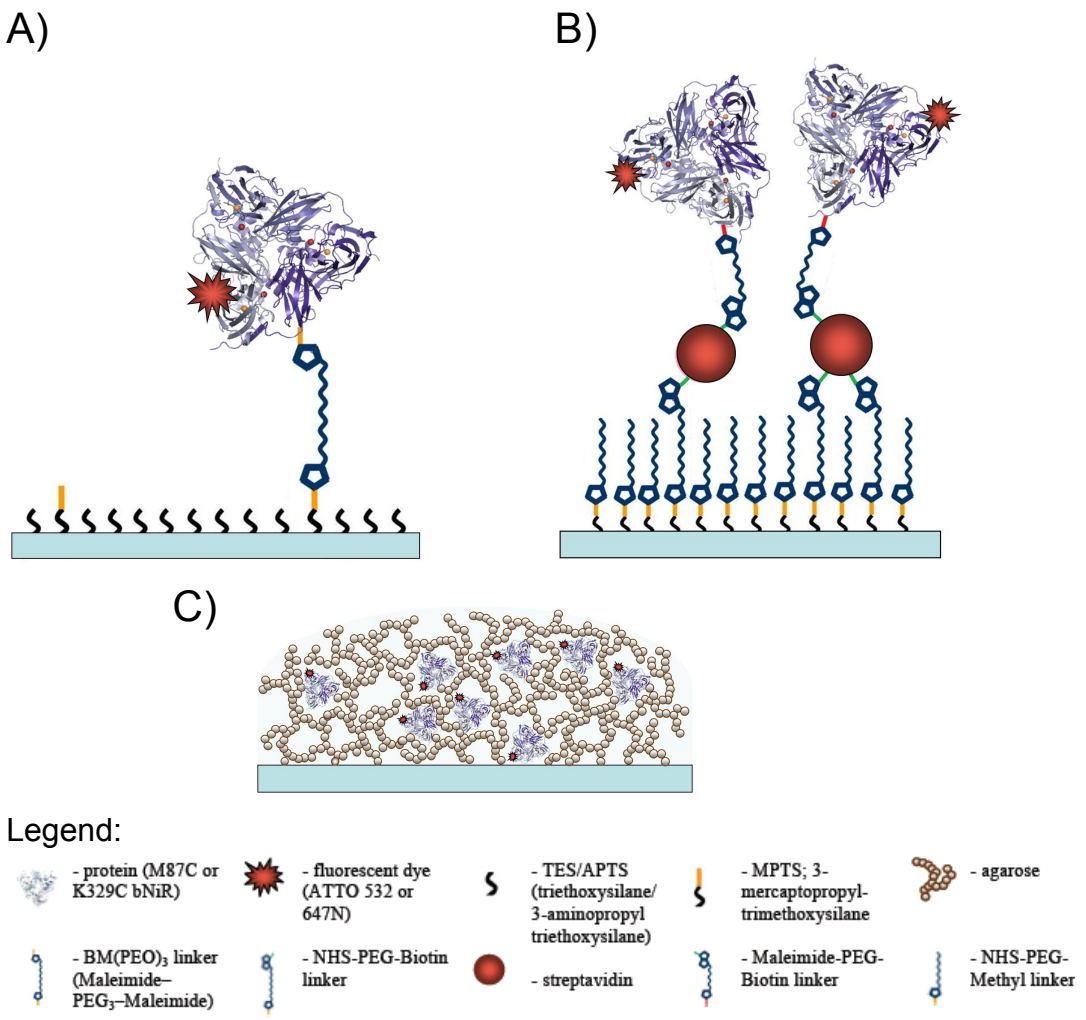

Figure 2.7 Protein immobilization schemes. (A) Covalent immobilization *via* a bis-functional linker on a TES/MPTS or an APTS/MPTS-coated glass slide. (B) Affinity-based immobilization on an APTS/streptavidin-coated glass slide *via* biotin/streptavidin interactions. (C) Trapping of molecules in a spin-coated agarose gel on a glass slide.

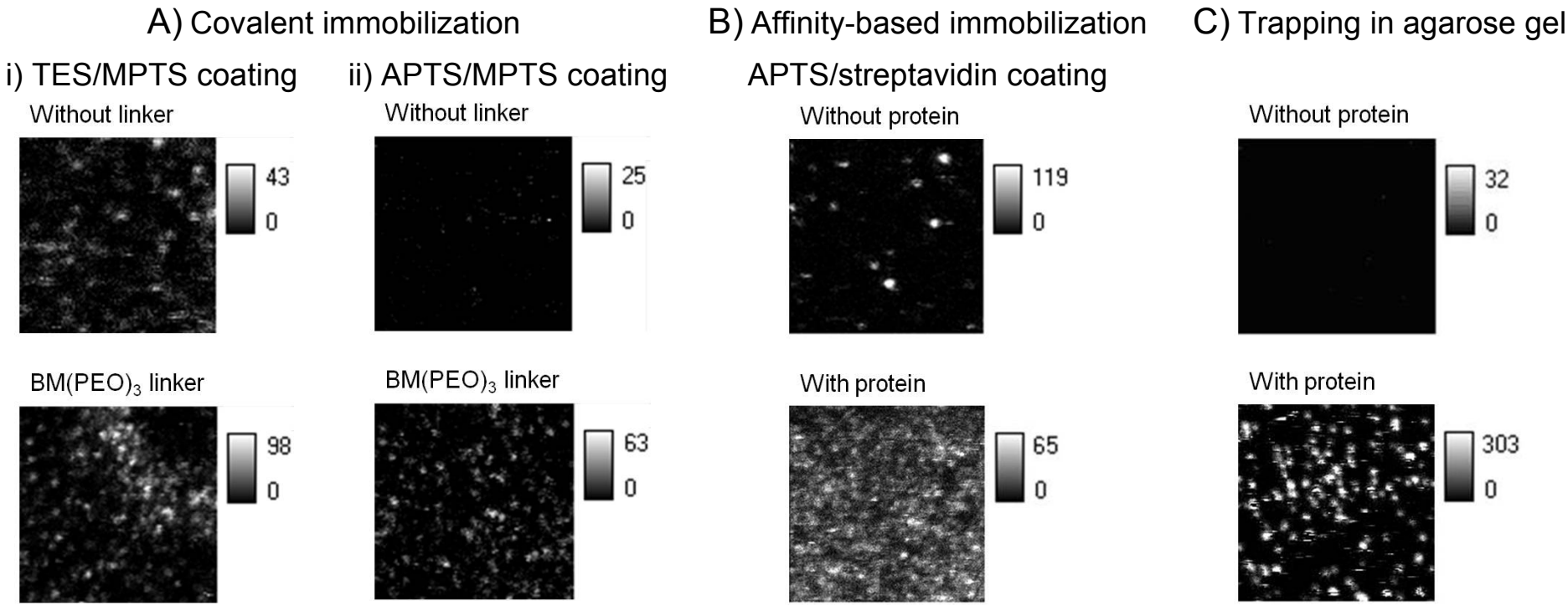

Figure 2.8 (A) Fluorescence intensity images (10×10 μm) of ATTO 532 labeled M87C bNiR immobilized on a silanized glass slide on (i) a TES/MPTS-coated and (ii) an APTS/MPTS-coated glass slides without (top) and with a bis-functional $BM(PEO)_3$ linker (bottom). (B) Fluorescence intensity images (20×20 μm) of an APTS/streptavidin-coated glass slides without (top) and with ATTO 647N labeled K329C bNiR with an NHS-PEG-biotin linker (bottom). (C) Fluorescence intensity images (15×15 μm) of 1 % agarose IV gel with (bottom) and without (top) ATTO 647N labeled K329C bNiR. All images: pixel size: 75-100 nm; dwell time per pixel: 4 ms.

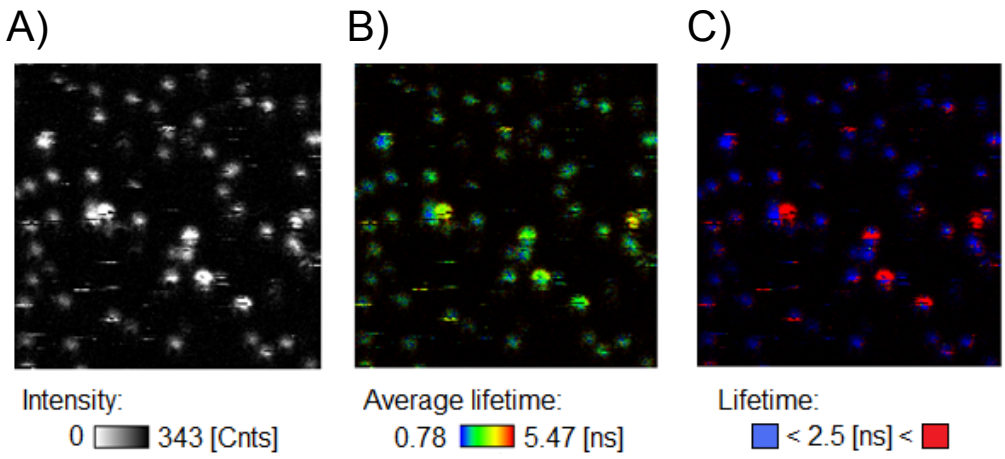

Figure 2.9 (A) Fluorescence intensity, (B) fluorescence average lifetime (so-called fast FLIM) and (C) false coloured lifetime confocal images (15×15 μm) after a double exponential fit of ATTO 647N labeled K329C bNiR molecules immobilized in agarose gel on a glass surface. The brightness in (A) reflects fluorescence intensity while the colour in (B) indicates the mean arrival times of fluorescence photons after the excitation laser pulse as a measure for the average lifetime, as implemented by SymPhoTime. The intensity range in (A) and colour scale range in (B) are from the minimum to maximum values. Lifetime images in (C) were generated by fitting the fluorescence decay observed for each pixel to a double exponential decay with fixed τ_1 = 1.1 ns and τ_2 = 3.7 ns, and using the maximum likelihood algorithm as implemented by SymPhoTime as described in Sections 2.3.15 and 2.3.16. Each pixel was false coloured either blue or red depending on whether the resulting average lifetime was smaller or larger than 2.5 ns, respectively. The surface was scanned from top to the bottom and from left to the right with a resolution of 75 nm per pixel and dwell time of 4 ms per pixel. Each spot corresponds to a single ATTO 647N labeled K329C bNiR molecule.

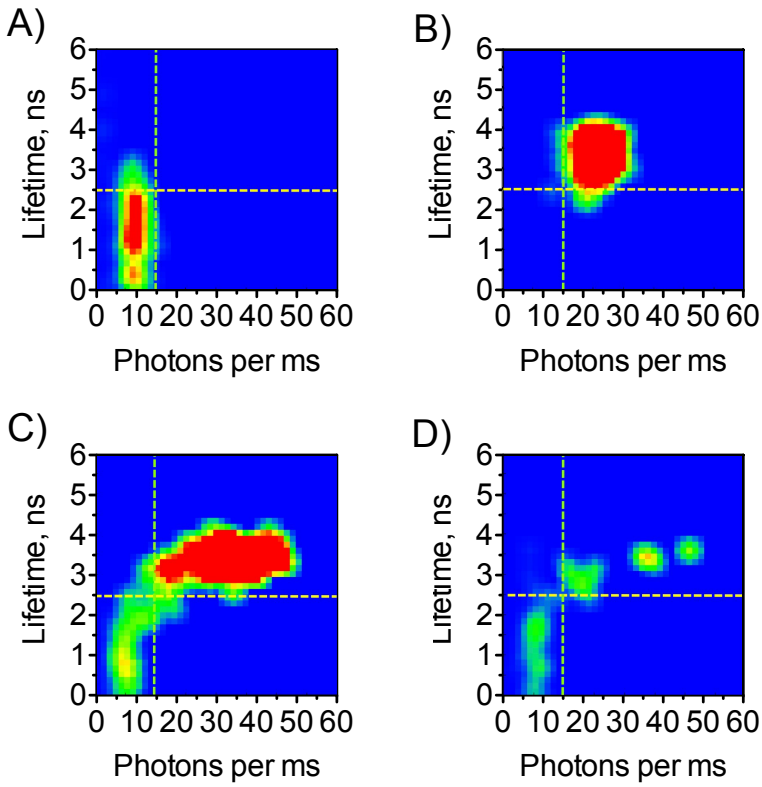

Figure 2.10 Correlograms linking the fluorescence intensity and fluorescence lifetime observed when monitoring individual ATTO 647N labeled K329C bNiR molecules in agarose gel for prolonged periods varying from 0.5 s to a few seconds. The examples displayed in the panels are from the 4 ms-binned time traces of individual molecules under (A) oxidizing (P_{ox} = 1.0), (B) reducing (P_{ox} = 0.02) and turnover, (C) P_{ox} = 0.15 and (D) P_{ox} = 0.7, conditions. The colour is indicative of the frequency of events occurring in the correlogram, with a colour change from green to red corresponding to an increase in occurrence. Yellow dashed lines depict the threshold of 15 photons per ms for the fluorescence intensity and 2.5 ns for the lifetime *(Result from Dr. Leandro C. Tabares).*

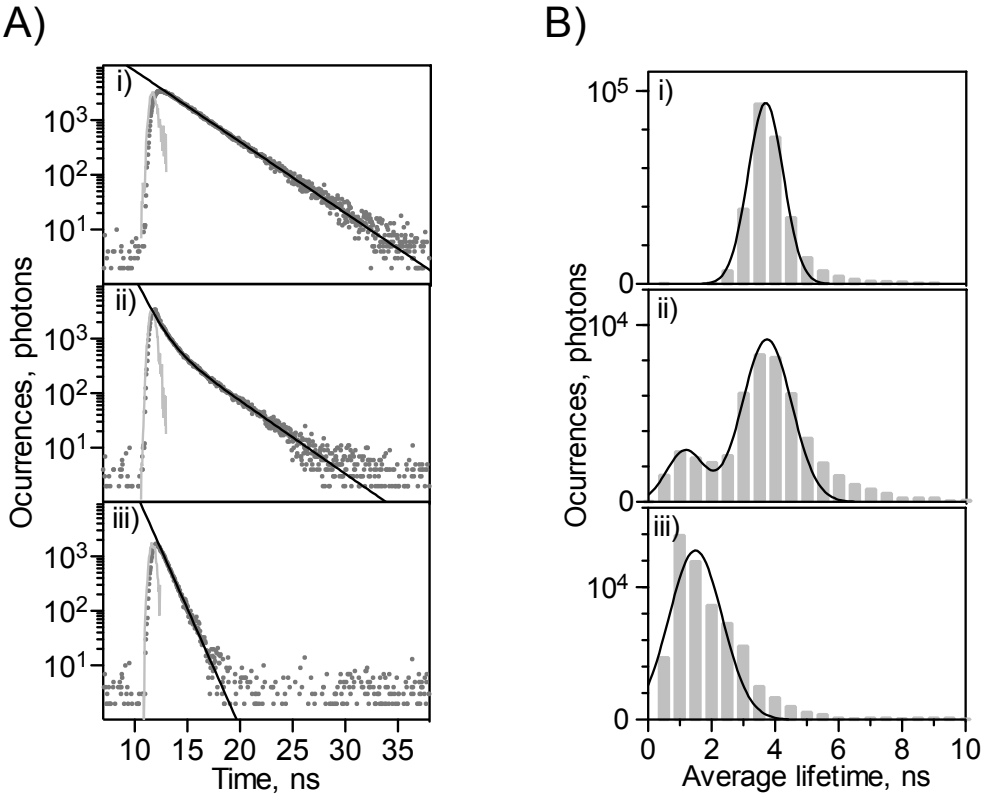

Figure 2.11 Fluorescence decay curves and lifetimes for ATTO 647N labeled K329C bNiR immobilized in agarose gel. Data correspond to an area (15×15 μm) containing around 40 spots. (A) Histograms of photon arrival times (•) for all the photons acquired during a full image scan in the presence of: (i) 10 mM ascorbate and 100 nM PES (reduced, τ = 3.7 ns); (ii) 10 mM ascorbate, 100 nM PES and 500 μM $NaNO_2$ (turnover, τ_1 = 1.1 ns, a_1 = 16 %, τ_2 = 3.7 ns, a_2 = 84 %); and (iii) 5 mM $NaNO_2$ (oxidized, τ = 1.1 ns). The gray lines represent IRF whilst the black lines represent the fits to the single (i and iii) and double (ii) exponential decays. Total number of detected photons after background correction: (i) 389254; (ii) 168705; (iii) 71725. (B) Histogram of fluorescence lifetimes per pixel (i.e. the frequency of photon counts corresponding to the individual mean lifetimes) in the presence of: (i) 10 mM ascorbate and 100 nM PES (reduced, τ = 3.7 ns); (ii) 10 mM ascorbate, 100 nM PES and 500 μM $NaNO_2$ (turnover, τ_1 = 1.2 ns, a_1 = 20 %, τ_2 = 3.7 ns, a_2 = 80 %); and (iii) 5 mM $NaNO_2$ (oxidized, τ = 1.5 ns). Black lines represent the fits to a single (i and iii) and double (ii) Gaussian distributions.

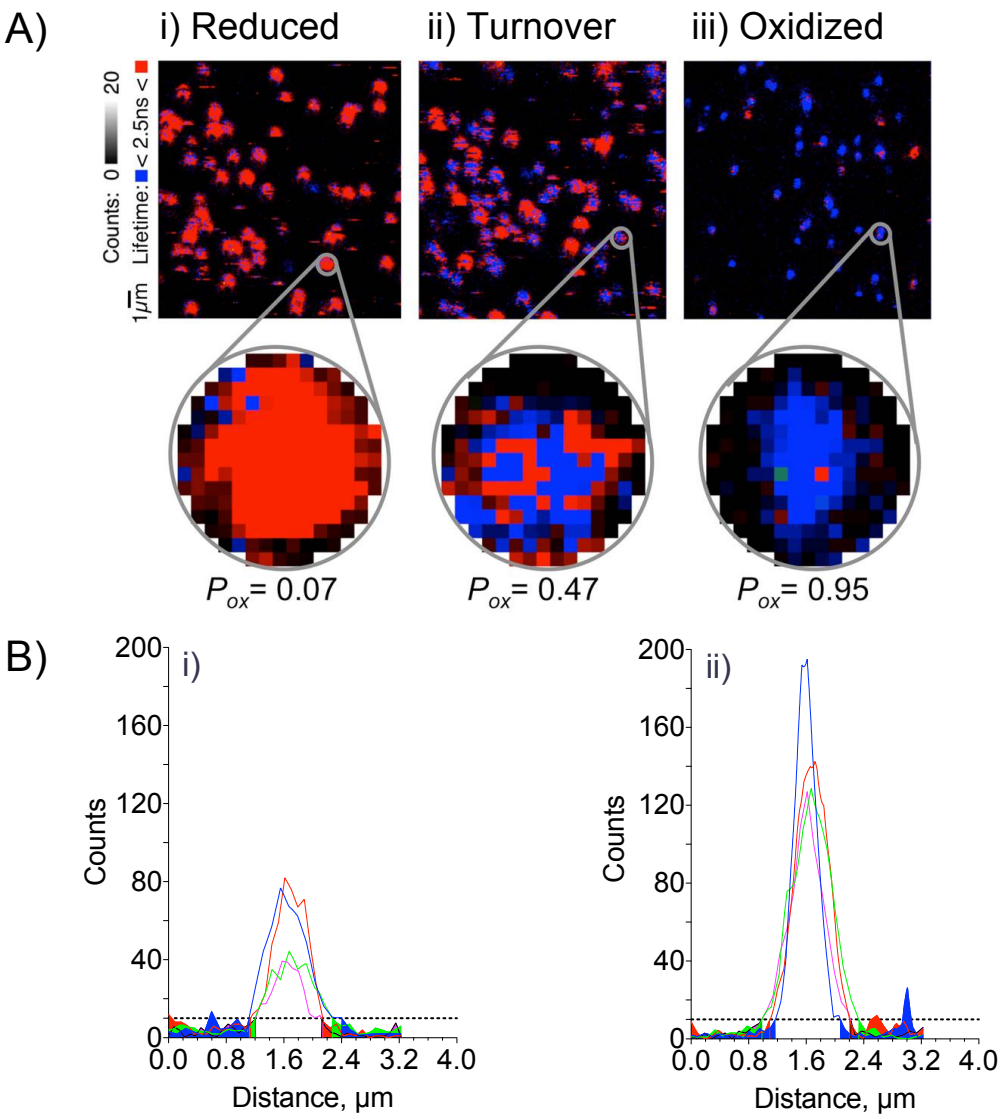

Figure 2.12 (A) FLIM images (15×15 μm, coloured as in Figure 2.9.C) of ATTO 647N labeled K329C bNiR immobilized in agarose gel in the presence of (i) 10 mM ascorbate and 100 nM PES, (ii) 10 mM ascorbate, 100 nM PES and 500 μM $NaNO_2$, and (iii) 5 mM $NaNO_2$; pixel size 75 nm, dwell time per pixel 4 ms. Fluorescence lifetimes: ■> 2.5 ns, ■< 2.5 ns. The insets: amplifications of the selected spots are shown for each FLIM image. For clarity and ease of comparison, brightness of the images was set from 0 to 20 counts per pixel, thus pixels with a signal stronger than 20 counts have been given the same (maximum) brightness. (B) Cross-section of the four randomly selected oxidized (i) and reduced (ii) spots from a FLIM image. The dotted lines indicate the threshold of 10 photons that was used as a cut-off for the analysis described in the main text. The coloured areas indicate the parts of the cross-sections that fall below the threshold or outside the 15 pixel diameter circle used for the spots selection.

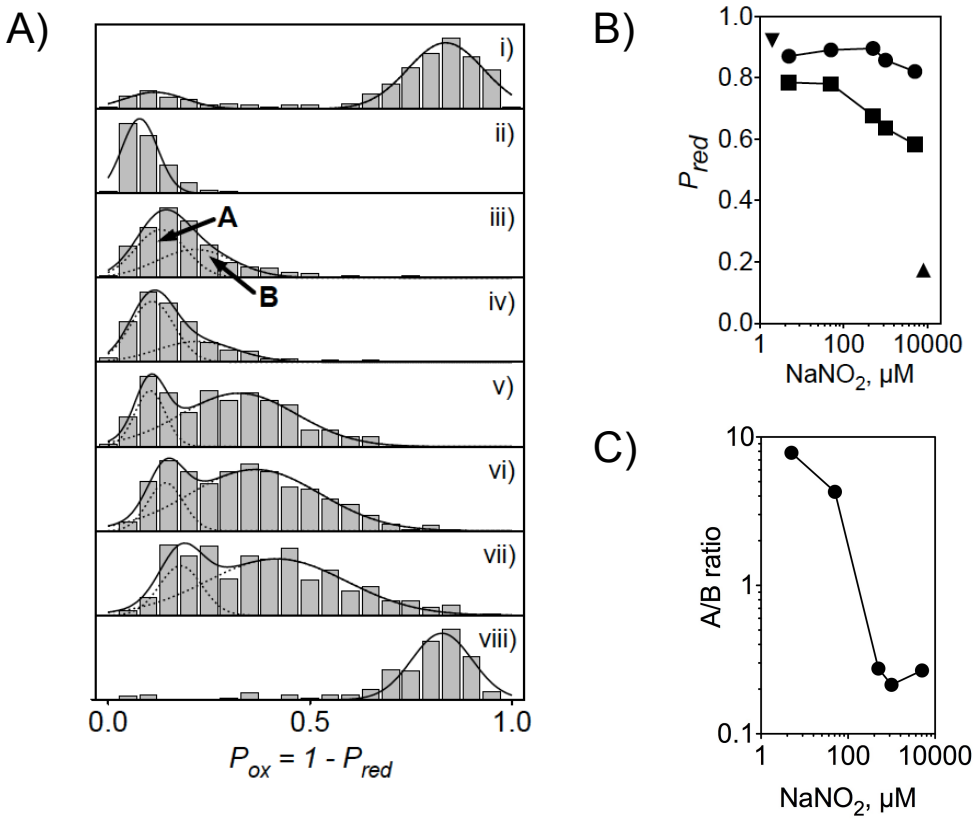

Figure 2.13 (A) Histograms of P_{ox} values for ATTO 647N labeled K329C bNiR immobilized in agarose gel: (i) in buffer (pH 7.5) with no reductant and oxidant present; (ii) under reducing conditions with 10 mM ascorbate and 100 nM PES; (iii) - (vii) turnover conditions with 10 mM ascorbate and 100 nM PES and varying amounts of $NaNO_2$: (iii) 5 µM, (iv) 50 µM, (v) 500 µM, (vi) 1 mM and (vii) 5 mM; (viii) under oxidizing conditions with 5 mM $NaNO_2$. The histograms in (ii) and (viii) were fit to a single Gaussian (—). For panel (i), the left and right distributions in the histogram were fit separately to a single Gaussian (—). In the panels (iii) - (vii), the fits (—) are the sum of two Gaussian distributions (┅). (B) Centers of the Gaussian distributions for populations **A** (●) and **B** (■) as a function of $NaNO_2$ concentration during turnover. The values for completely reduced (▼) and oxidized (▲) enzyme are also shown. (C) Ratio between the number of molecules in populations **A** and **B** during turnover as a function of $NaNO_2$ concentration.

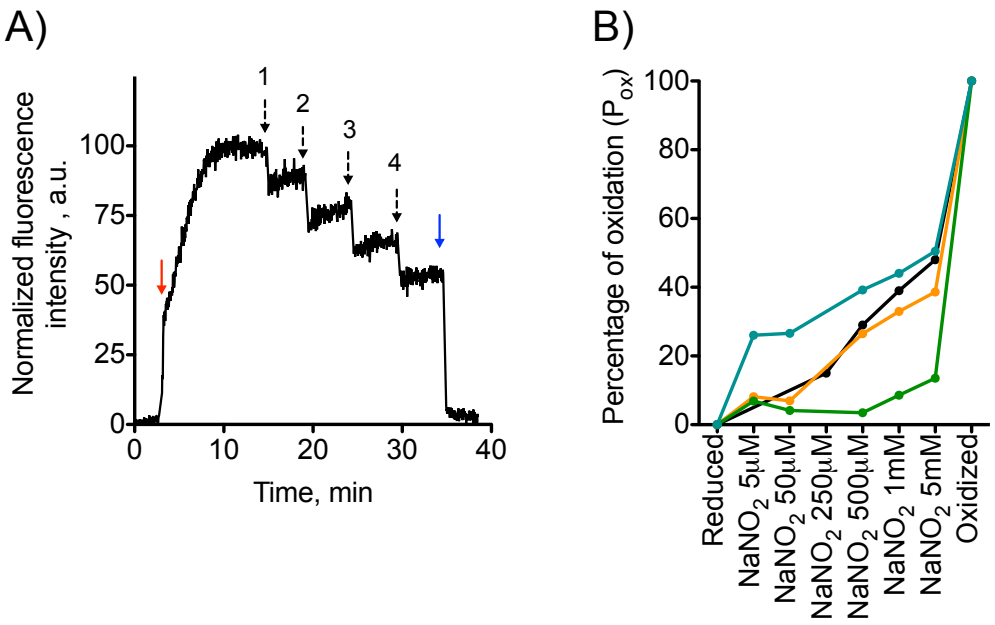

Figure 2.14 A) Normalized "in bulk" fluorescence intensity time trace of ATTO 647N labeled K329C bNiR, corrected for bleaching. Arrows indicate the addition of reductant (red arrow; 10 mM ascorbate and 100 nM PES), $NaNO_2$ (dashed, black arrows; 1: 250 µM, 2: 500 µM, 3: 1000 µM, 4: 5000 µM, final concentrations) and oxidant (blue arrow; 20 mM $K_3[Fe(CN)_6]$). B) Comparison of the mean P_{ox} values for population **A** (●), **B** (●) and **A** + **B** (●) with the "in bulk" (●) percentage of oxidation calculated from (A).

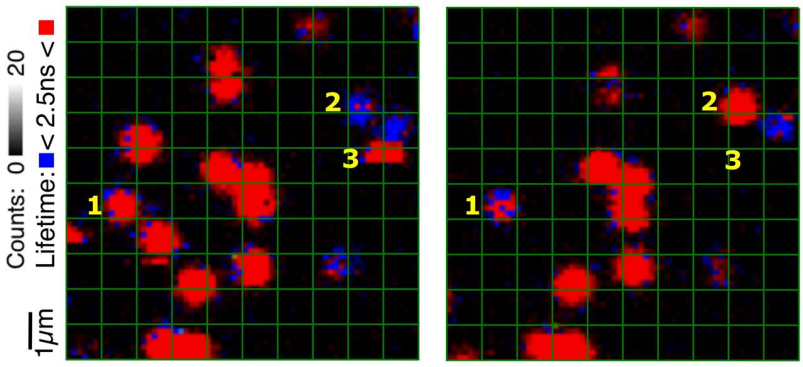

Figure 2.15 FLIM images (15×15 µm, pixel size 75 nm, dwell time per pixel 4 ms, coloured as in Figure 2.9.C) of ATTO 647N labeled K329C bNiR immobilized in agarose gel showing the switch between populations in the presence of 10 mM ascorbate, 100 nM PES and 500 µM $NaNO_2$ in 100 mM phosphate pH 7.5. Fluorescence lifetimes: ■> 2.5 ns, ■< 2.5 ns. The two images were taken of the same area 10 min apart (image on the left is the first one). The green grid was added to help to compare the position of molecules. The molecule marked as **1** switches from population **A** to **B** while the opposite happens for molecule **2**. A few molecules disappear when comparing the two images due to dye bleaching. In the left image a single step photo bleaching can be observed for molecule **3**. *(Results from Dr. Leandro C. Tabares)*

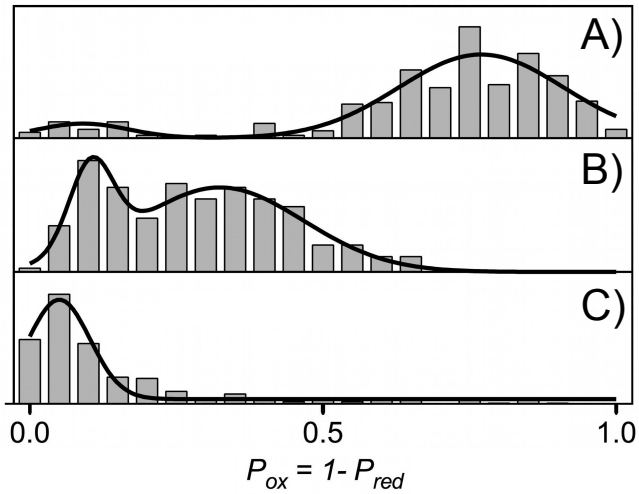

Figure 2.16 Histograms of P_{ox} values of ATTO 647N labeled K329C bNiR immobilized in agarose gel at (A) pH 5.0, (B) pH 7.5 and (C) pH 9.0 under turnover conditions: 10 mM ascorbate, 100 nM PES and 500 µM $NaNO_2$. The samples were measured in 100 mM ammonium acetate pH 5.0, 100 mM phosphate pH 7.5 and 100 mM sodium borate pH 9.0. *(Results from Dr. Leandro C. Tabares).*

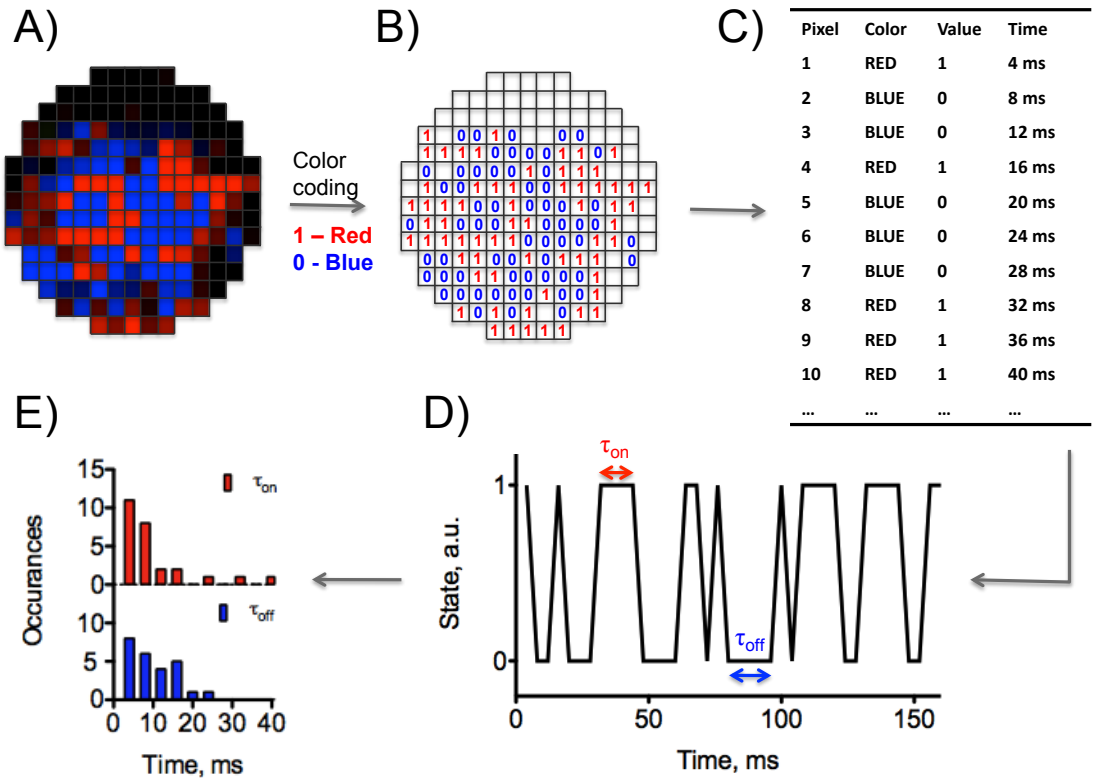

Figure 2.17 Analysis of the time dependent behavior of a single enzyme molecule represented as a spot with a diameter of 15 pixels. (A) The 75×75 nm pixels of the image are scanned sequentially from top to bottom row by row, left to right, with a dwell time of 4 ms per pixel. (B) A pixel is assigned a value of 0 or 1 depending on whether the fluorescence lifetime is shorter (■) or longer (■) than 2.5 ns, respectively. The values are collected in a table (C) and pixels below the set threshold were omitted. The pixel values were then plotted on a time axis (D), from which the occurrence of the "ON" and "OFF" waiting times (τ_{on} and τ_{off}) was plotted (E).

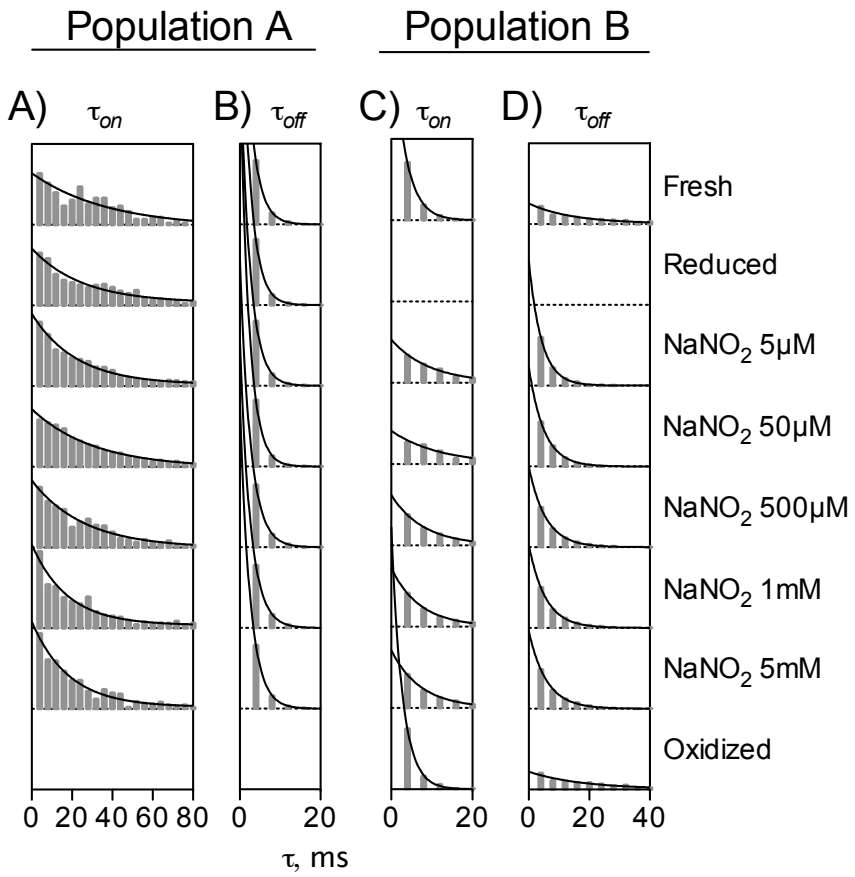

Figure 2.18 Histograms of the "ON" times, τ_{on} (A) and (C), and "OFF" times, τ_{off} (B) and (D), for the molecules from population **A** (A) and (B), and **B** (C) and (D). To limit cross contamination between the populations, for each condition, the crossing point of the Gaussian fit was determined (P_c) and populations **A** and **B** were defined as the collections of spots with $P_{ox} \leq P_c - 0.025$ and $P_{ox} \geq P_c + 0.025$, respectively. All histograms are fit to a single exponential function (——).

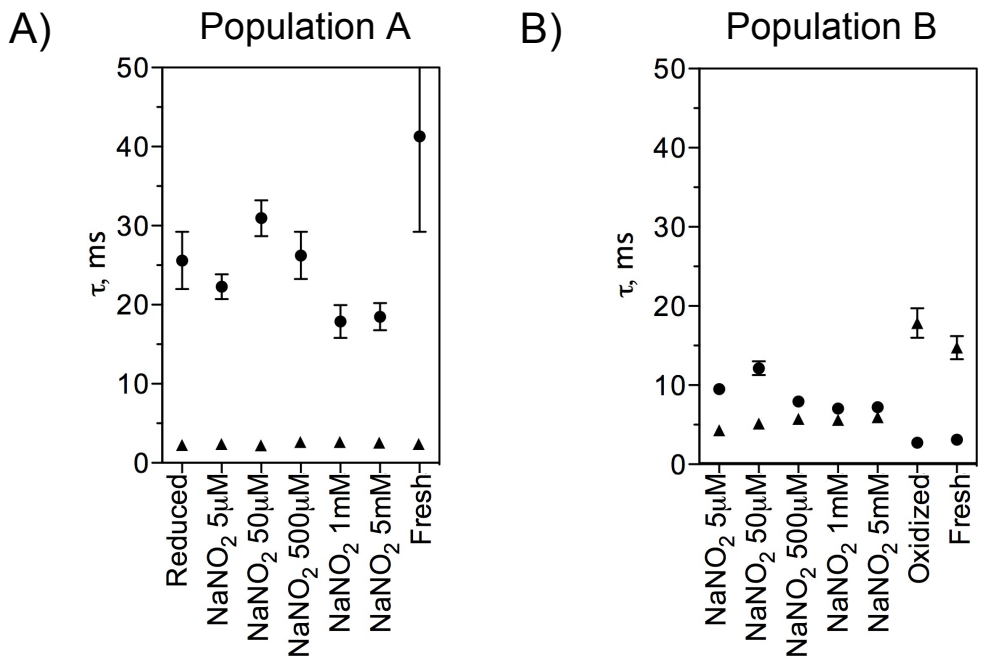

Figure 2.19 Lifetimes in the reduced (τ_{red}, ●) and the oxidized (τ_{ox}, ▲) states for (A) population **A** and (B) population **B** as determined from the single exponential fits of the histograms of waiting times (see Figure 2.18). Error bars represent the standard error of the fit (in cases where the error bars are not shown, the standard error is smaller than the symbol size).

2.5 Discussion

2.5.1 *Fluorescent labeling and "in-bulk" studies of bNiR*

The UV-Vis and EPR spectra of WT, M87C and K329C bNiR are very similar and therefore M87C and K329C mutations have little effect on the structure of the T1 or the T2 Cu sites of the enzyme. However, at pH 7.0, the activity of the M87C variant using BV as an artificial electron donor is lower than that of WT protein and the K329C variant. Additionally, Cys87-labeled ATTO 647N M87C bNiR could not be reduced with dithionite-reduced Az (data not shown), what is in agreement with previous findings that Met87 is involved in formation of the bNiR-Az complex [31]. Independent of the nature of electron donor, the K329C mutation has a limited effect on enzyme activity (Figure 2.5.D and Figure 2.6.B).

The contrast between reduced and oxidized states of the T1 Cu site of bNiR, which is reflected in *SR* values of fluorescence intensity and lifetime, is greater than that of labeled gNiR. K329C bNiR variant was chosen over M87C bNiR for studies on the mechanism of bNiR at the single molecule level, owing to the lower activity in NO_2^- reduction of the latter variant. The distance between the introduced Cys and the T1 Cu site within the monomer of K329C bNiR gave the optimal FRET and limited the concomitant detection of redox changes at the two other T1 Cu sites of the trimer. The *SR* values derived from fluorescence decay times for immobilized ATTO 647N labeled K329C bNiR (0.70), is in reasonable agreement with fluorescence intensity switching ratios observed for ABEL-trapped molecules (0.77) [122] and "in-bulk" measurements (0.86).

2.5.2 *Single molecule measurements of ATTO 647N labeled K329C bNiR*

The novel method of analyzing FLIM images of immobilized ATTO 647N labeled K329C bNiR revealed the existence of two populations (depicted as **A** and **B**, Figure 2.13), characterized by different lifetimes, τ_{red} and τ_{ox} (Figure 2.19), in the reduced (**RO** and **ROs,** bright part of manifold) and oxidized (**OO, OR** and **ORs**, dark part of manifold) states of the T1 Cu (Figure 2.20). The values for the ET rate between the T1 Cu and T2 Cu (corresponding to the RO $\rightleftharpoons$ OR and ROs $\rightleftharpoons$ ORs transitions in Figure 2.20.A) determined by pulse radiolysis or flash photolysis are in range of 180 - 330 s^{-1} and 265 - 770 s^{-1} for the forward and backward reaction, respectively [82,

83]. Therefore, for the single molecule experiments, the τ_{red} are estimated in order of ~ 3 - 6 ms, whilst τ_{ox} of ~ 1 - 4 ms. The values of τ_{red} and τ_{ox} obtained from FLIM analysis are higher than expected (especially for population **A**) and seem almost independent of NO_2^- concentration for both populations within the concentration range 5 μM to 5 mM (Figure 2.19). The comparison of τ_{red} values shows that the molecules from population **A** stay in the reduced state approximately 2 to 3-fold longer than molecules from population **B**, indicating that the ET between the T1 Cu and T2 Cu in population **A** takes longer than in population **B**. As the NO_2^- concentration increases, the distribution of populations **A** and **B** becomes broader (in particular for population **B**) and separation between populations is more visible, suggesting more pronounced heterogeneity between molecules. This has been observed before for gNiR and may reflect a distribution in rate of ET between the T1 Cu and T2 Cu related to structural disorder of the T1 and the T2 Cu sites [87]. Upon addition of NO_2^-, population **B** moves towards larger values of P_{ox}, which correlates with the increase in number of molecules from population **B** relative to population **A** (Figure 2.13.B and C).

Previous "in-bulk" activity and electrochemical measurements of gNiR have been interpreted according to the "random sequential" mechanism [70, 77] and modeled with a reaction scheme that distinguishes between a reduction-first and a substrate binding-first pathways, labeled as *A* and *B*, respectively, in Figure 2.20.A. The rate of ET between the T1 Cu and T2 Cu is known to depend on the ligand in the first coordination shell of the T2 Cu site, and at pH 7.5, in the absence of substrate this ligand is an OH^- group (pathway *A*) whilst in the presence of substrate, NO_2^- is bound (pathway *B*) [70]. Longer τ_{red} values for population **A** of immobilized K329C bNiR molecules are in agreement with ET to the T2 Cu coordinated by the OH^- ligand being slower then when NO_2^- binds [70, 86]. Therefore, we proposed that identified population **A** and **B** correspond to molecules that follow pathways *A* and *B*, respectively. It is important to note that the immobilized enzyme molecules seem to exhibit features reminiscent of an "ordered" mechanism, in the sense that once the bNiR molecule operates according to either pathway it will keep doing it for at least several turnovers [88, 123].

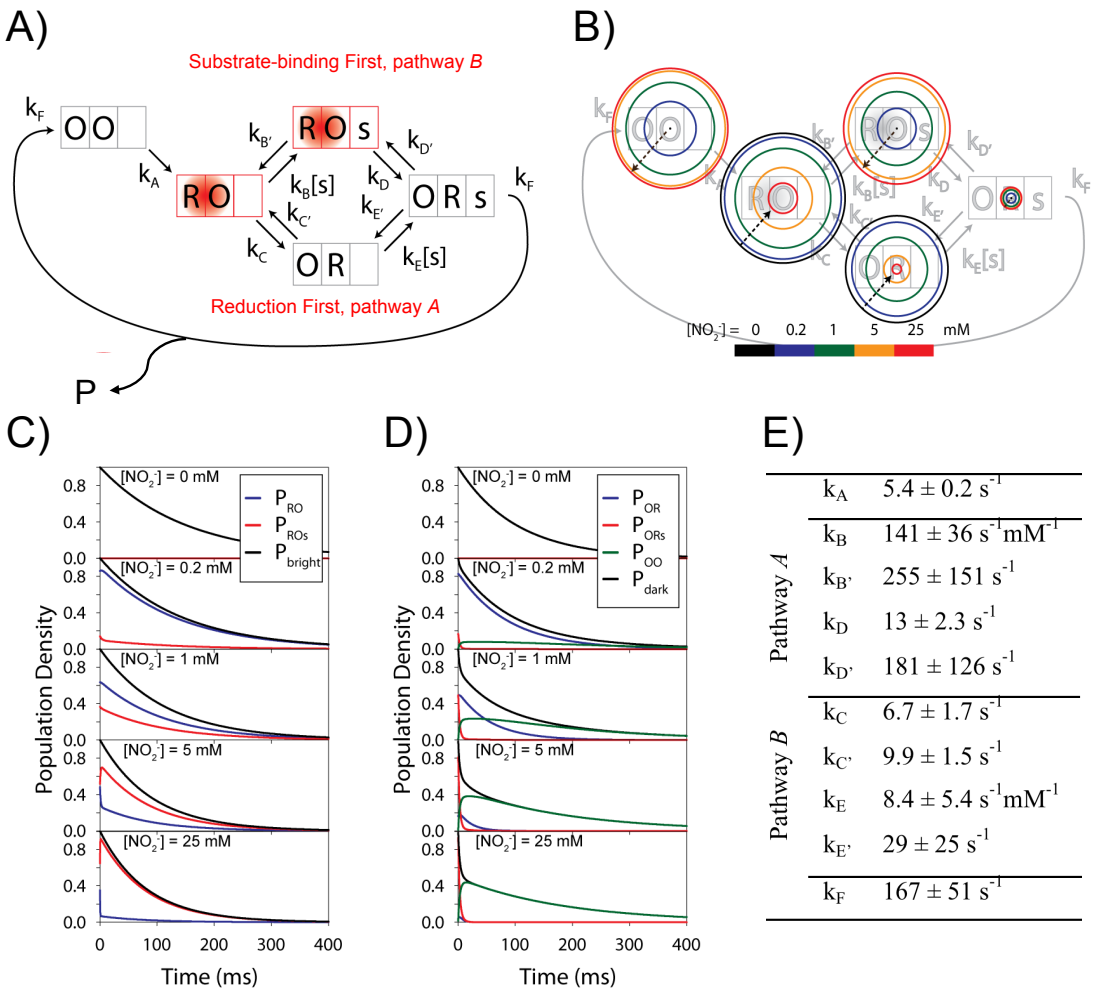

Pathway *A*	k_A	$5.4 \pm 0.2\ s^{-1}$
	k_B	$141 \pm 36\ s^{-1}mM^{-1}$
	$k_{B'}$	$255 \pm 151\ s^{-1}$
	k_D	$13 \pm 2.3\ s^{-1}$
	$k_{D'}$	$181 \pm 126\ s^{-1}$
Pathway *B*	k_C	$6.7 \pm 1.7\ s^{-1}$
	$k_{C'}$	$9.9 \pm 1.5\ s^{-1}$
	k_E	$8.4 \pm 5.4\ s^{-1}mM^{-1}$
	$k_{E'}$	$29 \pm 25\ s^{-1}$
	k_F	$167 \pm 51\ s^{-1}$

Figure 2.20 (A) "Random sequential" mechanism of NO_2^- reduction by CuNiRs as described by Wijma *et al.* [70]. The letters (**R** and **O**) in each box are, from left to right, the T1 Cu and T2 Cu. The letters **R** and **O** are the reduced and oxidized states, respectively, whilst NO_2^- and NO is **s** and **P**, respectively. Red-coloured states are highly fluorescent and referred as the bright part of the manifold, whilst non-coloured states are low fluorescent and referred as the dark part of manifold. The reduction-first and the substrate-binding first pathways are *A* and *B*, respectively. (B) Population distribution of each kinetic microstate of ATTO 647N labeled K329C bNiR during reduction of NO_2^- as a function of substrate concentration measured by ABEL trap in 10 mM Hepes pH 7.0 in 50 % glycerol at RT [122]. The circle area is directly proportional to the fractional population and each colour corresponds to a particular NO_2^- concentration, as shown on the colour bar. Population dynamics of each kinetic microstate in (C) bright and (D) dark manifold for each NO_2^- concentration, and (E) microscopic rate parameters for reduction of NO_2^- obtained for ABEL-trapped ATTO 647N labeled K329C bNiR molecules [122]. Images adapted from [122].

Parallel experiments of individually ABEL-trapped molecules of ATTO 647N labeled K329C bNiR probed in solution (10 mM Hepes pH 7.0 with 50 % glycerol) allowed a complete set of the kinetic parameters for the reduction of NO_2^- to be obtained [122]. The parameters were used to calculate the equilibrium population distribution of each kinetic state as a function of NO_2^- concentration (Figure 2.20.B). The population dynamics are described as the probabilities of occupying a particular state (**RO, ROs, OO, OR,** and **ORs**) as a function of time after entering pathway *A* or *B* (Figure 2.20.C and D). At low NO_2^- concentration, the enzyme molecules in the bright part of the manifold, follow pathway *A* in **RO** $\rightleftharpoons$ **OR** reaction, whilst at high NO_2^- concentration the population shifts rapidly from **RO** to **ROs** (**RO** $\rightleftharpoons$ **ROs** reaction), following pathway *B* what is in agreement with published results at pH > 6.5 [70]. The dark part of manifold can be entered through either **OR** or **ORs** states. At low NO_2^- concentrations, the enzyme is initially occupying the **OR** state (Figure 2.20.C), however, with increasing NO_2^- concentration, the probability of occupying **ROs** rather than **OR** states rapidly increases, with the majority of the population residing in the **OO** state (Figure 2.20.D). The 2-fold increase in the ET rates between the T1 Cu and T2 Cu (Figure 2.20.E) was determined between **RO** $\rightleftharpoons$ **OR** (k_C, Figure 2.20.A) and **RO** $\rightleftharpoons$ **ROs** (k_D, Figure 2.20.A) reactions, indicating that the ET to the T2 Cu site with coordinated OH^- is slower than when NO_2^- is bound, which is in agreement with the literature [70, 77]. Similar increase has been observed before [86], but since single molecule measurements using ABEL trap were performed in the presence of 50 % glycerol, a direct comparison of the kinetic rates is not possible.

2.5.3 *The populations distribution*

The FLIM analysis of NO_2^- reduction by ATTO 647N labeled K329C bNiR indicates a clear separation between the two distinct populations of enzyme molecules in the absence of substrate, which disappears when NO_2^- is added. Up to NO_2^- concentration of 50 μM, the P_{ox} distribution is broad and the separation becomes apparent only above the NO_2^- concentration of 500 μM. The population **B** separates considerably from population **A** as the substrate concentration increases. It is consistent with the change from the pathway *A* to *B* at NO_2^- concentration of ~ 520 μM that has been previously observed for immobilized gNiR [86]. Laser photoexcitation studies of ET between the T1 and T2 Cus suggest the existence of two apparent substrate-binding sites or two different affinities for NO_2^- [45, 47]. Krzeminski *et al.* have assigned these two

affinities as the different binding constants of NO_2^- to the reduced and oxidized T2 Cu site of immobilized ATTO 565 labeled L93C gNiR [86].

The increase in number of the individual enzyme molecules from population **B** upon increasing NO_2^- concentration observed during the FLIM measurements on immobilized bNiR (Figure 2.13.A and C) is consistent with the decrease in probability of finding molecules in **RO** state and concomitant growth of the **ROs** and **OO** populations observed during measurements of ABEL-trapped enzyme molecules (Figure 2.20.B). The molecules from population **B** spend less time in the reduced state than the molecules from population **A**, which suggests a faster depletion of the **RO** state from the pathway *B* than from the pathway *A*, in agreement with previously published results at pH > 6.5 [86, 122]. This increasing number of molecules in population **B** indicates the Michaelis-Menten constant relevant to route *B* (K_M^B) being much larger than the highest substrate concentration used in the experiment (5 mM), and therefore saturation with NO_2^- does not occur, in agreement with previous observations [70, 86].

The histograms of P_{ox} values, derived from FLIM of immobilized ATTO 647N labeled K329C bNiR, measured at three different pH values (pH 5.0, 7.5 and 9.0) show that at relatively high NO_2^- concentration (500 μM) at pH 5.0 molecules predominantly reside in population **B** whilst at 9.0 in population **A,** showing a lower degree of heterogeneity than at intermediate pH (pH 7.5) (Figure 2.16). At low pH and 500 μM NO_2^-, population **B** increases at the expense of population **A** what is an agreement with a decrease of the K_M^B value below pH 6.0 [70, 86]. The substrate inhibition at low pH (pH 5.45) and substrate activation at high pH (pH 6.85) of ET rate between the T1 Cu and T2 Cu has been observed by Krzeminski *et al.* [86]. At ~ 520 μM NO_2^- concentration, at pH 5.45, the ET rate between the T1 Cu and T2 Cu is almost 200-fold lower for **ROs** $\rightleftharpoons$ **ORs** than for **RO** $\rightleftharpoons$ **OR** transition [86] what is consistent with ET rate being slower with NO_2^- bound to the T2 Cu than when H_2O is bound [84, 85]. At low substrate concentration (< 520 μM), the ET rate is higher (almost 100-fold) at pH 5.45 than at 6.85 [86].

Wijma *et al.* proposed that there is an equilibrium between two forms of the reduced T2 Cu site of NiR. One of these is four-coordinate and is capable of binding NO_2^- whilst the other has the H_2O/OH^- ligand missing and is unable to bind NO_2^- (dead-end species, Figure 2.3.C) [70, 77]. At alkaline pH the equilibrium between these two is shifted towards the active form but at pH 5.5 almost half of NiR was found to be in the inactive form [77]. The conversion of the active to inactive form is slow (~ 0.1 s^{-1}) and can be reversed by the addition of NO_2^- [77]. The scheme discussed in

Figure 2.20.A does not account for the occurrence of this dead-end species. It could be argued that the increase in the number of molecules in population **B** with a concomitant decrease in those in population **A** upon increasing NO_2^- concentration at pH 7.5 is related to slow activation of the enzyme, and therefore, that population **A** corresponds to the reduced inactive species. This is unlikely as preliminary FLIM experiments at pH 9.0 showed that NiR predominantly resides in population **A** and that this is independent of NO_2^- concentration. At low pH (≤ 6.0) and low NO_2^- concentrations (50 - 250 μM) population **A** of ATTO 647N labeled K329C bNiR is negligible and the molecules reside predominantly in population **B** (the population distribution at pH 5.0 and at a NO_2^- concentration of 500 μM is shown in Figure 2.16). Only at high substrate concentrations (≥ 1 mM) do the number of molecules in population **A** significantly increases at the expense of population **B**.

Preliminary experiments show that ATTO 647N labeled K329C bNiR molecules interchange slowly between populations **A** and **B**, suggesting a large activation barrier between these two populations. This is possibly related to structural disorder around the T2 Cu site resulting in two conformations of the enzyme molecules. The fact that the population distribution of immobilized bNiR molecules depends on pH would suggest that this could be due to those residues responsible for proton delivery. Both, Asp92 and His249 (bNiR numbering) have been suggested to control the ET from the T1 to T2 Cu by delivering protons in an ET coupled protonation step [76, 124]. Proton-transfer coupling to the ET between the T1 and T2 Cu and NO_2^- reduction has been demonstrated [45 - 48] and at pH 7.0, the rate-limiting catalytic step is a single protonation event [45]. The conserved Asp92 is connected to the protein's surface *via* Asn90 and His254, which participate in the formation of two different proton channels. These channels were primarily identified in the crystal structures at different pH values, however, both can be observed in high-resolution crystal structures at pH 6.5 [36, 49, 50]. At pH 7.0, the Asn90 proton channel is sufficient to maintain essentially full enzymatic activity. Its disruption by mutating Asn90 to Ser (also in the Asn90Ser/His254Phe double mutant) results in an almost 70 % decrease in activity [45, 46]. However, proton delivery can be partially restored through the movement of the loop connecting Cys130 and His139 (both are T1 Cu ligands) that occurs upon binding of NO_2^- [46]. Although Asn90 has been recognized as the main proton source, the activities of the variants were only measured at pH 7.0. The His254 channel may be more significant at low pH. The influence of these proton channels on the heterogeneity of bNiR molecules could be examined by single molecule FLIM studies at low and high

pH using the Asn90Ser, His254Phe and Asn90Ser/His254Phe variants. Detailed analyses of population distributions and the time-dependent behavior of molecules of bNiR variants over a wide pH range would be necessary to quantify the influence of the proton delivery pathways on the enzyme's mechanism.

2.5 Conclusions

Single molecule measurements of bNiR provide a detailed insight into the catalytic mechanism of bNiR compared to previous "in-bulk" solution studies. Analysis of the FLIM images of agarose-immobilized ATTO 647N labeled K329C bNiR molecules indicate that the enzyme can follow either a substrate-binding first or a reduction first pathway, as described by the "random sequential" mechanism [70], consistent with reported results [86, 122]. The analysis of P_{ox} of single molecules of bNiR showed the presence of two populations, **A** and **B**, which distribution is dependent on the substrate concentration and pH. At pH 7.5, each of the populations of bNiR molecules follows one of the pathways of the "random sequential" mechanism, however, at high NO_2^- concentration, the substrate-binding pathway (corresponding to population **B**) seems to prevail over the reduction-first pathway (corresponding to population **A**), and the opposite happens at low substrate concentration. At extreme pH values (pH 5.0 and 9.0), in which enzyme shows different "in-bulk" behavior [70], the distinction between the two populations almost disappears. Population **A** prevails over population **B** at high pH, whilst at low pH the reverse occurs.

The crucial advantage of the presented FLIM measurements is not only the possibility of quick data collection for each full image scan but also that the long-term behavior of a molecule can be monitored while minimizing interference by bleaching. The main limitation of this method is that the signal is integrated over few milliseconds, and therefore events faster than the integration time cannot be easily probed. To enable observation of these faster events, higher time resolution measurements but with a longer trapping-window than can be achieved with the current ABEL trap, are necessary.

2.6 References

1) Averill B.A., 1996, Chem. Rev., 96, 2951-2964

2) Zumft W.G., 1997, Microbiol. Mol. Biol. Rev., 61, 533-616

3) Wasser I. M., de Vries S., Moenne-Loccoz P., Schroder I., Karlin K. D., 2002, Chem. Rev., 102, 1201-1234

4) Ferguson S.J., 1998, Curr. Opin. Chem. Biol., 2, 182-193

5) Merkle A.C., Lehnert N., 2012, Dalton Trans., 41, 3355-3368

6) Wijma H. J., Canters G. W., de Vries S., Verbeet M. P., 2004, Biochemistry, 43, 10467-10474

7) Coyne M. S., Arunakumari A., Averill B. A., Tiedje J. M., 1989, Appl. Environ. Microbiol., 55, 2924-2931

8) Kakutani T., Watanabe H., Arima K., Beppu T., 1981, J. Biochem., 89, 453-461

9) Iwasaki H., Matsubara T., 1972, J. Biochem., 71, 645-652

10) Masuko M., Iwasaki H., Sakurai T., Suzuki S., Nakamura A., 1984, J. Biochem., 96, 447-454

11) Zumft W.G., Gotzmann D.J., Kroneck P.M., 1987, Eur. J. Biochem., 168, 301-307

12) Sawada E., Satoh T., Kitamura H., 1978, Plant Cell Physiol., 19, 1339-1351

13) Pinho D., Besson S., Brondino C.D., Castro de B., Moura I., 2004, Eur. J. Biochem., 271, 2361-2369

14) Yamaguchi K., Kobayashi M., Kataoka K., Suzuki S., 2003, Biochem. Biophys. Res. Commun., 300, 36-40

15) Murphy M.E.P., Lindley P.F., Adman E.T., 1997, Protein Sci., 6, 761-770

16) Komori H., Hiyazaki K., Higuchi Y., 2009, FEBS Lett., 583, 1189-1195

17) Inoue T, Gotowda M., Deligeer, Kataoka K., Yamaguci K, Suzuki S., Watanabe H., Gohow M., Kai Y., 1998, J. Biochem, 124, 876-879

18) Solomon E. I., 2006, Inorg. Chem., 45, 8012-8025

19) Veselov A., Olesen K., Sienkiewicz A., Shapleigh J. P., Scholes C. P., 1998, Biochemistry, 37, 6095-6105

20) Olesen K., Veselov A., Zhao Y., Wang Y., Danner B., Scholes C. P., Shapleigh J. P., 1998, Biochemistry, 37, 6086-6094

21) Basumallick L., Szilagyi R. K., Zhao Y., Shapleigh J. P., Scoles C. P. Salomon E. I., 2003, J. Am. Chem. Soc., 125, 14784-14792

22) Sato K., Dennison C., 2006, Chem. Eur. J., 12, 6647-6659

23) Suzuki S., Kataoka K., Yamaguci K., 2000, Acc. Chem. Res., 33, 728-735

24) Dodd F.E., Hasnain S.S., Hunter W.N., Abraham Z.H., Debenham M., Kanzler H., Eldridge M., Eady R.R., Ambler R.P., Smith B.E., 1995, Biochemistry, 34, 10180-10186

25) Deligeer, Kataoka K., Yamaguchi K., Suzuki S., 2000, Bull. Chem. Soc. Jpn., 73, 1839-1840

26) Hormel S., Adman E.T., Walsh K., Beppu T., Titani K., 1986, FEBS Lett., 197, 301-314

27) Murphy L.M., Dodd F.E., Yousafzai F.K., Eady R.R., Hasnain S.S., 2002, J. Mol. Biol., 315, 859-871

28) Kukimoto M., Nishiyama M., Murphy M. E. P., Turley S., Adman E. T., Horinouchi S., Beppu T., 1995, Biochemistry, 33, 5246-5252

29) Libby E., Averill B. A., 1992, Biochem. Biophys. Res. Commun., 187, 1529 – 1535

30) Paraskevopoulos K., Hough M.A., Sawers R.G., Eady R.R., Hasnain S.S., 2007, J. Biol. Inorg. Chem., 12, 789-796

31) Barrett M.L., Harris R.L., Antonyuk S., Hough M.A., Ellis M.J., Sawers G., Eady R.R, Hasnain S.S., 2004, Biochemistry, 43, 16311-16319

32) Impagliazzo A., Ubbink M., 2004, J. Am. Chem. Soc., 126, 5658-5659

33) Impagliazzo A., Blok A.J., Cliff M.J., Ladbury J.E., Ubbink M., 2007, J. Am Chem. Soc., 129, 226-233

34) Nojiri M., Koteishi H., Nakagami T., Kobayashi K., Inoue T., Yamaguchi K., Suzuki S., 2009, Nature, 462, 117-120

35) Dodd F.E., Hasnain S.S., Abraham Z.H., Eady R.R., Smith B.E., 1997, Acta. Crystallogr., D53, 406-418

36) Ellis M.J., Dodd F.E., Sawers G., Eady R.R., Hasnain S.S., 2002, J. Mol. Biol., 328, 429-438

37) Adman E. T., Godden J. W., Turley S., 1995, J. Biol. Chem., 270, 27458-27474

38) Ellis M.J., Antonyuk S.V., Strange R.W., Sawers G., Eady R.R., Hasnain S.S., 2004, Inorg. Chem., 43, 7591-7593

39) Tocheva E.I., Rosell F.I., Mauk A.G., Murphy M.E., 2004, Science, 304, 867-870

40) Murphy M. E. P., Turley S., Adman E. T., 1997, J. Biol. Chem., 272, 28455-28460

41) The PyMOL Molecular Graphics System, Version 1.6.0.0 Schrödinger, LLC.

42) Lehnert N., Cormalissen U., Neese F., Ono T., Noguchi Y., Okamoto K., Fijisawa K., 2007, Inorg. Chem.. 46, 3916-3933

43) Boulanger M.J., Murphy M.E., 2003, Protein Sci., 12, 248-256

44) Ellis M.J., Prudencio M., Dodd F.E., Strange R.W., Sawers G., Eady R.R., Hasnain S.S., 2002, J. Mol. Biol., 316, 51-64

45) Brenner S., Heyes D.J., Hay S., Hough M.A., Eady R.R., Hasnain S.S., Scrutton N.S., 2009, J. Biol. Chem., 284, 25973-25983

46) Leferink, G.H., Han C., Antonyuk, S.V., Heyes, D.J., Rigby S.E.J., Hough M.A., Eady R.R., Scrutton N.S., Hasnain S.S., 2011, Biochemistry, 50, 4121-4131

47) Leferink N.G.H., Eady R.R., Hasnain S.S., Scrutton N.S., 2012, FEBS J. 279, 2174-2181

48) Leferink N.G.H., Pudney C.R., Brenner S., Heyes D.J., Eady R.R., Hasnain .S., Hay S., Rigby S.E.J., Scrutton N.S., 2012, FEBS Letters, 586, 578-584

49) Ellis M.J., Dodd F.E., Strange R.W., Prudencio M., Sawers G., Eady R.R., Hasnain S.S., 2001, Acta. Crystallogr. D57, 1110-1118*)*

50) Dodd F.E., Van Beeumen, J., Eady R.R., Hasnain S.S., 1998, J. Mol. Biol., 282, 369-382

51) Hough M.A., Eady, R.R., Hasnain S.S., 2008, Biochemistry, 47, 13547-13553

52) Antonyuk S. V., Strange R. W., Sawers G., Eady R. R., Hasnain S.S., 2005, Proc. Natl. Acad. Sci. USA, 102, 12041-12046

53) Merkle A.C., Lehnert N., 2009, Inorg. Chem., 48, 11504-11506

54) Tolman W.B., 1991, Inorg. Chem., 30, 4877-4880

55) Casella L., Carugo C., Gullotti M., Doldi S., Frassoni M., 1996, Inorg. Chem., 35, 1101-1113

56) Jiang F., Conry R.R., Bubacco L., Tyeklar Z., Jacobson R.R., Karlin K.D., Peisach J., 1993, J. Am. Chem. Soc., 115, 2093-2102

57) Komeda N., Nagao H., Adachi G.Y., Suzuki M., Uehara A., Tanaka K., 1993, Chem. Lett., 1521-1524

58) Komeda N., Nagao H., Kushi Y., Adachi G., Suzuki M., Uehara A., Tanaka K., 1995, Bull. Chem. Soc. Jpn., 68, 581-589

59) Halfen J.A., Tolman W.B., 1994, J. Am. Chem. Soc., 116, 5475-5476

60) Halfen J.A., Mahaparta S., Olmstead M.M., Tolman W.B., 1994, J. Am. Chem. Soc., 116, 2173-2174

61) Halfen J.A., Mahaptra S., Wilkinson E.C., Gengenbach A.J., Yound V.G., Que L., Tolman W.B., 1996, J. Am. Chem. Soc., 118, 763-776

62) Monzani E., Anthony G.J., Koolhaas A., Spandre A., Leggieri E., Casella L., Gullotti M., Nardin G., Randaccio L., Fontani M., Zanello P., Reedijk J., 2000, J. Biol. Inorg. Chem., 5, 251-261

63) Kujime M., Izumi C., Tomura M., Hada M., Fujii H., 2008, J. Am. Chem. Soc., 130, 6088-6089

64) Woollard-Shore J.G., Holland J.P., Jones M.W., Dilworth J.R., 2010, Dalton Trans., 39, 1576-1585

65) Wright A.M., Wu G.A., Hayton T.W., 2010, J. Am. Chem. Soc., 132, 14336-14337

66) Carrier S.M., Ruggiero C.E., Tolman W.B., 1992, J. Am. Chem. Soc., 114, 4407-4408

67) Ruggiero C.E., Carrier S.M., Antholine W.E., Whittaker J.W., Crames C.J., Tolman W.B., 1993, J. Am. Chem. Soc., 115, 11285-11298

68) Fujisawa K, Tateda A., Miyashita Y., Okamoto K., Paulat F., Praneeth V.K.V., Merkle A., Lehnert N., 2008, J. Am. Chem. Soc., 130, 1205-1213

69) Strange R.W., Murphy L.M., Dodd F.E., Abraham Z.H.L., Eady R.R., Smith B.E., Hasnain S.S., 1999, J. Mol. Biol., 287, 1001-1009

70) Wijma H.J., Jeuken L.J.C., Verbeet, M.P., Armstrong F.A., Canters G.W., 2006, J. Biol. Chem., 281, 16340-16346

71) De Marothy S.A., Blomberg M.R., Siegbahn P.E., 2007, J. Comput. Chem., 28, 528-539

72) Hough M.A., Antonyuk S.V., Strange, R.W., Eady, R.R., Hasnain S.S., 2008, J. Mol. Biol., 378, 353-361

73) Hough M.A., Ellis M.J., Antonyuk S., Strange R.W., Sawers G., Eady R.R., Hasnain S.S., 2005, J. Mol. Biol., 350, 300-309

74) Kataoka K., Furusawa H., Takagi K., Yamaguchi K., Suzuki S., 2000, J. Biochem., 127, 345-350

75) Suzuki S., Kataoka K., Yamaguci K., 2000, Acc. Chem. Res., 33, 728-735

76) Boulanger M. J., Kukimoto M, Nishiyama M., Horinouchi S., Murphy M. E. P., 2000, J. Biol. Chem., 275, 23957-23964

77) Wijma H. J., Jeuken L. J. C., Verbeet M. P., Armstrong F. A., Canters G. W., 2007, J. Am. Chem. Soc., 129, 8557-8565

78) Hulse C.L., Averill B.A., Tiedje J.M., 1989, J. Am. Chem. Soc., 111, 2322-2323

79) Suzuki S., Yoshimura T., Kohzuma T., Shidara S., Masuko M., Sakurai T., Iwasaki H., 1989, Biochem. Biophys. Res. Commun., 164, 1366-1372

80) Abraham Z. L., Smith B. E., Howes B. D., Lowe D. J., Eady R. R., 1997, J. Biochem., 324, 511-516

81) Sundararajan M., Hillier I.H., Burton N.A., 2007, J. Phys. Chem. B, 111, 5511-5517

82) Kobayashi K., Tagawa S., Deligeer, Suzuki S., 1999, J. Biochem., 126, 408-412

83) Farver O., Eady R.R., Abraham Z.H.L., Pecht I., 1998, FEBS Letters, 436, 239-242

84) Suzuki S., Deligeer, Yamaguchi K., Kataoka K., Kobayashi K., Tagawa S., Kohzuma T., Shidara S., Iwasaki H., 1997, J. Biol. Inorg. Chem., 2, 265-274

85) Suzuki S., Kohzuma T., Deligeer, Yamaguchi K., Nakamura N., Shidara S., Kobayashi K., Tagawa S., 1994, J. Am. Chem. Soc., 116, 11145-11146

86) Krzeminski L., Ndamba L., Canters G.W., Aartsma T.J., Evans S.D., Jeuken L.J.C, 2011, J. Am. Chem. Soc., 133, 15085-15093

87) Kuznetsova S., Zauner G., Aartsma T.J., Engelkamp H., Hatzakis N., Rowan A.E., Nolte R.J.M., Christianen P.C.M., Canters G.W., 2008, Proc. Natl. Acad. Sci. USA, 105, 3250-3255

88) Lu X. P., Xun L., Xie X. S., 1998, Science, 282, 1877-1882

89) Velonia K., Flomenbom O., Loos D., Masuo S., Cotlet M., Engelborghs Y., Hofkens J., Rowan A. E., Klafter J., Nolte R. J. M., De Schryver F. C., 2005, Angew. Chem. Int. Ed. Engl., 44, 560-564

90) English B. P., Min W., van Oijen A. M., Lee K. T., Luo G. B., Sun H. Y., Cherayil B. J., Kou S. C., Xie X. S., 2006, Nat. Chem. Biol., 2, 87-94

91) Smiley R. D., Hammes G. G., 2006, Chem. Rev., 106, 3080-3094

92) Edman L., Foldes-Papp Z., Wennmalm S., Rigler R., 1999, Chem. Phys., 247, 11-22

93) Bollinger L.M., Thomas G.E., 1961, Rev. Sci. Instrum., 32, 1044-1051*)*

94) Becker W., Bergmann A., Hink M.A., Konig K., Benndorf K., Biskup C., 2004, Microsc. Res. Techniq., 63, 58-66

95) Cohen A.E., Moerner W.E., 2008, Opt. Express., 16, 6941–6956

96) Rasnik I., McKinney S.A., Ha T., 2005, Acc. Chem. Res., 38, 542-548

97) Ha T., Rasnik I., Cheng W., Bobcock H.P., Gauss G.H., Lohman T.M., Chu S., 2002, Nature, 419, 638-641

98) Goldsmith R.H., Moerner W.E., 2010, Nat. Chem., 2, 179-186

99) Talaga D.S., Lau W.L., Roder H, Tang J., Jia Y., DeGrado W.F., Hochstrasser R.M., 2000, Proc. Natl. Acad. Sci. USA, 97, 13021–13026

100) Friedel M., Baumketner A., Shea J.E., 2006, Proc. Natl. Acad. Sci. USA, 103, 8396–8401

101) Cohen A.E., Moerner W.E., 2006, Proc. Natl. Acad. Sci. USA, 103, 4362–4365

102) Wang Q., Goldsmith R.H., Jiang Y., Bockenhouer S.P., Moerner W.E., 2012, Acc. Chem. Res., 45, 1955-1964

103) Schmauder R., Alagaratnam S., Chan C., Schmidt T., Canters G.W., Aartsma T.J., 2005, J. Biol. Chem., 10, 683-687

104) Kuznetsova S., Zauner G., Schmauder R., Mayboroda O.A., Deelder A.M., Aartsma T.J., Canters G.W., 2006, Anal. Biochem., 350, 52-60

105) Sorokina M., Koh H.R., Petel S.S., Ha T., 2009, J. Am. Chem. Soc., 131, 9630-9631

106) Tinnefeld P., Buschmann V., Herten D.P., Han K.T., Sauer M., 2000, Single Mol., 1, 215-223

107) Heilemann M., Herten D.P., Heintzmann R., Cremer C., Muller C., Tinnefeld P., Weston K.D., Wolfrum J., Sauer M., 2002, Anal. Chem., 74, 3511-3517

108) Gerritsen H.C., Draaijer A., van den Heuvel D.J., Agronskaia A.V., 2006, *Handbook of Biological Confocal Microscopy* (Ed.: Pawley J.B.), Springer, New York, pp. 516-534

109) Strianese M., Zauner G., Tepper A.W., Bubacco L., Breukink E., Aartsma T.J., Canters G.W., Tabares L.C., 2009, Anal. Biochem., 385, 242-248

110) Strianese M., De Martino F., Pavone V., Lombardi A., Canters G.W., Pellecchia C., 2010, J. Inorg. Biochem., 104, 619-624

111) Gustiananda M., Andreoni A., Tabares L.C., Tepper A.W., Fortunato L., Aartsma T.J., Canters G.W., 2012, Biosens. Bioelectron., 31, 419-425

112) Strianese M., Zauner G., Tabares L.C., Tepper A.W., De Martino F., Pellecchia C., Aartsma T.J., Canters G.W., 2013, Chemistry, 19, 14977-14982

113) Salverda J.M., Patil A.V., Mizzon G., Kuznetsova S., Zauner G., Akkilic N., Canters G.W., Davis J.J., Heering H.A., Aartsma T.J., 2010, Angew. Chem. Int. Ed. Engl., 49, 5776-5779*)*

114) Patil A.V., Davis J.J., 2010, J. Am. Chem. Soc., 132, 16938-16944

115) Krzeminski L., Cronin S., Ndamba L., Canters G.W., Aartsma T.J., Evans S.D., Jeuken L.J., 2011, J. Phys. Chem. B, 115, 12607-12614

116) van Oijen A.M., Blainey P.C., Crampton D.J., Richardsn C.C., Ellenberger T., Xie X.S., 2003, Science, 301, 1235-1238*)*

117) Shi J., Dertouzos J., Gafni A., Steel D., 2008, Methods Enzymol., 450, 129-157

118) Kakutani T., Watanabe H., Arima K., Beppu T., 1981, J. Biochem., 89, 463-472

119) Suzuki S., Kataoka K., Yamaguchi K., Inoue T., Kai Y., 1999, Coord. Chem. Rev., 190-192, 245-265

120) Nicolardi S., Andreoni A., Tabares L.C., van der Burgt Y.E., Canters G.W., Deelder A.M., Hensbergen P.J., 2012, Anal. Chem., 84, 2512-2520

121) Stirpe A., Sportelli L., Wijma H., Verbeet M.P., Guzzi R., 2007, Eur Biophys J., 36, 805-813

122) Goldsmith R.H., Tabares L.C., Kostrz D., Dennison C., Aartsma T.J., Canters G.W., Moerner W.E., 2011, Proc. Natl. Acad. Sci. USA, 108, 17269-17274

123) Edman L., Rigler R., 2000, Proc. Natl. Acad. Sci. USA, 97, 8266-8271
124) Boulanger M.J., Murphy M.E., 2001, Biochemistry, 40, 9132-9141

CHAPTER 3

Production of laccases from *Trametes versicolor* and *Streptomyces coelicolor* for studies on catalytic activity and fluorescence-based biosensing applications

3.1 Introduction

3.1.1 *Occurrence and physiological function of laccases*

Laccases (*p*-diphenol: dioxygen oxidoreductases, EC 1.10.3.2) are members of the multicopper oxidase (MCO) family of enzymes and catalyze the four-electron reduction of molecular oxygen (O_2) to water (H_2O) in four, one-electron reductions of four substrate molecules [1 - 5]. Laccases are widely distributed especially among plants, higher fungi and bacteria. While in plants they are involved in lignification, wound healing and iron metabolism [3, 6, 7], fungal laccases take part in lignin degradation, stress defense, pathogenesis and detoxification, and in development and morphogenesis of fungi [3 - 5, 8]. The presence of laccases was reported in larval and adult cuticles of several insects, where the protein is associated with the sclerotization process [9]. In bacteria the enzymes are involved in copper (Cu) homeostasis, sporulation and pigmentation of spores [10, 11].

3.1.2 *Reactivity of laccases*

The catalytic center of laccases consists of type 1 (T1), type 2 (T2) and binuclear type 3 (T3) Cu sites [12] (Chapter 1.2), and is similar to that found in ascorbate oxidase (AO) [13] and ceruloplasmin (Cp) [14]. The T2 and two T3 Cu ions form a trinuclear cluster that is commonly referred to as the T2/T3 Cu site (Chapter 1.2.4). The T1 Cu is the initial port of entry of electrons into the enzyme, whilst at the T2/T3 Cu site O_2 is reduced to H_2O. The T1 Cu sites of laccases posses a broad range of reduction potentials that has led to the classification of low (~ 430 mV versus the normal hydrogen electrode, NHE), mid (from 470 - 710 mV) and high (~ 800 mV) potential enzymes [1]. Reduction potential of the T2/T3 Cu site (determined only for several laccases) is usually similar that of the T1 Cu site [15, 16]. Laccases directly oxidize substrates with the reduction potentials lower to that of their T1 Cu site, with the rate of reaction being dependent on the reduction potential difference between the enzyme and the substrate [17, 18] (other factors such as steric hindrance of the substrate and size/shape of the substrate-binding pocket also affect the reaction rate [19, 20]). Therefore, high reduction potential of the T1 Cu site increases the range of oxidizable substrates. This and the broad substrate specificity make the high potential laccases especially promising for industrial and biotechnological purposes [3 - 5, 21 - 23].

Laccases catalyze the oxidation of a variety of aromatic compounds, including *ortho*- and *para*-substituted phenols, polyphenols, anilines, aryl diamines, methoxy-substituted phenols, hydroxyindols, benzenethiols and also some inorganic ions such as $[Mo(CN)_8]^{4-}$ and $[Fe(CN)_6]^{4-}$ (Figure 3.1.A) [1, 5]. Laccases remove a single electron from a phenolic substrate generating a free radical [24]. Depending on the conditions, this species can be transformed into a quinone or undergo non-enzymatic reactions like hydratation, disproportionation and polymerization. Non-phenolic substrates, phenols with reduction potential exceeding that of the T1 Cu site of laccase or molecules too bulky to enter the substrate-binding sites (for example lignin-like substrates) are not directly oxidized by the enzyme. However, catalysis can be carried out by the inclusion of low molecular weight organic compounds called mediators [25, 26] (Figure 3.1.B). The most common mediators are 2,2'-azinobis-3-ethylthiazoline-6-sulfonat (ABTS, also used as an artificial substrate), 1-hydro-xybenzotriazole (HOBT), N-hydro-xyphthalimide (NHPI) and 2,2,6,6-tetramethylpiperidine-1-oxyl (TEMPO).

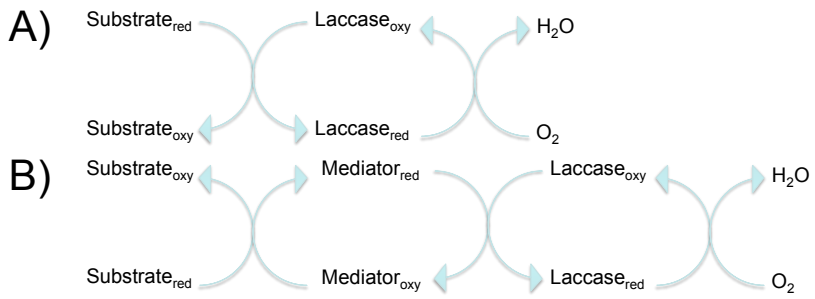

Figure 3.1 Schematic representations of laccase-catalyzed reactions in the absence (A) and in the presence (B) of redox mediators.

3.1.3 *Potential applications of laccases*

A number of potential applications for laccases have been investigated in several sectors [21, 27 - 31] including among others pharmaceutical [32, 33], pulp and paper bleaching [28], food and beverages [29, 34, 35], textiles [36], and cosmetic [37, 38] industries. The enzymes have been applied in organic synthesis [27], degradation of dyes and xenobiotics, bioremediation of coloured industrial effluents [30, 31, 39, 40], and wastewater treatment by degradation of a variety of persistent environmental pollutants [21, 41].

Laccases have been employed in the construction of biocathodes for biofuel cells [42 - 47]. The design involves the application of enzymes as biocatalysts for the

conversion of chemical energy into electrical current. Electricity that is generated from the oxidation of biofuels (glucose, glycerol or ethanol) coupled to concomitant reduction of O_2 to H_2O by laccases is expected to suffice for micro devices requiring relatively low power. To date, bioelectrodes with immobilized laccase from *Trametes versicolor* and small laccase (SLAC) from *Streptomyces coelicolor* [43, 46, 47] have great potential for successful use in biofuel cells.

In addition, laccases have been used in the construction of biosensors for clinical and environmental purposes [48]. The enzymes are mainly used for the determination of various phenolic compounds [49 - 59], plant flavonoids [60], O_2 [61], azides [62] and cyanides [63]. Selectivity and sensitivity of laccase-based biosensors have been improved by enzyme co-immobilization either with tyrosinase [64, 65], glucose dehydrogenase (GDH) [66 - 68] or peroxidases [69]. Biosensors based on the dual enzyme coupled system of laccase and GDH have been used for selective detection of morphine [66] and catecholamines [67, 68]. Detection of catecholamines at submicromolar detection limits has also been achieved using a laccase/peroxidase dual enzyme coupled system [69], laccase co-immobilized with an osmium redox polymer [70] and recently, using a laccase-based optical fiber biosensor [71].

3.1.4 *Heterologous expression of laccase from Trametes versicolor*

Production of laccases from native sources cannot meet the increasing demands for the enzyme, mainly due to low yields and long and expensive cultivation. Recombinant protein over-expression offers higher productivity at lower cost, and therefore, it is of importance for both industrial and biotechnological applications [72]. Additionally, protein engineering that requires a good over-expression system is often used to improve the biochemical (such as stability or substrate specificity) and catalytic efficiency of the enzyme [17, 72].

Among the best-characterized high potential laccases is that from the white-rot fungus *T. versicolor*. The fungus secretes several iso-forms [73, 74] that also differ in their glycosylation pattern. Hence the exact number of different laccases produced is not known [75, 76]. The difference in isoelectric point (pI values) of laccases has commonly been used as a criterion to identify these different iso-forms, and using this, two chromatographic fractions (A and B) have been separated by ion-exchange chromatography [77]. Isoelectric focusing has revealed that fraction A contains two components (pI 3.07 - 3.27), whilst fraction B has ten components (pI 4.64 - 6.76) [78,

79]. The production of active recombinant laccases from *T. versicolor* has previously been reported in plants [80, 81], yeast [73, 79, 82 - 94] and filamentous fungi [90, 95 - 98]. Filamentous fungi are generally good hosts for production of proteins but are more time consuming to work with compared to yeast [72]. No bacterial over-expression system producing an active *T. versicolor* laccase has been reported. However, laccases from *Cyathus bulleri* and *Ridigoporus lignosus* has been expressed in *Escherichia coli*, making them the first fungal laccases expressed in a bacterial host [99, 100].

3.1.5 *Characterization of the two- and three-domain MCOs*

The crystal structures of only fungal and bacterial laccases have been published. A structural model of the plant laccase from *Populus trichocarpa* is available [101]. The first crystal structure of a fungal laccase was solved for the T2 Cu depleted form of the enzyme from *Coprinus cinereus* [102]. Since then, a number of crystal structures of fungal laccases have been solved, including those from *T. versicolor* (TvL1KYA [75] and TvL1GYC [103]), *Pycnoporus cinnabarinus* [76], *Melanocarpus albomyces* [104], *Cerrena maxima* [105] and *R. lignosus* [106], all with a full complement of Cu ions. The enzymes are monomeric with three cupredoxin-like, metal-binding domains (MBD-1, MBD-2 and MBD-3, Chapter 1.3) The amino-acid sequences of the two crystallized iso-forms of *T. versicolor* laccases share ~ 80 % similarity, however, the crystal structures of TvL1KYA and TvL1GYC, superimpose with a root-mean square deviation (RMSD) of 0.343 Å for C^{α} atoms. A number of crystal structures of bacterial laccases have been determined. These include the monomeric, three-domain CotA from *Bacillus subtilis* [107] and the trimeric, two-domain laccases such as SLAC from *S. coelicolor* [108 - 110], mgLAC from metagenome database [111] and blue copper oxidase (BCO) from *Nitrosomonas europaea* [112].

Compared to three-domain laccases, two-domain laccases lack the second domain, however, a trimeric arrangement of those enzymes ensures stability and enables the same enzymatic function using different quaternary structure. Superposition of the structure of SLAC [108] with those of TvL1KYA and TvL1GYC gives RMSDs of 5.50 Å and 6.91 Å, respectively, for C^{α} atoms. Nakamura *et al.* suggested that the three-domain AO, three-domain laccases and six-domain Cp have evolved from cupredoxins *via* formation of trimeric two-domain MCOs [113] (for more details see Chapter 1.3). Three types (A, B and C) of these trimeric forms have been predicted and classified according to the location of T1 Cu sites [113]. Type A two-domain MCOs

contain a T1 Cu site in each domain, whereas type B (e.g. SLAC) and type C (e.g. mgLAC and BCO) house the T1 Cu site in MBD-2 and MBD-1, respectively. In three-domain laccases, the T1 Cu is located in MBD-3. The T2/T3 Cu cluster is located either between MBD-1 and MBD-2 of each two-neighboring chains of the trimer of the two-domain MCOs or at the interface of MBD-1 and MBD-3 of the three-domain MCOs.

3.1.6 *Structure of the active sites*

Crystallographic and spectroscopic studies of laccases have generated a detailed description of their active sites [1, 12, 75, 76, 102 - 106, 114 - 119] (Chapter 1.2). The three types of Cu sites in laccases differ in their spectroscopic properties [1, 116, 117, 120, 121]. The T1 Cu of TvL1KYA (and TvL1GYC) and SLAC is coordinated to two His and Cys in a trigonal planar [75, 103] and trigonal pyramidal [108] geometry, respectively (Chapter 1.3). A non-coordinating Phe in *T. versicolor* laccases is homologous to the axial Met ligand to the T1 Cu in SLAC. In some laccases (such as laccases from *M. albomyces* [104] or *R. lignosus* [106]), a non-coordinating axial Leu is present (Chapter 1.2.1). The T1 and the T2/3 Cus are 12 - 13 Å apart connected by a His(T3 Cu)-Cys(T1 Cu)-His(T3 Cu) motif, which is highly conserved among MCOs and is suggested to facilitate fast electron transfer (ET) between the Cu centers [1]. The T2 Cu, which is coordinated by two His residues and OH^-/H_2O, has a trigonal planar geometry, whereas both T3 Cus are coordinated by three His residues and a bridging oxygen ligand (OH^- or O^{2-}) in distorted tetrahedral geometries (Chapters 1.2.4 and 1.3).

3.1.7 *Catalytic mechanism of laccases*

Even though much effort has been devoted to describe the reduction of O_2 into H_2O by MCOs, the mechanism is still the subject of considerable debate. Solomon and coworkers have investigated in detail the kinetic and spectral features of intermediates present during O_2 reduction by MCOs [114, 122 - 126], mainly *Rhus vernificera* (Japanese lacquer tree) laccase [122, 126 - 128], and more recently Fet3p from *Saccharomyces cerevisiae* [128, 129]. Reduced laccase (4 Cu(I)) reacts with O_2 *via* two sequential two-electron transfer steps generating first a "peroxy" intermediate (PI, 2 Cu(I), 2 Cu(II)) [122, 130 - 133] followed by a "native" intermediate (NI, 4 Cu(II))

[122, 124] (Figure 3.2.A). The NI is structurally distinct from the fully oxidized resting form of the enzyme (RO) [124, 131 - 136]. The T2/T3 Cus in NI are bridged by μ_3-oxo ligand and the T3 Cus are additionally bridged by a μ_2-hydroxo moiety, whilst in RO only the μ_2-hydroxo between the T3 Cu is present (Figure 3.2.A). Rapid reduction of the NI indicates that NI rather than RO is the catalytically relevant fully oxidized form of the enzyme [122, 124, 137]. The formation of NI has been observed in native laccases [138, 139] (NI was also identified in the crystal structure of laccase from *Lentinus tigrinus* [140]), whilst PI has been trapped and characterized using the T1 Hg(II) derivative [122, 130, 131] and a C484S (T1 depleted, T1D) Fet3p variant [141, 142]. The NI and PI species are formed at similar rates (1.7×10^6 and 2.2×10^6 $M^{-1}s^{-1}$, respectively [130]) and the transition from PI to NI is very fast in the native enzyme ($k > 350\ s^{-1}$) [126]. Multiple studies indicate that PI is a kinetically competent precursor to NI [122, 143, 144].

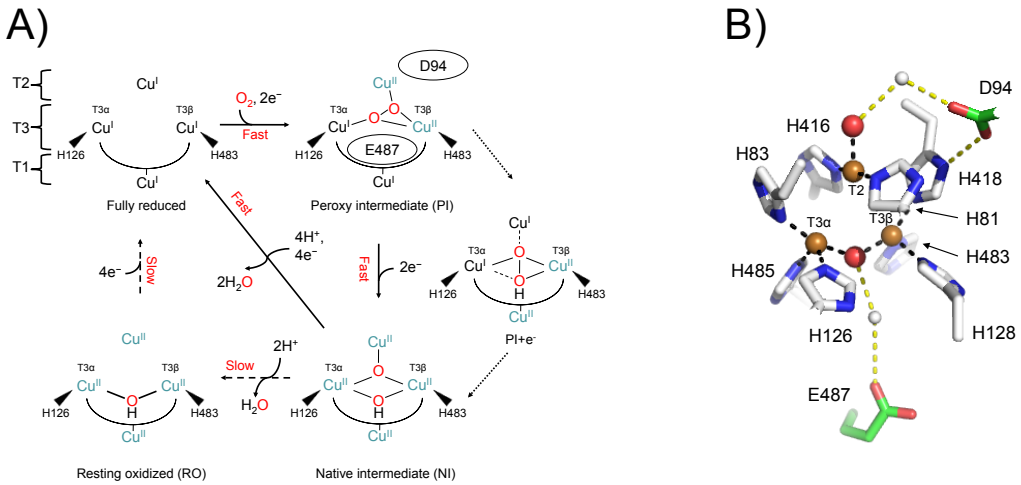

Figure 3.2 (A) Mechanism of O_2 reduction by Fet3p. Black solid arrows indicate the steps that take place in the catalytic cycle of the MCOs. Dashed arrows indicate steps that can be experimentally observed but are not part of the catalytic cycle. Dotted arrows indicate the transfer of an electron from the T1 Cu to the T2 Cu to create PI+e$^-$ that occurs on going from NI to PI but is not experimentally observed in the native enzyme (adapted from [125, 145]). (B) Structure of the active site of a resting oxidized AO [13] with the side chains numbered as in Fet3p [146]. The side chains of Asp94 and Glu487 are shown as green sticks. The T2 and T3 Cus are brown, H_2O/OH^- ligands are red and waters are gray spheres.

Figure 3.2.A shows the current understanding of the mechanism based on spectroscopic, kinetic and computational studies [4, 123, 125, 137]. The T2/T3 Cu ions

contribute differently to O_2 reactivity [147]. Mutation of the T3β Cu His483, but not of T3α Cu His126 ligand (Figure 3.2.B), strongly affects the electronic structure of the reduced enzyme, disabling fast two-electron reduction of O_2 to form PI [145, 147]. Formation of PI is a rate-determining step in O_2 reduction [114, 125], and the computational model of PI (Figure 3.2.A), in which O_2 is bound as peroxide bridge to the T2/T3 Cus, implicates the involvement of anionic Asp (Asp94 in Fet3p corresponding to the Asp77 in TvL1KYA), nearby the T2 Cu and the T3β Cu, in the stabilization of this intermediate [123, 126, 132, 144, 148]. In Fet3p, the carboxylate moiety of Asp94 is suggested to be involved in hydrogen bonding with the T2 Cu water-derived ligand (mediated by H_2O) and a T3β Cu His418 ligand (Figure 3.2.B), whereas the backbone carbonyl group hydrogen bonds with the T2 His81 ligand. The negative charge of Asp94 is suggested to stabilize the PI structure leading to the oxidation of the T2 Cu and the T3β Cu by lowering their reduction potentials. The computational model of PI is supported by experimental data on Fet3p, in which the D94A and D94N mutations result in complete loss of O_2 reactivity, but the D95E variant is still active [129, 149]. The T3α Cu is reduced first, followed by the reduction of the T2 Cu. Consequently T2 Cu-peroxide bonding is lost and PI adapts a transition structure ($PI+e^-$) with peroxide bound in between the T3α Cu(I) and T3β Cu(II). Fast ET from the T1 Cu to the T2 Cu promotes reductive cleavage of O−O peroxide bond accompanied by protonation (proton donated by Glu487 near the T3 Cus [129, 147], Asp456 in TvL1KYA) of one of the oxygens to produce NI [123, 125]. This intermediate is either rapidly reduced by substrate in the catalytic reaction, or, in the absence of a reducing substrate, very slowly decays to RO [122, 124, 137].

3.2 Scope of the chapter

The research described in this chapter deals with the development and characterization of laccase-based constructs, which utilize fluorescence detection for biosensing applications. This so-called FluoRox concept (Chapter 1.4.3) consists of a redox enzyme (herein laccase) with a fluorophore covalently attached to the protein's surface. This method not only permits the oxidized and the reduced states of the active site to be distinguished during redox reactions [150, 151], but also holds promise for improved sensitivity as compared to conventional electrochemical sensing techniques.

Primarily, work focused on the expression of the *lcc1* gene from *T. versicolor* in bacteria, yeast and filamentous fungi. A novel fungal expression system of active Lcc1

in *Schizophyllum commune* is presented. Recombinant protein has been isolated and spectrally characterized and a comparison made with native Laccase A from *T. versicolor* and the two-domain SLAC. The oxidation capacity of fungal laccases using phenolic and non-phenolic compounds has been evaluated. Preliminary studies on the relationship between the two- and three-domain laccases, in terms of the kinetics of the O_2 reduction, were performed. Furthermore, Lcc1, Laccase A and SLAC were fluorescently labeled with rhodamine dyes and these constructs were characterized.

3.3 Materials and methods

3.3.1 *Molecular cloning*

3.3.1.1 *Cloning for expression of Lcc1 in Escherichia coli*

The gene encoding Lcc1 (NCBI accession no. X84683) was amplified by polymerase chain reaction (PCR) using lcc1_pUC19 (kindly provided by Dr. M. Guo from Tianjin Agriculture College, People's Republic of China) as the template and the primers listed in Table 3.1. The PCR products were cloned into the NdeI and BamHI sites of pET29a (lcc1_pET29a construct; the gene subcloned from lcc1_pGEMT by Dr. Katsuko Sato and Rafal Zur), the NdeI and BamHI sites of pET44a (lcc1_pET44a construct encoding for Lcc1 fused N-terminally with N-utilization substance A (NusA) protein) and the NcoI and BamHI sites of pET22b (lcc1_pET22b construct with *lcc1* gene cloned upstream of the periplasmic PelB leader sequence). All constructs were verified by sequencing both strands.

3.3.1.2 *Cloning for expression of Lcc1 in Pichia methanolica and Pichia pastoris*

The gene encoding Lcc1 was amplified by PCR using lcc1_pE29a as the template and the primers listed in Table 3.1. The PCR product was cloned into the pGEMT and subcloned into the EcoRI and NotI sites of pMETαA (lcc1_pMETαA) and pPICZαA (lcc1_pPICZαA) upstream of the secretion α-factor signal peptide from *S. cerevisiae* (signal peptide was used to direct the secretion of the recombinant protein into the media). The constructs were verified by sequencing both strands.

3.3.1.3 *Cloning for expression of Lcc1 in Schizophyllum commune*

The circular (*lcc1-cDNA*) and genomic (*lcc1-gDNA*) genes encoding Lcc1 were amplified by PCR using lcc1_pET29a and *T. versicolor* genomic DNA as the templates, respectively, and the primers listed in Table 3.1. The full sequences of *clcc1* and *glcc1* can be found in Appendix C. The extraction and purification of genomic DNA from *T. versicolor* is described in Chapter 5.6. The 1497 bp (*lcc1-cDNA*) and 2052 bp-long (*lcc1-gDNA*) PCR products were cloned between the β-tubulin 2 promoter gene *tub 2* and the transcription termination signal, upstream of the SC3 signal sequence (the signal sequence was used for exporting the recombinant protein into the media), using the SmaI and BamHI sites of pKSPTubiT3 (unpublished results, kindly provided by Dr. Karin Scholtmeijer from Utrecht University, The Netherlands) to generate clcc1_pKSPTubiT3 and glcc1_pKSPTubiT3, respectively. The nourseothricin resistance cassette [152] was cloned into the EcoRI site of clcc1_pKSPTubiT3 (clcc1_pESCT) and glcc1_pKSPTubiT3 (glcc1_pESCT) to grant the selectivity of transformants in *S. commune*. All constructs were verified by sequencing both strands.

3.3.1.4 *Cloning for expression of Lcc1_cMYC and C452S_Lcc1_cMYC variants in Schizophyllum commune*

The gene encoding C-terminally fused Lcc1 was amplified by PCR using glcc1_pKSPTubiT3 as the template and the primers listed in Table 3.1. The PCR product was cloned into the SmaI and BamHI sites of pKSPTubiT3 (glcc1_cMYC_pKSPTubiT3), as described in Section 3.3.1.3. The C452S variant of Lcc1_cMYC was synthesized with QuickChange Mutagenesis Kit (Stratagene) using glcc1_cMYC_ pKSPTubiT3 as the template and the primers listed in Table 3.1 (C452S_glcc1_cMYC_pKSPTubiT3). The nourseothricin resistance cassette [152] was cloned into the EcoRI sites of glcc1_cMYC_pKSPTubiT3 and C452S_glcc1_cMYC_pKSPTubiT3, resulting in glcc1_cMYC_pESCT and C452S_glcc1_cMYC_pESCT, respectively. All constructs were verified by sequencing both strands.

Construct	Primer sequence 5' to 3'	Function
lcc1_pET22b	GTTCCATGGCTATCGGGCCTGTGAC	Forward primer; Lcc1 periplasmic expression in *E. coli.*
	GTTGGATCCTTAGAGGTCGGATGAGTCAAGAG	Reverse primer; Lcc1 periplasmic expression in *E. coli.*
lcc1_pET29a [a]	GAACATATGGCTATCGGGCCTGTGACCGAC	Forward primer; Lcc1 cytosolic expression in *E. coli.*
	GAAGGATCCTTAGAGGTCGGATGA	Reverse primer; Lcc1 cytosolic expression in *E. coli.*
lcc1_pET44a	GTTCACGTGGCAGCGCTATCGGGCCTGTGACC	Forward primer; NusA-fused Lcc1 cytosolic expression in *E. coli.*
	GTTGGATCCTTAGAGGTCGGATGAGTCAAGAG	Reverse primer; NusA-fused Lcc1 cytosolic expression in *E. coli.*
lcc1_pMETαA, lcc1_pPICZαA	CAAGAATTCGCTATCGGGCCTGTGACCGACCTC ACC	Forward primer; Lcc1 expression in *P. methanolica* and *P. pastoris*
	CAAGCGGCCGCTTAGAGGTCGGATGAGTCAAG AGC	Reverse primer; Lcc1 expression in *P. methanolica* and *P. pastoris*
clcc1_pKSPTubiT3 glcc1_pKSPTubiT3	GGAGCTATCGGGCCTGTGACCGACCTCACCATC	Forward primer; *lcc1-cDNA* and *lcc1-gDNA* cloning into pKSPTubiT3 vector for expression in *S. commune.*
	GTTGGATCCTTAGAGGTCGGATGAGTCAAGAG	Reverse primer; *lcc1-cDNA* and *lcc1-gDNA* cloning into pKSPTubiT3 vector for expression in *S. commune.*

[a] Primers designed by Rafal Zur

Table 3.1 List of primers used for cloning of Lcc1, Lcc1_cMYC, $SLAC_{long}$, $SLAC_{truncated}$ and preparation of the C452S_Lcc1_cMYC variant.

Construct	Primer sequence 5’ to 3’	Function
glcc1_cMYC_ pKSPTubiT3	GGAGCTATCGGGCCTGTGACCGACCTCACCATC	Forward primer for C-terminal cMYC tagging of Lcc1
	GTTTCTTGGATCCTCAGAGGTCCTCCTCGCTGAT GAGCTTCTGCTCGAGGTCGGATGAGTCAAGAGC GTTGTACG	Reverse primer for C-terminal cMYC tagging of Lcc1
C452S_glcc1_ cMYC_pKSPTubiT3	CAACCCCGGCCCCTGGTTCCTCCACTCTCACAT CGACTTCCACTTG	Forward primer; C452S mutagenesis of Lcc1_cMYC
	CAAGTGGAAGTCGATGTGAGAGTGGAGGAACC AGGGGCCGGGGTTG	Reverse primer; C452S mutagenesis of Lcc1_cMYC
SLAC(long)_pET22b	GTTGGAGTCTCATATGGACAGGCGAGGCTTTAA CC	Forward primer; $SLAC_{long}$ expression in *E. coli*
	GTTGGCCATCTCGAGTCAGTGCTCGTGTTCGTG TG	Reverse primer; $SLAC_{long}$ expression in *E. coli*
SLAC(truncated)_ pET22b	GTTGGAGTCTCATATGGGGGGCGAGGTGAGAC ACCTCAAG	Forward primer; $SLAC_{truncated}$ expression in *E. coli*
	GTTGGCCATCTCGAGTCAGTGCTCGTGTTCGTG TG	Reverse primer; $SLAC_{truncated}$ expression in *E. coli*

Table 3.1 List of primers used for cloning of Lcc1, Lcc1_cMYC, $SLAC_{long}$, $SLAC_{truncated}$ and preparation of the C452S_Lcc1_cMYC variant - continued.

3.3.1.5 *Cloning for expression of SLAC in Escherichia coli*

The gene encoding $SLAC_{long}$ (NCBI accession no. Q9XAL8) including the twin-arginine translocation (TAT) leader peptide (first 30 residues) was amplified by PCR as previously described [153] using *S. coelicolor* genomic DNA (kindly provided by Dr J. Stach from Newcastle University, UK) as the template and the primers listed in Table 3.1. The PCR product was cloned into the NdeI and XhoI sites of pET22b (SLAC(long)_pET22b). The leader sequence was removed by PCR using SLAC(long)_pET22b as the template and the primers listed in Table 3.1, and was also cloned into the NdeI and XhoI sites of pET22b (SLAC(truncated)_pET22b encoding for $SLAC_{truncated}$ that lacks the N-terminal 44 residues compared to $SLAC_{long}$). All the constructs were verified by sequencing both strands.

3.3.2 *Organisms used for over-expression of Lcc1, $SLAC_{long}$, $SLAC_{truncated}$*

The BL21 (DE3), Tuner (DE3) and Rosetta (DE3) strains were used for over-expression of Lcc1, $SLAC_{long}$, $SLAC_{truncated}$ in *E. coli*. *P. methanolica* PMAD11 (genotype: *ade2-11*) and *P. pastoris* X33 (genotype: wild type (WT)) strains were used for expression of Lcc1 in yeast. The competent cells were prepared as described in Chapters 5.3.2 (*E. coli*), 5.4.2 (*P. methanolica*) and 5.4.4 (*P. pastoris*). The *S. commune* WT 4-8 [154, 155] and KS8 [156, 157] strains were used for expression of Lcc1 and the variants. *S. commune* KS8 was obtained through a spontaneous event during cultivation of strain 72-3 which contains a deletion of the *SC3* gene [156, 157]. Mutation in the *thn* gene results in several morphological changes in KS8 strain such as production of a pungent smell, a higher radial growth rate and a lower biomass [158]. Protoplasts of *S. commune* WT and KS8 strains were prepared as described in Chapter 5.5.2.

3.3.3 *Expression studies of Lcc1*

3.3.3.1 *Lcc1 expression studies in Escherichia coli*

Small-scale expression of Lcc1 in the cytoplasm of *E. coli* was performed in Luria-Bertani (LB) media (Chapter 5.2.1) using BL21 (DE3), Rosetta (DE3) and Tuner (DE3) strains as described in Chapter 5.9.1. BL21 (DE3) cells transformed with lcc1_pET29a plasmid were grown at 30, 20, 10 and 4 °C; transformed Rosetta (DE3) cells at 30, 20

and 10 °C, whilst transformed Tuner (DE3) cells at 16 and 10 ºC. *E. coli* cells were grown in LB media at 37 °C until an OD_{600} of ~ 0.8 - 1.2 was reached. The cultures were cooled and 0.1 mM $Cu(NO_3)_2$ and/or 25 mM proline were added when necessary. Protein expression was induced with isopropyl β-D-1-thiogalactopyranoside (IPTG; 0.5 mM in BL21 (DE3) and Rosetta (DE3) and 0.05 - 0.2 mM in Tuner (DE3)). Cells were incubated at designated temperatures and 4 mL samples of the cultures were collected every few hours, sonicated and centrifuged for 10 minutes at 5000 g. 50 µL samples of sonicated cultures (representing all expressed proteins) and 50 µL of supernatant (representing soluble proteins) were lysed and analyzed using sodium dodecyl sulfate-polyacrylamide gel electrophoresis (SDS-PAGE) (Chapter 5.8.2).

E. coli BL21 (DE3) transformed with lcc1_pET44a and lcc1_pET22b were grown as described above for lcc1_pET29a. Over-expression of Lcc1_NusA was induced with 0.5 mM IPTG at an OD_{600} of ~ 0.9 - 1.4. Cells were incubated at 30 and 20 °C, and samples were collected and processed as previously. Periplasmic over-expression of Lcc1 was induced with 0.5 mM IPTG at an OD_{600} of ~ 0.6 - 0.8. Cells were incubated at 30 and 20 °C, and the samples were collected every few hours. Cells were spun down at 5000 g and the periplasmic fraction was isolated using osmotic shock-based method (Chapter 5.9.1). Samples (50 µL) were collected and processed as previously.

3.3.3.2 *Refolding of Lcc1 from Escherichia coli inclusion bodies*

E. coli BL21 (DE3) cells transformed with lcc1_pET29a were grown in LB at 37 °C until an OD_{600} of ~ 1.0 was reached. The Lcc1 over-expression was induced with 1.0 mM IPTG and the cells were incubated at 30 °C for 22 h. After harvesting, the cell pellet was re-suspended in 25 mM tris(hydroxymethyl)aminomethane (Tris) pH 7.5 and disrupted by sonication. The inclusion bodies (IB) containing the majority of Lcc1 were collected by centrifugation at 13500 g and subsequently stored at -20 °C. Lcc1 was refolded from IB in slow [159] and rapid [160] fashion using previously published procedures, with modifications, as described in Chapter 5.10.5.1. Different approaches used for the fast refolding of Lcc1 are summarized in Table 3.2.

3.3.3.3 *Studies on expression of Lcc1 in Pichia methanolica and Pichia pastoris*

The *P. methanolica* PMAD11 and *P. pastoris* X33 strains were transformed with lcc1_pMETαA and lcc1_pPICZαA, respectively, as described in Chapters 5.4.3 and 5.4.5. The *P. methanolica* PMAD11 and *P. pastoris* X33 transformants were screened for production of Lcc1 on minimal media plates containing 5 g/L of methanol (MtM-agar, Chapter 5.2.6) supplemented with 0.2 mM $Cu(NO_3)_2$ and 0.2 mM ABTS as described in Section 3.3.17. Transformants of *P. methanolica* PMAD11 with the highest laccase production identified by the largest green halo around the colonies (transformants of *P. pastoris* X33 did not develop the green halo) were used for Lcc1 expression, as previously described [94].

3.3.3.4 *Studies on expression of Lcc1 in Schizophyllum commune*

Small-scale expression of Lcc1 in *S. commune* (Chapter 5.9.2) was performed using WT and KS8 strains transformed with either clcc1_pESCT or glcc1_pESCT as described in Chapter 5.5.3. Lcc1-secreting transformants were selected on minimal media (MM, Chapter 5.2.7) agar supplemented with 0.2 mM $Cu(NO_3)_2$ and 0.2 mM ABTS, as described in Section 3.3.17. Transformant with the highest laccase production identified by the largest green halo around colonies was used for Lcc1 expression studies. To examine the effect of media composition on secretion of Lcc1, the KS8 strain containing glcc1_pESCT was grown in 25 mL liquid standing cultures using MM, complete medium (CM, Chapter 5.2.8) and production media (PM, Chapter 5.2.9). The effect of cultivation temperature (23 and 30 °C), pH (6.6, 7.0, 7.4 and 8.0) and $Cu(NO_3)_2$ concentration (0 - 4 mM) in the media on Lcc1 secretion was also investigated. Samples (1 mL) were taken daily for measurements of protein expression (as in Section 3.3.17).

3.3.3.5 *Studies on expression of cMYC tagged Lcc1 and the C452S variant in Schizophyllum commune*

The *S. commune* KS8 strain was transformed with glcc1_cMYC_pESCT and C452S_glcc1_cMYC_pESCT encoding for cMYC tagged variants of Lcc1 and C452S (T1D) Lcc1, as described in Chapter 5.5.3. The *S. commune* KS8 strains containing glcc1_cMYC_pESCT and C452S_glcc1_cMYC_pESCT were selected by

sandwich immunodetection (experiment carried out by Dr. Karin Scholtmeijer) using anti-cMYC antibody conjugated with alkaline phosphatase (Acris SM1863AP), as described in Chapter 5.8.4. Selected *S. commune* KS8 strains containing glcc1_cMYC_pESCT and C452S_glcc1_cMYC_pESCT were cultured at 30 °C in CM medium, pH 7.0, containing 2.0 mM $Cu(NO_3)_2$, as described in Chapter 5.10.7. After 12 days of growth, the supernatant was collected and incubated overnight at 4 °C with a diethylaminoethyl (DEAE) Fast Flow Sepharose (GE Healthcare) equilibrated in 20 mM phosphate pH 7.0. The next day, the supernatant was filtered out, the DEAE Fast Flow Sepharose was washed with 20 mM phosphate pH 7.0 and the bound proteins were eluted with 50 mL of 0.5 M NaCl. The eluents were subsequently concentrated by ultrafiltration (Amicon ultra 4, 30 kDa molecular weight cut off (MWCO) membrane, Chapter 5.14.2) and separated by SDS-PAGE. The proteins were electrotransfered to a cellulose membrane as described in Chapter 5.8.3 and detected using mouse anti-cMYC antibody (Sigma) in combination with rabbit anti-mouse Ig conjugated with alkaline phosphatase (Promega).

3.3.4 *Expression and purification of proteins*

The proteins $SLAC_{long}$ and $SLAC_{truncated}$ were expressed in *E. coli* and purified using previously published procedure [153], with modifications, as described in Chapter 5.10.1. Laccase A was isolated from crude acetone powder from *T. versicolor*, as described in Chapter 5.10.4. Lcc1 was expressed in *E. coli*, *P. methanolica* PMAD11 [94] and *S. commune* KS8 and purified, as described in Chapters 5.10.5, 5.10.6 and 5.10.7 respectively. $SLAC_{long}$, $SLAC_{truncated}$ concentrations were estimated using extinction coefficient (ε) of 4400 $M^{-1}cm^{-1}$ at 590 nm [153], whilst concentration of Lcc1 and Laccase A was estimated using ε of 4900 $M^{-1}cm^{-1}$ at 610 nm (at pH 6.0) [107].

3.3.5 *Determination of proteins' apparent molecular weight by gel-filtration*

The apparent molecular weight (MW^{app}) of proteins was determined as described in Chapter 5.13.4 using a HiLoad Superdex 200 16/60 (GE Healthcare) gel-filtration column in 20 mM Tris pH 7.5 containing 200 mM NaCl ($SLAC_{long}$, $SLAC_{truncated}$) or a HiLoad Superdex 75 16/60 (GE Healthcare) gel-filtration column in 50 mM phosphate buffer pH 6.0 containing 200 mM NaCl (Lcc1 and Laccase A).

3.3.6 *Determination of proteins' molecular weight by mass spectrometry*

The molecular weights (MW) of $SLAC_{long}$, $SLAC_{truncated}$ and Lcc1 were determined by matrix-assisted laser desorption ionization time-of-flight mass spectrometry, MALDI-TOF-MS, as described in Chapter 5.12.1.

3.3.7 *Metal content determination*

The metal (Cu and Zn) content of purified proteins was determined with a Thermo Electron M Series Atomic Absorption Spectrometer (AAS), as described in Chapter 5.12.4.

3.3.8 *N-terminal sequencing of Laccase A from Trametes versicolor*

The N-terminal sequencing of Laccase A was performed by Dr. Joe Gray (Pinnacle, Newcastle University) using a Beckman LF3000 gas-phase protein micro-sequencer.

3.3.9 *Fluorescence spectroscopy*

Fluorescence spectra and time course measurements were performed on a Cary Eclipse Fluorescence Spectrophotometer (Varian Inc., Agilent Technologies), as described in Chapter 5.12.6. ATTO 647N and ATTO 532 were excited at 630 and 520 nm, respectively, and the emission was measured at 657 and 550 nm, respectively. Trp residues were excited at 285 nm, with emission monitored at 334 nm. The protein samples were prepared in 50 mM phosphate pH 6.0 (Lcc1 and Laccase A) or pH 7.5 ($SLAC_{truncated}$) in the anaerobic chamber (Belle Technology, $[O_2] << 2$ ppm) in septum sealed gas tight 3 mL cuvette. The proteins were reduced with anaerobic 1 mM (final concentration) hydroxylamine, injected using a gas tight syringe (Hamilton).

3.3.10 *Circular dichroism spectroscopy*

Far-UV (190 - 260 nm) and visible (300 - 700 nm) circular dichroism (CD) spectra of proteins were acquired on a Jasco J-810 spectrometer, as described in Chapter 5.12.3. For far-UV CD measurements, the $SLAC_{truncated}$, Laccase A and Lcc1 concentrations

were 1.0, 1.0 and 0.64 mg/mL, respectively, whilst for visible CD they were 9.1, 5.5 and 5.8 mg/mL, respectively.

3.3.11 *UV-Vis absorption spectroscopy*

UV-Vis spectra were acquired on a Perkin Elmer λ 35 spectrophotometer equipped with a Parkin Elmer PTP-1 peltier or a Varian Cary 50 spectrophotometer (Varian Inc., Agilent Technologies), as described in Chapter 5.12.2.

3.3.12 *Continuous wave electron paramagnetic resonance spectroscopy*

Continuous wave (cw), X-band (9.48 GHz) electron paramagnetic resonance (EPR) spectra of $SLAC_{truncated}$, Laccase A and Lcc1 were acquired at ~ 40 or ~ 80 K with a Bruker EMX EPR spectrometer equipped with a TE_{102} cavity and an ESR900 cryostat (Oxford Instruments), as described in Chapter 5.12.5.

3.3.13 *Detection of the transient intermediate in Laccase A*

The intermediate formed during anaerobic reduction of Laccase A and Lcc1 by hydroxylamine was detected at RT using a Varian Cary 50 spectrophotometer in O_2-free Ar-degassed 50 mM phosphate pH 6.0 in a 3 mL septum sealed gas tight cuvette. Concentrated protein was diluted into an anaerobic buffer to give a final concentration of 14 - 27 μM. A gentle flow of O_2-free Ar was passed over the solution for additional 15 min. The reaction was initiated by injecting an anaerobic hydroxylamine (1 mM), using a gas tight syringe. The optical spectra were acquired every 6.7 s until total reduction of the protein had been achieved. For the detection of the intermediate during aerobic turnover of hydroxylamine by Laccase A, a similar procedure was followed, but the reaction was carried out in air-saturated, 100 mM phosphate pH 6.0.

For detection of the intermediate using cw X-band EPR, ~ 1 mM of anaerobic Laccase A in 42 mM phosphate pH 6.0 plus 15 % glycerol was incubated for around 2 h in the anaerobic chamber with an excess of hydroxylamine to afford complete reduction of the Cu centers. The enzyme was re-oxidized with an excess of O_2, after which it was immediately frozen in liquid N_2. The whole procedure was completed within 10 s from the start of the incubation with O_2. After acquisition of the first EPR spectrum at

~ 40 K, the sample was then warmed up to RT and, after a certain time interval (30 s, 1 and 5 min), frozen in liquid N_2 and its spectrum re-measured.

3.3.14 *Protein labeling with fluorescent dyes*

Prior to labeling with ATTO 647N or ATTO 532 N-hydroxysuccinimide (NHS) ester modified fluorescent dyes, Laccase A and Lcc1 were exchanged into 100 mM phosphate pH 6.0, whilst $SLAC_{truncated}$ was exchanged into 100 mM phosphate pH 7.5. The proteins were labeled anaerobically using modified versions of published protocols [150, 151], as described in Chapter 5.11. Typically, the dye to protein labeling ratios were kept in the range of 40 to 80 % per protein's monomer.

3.3.15 *Creation of structural model of Lcc1*

Structure modeling of Lcc1 was performed with I-TASSER software [161] using the crystal structure of TvL1KYA (pdb file: 1KYA) as the template. The template modeling (TM) score of 0.99 ± 0.04 and an RMSD between the main chain atoms of the modeled structure and the template of 3.1 ± 2.2 Å were calculated. The TM-score indicates the difference between the modeled structure and the template by a score of 0 to 1, where 1 indicates a perfect match between two structures. To predict the substrate-binding sites of Lcc1, the model was overlaid onto the crystal structure of TvL1KYA containing one molecule of 2,5-xylidine. PyMol software was used to calculate qualitative electrostatic surface representations and to visualize the structural model [162].

3.3.16 *Kinetic measurements on ATTO 532 labeled Laccase A using stopped flow spectrophotometer*

Stopped flow experiments were performed as previously described [163] using an SX18MV Applied Photophysics stopped flow spectrophotometer with fluorescence detection. An increase in fluorescence intensity at 340 and 550 nm, in parallel with a disappearance of the absorbance at 330 and 610 nm of N-terminally ATTO 532 labeled Laccase A, respectively, was followed. An optical cut off filter of 304 nm and a notch filter (which blocks 532 nm laser light) were used for detection of the emission from Trp ($\lambda_{excitation}$ = 280 nm, $\lambda_{emission}$ = 340 nm) and ATTO 532 ($\lambda_{excitation}$ = 532 nm, $\lambda_{emission}$ = 550 nm), respectively. Prior to the measurements, O_2 was removed from the

internal flow lines of the apparatus by flushing with an anaerobic solution of sodium dithionite. The sample syringes were sealed with septa and gentle flow of O_2-free Ar was passed over the system for additional 45 min. Anaerobic, concentrated Laccase A and ATTO 532 labeled Laccase A were mixed and diluted into 100 mM phosphate pH 6.0 to provide the final concentrations (in the syringe) of 3.56 μM and 0.14 μM, respectively. The other syringe contained an anaerobic solution of sodium ascorbate (600 μM) in 100 mM phosphate pH 6.0. To maintain anaerobic conditions, O_2-free Ar was gently bubble through the samples during the experiments.

3.3.17 *Laccase activity assays*

The initial selection of Lcc1 secreting transformants was performed using an on-plate activity assay. Transformed *P. methanolica* PMAD11, *P. pastoris* X33 and *S. commune* WT and KS8 strains were grown for 3 days at 30 °C on MtM-agar (expression in yeast) or MM-agar (expression in *S. commune*) plates containing 0.2 mM $Cu(NO_3)_2$ and 0.2 mM ABTS. After additional 10 - 24 h incubation at 4 °C the colonies were checked for the development of a green halo.

Laccase activity in culture supernatant was determined using ABTS as the substrate. 1 mL aliquots of culture were collected every 1 - 3 days and centrifuged. The reaction mixture consisted of 100 μL of 10 mM ABTS added to 900 μL of McIlvaine buffer (0.1 M citric acid/0.2 M K_2HPO_4) pH 4.0. The reaction was initiated by addition of 100 μL of filtered culture. Oxidation of ABTS was followed at 420 nm (ε_{420} = 36000 $M^{-1}cm^{-1}$ [164]). The activity is expressed as nanokatal×mL^{-1} (nkat×mL^{-1}), which is defined as the amount of enzyme catalyzing the oxidation of 1 nmol ABTS per second (10^{-9} mol×s^{-1}×mL^{-1}) [165].

The influences of pH (McIlvaine buffer pH 2.2 - 7.0, and 100 mM phosphate pH 7.4 and 7.8) and temperature (15 to 70 °C) on the activity of laccases were determined using 2 mM of both 2,6-dimethylphenol (2,6-DMP) and ABTS (the effect of temperature was measured at pH 4.0 (Laccase A) and pH 5.4 (Lcc1)). Prior to measurements at different temperatures, the reaction mixture was incubated for 15 min at the designated temperature and the reaction was initiated by the addition of protein. The relative activity was calculated from the initial rates of product formation, which was determined spectrophotometrically by following the conversion of 2,6-DMP to 3,5,3',5'-tetramethoxydiphenoquinone at 468 nm (ε_{468} = 14800 $M^{-1}cm^{-1}$ [166]) and ABTS to ABTS radical at 420 nm (Appendix A).

Enzyme kinetics was investigated by assaying laccase activity at a range of substrate concentrations. The initial rates of product formation were used to determine the substrate-dependent reaction velocities. The Michaelis-Menten constant (K_M) and catalytic rate constant (k_{cat}) were derived from the nonlinear fit of the data to the Michaelis-Menten equation (Equation 3.1).

$$v_0 = \frac{d[P]}{dt} = \frac{v_{max}[S]}{K_M + [S]} = k_{cat}[E]\frac{[S]}{K_M + [S]} \qquad \text{(Equation 3.1),}$$

where v_0 is the initial velocity of the reaction, v_{max} is the maximal velocity of the reaction, [P] is the product concentration, [S] the substrate concentration, and [E] is enzyme concentration.

3.4 Results

3.4.1 *Over-expression studies of Lcc1*

3.4.1.1 *Lcc1 over-expression in Escherichia coli*

The expression level of Lcc1 (band with an MW^{app} of 55 kDa on an SDS-PAGE gel) in the cytoplasm of *E. coli* BL21 (DE3) was high (Figure 3.3), however, most of the protein was found in an insoluble form. All attempts to obtain active Lcc1 from IB were unsuccessful (Table 3.2). The refolded enzyme contained negligible Cu and did not show spectral features and activity typical of laccase (Figure 3.4). Higher expression levels seem to result in the presence of a greater proportion of insoluble protein. Tuning protein expression by adjusting IPTG concentration did not improve expression of soluble Lcc1 (Figure 3.3.C). Although lower expression was obtained in *E. coli* Rosetta (DE3), which enhances the expression of proteins containing rare codons, most of Lcc1 was still found in IB (Figure 3.3.D). A small increase in the production of soluble Lcc1 in *E. coli* BL21 (DE3) was obtained by the addition of 0.1 mM $Cu(NO_3)_2$ and 25 mM proline to the media and decreasing the growth temperature to 10 °C (Figure 3.3.A). A significant improvement was obtained by expressing the enzyme as an N-terminal fusion to the NusA protein (Figure 3.3.E). The NusA tag has previously been reported to promote cytoplasmic solubility of its fusion partners [167]. Export of Lcc1 to the periplasm of *E. coli* failed, but a higher percentage of expressed soluble protein was

observed (Figure 3.3.F). In all cases, however, the purified enzyme did not show any laccase activity and spectral features typical of laccases.

3.4.1.2 *Lcc1 over-expression in Pichia methanolica and Picha pastoris*

The majority of *P. methanolica* PMAD11 colonies transformed with *lcc1* showed laccase activity using an on-plate assay (in the presence of methanol as inducer), whilst none of the *P. pastoris* X33 colonies carrying the *lcc1* gene did (data not shown). Strains transformed with the empty vectors did not show laccase activity. A shaken culture of *P. methanolica* PMAD11 colony transformed with *lcc1* had a maximal activity of ~ 7.3 nkat/mL on the day of harvest, which is significantly lower than reported values [94]. This very low expression level hampered efficient Lcc1 purification and the protein could only be partially purified from *P. methanolica* cultures (data not shown). The MW^{app} of the enzyme is ~ 80 kDa from an SDS-PAGE gel and ~ 100 kDa from gel-filtration column, both of which are significantly heavier than the reported value (64 kDa) [94].

3.4.1.3 *Lcc1 over-expression in Schizophyllum commune*

Lcc1 secretion from transformed *S. commune* was detected using an on-plate assay. Around 50 % of stable WT and KS8 strains transformed with clcc1_pESCT developed green halos around colonies (Figure 3.5.A), whilst empty WT and KS8 strains, which were grown as controls, showed no laccase activity (data not shown). This result confirms that the SC3 signal peptide is functional for Lcc1 secretion in *S. commune*. The average ratio of the halo and the colony diameters is 0.91 ± 0.07 for the WT strains and 0.87 ± 0.08 for KS8 strains (Figure 3.5.A and 3.5.B), indicating that the expression of Lcc1 is similar in both strains. However, based on activity assays in media, Lcc1 expression was approximately 40 % higher in the KS8 compared to the WT strain (Figure 3.5.C). Expression levels reached maximum values after 8 - 9 days of growth for the WT strain (~ 25 nkat/mL) and 11 - 13 days for KS8 strain (~ 40 nkat/mL) and remained constant when cultivation was continued further. *S. commune* WT secretes around 2.9 g/L of the polysaccharide schizophyllan (SPG) (unpublished results, Dr. Karin Scholtmeijer), which dramatically increases the viscosity of the medium, whilst Lcc1-expressing KS8 does not produce SPG. Although the presence of SPG is

probably not responsible for the lower expression of Lcc1 (unpublished results, Dr. Karin Scholtmeijer), increased viscosity hampers efficient protein purification.

It has been reported that the presence of introns in the coding gene improves heterologous expression of proteins in *S. commune* [168]. 68 % of stable *S. commune* KS8 strains transformed with glcc1_pESCT secreted Lcc1, as determined using an on-plate assay. Figures 3.5.A and 3.5.B show higher halo to colony ratios (1.75 ± 0.95) for these KS8 strains compared to the KS8 strains transformed with clcc1_pESCT, indicating that the presence of introns indeed increases the expression of Lcc1. In the liquid cultures these transformants showed an almost 4-fold increase in activity compared to KS8 strains transformed with clcc1_pESCT (Figure 3.5.D).

Similar activity levels of cultures grown in CM and MM suggest that the composition of media has limited influence on KS8 strain growth and Lcc1 expression (Figure 3.6.A). However, the level of contaminants present in MM hampered Lcc1 purification (data not shown). The addition of ethanol (PM medium) inhibited the growth of KS8 strain (data not shown). The presence of $Cu(NO_3)_2$ is essential for the expression of active Lcc1, however, the elevated concentration (4 mM) adversely affects the growth of KS8 strain (Figure 3.6.B). The initial pH of the media has very little effect on Lcc1 expression in the 6.6 to 8.0 range (Figure 3.6.C). Almost 2-fold higher production of active Lcc1 was observed for the fungus grown at 30 °C than at 23 °C (Figure 3.6.D).

3.4.1.4 *Over-expression of cMYC tagged Lcc1 and T1D Lcc1 in Schizophyllum commune*

S. commune KS8 transformants expressing the C452S (T1D) Lcc1 variant were selected using sandwich immunodetection (Figure 3.7.A). The C452S mutation disrupts the T1 Cu site, thus inactivates the protein. To facilitate immunodetection, Lcc1 and C452S_Lcc1 were tagged C-terminally with a single cMYC peptide (sequence: N'-EQKLISSEEDL-'C). The western blot analysis (Figure 3.7.B) showed that *S. commune* KS8 strains transformed with glcc1_cMYC_pESCT or C452S_glcc1_cMYC_pESCT successfully selected by sandwich immunodetection using anti-cMYC antibody (Figure 3.7.A), secrete Lcc1_cMYC and T1D Lcc1_cMYC as full-length forms (~ 65 kDa). However, the proteins do not show any activity when grown on either the $Cu(NO_3)_2$ and ABTS containing MM-agar (Figure 3.7.C) or in liquid cultures (data not shown).

3.4.2 *Purification of Lcc1, Laccase A, $SLAC_{long}$ and $SLAC_{truncated}$*

Typically, around 5 mg of purified Lcc1 per one litre of media was obtained from expression in *S. commune* KS8 strain, whilst approximately 35 mg of pure Laccase A was obtained from 1 g of crude *T. versicolor* acetone powder. Lcc1 and Laccase A were pure, giving single bands on SDS-PAGE gels at ~ 64 kDa (Figure 3.8.A and 3.8.B). The elution volumes of Lcc1 and Laccase A (65.8 and 68.0 ml) on the gel-filtration column correspond to MW^{app}s of ~ 50 and ~ 43 kDa, respectively, indicative of the proteins being stable monomers in solution (Table 3.3). MALDI-TOF-MS of Lcc1 gives a range of masses, with a mean value of ~ 60.3 kDa (Laccase A was not analyzed). The calculated MW of the *lcc1* gene translation product is 53350.9 Da (Table 3.3), indicating an average glycosylation level of ~ 12 %, similar to that of TvL1KYA [75] and TvL1GYC [103]. Lcc1 and Laccase A were isolated with 3.53 ± 0.29 and 3.81 ± 0.19 equivalents of Cu per monomer and negligible Zn (Table 3.4).

Purified $SLAC_{long}$ (SLAC variant containing the 30 residues-long TAT-leader sequence, ~ 100 mg/L of culture) has an MW^{app} of ~ 40 kDa by SDS-PAGE gel and elutes at 68.9 ml on the gel-filtration column, corresponding to an MW^{app} of 147 kDa, indicative of the protein being a stable oligomer in solution. However, the observed apparent masses of both the monomer and the oligomer are significantly heavier than reported values of 32 and 81 kDa, respectively [108, 153]. MALDI-TOF-MS gives several peaks for $SLAC_{long}$, with the heaviest form having a mass of 36919.9 Da (Table 3.3). The calculated MW of $SLAC_{long}$ is 36875.0 Da, indicating that its TAT-leader peptide is not cleaved during expression, resulting in heterogeneity. This finding is contrary to what was observed by Machczynski *et al.* and Skalova *et al.*, who reported that the TAT-leader sequence is cleaved during protein expression in *E. coli* [153] and *A. oryzae* [108], respectively. The N-terminal and C-terminal sequencing showed that SLAC expressed in *E. coli* [153] lacks the first 34 - 42 residues and the ending 7 residues, respectively. Similar truncations were observed for SLAC expressed in *A. oryzae* [108].

Expression of $SLAC_{truncated}$, lacking the N-terminal 44 residues (this truncation point was based on the crystal structure of SLAC (pdb file: 3CG8, [108]), which starts at residue 45), yielded a protein (~ 100 mg/L of culture), which gives a single band on an SDS-PAGE gel with an MW^{app} of ~ 37 kDa (Figure 3.8.C). MALDI-TOF-MS gives a single peak of 32591.6 Da (Table 3.3), which is very close to the theoretical value (32587.0 Da). The gel-filtration elution volume of 74.3 mL (MW^{app} of 104.3 kDa)

indicates that $SLAC_{truncated}$ is a stable trimer in solution. AAS quantifies 3.38 ± 0.16 equivalents of Cu per monomer of $SLAC_{truncated}$ and negligible Zn (Table 3.4).

3.4.3 *Structural comparison and stability of Lcc1, Laccase A and $SLAC_{truncated}$*

Edman degradation data from the N-terminus of Laccase A identifies the first six residues as G I G P V A. This fragment is identical to the N-terminal sequence in TvL1KYA [75], which is different to that of TvL1GYC (A I G P A A) [103]. Lcc1 shares only 71.7 % sequence similarity with TvL1KYA and 70.1 % with TvL1GYC (Figure 3.9). The structural model of Lcc1 predicts that His396, His457 and Cys452 coordinate the T1 Cu. Similar to TvL1KYA and TvL1GYC, Lcc1 has a non-coordinating Phe462 residue in the axial position of the T1 Cu site, and therefore, is expected to exhibit a reduction potential higher than 700 mV versus NHE. The T2/T3 Cu ions are coordinated by His64, His66, His109, His111, His399, His401, His451 and His453. The T1 Cu is linked with the T2/T3 Cu cluster by the conserved His451(T3 Cu)-Cys452(T1 Cu)-His453(T3 Cu) motif.

Secondary structure compositions of purified Laccase A, Lcc1 and $SLAC_{truncated}$ have been estimated using far-UV CD spectroscopy. The far-UV CD spectrum of Lcc1 resembles that of Laccase A and shows a maximum (+) at 196 nm and the minimum (-) at ~ 216 nm (Figure 3.8.D). The spectrum of $SLAC_{truncated}$ exhibits three bands at 201 nm (+), 222 nm (−) and 230 nm (+) (Figure 3.8.D). The obtained secondary structure composition of Laccase A, $SLAC_{truncated}$ and Lcc1 are in relatively good agreement with those calculated from the structures of TvL1KYA [75], SLAC [109] and the structural model of Lcc1 (Table 3.5). While Lcc1 and Laccase A have similar secondary structure composition, $SLAC_{truncated}$ shows significant increase in the percentage of β-strand and a lowered α-helical content.

Laccase A and Lcc1 are relatively stable (based on activity measurements with ABTS and 2,6-DMP) in the 4.0 to 7.0 pH range for at least 60 min (at 21 °C), however, this stability decreased with pH. After 60 min incubation at pH 2.2 Laccase A still retained ~ 50 % of the initial activity (Figure 3.8.E), whilst Lcc1 activity was completely abolished (Figure 3.8.F).

3.4.4 *Spectroscopic characterization of Lcc1, Laccase A and SLAC$_{truncated}$*

The UV-Vis spectra are dominated by the T1 Cu S(Cys)π→Cu(II) $d_{x^2-y^2}$ LMCT bands at 610 nm for Lcc1 and Laccase A and 590 nm for $SLAC_{truncated}$ (Figure 3.10.A and Table 3.4). The relative absorption at 280 and 610 nm (A_{280}/A_{610} ratio) is ~ 17 for Lcc1 and Laccase A (at pH 6.0). The A_{280}/A_{590} ratio of $SLAC_{truncated}$ is ~ 12 (pH 7.5), which is in good agreement with the reported value [153]. The binuclear T3 Cu site of laccases demonstrates an intense bridging OH^- to Cu(II) LMCT transition band at ~ 330 nm. The A_{280}/A_{330} ratio for Lcc1 is ~ 24, which is higher than that for Laccase A (~ 10) and $SLAC_{truncated}$ (~ 15) and it does not change after additional incubation of Lcc1 with copper.

The visible CD spectra contain transitions mainly involving the T1 Cu (transitions involving T3 Cus are of low intensity). The spectra of Laccase A and Lcc1 (Figure 3.10.B) are similar and in good agreement with those reported earlier for fungal laccases [117, 169, 170]. Three intense bands at 438 nm (22830 cm^{-1}; −), 530 nm (18870 cm^{-1}; +) and 630 nm (15870 cm^{-1}; −) can be distinguished. The visible CD spectrum of $SLAC_{truncated}$ (Figure 3.10.B) is decidedly different to those of the fungal laccases and resembles that of plastocyanin [171]. In particular, between 450 and 700 nm $SLAC_{truncated}$ shows a broad asymmetric positive maximum, whereas Laccase A and Lcc1 display two oppositely signed bands. The visible CD spectrum of $SLAC_{truncated}$ is characterized by intense bands at 438 nm (22830 cm^{-1}; −), 540 nm (18520 cm^{-1}; +) and 700 nm (14280 cm^{-1}; −). By comparison with the well-characterized spectra of plastocyanin [172], fungal laccase from *Polyporus pinsitis* [169] and its F463M variant (containing Met instead of Phe residue in the axial position, [169]), the bands at 438 and 530 nm (and 540 nm for $SLAC_{truncated}$) can been assigned as N(His)π→Cu(II) $d_{x^2-y^2}$ and a S(Cys)pseudo-σ→Cu(II) $d_{x^2-y^2}$ LMCT transitions at the T1 Cu site, respectively (Table 3.6). Although the S(Cys)π→Cu(II) $d_{x^2-y^2}$ LMCT transition dominates the UV-Vis absorption spectrum, this band cannot be resolved in the visible CD spectrum. The low-energy bands at 630 nm observed in Lcc1 and Laccase A spectra, and at 700 nm (14280 cm^{-1}) in the $SLAC_{truncated}$ spectrum, can be assigned to $d_{xz}\rightarrow d_{x^2-y^2}$ (fungal laccases) and $d_{yz}\rightarrow d_{x^2-y^2}$ ($SLAC_{truncated}$) ligand field (LF) transitions at the T1 Cu site [169, 170, 173]. The LF transition in *T. versicolor* laccases, which is shifted to higher energy, indicates increased ligand field strength relative to plastocyanin and F463M laccases. This has previously been interpreted as being due to the lack of an

axial Met ligand and a more trigonal planar geometry in the T1 Cu sites of fungal laccases [169] and Fet3p [173].

The T1 Cu site of Laccase A, Lcc1 demonstrate an axial EPR spectrum (Figure 3.10.C) similar to those reported earlier for fungal laccases [169]. The T2 Cu site is also axial, but its overlap with the T1 Cu signal prevents from accurate deconvolution. The T1 and T2 Cu sites of $SLAC_{truncated}$ (Figure 3.10.C) also demonstrate the axial EPR signals with hyperfine coupling (A_z) in the g_z region of 76×10^{-4} and 107×10^{-4} cm^{-1}, respectively, consistent with previously reported values [153] (Table 3.4).

3.4.5 *Kinetic parameters for the reactions of Laccase A, Lcc1, $SLAC_{long}$ and $SLAC_{truncated}$ with 2,6-DMP and ABTS*

The influence of pH on the activity of Laccase A and Lcc1 was determined for phenolic (2,6-DMP) and nonphenolic (ABTS) substrates (structures available in Appendix A). Both enzymes oxidise 2,6-DMP in a pH-dependent manner showing the highest activity between pH 4.0 and 6.0 (Figures 3.11.A), which is slightly higher than the average for fungal laccases (pH 4.0) [174]. At alkaline pH the activity of laccases is negatively influenced by the OH^- ion inhibition (at the T2/T3 Cu cluster), but positively affected by the lower reduction potential of the phenolic substrates [18]. The combination of these two effects contributes to the bell-shaped dependence of activity on pH. Both enzymes show maximum catalytic efficiency (expressed as k_{cat}/K_M) at pH 5.4, but the value is 2-fold higher for Laccase A than for Lcc1 (Figures 3.12.A and 3.12.B). The affinity of Laccase A and Lcc1 for 2,6-DMP increases with pH but does not reach the maximum at the optimal pH (Figures 3.12.C and 3.12.D). k_{cat} shows the standard bell-shaped dependence on pH reaching a maximum at approximately pH 3.0 for Laccase A (Figure 3.12.E), and a plateau at ~ pH 4.0 for Lcc1 (Figure 3.12.F). When ABTS is used as the substrate (Figure 3.11.B), both enzymes show a linear dependence of activity on pH (decreasing as the pH becomes more alkaline due to the OH^- ion binding at the T2/T3 Cu cluster [18]), which is similar to other fungal laccases [174].

The oxidation of both 2,6-DMP and ABTS is optimal at 45 °C for Laccase A, but is at 45 and 35 °C for Lcc1 (Figures 3.11.C and 3.11.D), somewhat lower than the optimum temperature range (50 - 70 °C) of the majority of fungal laccases [5, 174]. The kinetic parameters (K_M and k_{cat}) for the Laccase A-catalyzed oxidation of both ABTS and 2,6-DMP were determined at pH 4.0 at 21 and 45 °C, whereas for Lcc1

reactivity with ABTS (at 21 and 35 °C) and 2,6-DMP (at 21 and 45 °C) was measured at pH 4.0 and 5.4, respectively (Figure 3.13). Laccase A shows similar affinity for both substrates that decreases when the temperature increases. However, k_{cat}/K_M is almost unaffected by temperature (Table 3.7). The affinity of Lcc1 for ABTS increases 1.4-fold at higher temperature, whereas for 2,6-DMP it is unaffected by temperature. At 35 °C, k_{cat}/K_M for Lcc1 with ABTS increases 2-fold compared to that at 21 °C but is still lower than that of Laccase A. A 2-fold increase with temperature of the k_{cat}/K_M with 2,6-DMP results in Lcc1 being more efficient in the oxidation of this substrate than Laccase A (Table 3.7).

The kinetic parameters of $SLAC_{long}$ and $SLAC_{truncated}$ were determined with 2,6-DMP at pH 8.0 (Figure 3.13.E). $SLAC_{truncated}$ has substantially lower affinity (~ 30 and 220-fold higher K_M and ~ 40 and 230-fold lower k_{cat}) towards 2,6-DMP than Lcc1 and Laccase A (Table 3.7). Removal of the N-terminal 44 residues appears to change the activity of the enzyme. The K_M (6.6 mM) and k_{cat}/K_M (0.97 $mM^{-1}s^{-1}$) values for $SLAC_{truncated}$ are ~ 2 to 6-fold and ~ 0.9 to 7-fold higher respectively than previously reported [153, 175, 176]. The K_M of SLAC is almost 2-fold higher than for $SLAC_{long}$ (3.75 mM, data not shown), however k_{cat}/K_M remains almost unaffected. The role of the missing residues is unknown. The N-terminus points to the opposite direction of the T2/T3 Cu cluster and predicted shallow substrate-binding cavity (center of the trimer), making it unlikely for the TAT-signal peptide to approach the substrate-binding pocket [108].

3.4.6 *Preliminary studies on transient species present during the catalytic cycle of Laccase A*

Reduction of Laccase A with hydroxylamine in O_2-containing buffer resulted in the gradual disappearance of absorption bands at 330 and 610 nm (Figure 3.14.A). The reduction process was complete within 90 min (Figure 3.14.B). Reaction of the reduced sample with O_2 resulted in full recovery of absorption at 330 nm and only partial recovery of the 610 nm band (data not shown). However, reduction of the protein in anaerobic buffer resulted in the initial formation of a band at 420 nm (within a dead time of the measurement), which subsequently disappeared within a few minutes along with (but slower) the 330 and 610 nm bands (Figures 3.14.C and 3.14.D). After the addition of O_2-containing buffer to the fully reduced sample, the 420 nm band re-appeared together with the partial recovery of the 330 and 610 nm bands (data not

shown). A similar band at ~ 420 nm was also been observed during anaerobic reduction of Lcc1 and subsequent oxidation (data not shown).

To investigate whether this transient species (giving rise to the 420 nm band) is paramagnetic, X-band EPR spectra were obtained during the oxidation of hydroxylamine-reduced Laccase A. Reduced Laccase A was mixed (under anaerobic conditions) with an excess of O_2 and frozen in liquid nitrogen. The results are inconclusive as the EPR spectra in the g = 2 region are complex and consists of several intense overlapping signals that can be attributed to the T1 and T2 Cu(II)s (data not shown).

3.4.7 *Preliminary studies on fluorescently labeled laccases*

The absorption bands of Laccase A (Figure 3.15.A), Lcc1 and $SLAC_{truncated}$ at ~ 600 nm (T1 Cu(II)) and ~ 330 nm (T2/T3 Cu(II)) are absent when the proteins are reduced. The emission spectra of Laccase A (Figure 3.15.B), Lcc1 and $SLAC_{truncated}$ are dominated by fluorescence from Trp residues (7, 6 and 5 Trp residues in Laccase A, Lcc1 and $SLAC_{truncated}$ respectively) showing a maximum at around 333 nm. This emission overlaps significantly with the 330 nm absorption band of the T2/T3 Cu(II) cluster. Therefore, in the oxidized state of the protein, this fluorescence is quenched by Förster Resonance Energy Transfer (FRET, Chapter 1.4.3) to the 330 nm absorption band. In the reduced state, the absorption band at 330 nm is absent, and therefore, the quenching of fluorescence is limited. This change is reflected in an increase in fluorescence intensity. (Figure 3.15.C). The switching ratios (*SR*s, Chapter 5.12.6) under anaerobic conditions are 0.48 for Laccase A, 0.30 for Lcc1 and 0.36 for $SLAC_{truncated}$.

To monitor redox changes at the T1 Cu site *via* fluorescence, Lcc1 and Laccase A were N-terminally labeled with ATTO 532 or ATTO 647N dyes, whereas $SLAC_{truncated}$ was N-terminally labeled with ATTO 590 (structures of dyes are shown in Appendix A). The emission spectra of the dyes (maxima at 553, 624 and 669 nm for ATTO 532, ATTO 590 and ATTO 647N, respectively) overlap with the absorption band of the T1 Cu site of Lcc1, Laccase A and $SLAC_{truncated}$ at ~ 600 nm. In the oxidized state of the proteins, the fluorescence of the dye is quenched by FRET to the 600 nm absorption band, whilst in the reduced state this quenching is limited. The two-phase increase in Trp and ATTO 647N fluorescence emission observed for ATTO 647N labeled Laccase A and Lcc1 upon reduction is different to the one-phase increase for

ATTO 590 labeled SLAC (and other fluorescently labeled T1 Cu-containing proteins, see Chapter 1.3 and Chapter 2). These unusual reduction kinetics for the fungal laccases are probably due to trace amounts of oxygen present in the reaction mixture. The reduction kinetics are sensitive to the oxygen concentration, which is hard to contol, even for experiments performed in an anaerobic chamber. The fluorescence *SR*s are 0.44 for ATTO 647N labeled Lcc1, 0.64 for ATTO 647N labeled Laccase A and 0.63 for ATTO 590 labeled $SLAC_{truncated}$ (Figure 3.16.A). Labeled $SLAC_{truncated}$ is stable, whereas labeled Lcc1 and Laccase A are not and their *SR*s decrease within hours (this decrease is faster for labeled Lcc1 than for Laccase A, data not shown). The kinetics of reduction of ATTO 532 labeled Laccase A was studied using stopped-flow spectrophotometry. ATTO 532 and Trp emission traces superimpose with the corresponding absorbance traces (values multiplied by -1) and follow the same kinetics, showing that reduction of the T1 Cu site and T2/T3 Cu cluster can be monitored simultaneously and independent of each other using FRET-based approach (Figure 3.16.B).

Denaturating mixture	Refolding mixture	Observations
6 M Gdn [a], 50 mM EDTA [b], 2 mM DTT [c] in 0.1 M Hepes [d], pH 8.0	10 mM Hepes, pH 8.0, 5 mM DTT	Protein exchanged into 250 mM NH_4Ac [e] pH 8.0 by ultrafiltration and incubated with 5 mM $CuSO_4$. **Protein precipitated.**
6 M Urea, 50 mM EDTA, 2 mM DTT in 0.1 M Hepes, pH 8.0		
6 M Urea, 50 mM EDTA, 2 mM DTT in 0.1 M Hepes, pH 8.0	10 mM Hepes, pH 8.0, 5 mM DTT	Protein dialysed against 125 mM NH_4Ac pH 8.0 and incubated with $CuSO_4$: (a) 5 mM **(protein precipitated)**, (b) 2.5 mM **(no Cu incorporation, Lcc1 inactive with ABTS)**, (c) 1 mM **(no Cu incorporation, Lcc1 inactive with ABTS).**
	10 mM Hepes, pH 8.0;	**Protein precipitated.**
6 M Urea, 10 or 30 mM EDTA, 2 mM DTT in 0.1 M Hepes, pH 8.0	10 mM Hepes, pH 8.0, 2 mM DTT	Protein dialysed against 125 mM NH_4Ac pH 8.0 and incubated with 1 and 2.5 mM $CuSO_4$. **Protein inactive with ABTS.**
6 M Urea, 10 or 30 mM EDTA, 2 mM DTT in 0.1 M Hepes, pH 8.0	10 mM Hepes, pH 8.0, 2 mM DTT, 1 or 2 mM $CuSO_4$	**Protein inactive with ABTS.**

[a] Guanidinium chloride [b] Ethylenediaminetetraacetic acid. [c] Dithiothreitol. [d] 4-(2-hydroxyethyl)-1-piperazineethanesulfonic acid. [e] Ammonium acetate.

Table 3.2 Experimental conditions for fast refolding of Lcc1 from IB.

Protein	MW, Da		V_e, mL	MW^{app}, kDa
	Experimental mass	Theoretical mass		
Lcc1	60226.4	53350.9 [a]	65.8	49.6
Laccase A	[b]	[b]	68.0	42.7
$SLAC_{long}$	36919.9 35138.4 34597.1	36875.0 [a]	68.9	147
$SLAC_{truncated}$	32591.6	32587.0 [a]	74.3	104 [c]

[a] MW excluding the N-terminal Met residue. [b] Not determined. [c] MW^{app} corresponds to the trimeric form of the protein.

Table 3.3 MALDI-TOF-MS and the gel-filtration data for Lcc1, Laccase A, $SLAC_{long}$ and $SLAC_{truncated}$.

Spectral properties	Protein		
	Laccase A	Lcc1	$SLAC_{truncated}$
	UV-Vis [a]		
$\lambda_{max\ (1)}$, nm	330	330	330
$\lambda_{max\ (2)}$, nm	610	610	590
$\varepsilon_{max\ (2)}$, $M^{-1}cm^{-1}$	4900 [b]	4900	4400 [c]
$A_{280}/A_{max(1)}$	~ 10	~ 24	~ 15
$A_{280}/A_{max(2)}$	~ 17	~ 17	~ 12
	T1 Cu (T2 Cu) EPR parameters [d]		
g_x	2.042	2.042	2.032 (2.048)
g_y	2.042	2.042	2.049 (2.055)
g_z	2.191 (2.227) [e]	2.191 (2.244) [e]	2.233 (2.362)
A_x, 10^{-4} cm^{-1}	9.3	9.3	9.3 (0.0)
A_y, 10^{-4} cm^{-1}	9.6	9.6	9.6 (0.0)
A_z, 10^{-4} cm^{-1}	80 (199) [e]	80 (178) [e]	77 (107)
	Metal content per monomer		
Cu/monomer	3.81 ± 0.19	3.53 ± 0.29	3.38 ± 0.16
Zn/monomer	Negligible	Negligible	Negligible
	Intrinsic fluorescence [a]		
$\lambda_{excitation}$, nm	280	278	280
$\lambda_{emission}$, nm	332	333	333
SR	0.48	0.30	0.36
	ATTO 647N labeled Laccase A and Lcc1 or ATTO 590 labeled SLAC [a]		
SR	0.64	0.44	0.63

[a] In 50 mM phosphate pH 6.0 (Lcc1 and Laccase A) and 20 mM Tris pH 7.5 ($SLAC_{truncated}$) at room temperature (RT). [b] Taken from [117]. [c] Taken from [153]. [d] In 50 mM phosphate pH 6.0 (Lcc1 and Laccase A) and 20 mM Tris pH 7.5 containing 200 mM NaCl ($SLAC_{truncated}$) at ~ 80 K. [e] The T1 and T2 Cu(II)s signals overlap, thus the parameters obtained are less precise.

Table 3.4 Comparison of spectral properties of Laccase A, Lcc1 and $SLAC_{truncated}$.

Protein	Data analyzed	Fitting NRMSD [a]	Secondary structure, %			
			Helix	β-sheet	Turn	Random Coil
Laccase A	Far-UV CD [b]	0.025	9.0	36.0	23.0	32.0
	Crystal structure [c]		9.4	31.3	30.5	16.6
Lcc1	Far-UV CD [b]	0.016	11.0	36.0	23.0	31.0
	Homology model [c]		10.8	33.5	32.3	23.4
$SLAC_{truncated}$	Far-UV CD [d]	0.034	3.0	47.0	22.0	27.0
	Crystal structure [c]		6.6	46.5	27.5	19.4

[a] Normalised to 1 root-mean square deviation [177] for fitting of the far-UV CD spectra in the 190 - 240 nm range using the CDSSTR analysis method [178], protein reference set 4, as implemented by Dichroweb [179]. [b] In 10 mM phosphate pH 6.0 at 25 °C. [c] The crystal structures of Laccase A (pdb code: 1KYA) [75] and SLAC (pdb code: 3KW8) [109] and the structural model of Lcc1 created with I-TASSER [161] using 1KYA as the template were used. [d] In 10 mM phosphate pH 7.0 at 25 °C.

Table 3.5 Comparison of the secondary structure content determined from available structures or a homology model, using STRIDE [180], with those calculated from far-UV CD spectra using Dichroweb [179].

Transition	Energy, cm^{-1} (λ, nm)						
	Laccase A [a]	Lcc1 [a]	$SLAC_{truncated}$ [b]	*P. pinsitis* laccase [a, c]	*P. pinsitis* F463M laccase [b, c]	*M. thermophila* laccase [c, d]	Plastocyanin [b, c, e]
$d_{z^2} \rightarrow d_{x^2-y^2}$	*f*	*f*	*f*	6900 (1450)	6500 (1539)	6500 (1539)	5000 (2000)
$d_{xy} \rightarrow d_{x^2-y^2}$	*f*	*f*	*f*	13270 (754)	12370 (808)	13160 (760)	10800 (926)
$d_{yz} \rightarrow d_{x^2-y^2}$	*f*	*f*	~ 14280 (~ 700)	14350 (697)	13700 (730)	14290 (700)	12800 (781)
$d_{xz} \rightarrow d_{x^2-y^2}$	15870 (630)	15870 (630)	*f*	15860 (630)	14880 (672)	15470 (646)	13950 (717)
S(Cys)π→Cu(II) $d_{x^2-y^2}$	16390 (610) [g]	16390 (610) [g]	16950 (590) [g]	16450 (608)	16630 (601)	16610 (602)	16700 (599)
S(Cys)pseudo-σ→ Cu(II) $d_{x^2-y^2}$	18870 (530)	18870 (530)	18520 (540)	18860 (530)	18540 (539)	18650 (536)	18700 (535)
N(His)π→Cu(II) $d_{x^2-y^2}$	22830 (438)	22830 (438)	22830 (438)	*f*	*f*	*f*	21390 (468)

[a] Proteins containing a T1 Cu site with Phe in the axial position. [b] Proteins containing a T1 Cu site with Met in the axial position. [c] Taken from [169]. [d] Proteins containing a T1 Cu site with Leu in the axial position. [e] Taken from [172]. [f] Not determined. [g] Values are taken from the UV-Vis spectrum.

Table 3.6 Comparison of the LMCT and LF transitions from UV-Vis absorption and visible CD spectra.

Substrate	Temperature, °C	K_M, μM	k_{cat}, s^{-1}	k_{cat}/K_M, $\mu M^{-1}s^{-1}$
	Laccase A			
ABTS, pH 4.0	21	31.5 ± 4.1	404 ± 10	12.8 ± 1.2
	45 [a]	49.0 ± 4.0	817 ± 29	16.7 ± 1.0
2,6-DMP, pH 4.0	21	29.7 ± 1.8	265 ± 6	8.9 ± 0.3
	45 [a]	46.7 ± 1.6	483 ± 6	10.3 ± 0.2
	Lcc1			
ABTS, pH 4.0	21	1011 ± 7	2475 ± 148	2.4 ± 0.2
	35 [a]	743 ± 3	3796 ± 158	5.1 ± 0.2
2,6-DMP, pH 5.4	21	223 ± 8	1457 ± 107	6.5 ± 0.3
	45 [a]	245 ± 10	3304 ± 46	13.5 ± 0.4
	$SLAC_{truncated}$			
2,6-DMP, pH 8.0	21	6601 ± 263	6.4 ± 0.3	$(9.7 \pm 0.1)\times10^{-4}$

[a] Single measurement.

Table 3.7 Turnover number (k_{cat}), Michaelis-Menten constant (K_M) and catalytic constant (k_{cat}/K_M) of Laccase A, Lcc1 and $SLAC_{truncated}$ with ABTS and 2,6-DMP.

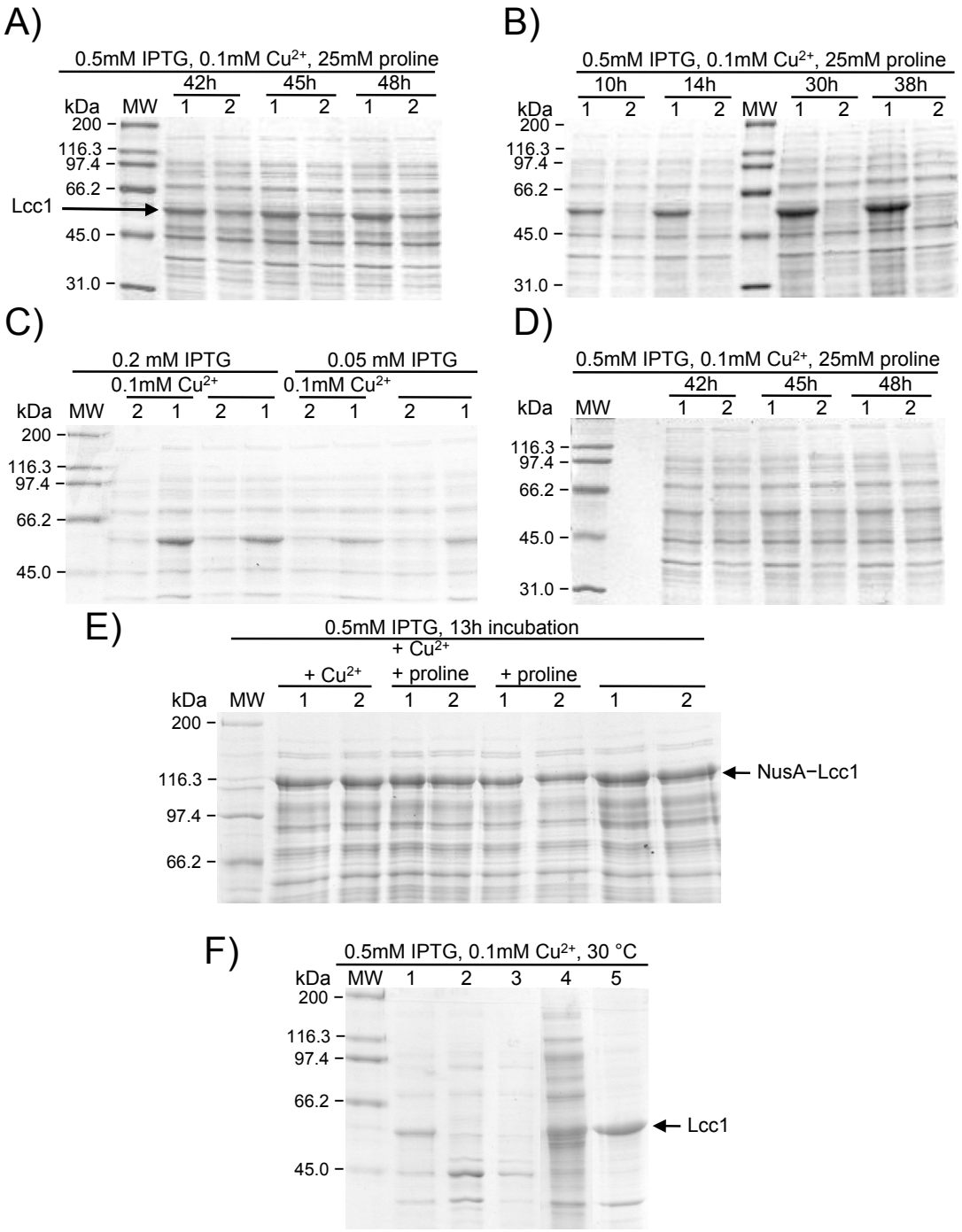

Figure 3.3 SDS-PAGE gels of Lcc1 expression in *E. coli.* Cytoplasmic expression of Lcc1 in BL21 (DE3) at (A) 10 °C and (B) 20 °C; (C) Tuner at 20 °C and (D) Rosetta (DE3) at 20 °C. (E) Cytoplasmic expression of Lcc1 fused to NusA in BL21 (DE3) at 30 °C. Cells were grown with or without 0.1 mM $Cu(NO_3)_2$ and 25 mM proline. (F) Periplasmic expression of Lcc1 in BL21 (DE3). Legend: 1 - expressed proteins, 2 - soluble proteins, 3 - soluble proteins in periplasmic fraction, 4 - soluble proteins in cytoplasmic fraction, 5 - insoluble proteins (pellet).

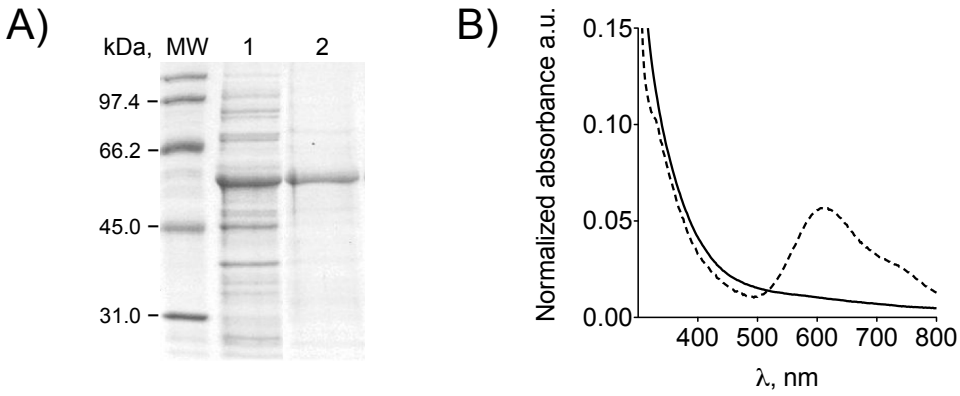

Figure 3.4 Refolding of Lcc1 from IB. (A) SDS-PAGE gel of refolded Lcc1 from IB. Legend: 1 - expressed proteins, 2 - soluble, pure Lcc1 refolded from IB. (B) UV-Vis spectra of Laccase A (▬ ▪ ▬) and pure, refolded Lcc1 (▬) after attempted reconstitution with copper. Spectra were acquired at RT in 50 mM phosphate pH 6.0.

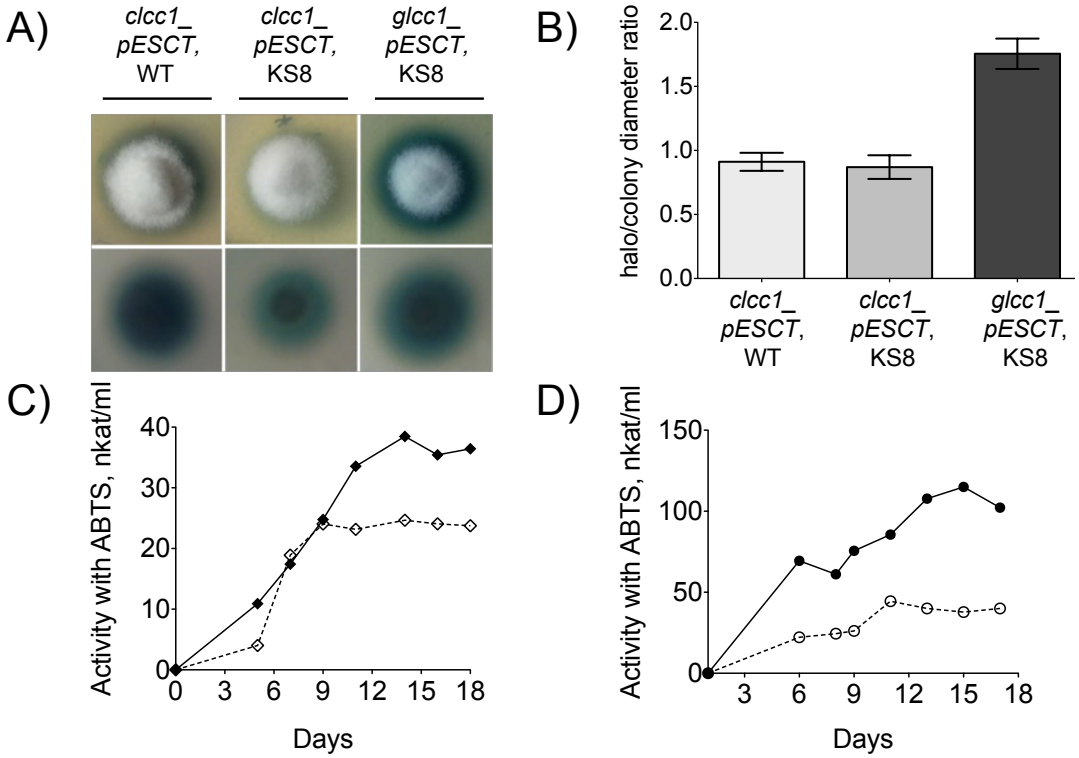

Figure 3.5 (A) On-plate activity assay of *S. commune* WT transformed with clcc1_pESCT and KS8 transformed with clcc1_pESCT and glcc1_pESCT. *Top row:* front of the colony; *bottom row*: other side of the colony. (B) Comparison of the halo to colony ratio of WT and KS8-strains. Activity of Lcc1 secreted by (C) WT (◇) and KS8 (◆) strains transformed with clcc1_pESCT and (D) KS8 strains transformed with clcc1_pESCT (○) and glcc1_pESCT (●) (D) grown (30 °C) in liquid cultures MM at pH 7.0 and in the presence of 2 mM $Cu(NO_3)_2$. Activity was determined (RT) at pH 4.0 with 0.91 mM ABTS as the substrate.

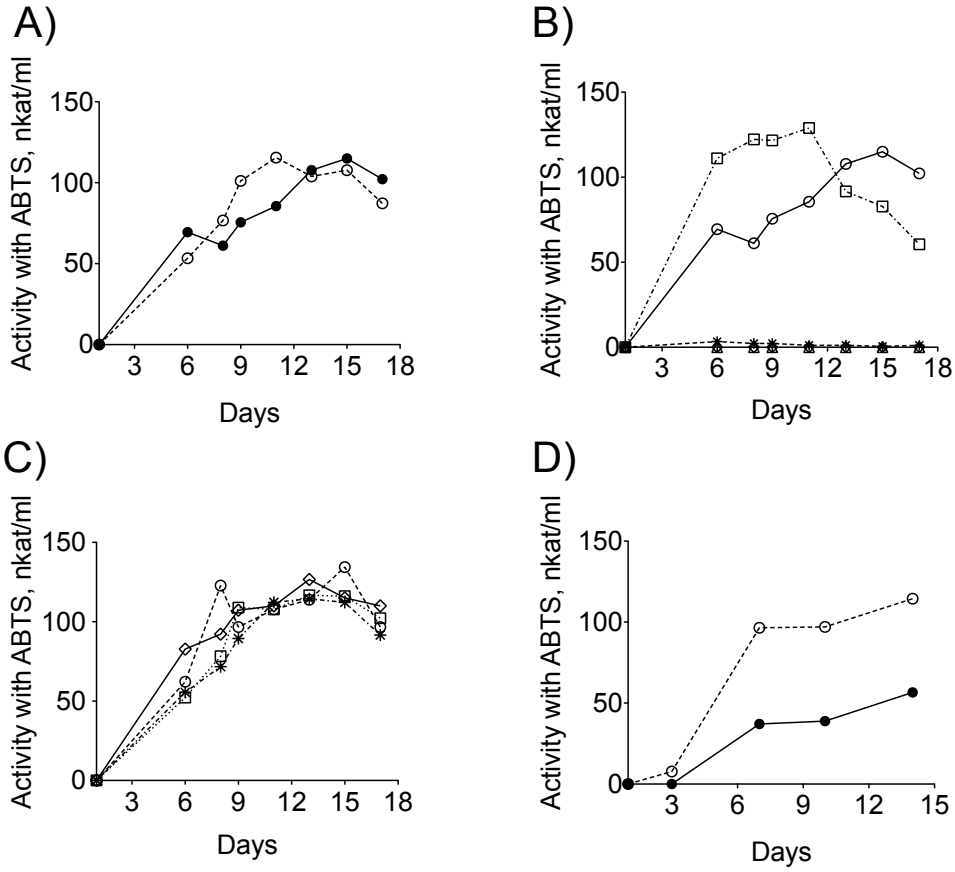

Figure 3.6 The influence of (A) medium composition, (B) $Cu(NO_3)_2$ concentration, (C) pH and (D) temperature on activity of Lcc1 in media during 15 - 17 days of growth. Lcc1 was secreted by *S. commune* KS8 transformed with glcc1_pESCT grown (30 °C) in liquid standing cultures in: (A) MM (○) and CM (●) pH 7.0 with 2 mM $Cu(NO_3)_2$; (B) in CM at pH 7.0 in the absence (△) and presence of 1 (□), 2 (○), 3 (◇) and 4 mM (✳) $Cu(NO_3)_2$; (C) in CM at pH 6.6 (◇), 7.0 (○), 7.4 (□) and 8.0 (✳) with 2 mM $Cu(NO_3)_2$; (D) in CM at 23 °C (●) and 30 °C (○) at pH 7.0 with 2 mM $Cu(NO_3)_2$. Activity was measured at pH 4.0 (RT) with 0.91 mM ABTS as the substrate.

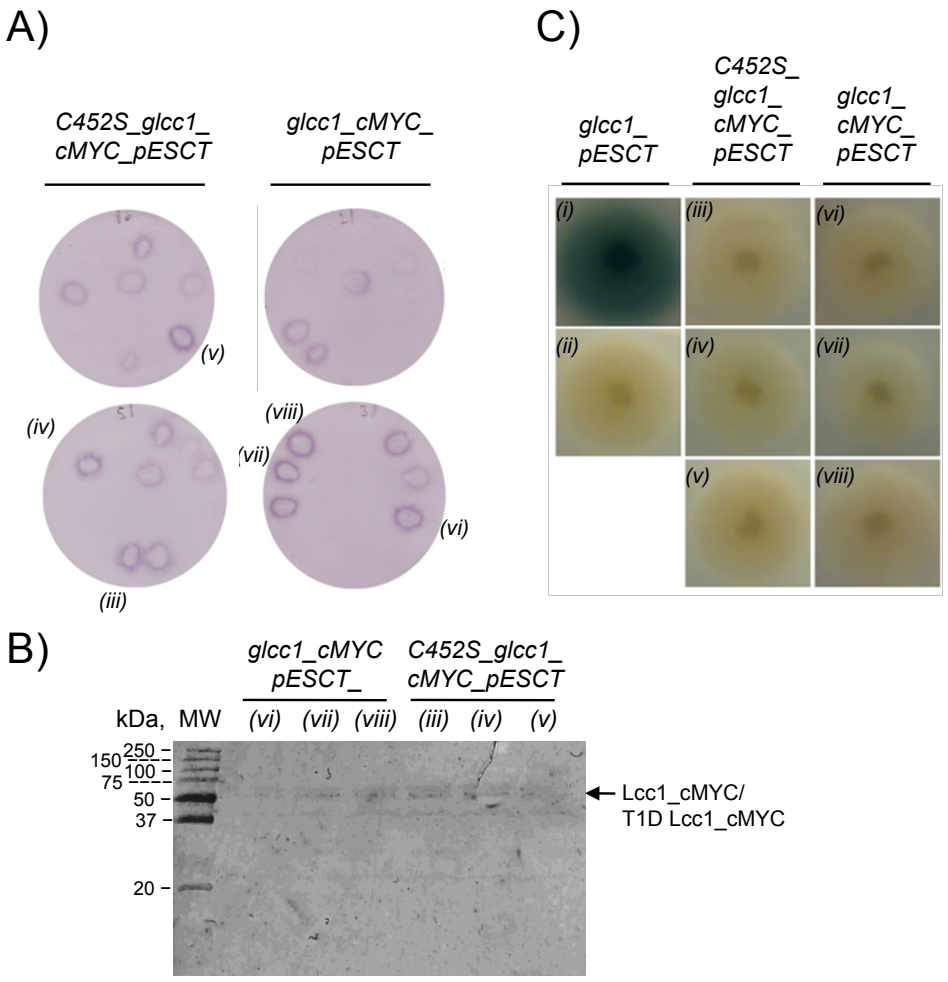

Figure 3.7 (A) On-plate screen assay of *S. commune* KS8 transformed with C452S_glcc1_cMYC_pESCT and glcc1_cMYC_pESCT *via* sandwich immunodetection using the anti-MYC alkaline phosphatase conjugated antibody (results provided by Dr. K. Scholtmeijer). (B) Western blot of C452S_Lcc1_cMYC (selected transformants: *iii* - *v*) and Lcc1_cMYC (selected transformants: *vi* - *viii*) expressed in liquid culture. (C) On-plate activity assay of *S. commune* KS8 transformed with glcc1_pESCT (*i* - *positive control* (Figure 3.5.A) and *ii* - *negative control*), glcc1_cMYC_pESCT (*iii* - *v*) and C452S_glcc1_cMYC_pESCT (*vi* - *vii*). Colonies were grown for 3 days on MM plates in the presence of 0.2 mM ABTS and 0.2 mM $Cu(NO_3)_2$.

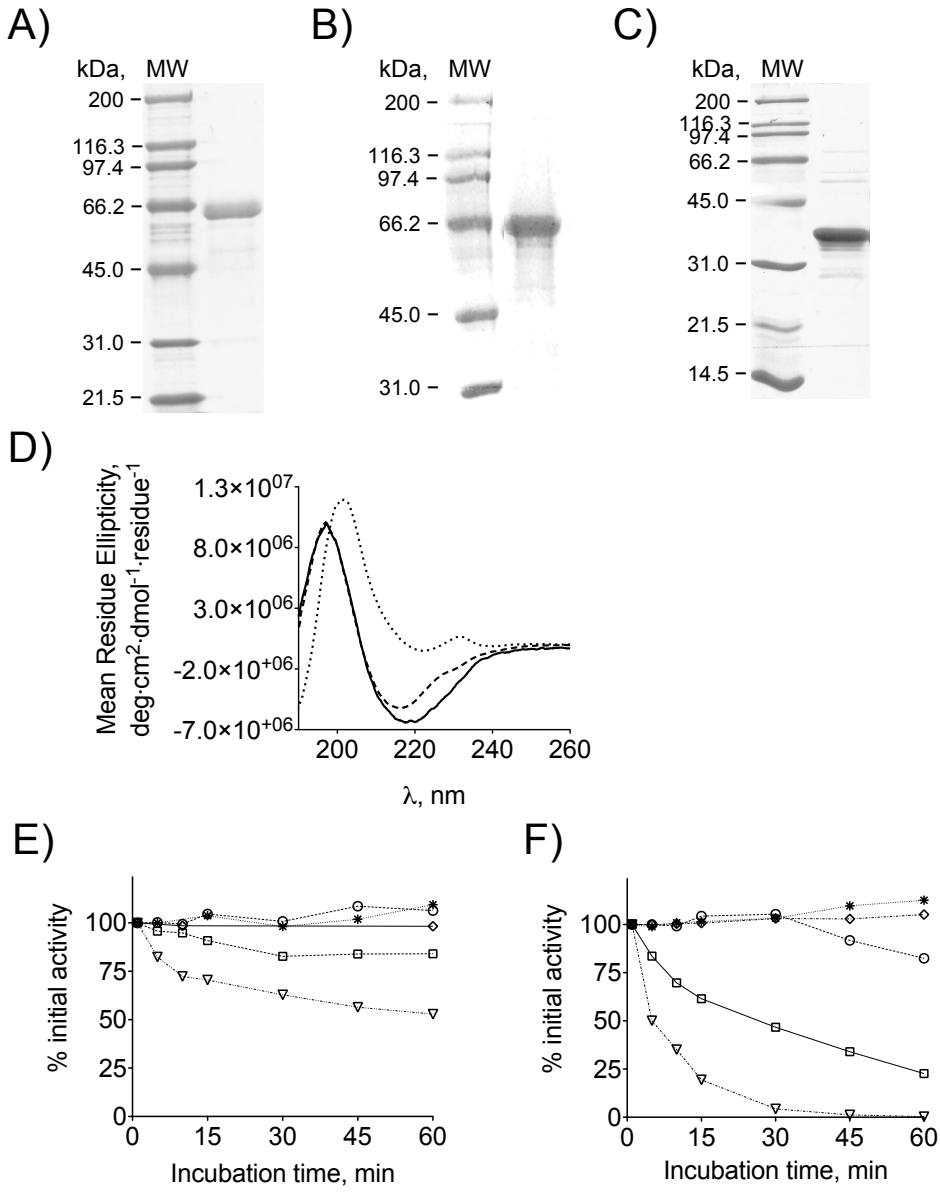

Figure 3.8 SDS-PAGE gels of (A) Laccase A purified from crude acetone powder of *T. versicolor*, (B) Lcc1 expressed by *S. commune* KS8 strain transformed with glcc1_cMYC_pESCT and (C) SLAC expressed in *E. coli*. (D) Far-UV CD spectra of Laccase A (- - -), Lcc1 (—) and SLAC (···) at 25 °C. The spectra of Laccase A and Lcc1 were acquired in 10 mM phosphate pH 6.0, whereas SLAC is in 10 mM phosphate pH 7.0. Stability of (E) Laccase A and (F) Lcc1 measured using activity at pH 2.2 (▽), pH 3.0 (□), pH 4.0 (○), pH 5.4 (◇) and pH 7.0 (✳). Activity was measured at 21 °C with 2 mM 2,6-DMP (pH 7.0, 5.4 and 4.0) and 2 mM ABTS (pH 3.0 and 2.2).

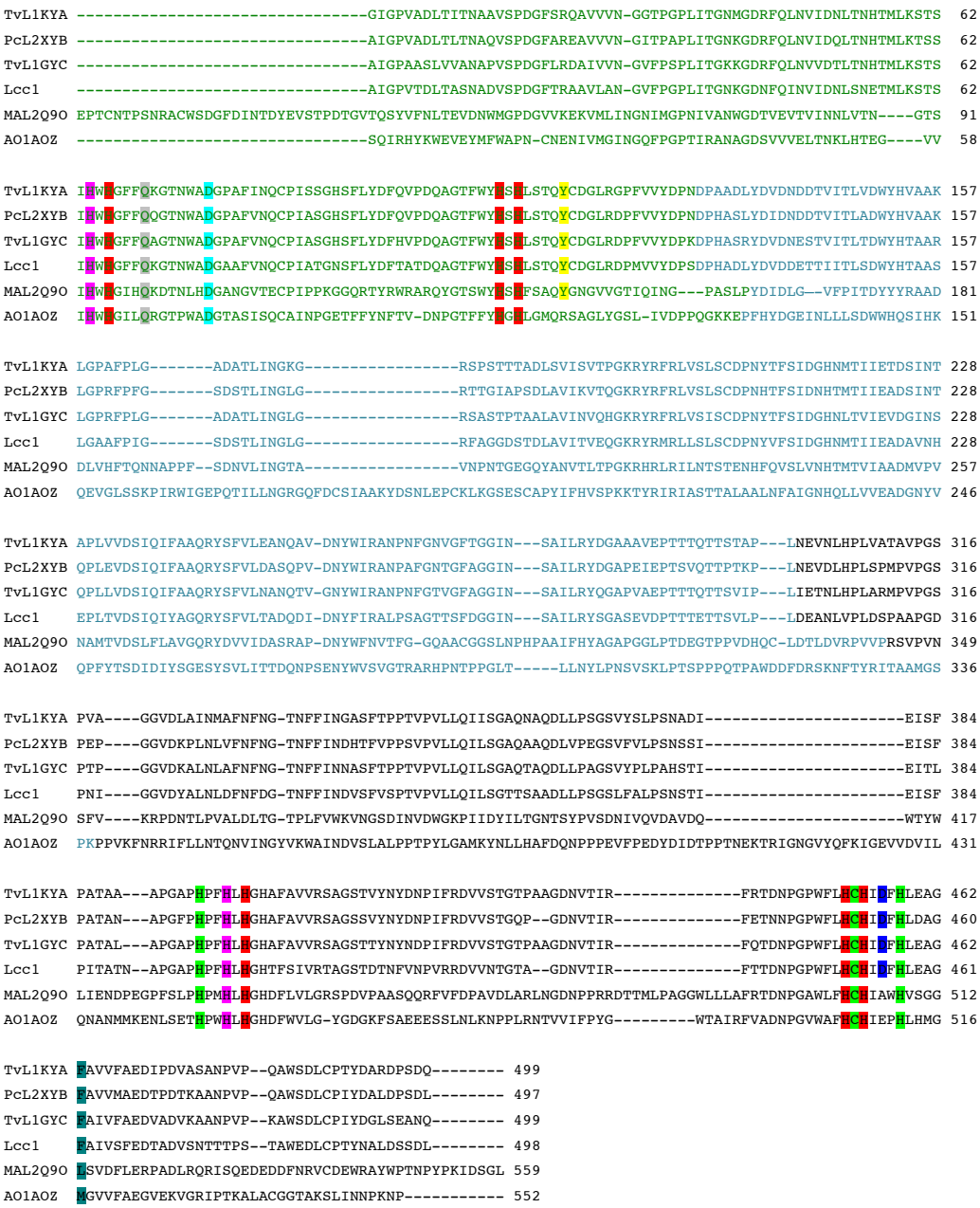

Figure 3.9 Sequence alignment of the three-domain laccases: TvL1KYA from *T. versicolor* [75], PcL from *P. cinnabarinus* (PcL2XYB [76]), TvL1GYC from *T. versicolor* [103], Lcc1 from *T. versicolor*, MaL from *M. albomyces* (MaL2Q9O [104]) and AO from zucchini (AO1AOZ [13]). The residues coordinating to the T1, T2 and T3 Cus are highlighted in green, purple and red, respectively. The Phe, Leu and Met in the axial position at the T1 Cu site are highlighted in teal. The conserved Gln (Gln70 in TvL1KYA), Asp (Asp77 TvL1KYA) and Tyr (Tyr116 in TvL1KYA) are highlighted in gray, cyan and yellow, respectively. The Asp (Asp456 in TvL1KYA) corresponding to Glu487 in Fet3p is highlighted in navy blue. Domain 1, 2 and 3 are green, blue and black, respectively. The sequence alignment was obtained using ClustalX.

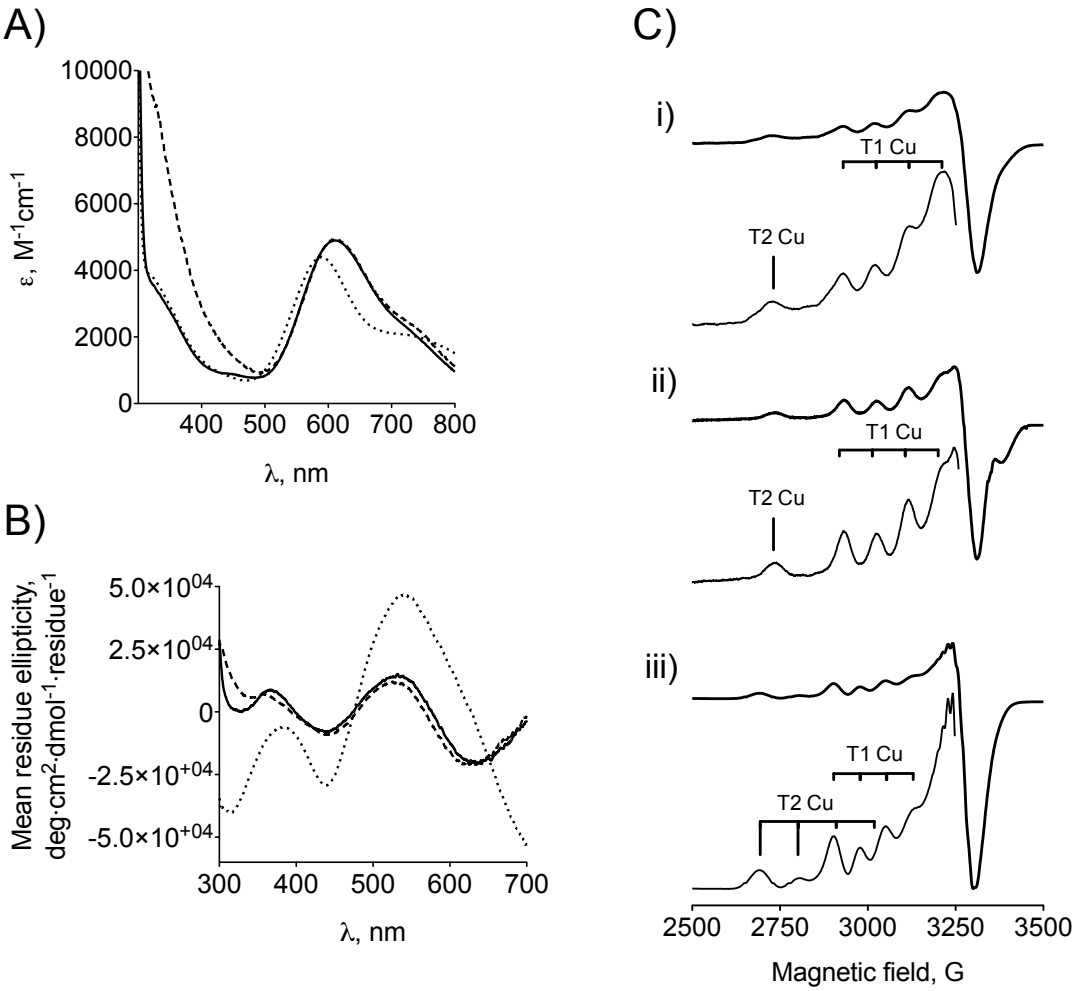

Figure 3.10 UV-Vis absorption (A) and visible CD (B) spectra of Lcc1 (—), Laccase A (- - -) and $SLAC_{truncated}$ (···). Spectra of Lcc1 and Laccase A were acquired in 50 mM phosphate pH 6.0, whilst $SLAC_{truncated}$ was in 50 mM phosphate pH 7.0. (C) EPR spectra of Lcc1 (i), Laccase A (ii) and $SLAC_{truncated}$ (iii) at ~ 80 K. The spectra of Lcc1 and Laccase A were acquired in 50 mM phosphate pH 6.0, whilst $SLAC_{truncated}$ in 20 mM Tris pH 7.5 containing 200 mM NaCl.

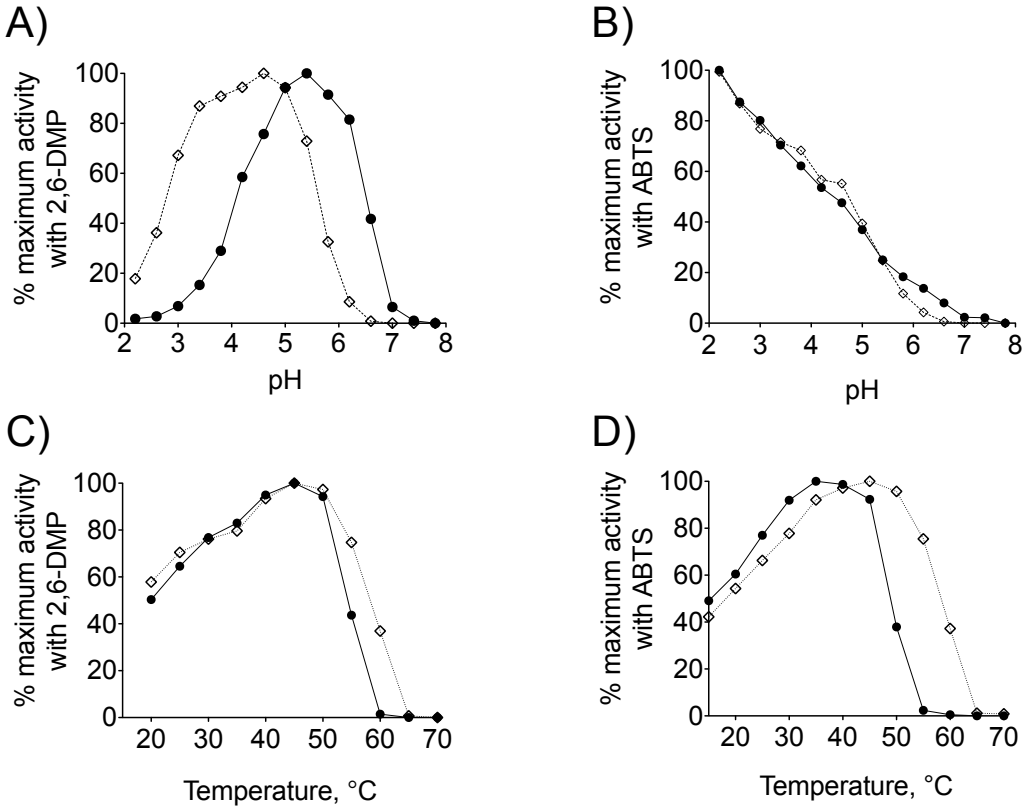

Figure 3.11 The effect of pH (21 °C) on the activity of Laccase A (◇) and Lcc1 (●) measured with (A) 2 mM 2,6-DMP and (B) 2 mM ABTS. The effect of temperature (15 - 70 °C) on activity of Laccase A (◇, pH 4.0) and Lcc1 (●, pH 5.4) measured with (C) 2 mM 2,6-DMP and (D) 2 mM ABTS.

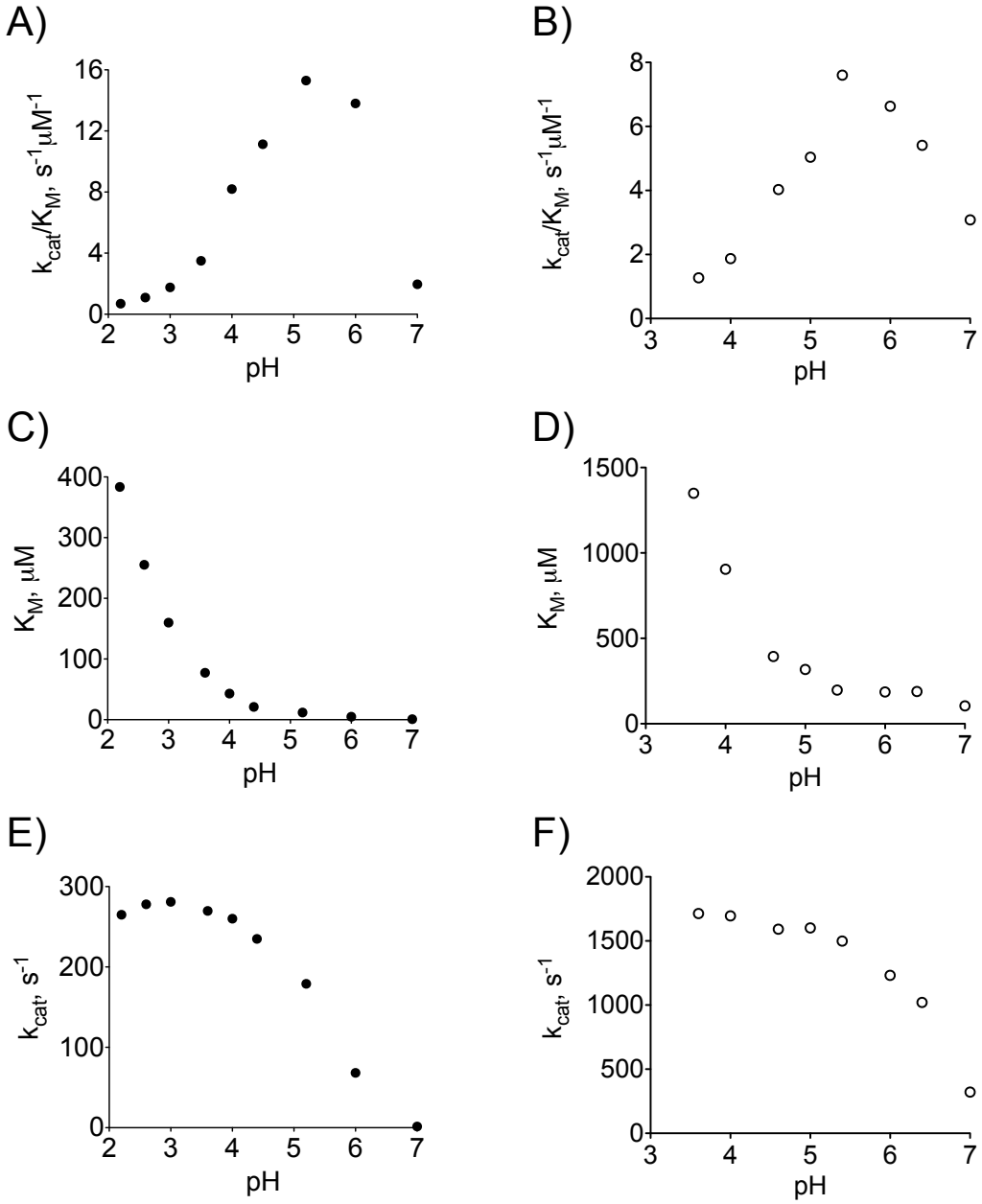

Figure 3.12 Plots of k_{cat}/K_M (A and B), K_M (C and D) and k_{cat} (E, and F) versus pH for the reaction of Laccase A (●) and Lcc1 (O) with 2,6-DMP at 21 °C.

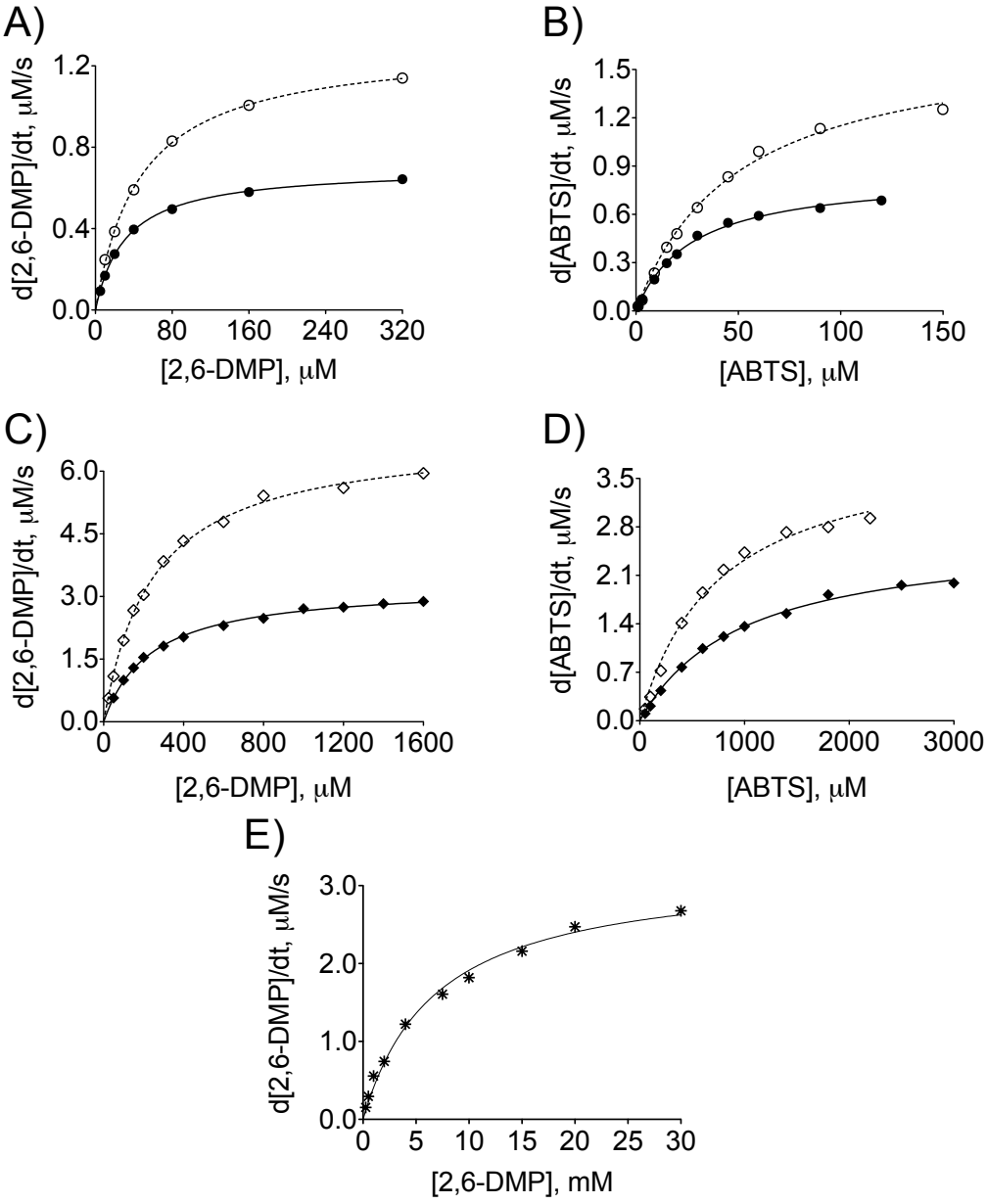

Figure 3.13 Michaelis-Menten plots for the reaction of Laccase A, Lcc1 and $SLAC_{truncated}$ with 2,6-DMP and ABTS giving the parameters obtained listed in Table 3.7. Activity of Laccase A with 2,6-DMP (A, 2.7 nM Laccase A) and ABTS (B, 2.1 nM Laccase A) measured in 100 mM citrate/phosphate buffer pH 4.0 at 21 (●) and 45 (⊖) °C. (C) Activity of Lcc1 (2.1 nM) with 2,6-DMP measured in 100 mM citrate/phosphate buffer pH 5.4 at 21 (◆) and 45 (◇) °C. (D) Activity of Lcc1 (1.0 nM) with ABTS measured in 100 mM citrate/phosphate buffer pH 4.0 at 21 (◆) and 35 (◇) °C. (E) Activity of SLAC (504 nM) with 2,6-DMP measured in 100 mM phosphate pH 8.0 at 21 °C.

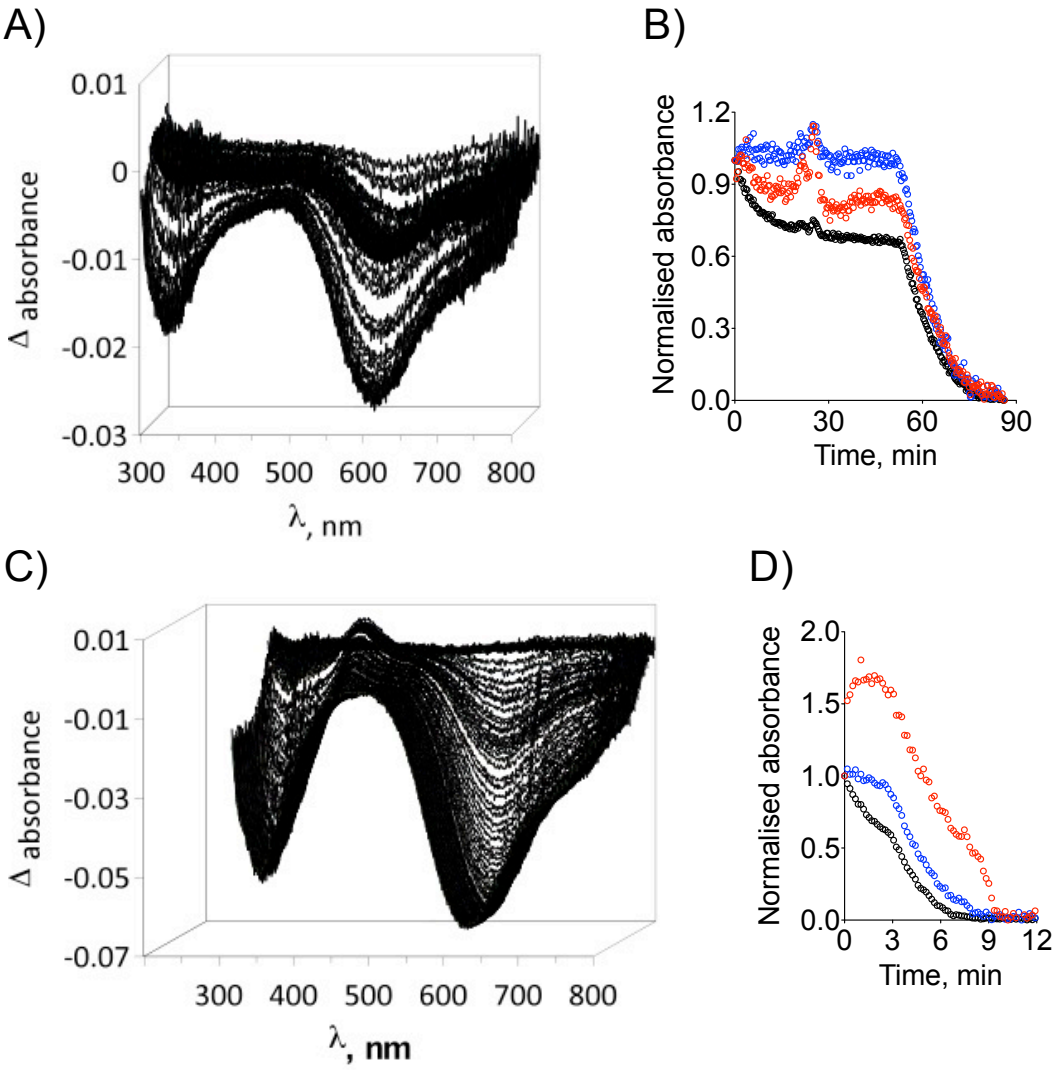

Figure 3.14 Difference absorption spectra (spectrum minus that of the oxidized protein) of (A) Laccase A (27 µM) reduced with 2 mM hydroxylamine in O_2-containing buffer and (C) the same protein (14 µM) reduced with 1 mM hydroxylamine in anaerobic buffer. Time-dependent changes in absorbance intensity at 610 nm (O), 420 nm (O) and 330 nm (O) after addition of hydroxylamine under (B) aerobic and (D) anaerobic conditions are also shown. Measurements were performed at RT in 100 mM phosphate pH 6.0.

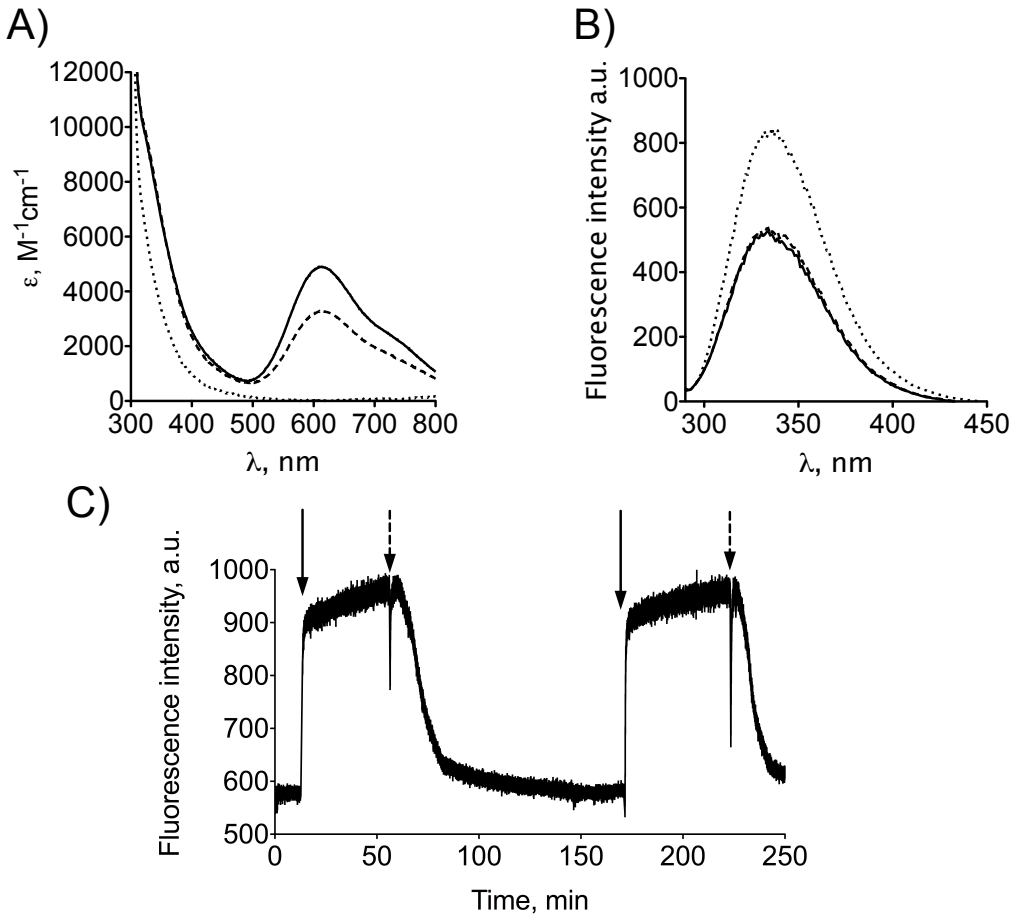

Figure 3.15 UV-Vis (A) and Trp (B) fluorescence emission spectra of oxidized (—), ascorbate-reduced (···) and oxygen re-oxidized (- - -) Laccase A. (C) Intensity changes in the emission (divided by the initial fluorescence intensity) upon reduction and oxidation of Laccase A (5.37 μM). Fluorescence was followed at 334 nm using an excitation wavelength of 285 nm. Solid arrows in (C) and (D) indicate the addition of reductant (ascorbate), whereas dashed arrows indicate exposure to oxygen. Measurements were performed in 50 mM phosphate pH 6.0 at RT.

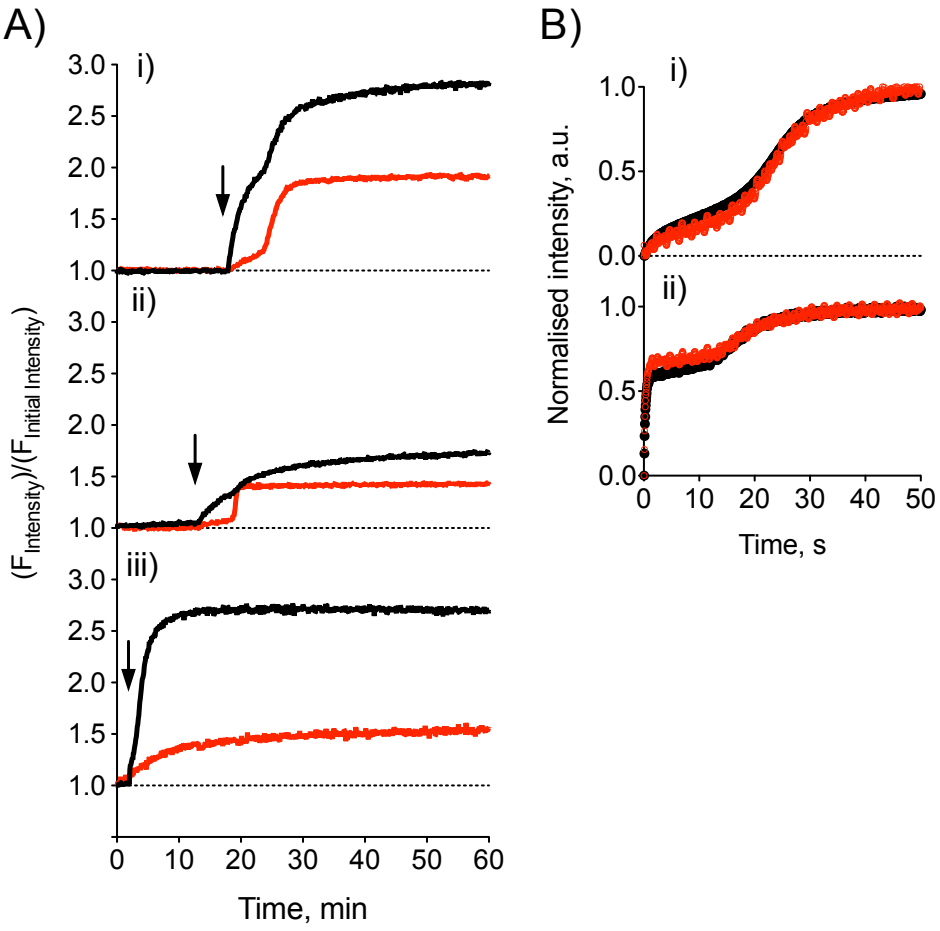

Figure 3.16 (B) Fluorescence intensity changes (divided by the initial fluorescence intensity) upon reduction of (i) ATTO 647N labeled Laccase A (45 nM), (ii) ATTO 647N labeled Lcc1 (60 nM) in 50 mM phosphate pH 6.0 and (iii) ATTO 590 labeled $SLAC_{truncated}$ (38 nM) in 50 mM phosphate pH 7.5. ATTO 647N and ATTO 590 fluorescence (—) was followed at 657 nm (λ_{exc} = 630 nm) and 630 nm (λ_{exc} = 590 nm), respectively. Trp emission (—) was followed at 334 nm (λ_{exc} = 285 nm). The arrows indicate when hydroxylamine (1 mM) was added. (A) A comparison of emission and corresponding absorbance (multiplied by -1) observed during the reduction of ATTO 532 labeled Laccase A (70 nM) by ascorbate in 100 mM phosphate pH 6.0, under anaerobic conditions: (i) Trp fluorescence at 340 nm (O, λ_{ex} = 280 nm) compared with the absorbance at 330 nm (●); (ii) ATTO 532 fluorescence at 550 nm (O, λ_{ex} = 532 nm) compared with absorbance at 610 nm (●).

3.5 Discussion

3.5.1 *Expression and characterization of laccases*

Industrial and biotechnological applications of laccases require large scale production of stable and active enzymes. High yields of low potential laccases can be obtained from bacterial sources and ascomycate fungi. The more desirable high potential laccases originate from basidiomycetes fungi, and these are generally difficult to express heterologously in an active form [27, 72]. So far, heterologous expression of fungal enzymes has only been partially successful, when evaluated in terms of yield, protein stability or activity. Therefore development of efficient expression system for high potential laccases and engineering of bacterial laccases with enhanced activity is of special interest [17, 72].

The expression of Lcc1 in *E. coli* resulted in insoluble aggregates in IB. Modifications to the expression procedure led to an increase in the amount of soluble Lcc1, however, this protein was not active with ABTS and did not show the spectral features typical of laccase. Expression of active fungal laccase in *E. coli* is challenging, probably owing to the lack of post-translational modifications, and particularly glycosylation. These findings are consistent with previous observations on laccase from *Coriolus versicolor*, in which the protein loses activity when the sugars are selectively removed [181]. Several roles for carbohydrate moieties attached to laccase have been suggested, including stabilization of the Cu centers, directing protein secretion, protection against proteolysis and enhancing thermostability [182]. Glycans have also been shown to influence laccase activity [183].

Yeast expression systems are economical and in most cases result in relatively high protein yields. The ability of yeast to perform eukaryote-specific post-translational modifications, particularly glycosylation is highly advantageous for expression of fungal laccases. However, different yeasts do not process laccases with the same efficiency. Johnsson *et al.* reported that Lcc1 could be successfully expressed in *P. pastoris* (using the pHIL expression vector) [85, 87] but not in *S. cerevisae* [79], whereas Lcc2 was expressed in both organisms [79, 83, 90]. Herein, active Lcc1 was successfully expressed in *P. methanolica* PMAD11 but not in *P. pastoris* X33 strain (using the pPICZαA expression vector). The latter system has recently been successfully applied for the expression of the fungal laccase from *Cyathus bulleri* [184]. Expression of Lcc1 in *P. methanolica* resulted in secretion of protein with an MW^{app}

much heavier than reported, most probably due to hyperglycosylation. Additionally, the production yield of protein was lower than expected (10 mg/L, [94]).

Expression systems using filamentous fungi as hosts are interesting owing to their ability to produce proteins in high yields. For instance, homologous over-expression of laccases in *Trametes* sp. 420 [185] and *P. cinnabarinus* [165] yielded 310 mg/L and 1.2 g/L of protein, respectively. *S. commune* is considered a model basidiomycete fungus as a full genome sequence is available [155] and genetic modification of this organism is relatively easy. It has a short life cycle (10 days) and grows on simple media that facilitates fungus cultivation and lowers costs. Purification of proteins expressed in *S. commune* WT is complicated by the production of large amounts of SPG in the culture media of this fungus. However, the KS8 strain does not produce SPG [158, 186, 187] making it a preferential host for protein production.

Expression of Lcc1 by *S. commune* KS8 resulted in maximal laccase activity ranging from 150 - 240 nkat/mL. The expression level of purified Lcc1 (~ 5 mg/L of media) is lower than those reported in *P. methanolica* [94] and *P. pastoris* [67]. Increasing temperature and lowering aeration during cultivation as well as increasing $Cu(NO_3)_2$ concentration have been identified as factors affecting the level of Lcc1 production in the KS8 strain. The expression levels of Lcc1 increased when aeration of media decreased, therefore liquid-standing cultures instead of shake flask cultures were used for the growth of *S. commune* expressing Lcc1. Oxygen-limited conditions have previously been reported to result in higher level of laccase secretion in *S. cereviasae* [83]. In contrast to expression in yeast [86, 87, 93], decreasing the temperature of cultivation did not result in an increase in protein production. The effect of the initial pH of the cultivation media on enzyme expression was lower than that observed in *S. cereviasae* [79], *P. pastoris* [85, 87] and *P. methanolica* [93, 94].

Activity-based method of detecting successful Lcc1-secreting transformants of *S. commune*, limits the expression system to the active variants of Lcc1. The method can be extended to inactive variants by using antibodies directed against Lcc1 or an epitope tagged to the protein. Surprisingly, the C-terminal fusion of Lcc1 with a single cMYC epitope led to the production of Lcc1_cMYC that was inactive with ABTS and 2,6-DMP. The ascomycate laccases such as MaL from *M. albomyces* [104] contain a conserved Asp-Ser-Gly-Leu motif at the C-terminus (so-called “C-terminal plug”) pointing towards the T2/T3 Cu cluster and obstructing the solvent channel. The carboxylate group of this C-terminal Leu is in a hydrogen bonding contact (2.8 Å) with a T3 Cu coordinating Nδ1 atom of His140 [104], and its position is critical for the

enzyme activity [188]. Laccases from *T. versicolor* do not have an analogous motif and the C-terminus (~ 16 Å from Nδ1 atom of His111 in TvL1KYA) is nine-residue shorter than that of MaL. Unexpectedly therefore the 11-residue long cMYC epitope in Lcc1 interacts with the T2/T3 Cu cluster (similar to the "C-terminal plug" in MaL) and results in loss of protein activity.

The oxidation of the phenolic substrate 2,6-DMP is optimal for Lcc1 and Laccase A at slightly acidic pH, whilst SLAC shows maximal activity in alkaline solutions [153]. At RT, the affinity of Lcc1 for 2,6-DMP and ABTS is lower than that of Laccase A. The k_{cat}/K_M for Lcc1 with 2,6-DMP is ~ 2.6-fold lower compared to that of Laccase A, and almost 7000-fold higher than that of $SLAC_{truncated}$. The activity for oxidation of ABTS by Lcc1 and Laccase A is very high (maximal at 35 and 45 °C, respectively), especially at low pH, however, the activity is compromised by low stability of the proteins at acidic pH.

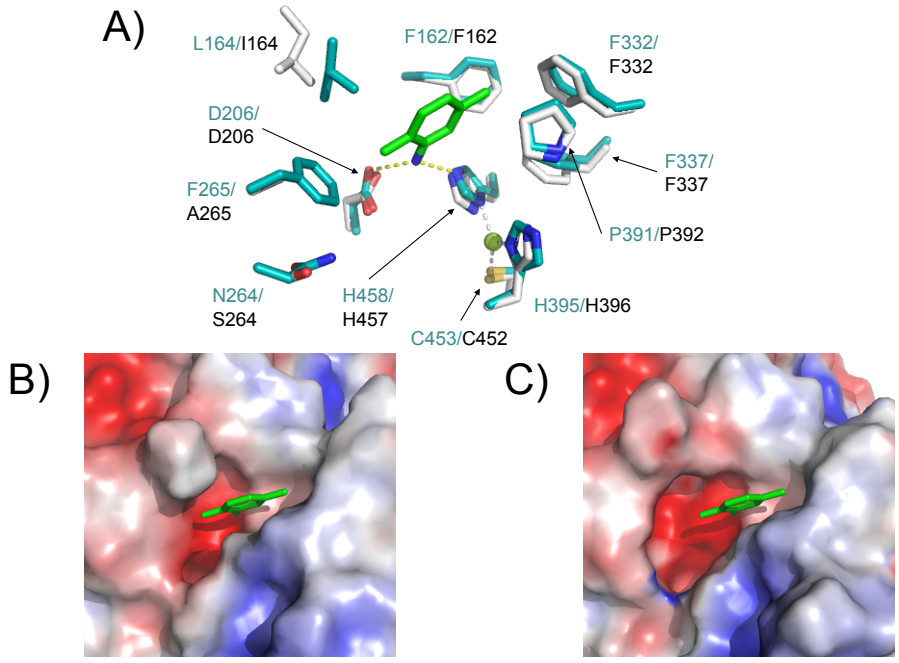

Figure 3.17 (A) 2,6-dimethylbenzene-1-amine (2,5-xylidine, C^{α} in green) and neighboring interacting residues in the substrate cavity of TvL1KYA [75] (teal) superimposed on structural model of Lcc1 (gray). The T1 Cu is shown as a lime sphere. Qualitative electrostatic surface representation in the substrate-binding cavity of (B) TvL1KYA (1KYA crystallized with 2,5-xylidine) and (C) Lcc1 (superimposed on 1KYA). Surface generated in PyMol using protein contact potential with negative charge red and positive charge blue.

The structure of TvL1KYA is the only structure of *T. versicolor* laccase that was co-crystallized with an organic substrate, 2,5-xylidine, in the substrate-binding cavity [75]. This pocket is located at the boundary between MBD-2 and MBD-3 and is paved with a series of hydrophobic residues, such as Phe162, Leu164, Phe265, Phe332, Phe337 and Pro391, which may be involved in the protein-substrate interactions. The superposition of the structural model of Lcc1 with the crystal structure of TvL1KYA shows that the conserved among laccases, catalytically essential His (His458 and His457 for TvL1KYA and Lcc1, respectively) and Asp (Asp206 and Asp206 for TvL1KYA and Lcc1, respectively) are located at the rear wall of this cavity, with their side chains groups pointing towards the substrate-binding pocket. The imidazole Nε2 atom of His458 in TvL1KYA is within hydrogen-bonding distance of the amino nitrogen of 2,5-xylidine, and is considered important for ET between the substrate and the T1 Cu site [75, 189]. The amino group of 2,5-xylidine also forms a hydrogen bond with the side chain Oδ2 atom of Asp206 (Figure 3.17.A). This residue is suggested to play an important role in binding and orienting the substrate molecule [75, 189]. The shape and volume of the hydrophobic substrate-binding pocket varies between laccases. A comparison of the cavities of TvL1KYA and Lcc1 indicates the presence of three amino acid differences: Leu164/Ile164, Phe265/Ala265 and Asn264/Ser264 in TvL1KYA/Lcc1 (Figure 3.17.A). As a result, the cavity of TvL1KYA (Figure 3.17.B) is smaller than that of Lcc1 (Figure 3.17.C). Broadening of a substrate-binding pocket has also been observed in *T. versicolor* Lcc1δ that contains Val164 and Ala265 (as found in Lcc1) and shows similar to Lcc1 low affinities and high turnover rates with ABTS (K_M of 2262 ± 103 μM and k_{cat} of 798 ± 44 s^{-1} at pH 5.0 (RT)) [190]. The influence of residues at positions 164 and 265 (localized ~ 4 and 5 Å from 2,5-xylidine, respectively, in TvL1KYA [75]) on substrate binding and stabilization in *T. versicolor* laccases was previously investigated by site-directed mutagenesis [190, 191]. Mutations to both residues have negative influence on enzyme/substrate interaction and reduce the oxidation ability of the enzyme with respect to bulky phenolic substrates such as anthracene (polycyclic aromatic hydrocarbon) [191] and *ortho*- and *meta*-substituted di-t-Bu phenols [190]. Replacement of Phe265 to Ala (as found in Lcc1) lowered 2-fold the affinity of TvL1KYA for 2,6-DMP but did not change the affinity for ABTS [191]. Therefore one of the reasons for decreased activity of Lcc1 with 2,6-DMP (K_M almost 10-fold lower compared to that of TvL1KYA) could be a depletion of hydrophobic interaction between the smaller Ala265 and the substrate molecule. X-ray structural data of CotA crystallized with ABTS showed that the

substrate molecule is bent and only partially buried inside the substrate-binding cavity, with one of the sulfonate O atoms forming a hydrogen bond with Gly323 (3.5 Å) [192]. Assuming similar positioning of ABTS within a substrate-binding pocket of TvL1KYA, the molecule might be stabilized through a hydrogen bond between the O sulfonate atom and side chain N donor of Asn264. The absence of a similar hydrogen bond in Lcc1 (due to the N264S replacement) could result in decreased affinity of Lcc1 for ABTS compared to TvL1KYA.

3.5.2 *Comparison between three-domain laccases and two-domain laccases*

Recently, direct involvement of Tyr108 in the catalytic cycle of SLAC has been demonstrated [110, 193] (Figure 3.18). The exact role of the residue is not known, but Gupta *et al.* hypothesize that it provides an additional electron, therefore reducing the lifetime of a three electron loaded intermediate (PI+e^-). In this way Tyr108 would act as a "kinetic buffer" of redox equivalents, which prevents the generation of reactive oxygen species and possible damage to the enzyme [110]. The temporary tyrosyl (Tyr) radical was observed during oxidation of reduced WT SLAC and the C288S (T1D) variant and is characterized by an absorption band at ~ 410 nm and EPR signals in the g = 2 and 4 regions [193]. The EPR signals are thought to arise from exchange coupling of two unpaired spins, one residing at the T2/T3 Cu cluster and the other on Tyr108. This residue is located ~ 5 Å from the T2 Cu, at the interface of two subunits of the trimer and its absence in the Y108F and Y108A T1D SLAC variants was found to disrupt enzyme activity [110].

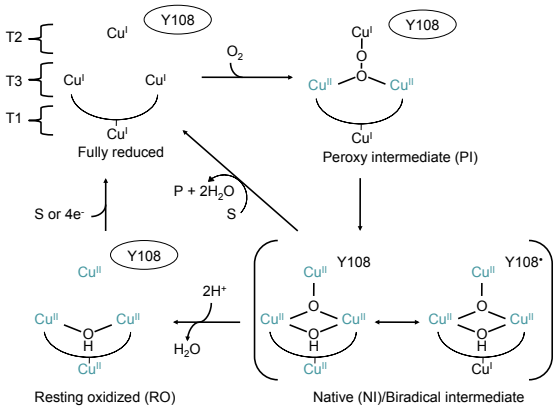

Figure 3.18 Proposed pathway of O_2 reduction to H_2O by SLAC, which includes the role of Tyr radical (adapted from [110]). Reduced and oxidized Cu sites are depicted in blue and black, respectively. S indicates the substrate, while P is the reaction product.

Preliminary results assessing a possible role of a Tyr radical in the catalytic cycle of fungal three-domain laccases showed that under oxygen-limited conditions during the reduction of resting oxidized Laccase A and Lcc1 by hydroxylamine, an absorption band at ~ 420 nm is observed. The presence of this band was also observed during re-oxidation of hydroxylamine-reduced Laccase A and Lcc1. The spectral fingerprint is clearly different from those of PI (peroxy intermediate, with the LMCT band at 340 nm) and NI (native intermediate, with the LMCT bands at 318 and 365 nm) described by Solomon and coworkers [114, 122 - 126, 130], and can be assigned to a Tyr radical. The formation of a radical during oxidation of hydroxylamine-reduced Laccase A was not observed by EPR as high intensity signals of the T1 and the T2 Cus overlap in the g = 2 region (the EPR signal in g = 4 was also not observed, data not shown). The attempts to prepare T1D Lcc1 variant, in which Cys452 is replaced with Ser were unsuccessful. Detailed experiments, including the kinetics of formation and decay of the intermediate are necessary to determine if the transient species indeed corresponds to a Tyr radical.

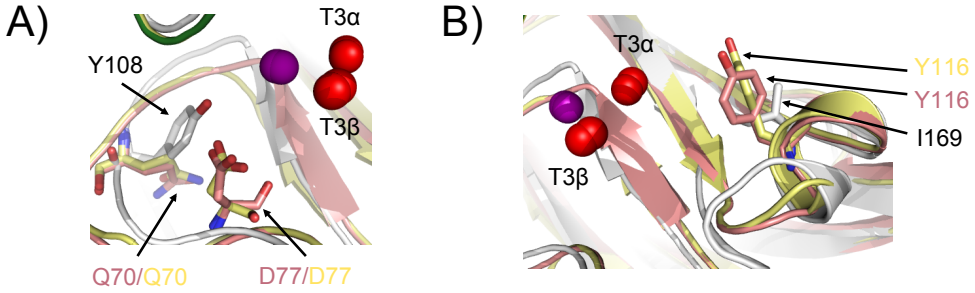

Figure 3.19 Overlaid T2/T3 Cu sites of SLAC (gray, [108]), structural model of Lcc1 (yellow) and TvL1KYA (MBD-1, -2 and -3 are pink, blue and green, respectively, [75]) around Tyr108 in SLAC (A) and Tyr116 in TvL1KYA and Lcc1 (B). Tyr108 and Ile169 of SLAC are gray sticks; Gln70, Asp77 and Tyr116 of TvL1KYA and Lcc1 are pink and yellow sticks, respectively. The T2 and T3 Cus of SLAC and TvL1KYA are purple and red spheres, respectively.

Tyr108 of SLAC is conserved not only among homologous, two-domain MCOs but also in six-domain Cp (Tyr107, pdb file: 2J5W). Furthermore, the appearance of a 410 nm feature was previously observed during oxidation of fully reduced Cp but the nature of the intermediate was not investigated further [194, 195]. The involvement of the Tyr radical in the catalytic cycles of SLAC and Cp would support the evolution postulates, in which the two-domain laccases are proposed to be ancestors to the

six-domain Cp [113, 196]. The superposition of crystal structures of AO, TvL1KYA, TvL1GYC and the homology model of Lcc1 with that of SLAC showed that Tyr108 in the two-domain laccase is replaced with Gln70 and Gln66 in the three-domain laccases (Figure 3.19.A) and AO, respectively, with the side chains of Tyr108 and Gln70/Gln66 pointing in the opposite directions. The side chain of Tyr108 partially overlaps with Asp77 in the three-domain laccases (Figure 3.19.A) and Asp73 in AO that is thought to participate in formation of PI [122]. Structural and sequence comparisons of the two- and three-domain MCOs show that Tyr116 of laccases from *T. versicolor* (Figure 3.19.B), which is located ~ 6, 8 and 10 Å from the T3α, T3β and T2 Cus, respectively, is conserved among three-domain laccases (Figure 3.9). The corresponding residue in the structurally similar three-domain AO and SLAC is not a Tyr but Arg111 (Figure 3.9) and Ile169 (Figure 3.19), respectively. The investigation of Tyr116 variants of T1D Lcc1 is required to assess if this residue is involved in activity of this enzyme.

3.5.3 *Preliminary fluorescence studies on laccases*

Sensitive fluorescence-based biosensors for the detection of O_2 [197 - 199], histamine [200], nitric oxide [201] and phenols [202] have recently been developed. These biosensors belong to a new generation of devices, which combine the substrate selectivity of proteins and the high sensitivity of fluorescence detection. In this approach the detection of a protein's oxidation state is based on radiationless FRET from the attached fluorescent label to the prosthetic group of the redox protein (Chapter 1.4.3). Redox-induced changes in the spectral features of the prosthetic group are therefore translated into changes in emission [150, 151]. The FluoRox principle can be adapted to all redox proteins, including laccases, whose absorption spectrum changes upon redox interconversion. In laccases, this method allows for individual assessment of the oxidation state of the T1 Cu and the T2/T3 Cu cluster and can be applied to study enzyme catalysis. The method also has great potential for the development of novel laccase-based biosensors (Figure 3.20) to measure the conversion of various compounds such as chlorinated phenols, synthetic dyes and polycyclic aromatic hydrocarbons [3, 21, 174]. The determination of trace amounts of these compounds and their derivatives is of environmental importance as they are released by numerous industries, in particular during the manufacture of drugs and dyes, fuel burning, and are present in wastewaters from pulp and paper production.

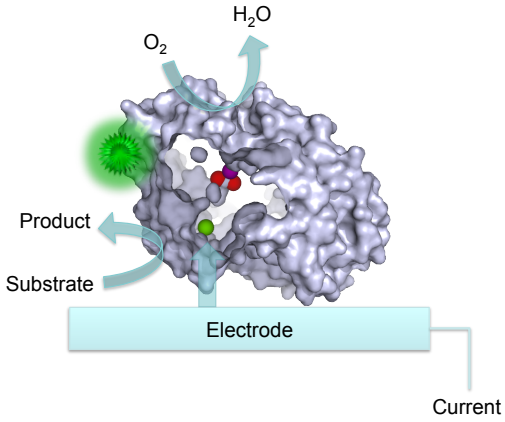

Figure 3.20 Schematic representation of a biosensor using laccase and the FluoRox principle. A fluorescently labeled enzyme is immobilized on a transparent or semi-transparent electrode surface. The fluorescence intensity depends on the oxidation state of the active centre, which changes upon reactions with the electrode or analytes. The T1, T2 and T3 Cus are green, magenta and red spheres, respectively. The fluorescent label is depicted as a green star.

The detection unit of FluoRox biosensor (a fluorescently labeled enzyme) ought to have increased sensitivity by exhibiting a high fluorescence *SR* in order to enhance the contrast between the reduced and oxidized forms of the enzyme. Föster theory (Chapter 1.4.2) predicts that the quenching efficiency (and *SR* of the label) will depend on the distance, the orientation and the spectral overlap between the electron donor (e.g. fluorescent dye and Trp) and the acceptor (e.g. the T1 and T2/T3 Cus). The relatively low fluorescence *SR* of N-terminally labeled Lcc1 (0.30) and $SLAC_{truncated}$ (0.36) can be improved by changing the attachment point of the dye. This can be achieved by introducing surface exposed Cys residues as targets for maleimide-modified fluorescence dyes, permitting more specific labeling (as in Chapter 2). Gly433 or Ala325 located 16 and 20 Å respectively from the T1 Cu are possibilities for introducing Cys residues in Lcc1. Due to the trimeric arrangement of SLAC, the location of the introduced Cys needs to be chosen so that the distance between the label and the T1 Cu site within the same monomer is optimal for FRET, whilst limiting the influence of redox changes at the two other T1 Cu sites of the trimer (as in Chapter 2). The ATTO 647N maleimide conjugated K204C SLAC variant (Lys204 is located 16 Å from the T1 Cu within the same monomer and 26/30 Å from the T1 Cus in the other monomers), which was recently used for the measurements at the single molecule level, showed the increased *SR* value to ~ 0.8 [203]. Increasing the spectral overlap between the emission spectrum of the dye and the absorption spectrum of the T1 Cu site could

further enhance the fluorescence *SR*. However, using various different rhodamine-based dyes for the labeling of Lcc1, Laccase A and $SLAC_{truncated}$ resulted in little improvement of the *SR* values.

Major challenges for the development of FluoRox-based biosensors for industrial applications are shelf life of the fluorescently labeled enzymes and immobilization of the labeled proteins in a stable and active form on conducting surfaces (transparent or semi-transparent). The stability of $SLAC_{truncated}$, which is N-terminally labeled with rhodamine-based fluorescent dyes, is relatively good, with the construct retaining its *SR* value for several days at 4 °C. However, the stability of labeled Laccase A and Lcc1 is very poor, with the *SR* decaying after ~ 24 h for Laccase A and within a few hours for Lcc1. The ability of fungal laccases to catalyze the conversion of aromatic compounds with high efficiency indicates that the rhodamine-based fluorescent dyes are probably degraded by the enzymes (broader substrate-binding pocket of Lcc1 might enable a better binding and faster conversion of dyes), and therefore cannot be used for labeling. This problem would be overcome by using an alternative donor such as quantum dots.

3.6 Conclusions

Lcc1 from *T. versicolor* has been successfully expressed in *S. commune* KS8. The production of laccase was found to depend on several factors, including cultivation temperature, $Cu(NO_3)_2$ concentration, and culture aeration. The expression level obtained so far is sufficient for biochemical characterization and preliminary measurements on the catalytic activity of the enzyme, but it is too low to be useful for industrial purposes. Further optimization of the expression protocol (on both protein expression and purification efficiency levels) is necessary to enhance the production of Lcc1.

Fluorescence-based tracking of redox events independently at the T1 and the T2/T3 Cu sites of laccases is possible. Therefore, a laccase-based FluoRox construct can be used not only for biosensing but also to provide detailed insight into the kinetics of the internal ET processes between the Cu centers in the enzyme. In contrast to $SLAC_{truncated}$, fungal laccases exhibit a very high conversion rate of organic compounds (including dyes), and therefore, the preparation of a stable FluoRox device requires labeling with different than rhodamine-based fluorophores.

3.7 References

1) Solomon E.I., Sundaram U.M., Machonkin T.E., 1996, Chem. Rev., 96, 2563-2605

2) Messerschmidt A., Huber R., 1990, Eur. J. Biochem., 26, 341-352

3) Mayer A.M., Staples R.C., 2002, Phytochemistry, 60, 551-565

4) Giardina P., Faraco V., Pezzella C., Pisctielli A., VanhulleS., Sannia G., 2010, Cell. Mol. Life Sci., 67, 369-385

5) Morozova O.V., Shumakovich G.P., Gorbacheva M.A., Shleev S.V., Yaropolov A.I., 2007, Biochemistry (Mosc), 72, 1136-1150

6) Hüttermann A., Mai C., Kharazipour A., 2001, Appl. Microbiol. Biotechnol., 55, 387-394

7) Hoopes J.T., Dean J.F., 2004, Plant. Physiol. Biochem., 42, 27-33

8) Thurston C.F., 1994, Microbiology, 140, 19-26

9) Dittmer N.T., Suderman R.J., Jiang H., Zhu Y.C., Gorman M.J., Kramer K.J., Kanost M.R., 2004, Insect Biochem. Mol. Biol., 34, 29-41

10) Sharma P., Goel R., Capalash N., 2007, World J. Microbiol. Biotechnol., 23, 823-832

11) Martins L.O., Soares C.M., Pereira MM.., Teixeira M., Costa T., Jones G.H., Henriques A.O., 2002, J. Biol. Chem., 277, 18849-18859

12) Kosman D.J., 2010, J. Biol. Inorg. Chem., 15, 15-28

13) Messerschmidt A., Ladenstein R., Huber R., Bolognesi M., Avigliano L., Petruzzelli R., Rossi A., Finazzi-Agró A., 1992, J. Mol. Biol., 224, 179-205

14) Bento I., Peixoto C., Zaitsev V.N., Lindley P.F., 2007, Acta Crystallogr. D Biol. Crystallogr., 63, 240-248

15) Reinhammar B.R.M., 1972, Biochim. Biophys. Acta, 275, 245-259

16) Farver O., Goldberg M., Wherland S., Pecht I., 1978, Proc. Natl. Acad. Sci. USA, 75, 5245-5249

17) Rodgers C.J., Blanford C.F., Giddens S.R., Skamnioti P., Armstrong F.A., Gurr S.J., 2010, Trends Biotechnol., 28, 63-72

18) Xu F., 1997, J. Biol. Chem., 272, 924-928

19) Xu F., Berka R.M., Wahleithner J.A., Nelson B.A., Shuster J.R., Brown S.H., Palmer A.E., Solomon E.I., 1998, Biochem. J., 334, 63-70

20) Tadesse M.A., D'Annibale A., Galli C., Gentili P., Sergo F., 2008, Org. Biomol. Chem., 6, 868-878

21) Rodrigez Couto S., Toca Herrera J.L., 2006, Biotechnol. Adv., 24, 500-513

22) Riva S., 2006, Trends Biotechnol., 24, 219-226

23) Osma J.F., Toca-Herrera J.L., Rodríguez-Couto S., 2010, Enzyme. Res., 2010:918761, doi: 10.4061/2010/918761

24) Sanchez-Amat A., Solano F., 1997, Biochem. Biophys. Res. Commun., 240, 787-792

25) Shleev S.V., Khan I.G., Gazaryan I.G., Morozova O.V., Yaropolov A.I., 2003, Appl. Biochem. Biotechnol., 111, 167-184

26) Li K., Xu F., Eriksson K.E., 1999, Appl. Environ. Microbiol., 65, 2654-2660

27) Kunamneni A., Camarero S., García-Burgos C., Plou F.J., Ballesteros A., Alcalde M., 2008, Microb. Cell Fact., 7:32, doi: 10.1186/1475-2859-7-32

28) Virk A.P., Sharma P., Capalash N., 2012, Biotechnol. Prog., 28, 21-32

29) Brijwani K., Rigdon A., Vadlani P.V., 2010, Enzyme. Res., 2010:149748, doi: 10.4061/2010/149748

30) Pointing S.B., 2001, Appl. Microbiol. Biotechnol., 57, 20-33

31) Cameron M.D., Timofeevski S., Aust S.D., 2000, Appl. Microbiol. Biotechnol., 54, 751-758

32) Mikolasch A., Schauer F., 2009, Appl. Microbiol. Biotechnol., 82, 605-624

33) Mikolasch A., Manda K., Schlüter R., Lalk M., Witt S., Seefeldt S., Hammer E., Schauer F., Jülich W.D., Lindequist U., 2012, Biotechnol. Appl. Biochem., 59, 295-306

34) Minussi R.C., Pastore G.M., Duran N., 2002, Trends Food Sci. Technol., 13, 205-216

35) Selinheimo E., Kruus K., Buchert J., Hopia A., Autio K., 2006, J. Cereal. Sci., 43, 152-159

36) Setti L., Giuliani S., Spinozzi G., Pifferi P.G., 1999, Enzyme Microb. Technol., 25, 285-289

37) Roure M., Delattre P., Froger H., 1992, Eur. Pat. Appl., EP0504005

38) Golz-Berner K., Walzel B., Zastrow L., Doucet O., 2004, Int. Pat. Appl., WO2004017931

39) Soares G.M., Costa-Ferreira M., Pessoa de Amorim M.T., 2001, Bioresour. Technol., 79, 171-177

40) Karigar C.S., Rao S.S., 2011, Enzyme Res., 2011:805187

41) Bergbauer M., Eggert C., Kraepelin G., 1991, Appl. Microbiol. Biotechnol., 35, 105-109

42) Bullen R.A., Arnot T.C., Lakeman J.B., Walsk F.C., 2006, Biosens. Bioelectron., 21, 2015-2045

43) Gallaway J., Wheeldon I., Rincon R., Atanassov P., Banta S., Barton S.C., 2008, Biosens. Bioelectron., 23, 1229-1235

44) Tan Y., Deng W., Ge B., Xie Q., Huang J., Yao S., 2009, Biosens. Bioelectron., 24, 2225-2231

45) Nazaruk E., Sadowska K., Biernat J.F., Rogalski J., Ginalska G., Bilewicz R., 2010, Anal. Bioanal. Chem., 398, 1651-1660

46) Zebda A., Gondran C., Le Goff A., Holzinger M., Cinquin P., Cosnier S., 2011, Nat. Commun., 2:370, doi: 10.1038/ncomms1365

47) Wheeldon I.R., Gallaway J.W., Barton S.C., Banta S., 2008, Proc. Natl. Acad. Sci. USA, 105, 15275-15280

48) Duran N., Rosa M.A., D'Annibale A., Gianfreda L., 2002, Enzyme and Microb. Tech., 31, 907-931

49) Timur S., Pazarlioglu N., Pilloton R., Telefoncu A., 2004, Sens. Actuators. B Chem., 97, 132-136

50) Kulys J., Vidziunaite R., 2003, Biosens. Bioelectron., 18, 319-325

51) Roy J.J., Abraham T.E., Abhijith K.S., Kumar P.V.S., Thakur M.S., 2005, Biosens. Bioelectron., 21, 206-211

52) Jarosz-Wilkolazka A., Ruzgas T., Gorton L., 2005, Talanta, 66, 1219-1224

53) Haghighi B., Gorton L., Ruzgas T., Jonsson L.J., 2003, Anal. Chim. Acta, 487, 3-14

54) Freire R.S., Duran N., Kubota L.T., 2002, Anal. Chim. Acta, 463, 229-238

55) Marko-Varga G., Emneus J., Gorton L., Ruzgas T., 1995, Trends Anal. Chem., 14, 319-328

56) Liu J., Niu J., Yin L., Jiang F., 2011, Analyst., 136, 4802-4808

57) Rawal R., Chawla S., Pundir C.S., 2011, Anal. Biochem., 419, 196-204

58) Sezgintürk M.K., Odaci D., Pazarlioğlu N., Pilloton R., Dinçkaya E., Telefoncu A., Timur S., 2010, Artif. Cells Blood Substit. Immobil. Biotechnol., 38, 192-199

59) Sanz J., de Marcos S., Galban J., 2012, Anal. Bioanal. Chem., 404, 351-359

60) Jarosz-Wilkolazka A., Ruzgas T., Gorton L., 2004, Enzyme Microb. Technol., 35, 238-241

61) Gardiol A.E., Hernandez R.J., Reinhammar B., Harte B.R., 1996, Enzyme Microb. Technol., 18, 347-352

62) Leech D., Daigle F., 1998, Analyst., 123, 1971-1974

63) Deng L., Chen C., Zhou M., Guo S., Wang E., Dong S., 2010, Anal. Chem., 82, 4283-4287

64) ElKaoutit M., Naranjo-Rodriguez I., Temsamani K.R., Dominguez de la Vega M., Hidalgo-Hidalgo de Cisneros J.L., 2007, J. Agric. Food Chem., 55, 8011-8018

65) El Kaoutit M., Naranjo-Rodriguez I., Temsamani K.R., Dominguez M., Hidalgo-Hidalgo de Cisneros J.L., 2008, Talanta, 75, 1348-1355

66) Bauer C.G., Kuhn A., Gajovic N., Skorobogatko O., Holt P.J., Bruce N.C., Makower A., Lowe C.R., Scheller F.W., 1999, Fresenius' J. Anal. Chem., 364, 179-183

67) Lisdat F., Wollenberger U., Makower A., Hortnag H., Pfeiffer D., Scheller F.W., 1997, Biosens. Bioelectron., 12, 1199-1211

68) Szeponik J., Moller B., Pfeiffer D., Lisdat F., Wollenberger U., Makower A., Scheller F.W., 1997, Biosens. Bioelectron., 12, 947-952

69) Leite O.D., Lupetti K.O., Fatibello-Filho O., Vieira I.C., de M. Barbosa A., 2003, Talanta, 59, 889-896

70) Ferry Y., Leech D., 2005, Electroanalysis, 17, 2113-2119

71) Silva L.I.B., Ferreira F.D.P., Freitas A.C., Rocha-Santos T.A.P., Duarte A.C., 2009, Talanta, 80, 853-857

72) Piscitelli A., Pezzella C., Giardina P., Faraco V., Giovanni S., 2010, Bioeng. Bugs., 1, 252-264

73) Necochea R., Valderrama B., Díaz-Sandoval S., Folch-Mallol J.L., Vázquez-Duhalt R., Iturriaga G., 2005, FEMS Microbiol. Lett., 244, 235-241

74) Mikuni J., Morohoshi N., 1997, FEMS Microbiol. Lett., 155, 79-84

75) Bertrand T., Jolivalt C., Briozzo P., Caminade E., Joly N., Madzak C., Mougin C., 2002, Biochemistry, 41, 7325-7333

76) Antorini M., Herpoël-Gimbert I., Choinowski T., Sigoillot J.C., Asther M., Winterhalter K., Piontek K., 2002, Biochim. Biophys. Acta., 1594, 109-114

77) Fåhraeus G., Reinhammar B., 1967, Acta Chem. Scand., 21, 2367-2378

78) Jonsson M., Pettersson E., Reinhammar B., 1968, Acta Chem. Scand., 22, 2135-2140

79) Cassland P., Jönsson L.J., 1999, Appl. Microbiol. Biotechnol., 52, 393-400

80) Bailey M.R., Woodard S.L., Callaway E., Beifuss K., Magallanes Lundback M., Lane J.R., Horn M.E., Mallubhotla H., Delaney D.D., Ward M., Van Gastel F., Howard J.A., Hood E.E., 2004, Appl. Microbiol. Biotechnol., 63, 390-397

81) Sonoki T., Kajita S., Ikeda S., Uesugi M., Tatsumi K., Katayama Y., Iimura Y., 2005, Appl. Microbiol. Biotechnol., 67, 138-142

82) Madzak C., Mimmi M.C., Caminade E., Brault A., Baumberger S., Briozzo P., Mougin C., Jolivalt C., 2006, Protein Eng. Des. Sel., 19, 77-84*)*

83) Larsson S, Cassland P, Jönsson LJ., 2001, Appl. Environ. Microbiol., 67, 1163-1170

84) Uldschmid A., Dombi R., Marbach K., 2003, Microbiology, 149, 2039-2048

85) Jönsson L.J., Saloheimo M., Penttilä M., 1997, Curr. Genet., 32, 425-430

86) O'Callaghan J., O'Brien J.J., McClean K., Dobson A.D.W., 2002, J. Ind. Microbiol. Biotechnol., 29, 55-59

87) Hong F., Meinander N.Q., Jönsson L.J., 2002, Biotechnol. Bioeng., 79, 438-449

88) Gelo-Pujic M., Kim H.H., Butlin N.G., Palmore G.T., 1999, Appl. Environ. Microbiol., 65, 5515-5521

89) Brown M.A., Zhao Z., Mauk A.G., 2002, Inorg. Chim. Acta., 331, 232-238

90) Bohlin C., Jönsson L.J., Roth R., van Zyl W.H., 2006, Appl. Biochem. Biotechnol., 129, 195-214

91) Jolivalt C., Madzak C., Brault A., Caminade E., Malosse C., Mougin C., 2005, Appl. Microbiol. Biotechnol., 66, 450-450

92) Guo M., Lu F., Pu J., Bai D., Du L., 2005, Appl. Microbiol. Biotechnol, 69, 178-183

93) Guo M., Lu F., Du L., Pu J., Bai D., 2006, Appl. Microbiol. Biotechnol., 71, 848, 852

94) Guo M., Lu F., Liu M., Li T., Pu J., Wang N., Liang P., Zhang C., 2008, Biotechnol. Lett., 30, 2091-2096

95) Fujihiro S., Higuchi R., Hisamatsu S., Sonoki S., 2009, Appl. Microbiol. Biotechnol., 82, 853-860

96) Valkonen M., Ward M., Wang H., Penttilä M., Saloheimo M., 2003, Appl. Environ. Microbiol., 69, 6979-6986

97) Wang Y., Xue W., Sims A.H., Zhao C., Wang A., Tang G., Qin J., Wang H., 2008, Fungal Genet. Biol., 45, 17-27

98) Téllez-Jurado A., Arana-Cuenca A., González Becerra A.E., Viniegra-González G., Loera O., 2006, Enzyme Microb. Technol., 38, 665–669

99) Salony, Garg N., Baranwal R., Chhabra M., Mishra S., Chaudhuri T.K., Bisaria V.S., 2008, Biochim. Biophys. Acta., 1784, 259-268

100) Nicolini C., Bruzzese D., Cambria M.T., Bragazzi N. L., Pechkova E., 2013, J. Cell Biochem., 114, 599-605

101) Dwivedi U.N., Singh P., Pandey V.P., Kumar A., 2011, J. Molec. Catal. B, 68, 117-128

102) Ducros V., Brzozowski A.M., Wilson K.S., Brown S.H., Ostergaard P., Schneider P., Yaver D.S., Pedersen A.H., Davies G.J., 1998, Nat. Struct. Biol., 5, 310-316
103) Piontek K., Antorini M., Choinowski T., 2002, J. Biol. Chem., 277, 37663-37669
104) Hakulinen N., Kruus K., Koivula A., Rouvinen J., 2006, Biochem. Biophys. Res. Commun., 350, 929-934
105) Lyashenko A.V., Bento I., Zaitsev V.N., Zhukhlistova N.E., Zhukova Y.N., Gabdoulkhakov A.G., Morgunova E.Y., Voelter W., Kachalova G.S., Stepanova E.V., Koroleva O.V., Lamzin V.S., Tishkov V.I., Betzel C., Lindley P.F., Mikhailov A.M., 2006, J. Biol. Inorg. Chem., 11, 963-973
106) Garavaglia S., Cambria M.T., Miglio M., Ragusa S., Iacobazzi V., Palmieri F., D'Ambrosio C., Scaloni A., Rizzi M., 2004, J. Mol. Biol., 342, 1519-1531
107) Enguita F.J., Martins L.O., Henriques A.O., Carrondo M.A., 2003, J. Biol. Chem., 278, 19416-19425
108) Skálová T., Dohnálek J., Østergaard L.H., Østergaard P.R., Kolenko P., Dusková J., Stepánková A., Hasek J., 2009, J. Mol. Biol., 385, 1165-1178
109) Skálová T., Dušková J., Hašek J., Stěpánková A., Koval T., Østergaard L.H., Dohnálek J., 2011, Acta Crystallogr. Sect. F Struct. Biol. Cryst. Commun., 67, 27-32
110) Gupta A., Nederlof I., Sottini S., Tepper A.W., Groenen E.J., Thomassen E.A., Canters G.W., 2012, J. Am. Chem. Soc., 134, 18213-18216
111) Komori H., Miyazaki K., Higuchi Y., 2009, FEBS Lett., 583, 1189-1195
112) Lawton T.J., Sayavedra-Soto L.A., Arp D.J., Rosenzweig A.C., 2009, J. Biol. Chem., 284, 10174-10180
113) Nakamura K., Go N., 2005, Cell. Mol. Life Sci., 62, 2050-2066
114) Solomon E.I., Chen P., Metz M., Lee S.K., Palmer A.E., 2001, Angew. Chem. Int. Ed. Engl., 40, 4570-4590
115) Solomon E.I., Ginsbach J.W., Heppner D.E., Kieber-Emmons M.T., Kjaergaard C.H., Smeets P.J., Tian L., Woertink J.S., 2011, Faraday Discuss., 148, 97-108
116) Solomon E.I., Here J.W., Gray H.B., 1976, Proc. Natl. Acad. Sci. USA, 73, 1389-1393
117) Dooley D.M., Rawlings J. Dawson J.H., Stephens P.J., Andréasson L.E., Malmström B.G., Gray H.B., 1979, J. Am. Chem. Soc., 101, 5038-5046
118) Solomon, E. I., Penfield, K. W., Gewirth, A. A., Lowery, M. D., Shadle, S. E., Guckert, J. A., LaCroix, L. B., 1996, Inorg. Chim. Acta, 243, 67-78
119) Solomon E.I., Lowery M.D., 1993, Science, 259, 1575-1581
120) Yoon J., Fujii S., Solomon E.I., 2009, Proc. Natl. Acad. Sci. USA, 106, 6585-6590

121) Solomon E.I., Lowery M.D., LaCroix L.B., Root D.E., 1993, Methods Enzymol., 226, 1-33

122) Lee S.K., George S.D., Antholine W.E., Hedman B., Hodgson K.O., Solomon E.I., 2002, J. Am. Chem. Soc., 124, 6180-6193

123) Yoon J., Solomon E.I., 2007, J. Am. Chem. Soc., 129, 13127-13136

124) Yoon J., Liboiron B.D., Sarangi R., Hodgson K.O., Hedman B., Solomon E.I., 2007, Proc. Natl. Acad. Sci. USA, 104, 13609-13614

125) Solomon E.I., Augustine A.J., Yoon J., 2008, Dalton Trans., 30, 3921-3932

126) Palmer A.E., Lee S.K., Solomon E.I., 2001, J. Am. Chem.. Soc., 123, 6591-6599

127) Zoppellaro G., Sakurai T., Huang H., 2001, J. Biochem., 129, 949-953

128) Augustine A.J., Kragh M.E., Sarangi R., Fujii S., Liboiron B.D., Stoj C.S., Kosman D.J., Hodgson K.O., Hedman B., Solomon E.I., 2008, Biochemistry, 47, 2036-205

129) Augustine A.J., Quintanar L., Stoj C.S., Kosman D.J., Solomon E.I., 2007, J. Am. Chem. Soc., 129, 13118-13126

130) Cole J.L., Clark P.A., Solomon E.I., 1990, J. Am. Chem. Soc. 112, 9534-9548

131) Quintanar L., Yoon J., Aznar C.P., Palmer A.E., Andersson K.K., Britt R.D., Solomon E.I., 2005, J. Am. Chem. Soc., 127, 13832-13845

132) Rulísek L., Solomon E.I., Ryde U., 2005, Inorg. Chem., 44, 5612-5628

133) Yoon J., Mirica L.M., Stack T.D., Solomon E.I., 2004, J. Am. Chem. Soc., 126, 12586-12595

134) Yoon J., Mirica L.M., Stack T.D., Solomon E.I., 2005, J. Am. Chem. Soc., 127, 13680-13693

135) Yoon J., Solomon E.I., 2005, Inorg. Chem., 44, 8076-8086

136) Chalupský J., Neese F., Solomon E.I., Ryde U., Rulísek L., 2006, Inorg. Chem., 45, 11051-11059

137) Heppner DE, Kjaergaard CH, Solomon EI., 2013, J. Am. Chem. Soc., 135, 12212-12215

138) Andréasson L.E., Brändén R., Reinhammar B., 1976, Biochim. Biophys. Acta, 438, 370-379

139) Andréasson L.E., Reinhammar B., 1976, Biochim. Biophys. Acta, 445, 579-597

140) Ferraroni M., Myasoedova N.M., Schmatchenko V., Leontievsky A.A., Golovleva L.A., Scozzafava A., Briganti F., 2007, BMC Struct. Biol., 7, 60-72

141) Blackburn N.J., Ralle M., Hassett R., Kosman D.J., 2000, Biochemistry, 39, 2316-2324

142) Palmer A.E., Quintanar L., Severance S., Wang T.P., Kosman D.J., Solomon E.I., 2002, Biochemistry, 41, 6438-6448

143) Cole J.L., Ballou D.P., Solomon E. I., 1991, J. Am. Chem. Soc. 113, 8544-8546

144) Shin W., Sundaram U.M., Cole J.L., Zhang H.H., Hedman B., Hodgson K.O., Solomon E.I., 1996, J. Am. Chem. Soc., 118, 3202-3215

145) Kjaergaard C.H., Qayyum M.F., Augustine A.J., Ziegler L., Kosman D.J., Hodgson K.O., Hedman B., Solomon E.I., 2013, Biochemistry, 52, 3702-3711

146) Taylor A.B., Stoj C.S., Ziegler L., Kosman D.J., Hart P.J., 2005, Proc. Natl. Acad. Sci. USA, 102, 15459-15464

147) Augustine A.J., Kjaergaard C., Qayyum M., Ziegler L., Kosman D.J., Hodgson K.O., Hedman B., Solomon E.I., 2010, J. Am. Chem. Soc., 132, 6057-6067

148) Sundaram U.M., Zhang H.H., Hedman B., Hodgson K.O., Solomon E.I., 1997, J. Am. Chem. Soc., 119, 12525-12540

149) Quintanar L., Stoj C., Wang T.P., Kosman D.J., Solomon E.I., 2005, Biochemistry, 44, 6081-6091

150) Schmauder R., Alagaratnam S., Chan C., Schmidt T., Canters G.W., Aartsma T.J., 2005, J. Biol. Chem., 10, 683-687

151) Kuznetsova S., Zauner G., Schmauder R., Mayboroda O.A., Deelder A.M., Aartsma T.J., Canters G.W., 2006, Anal. Biochem., 350, 52-60

152) van Peer A.F., de Bekker C., Vinck A., Wösten H.A., Lugones L.G., 2009, Appl. Environ. Microbiol., 75, 1243-1247

153) Machczynski M.C., Vijgenboom E., Samyn B., Canters G.W., 2004, Protein Sci., 13, 2388-2397

154) Fowler T.J., Mitton M.F., 2000, Genetics, 156, 1585-1594

155) Ohm R.A., de Jong J.F., Lugones L.G., Aerts A., Kothe E., Stajich J.E., de Vries R.P., Record E., Levasseur A., Baker S.E., Bartholomew K.A., Coutinho P.M., Erdmann S., Fowler T.J., Gathman A.C., Lombard V., Henrissat B., Knabe N., Kües U., Lilly W.W., Lindquist E., Lucas S., Magnuson J.K., Piumi F., Raudaskoski M., Salamov A., Schmutz J., Schwarze F.W., van Kuyk P.A., Horton J.S., Grigoriev I.V., Wösten H.A., 2010, Nature Biotechnol., 28, 957-963

156) Wösten H.A., Schuren F.H., Wessels J.G., 1994, EMBO J., 13, 5848-5854

157) van Wetter M.A., Schuren F.H.J., Schuurs T.A., Wessels J.G.H., 1996, FEMS Microbiol. Lett., 140, 265-269

158) Schwalb M.N., Miles P.G., 1967, Am. J. Bot., 54, 440-446

159) Harrison M.D., Dennison C., 2004, Proteins, 155, 426-435

160) Diederix RE, Canters GW, Dennison C., 2000, Biochemistry, 39, 9551-9560

161) Roy A., Kucukural A., Zhang Y., 2010, Nat. Protoc., 5, 725-738

162) The PyMOL Molecular Graphics System, Version 1.6.0.0 Schrödinger, LLC.

163) Tepper A.W., Aartsma T.J., Canters G.W., 2011, Faraday Discuss., 148, 161-171*)*

164) Childs R.E., Bardsley W.G., 1975, Biochem. J., 145, 93-103

165) Alves A.M., Record E., Lomascolo A., Scholtmeijer K., Asther M., Wessels J.G., Wösten H.A., 2004, Appl. Environ. Microbiol., 70, 6379-6384

166) Solano F., Lucas-Elío P., López-Serrano D., Fernández E., Sanchez-Amat A., 2001, FEMS Microbiol. Lett., 204, 175-181

167) Kim S., Lee S.B., 2008, Protein Expr. Purif., 62, 116-119

168) Lugones L.G., Scholtmeijer K., Klootwijk R., Wssels J.G.H., 1999, Mol. Microbiol., 32, 681-689

169) Palmer A.E., Randall D.W., Xu F., Solomon E.I., 1999, J. Am. Chem. Soc., 121, 7138-7149

170) Palmer A.E., Szilagyi R.K., Cherry J.R., Jones A., Xu F., Solomon E.I., 2003, Inorg. Chem., 42, 4006-4017

171) Gewirth A.A., Solomon E.I., 1988, J. Am. Chem. Soc., 110, 3811-3819

172) LaCroix L.B., Shadle S.E., Wang Y., Averill B.A., Hedman B., Hodgson K.O., Solomon E.I., 1996, J. Am. Chem. Soc., 118, 7775-7768

173) Machonkin T.E., Quintanar L., Palmer A.E., Hassett R., Severance S., Kosman D.J., Solomon E.I., 2001, J. Am. Chem.. Soc., 123, 5507-5517

174) Baldrian P., 2005, FEMS Microbiol. Rev., 30, 215-242

175) Sherif M., Waung D., Korbeci B., Mavisakalyan V., Flick R., Brown G., Abou-Zaid M., Yakunin A.F., Master E.R., 2013, Microb. Biotechnol., 6, 588-597

176) Toscano M.D., De Maria L., Lobedanz S., Ostergaard L.H., 2013, Chembiochem., 14, 1209-1211

177) Mao D., Wachter E., Wallace B.A., 1982, Biochemistry, 21, 4960-4968

178) Johnson W.C., 1999, Proteins, 35, 307-312

179) Whitmore L., Wallace B.A., 2004, Nucleic Acids Res., 32, W668-73

180) Heinig M., Frishman D., 2004, Nucl. Acids Res., 32, W500-2

181) Yoshitake A., Katayama Y., Nakamura M., Iimura Y., Kawai S., Morohoshi N., 1993, J. Gen. Microbiol., 139, 179-185

182) Hildén K., Hakala T.K., Lundell T., 2009, Biotechnol. Lett., 31, 1117-1128

183) Vite-Vallejo O., Palomares L.A., Dantán-González E., Ayala-Castro H.G., Martínez-Anaya C., Valderrama B., Folch-Mallol J., 2009, Enzyme Microb. Technol., 45, 233-239

184) Garg N., Bieler N., Kenzom T., Chhabra M., Ansorge-Schumacher M., Mishra S., 2012, BMC Biotechnol., 12, 75-87

185) Tong P., Hong Y., Xiao Y., Zhang M., Tu X., Cui T., 2007, Biotechnol. Lett., 29, 295-301

186) Raper J.R., Miles P.G., 1958, Genetics, 43, 530-546

187) Wessels J.G., de Vries O.M., Asgeirsdóttir S.A., Springer J., 1991, J. Gen. Microbiol., 137, 2439-2445

188) Andberg M., Hakulinen N., Auer S., Saloheimo M., Koivula A., Rouvinen J., Kruus K., 2009, FEBS J., 276, 6285-6300

189) Garzillo A.M., Colao MC., Buonocore V., Oliva R., Falcigno L., Saviano M., Santoro A.M., Zappala R., Bonomo R.P., Bianco C., Giardina P., Palmieri G., Sannia G., 2011, J. Protein Chem., 20, 191-201

190) Koschorreck K., Richter S.M., Swierczek A., Beifuss U., Schmid R.D., Urlacher V.B., 2008, Arch. Biochem. Biophys., 474, 213-219

191) Galli C., Gentili P., Jolivalt C., Madzak C., Vadalà R., 2011, Appl. Microbiol. Biotechnol., 91, 123-131

192) Enguita F.J., Marcal D., Martins L.O., Grenha R., Henriques A.O., Lindley P.F., Carrondo M.A., 2004, J. Biol. Chem., 279, 23472-23476

193) Tepper A.W., Milikisyants S., Sottini S., Vijgenboom E., Groenen E.J., Canters G.W., 2009, J. Am. Chem. Soc., 131, 11680-11682

194) Manabe T., Manabe N., Hiromi K., Hatano H., 1972, FEBS Lett., 23, 268-270

195) Manabe T., Hatano, Hiromi K., 1973, J. Biochem., 73, 1169-1174

196) Murphy M.E., Lindley P.F., Adman E.T., 1997, Protein Sci., 6, 761-770

197) Zauner G., Strianese M., Bubacco L., Aartsma T.J., Tepper A.W.J.W., Canters G.W., 2008, Inorg. Chim. Acta., 361, 1116-1121

198) Strianese M., Zauner G., Tepper A.W., Bubacco L., Breukink E., Aartsma T.J., Canters G.W., Tabares L.C., 2009, Anal. Biochem., 385, 242-248

199) Zauner G., Lonardi E., Bubacco L., Aartsma T.J., Canters G.W., Tepper A.W., 2007, Chemistry, 13, 7085-7090

200) Gustiananda M., Andreoni A., Tabares L.C., Tepper A.W., Fortunato L., Aartsma T.J., Canters G.W., 2012, Biosens. Bioelectron., 31, 419-425

201) Strianese M., De Martino F., Pavone V., Lombardi A., Canters G.W., Pellecchia C., 2010, J. Inorg. Biochem., 104, 619-624

202) Strianese M., Zauner G., Tabares L.C., Tepper A.W., De Martino F., Pellecchia C., Aartsma T.J., Canters G.W., 2013, Chemistry, 19, 14977-14982

203) Gupta A., Aartsma T.J., Canters G.W., 2014, J. Am. Chem. Soc., doi: 10.1021/ja411078b

CHAPTER 4

Engineering copper sites using cupredoxin-like domains in SLAC from *Streptomyces coelicolor* and bNiR from *Alcaligenes xylosoxidans.*

4.1 Introduction

The ultimate goal of protein design is the creation of new proteins with specific and predictable structure and function. The *de novo* design and the modification of existing sites in natural metal-binding proteins, not only deepens the understanding of protein structure/function relationship, but also is important for engineering proteins for industrial applications. Site- and loop-directed mutagenesis has been especially successful in evaluating the role of the first and second coordination spheres of mainly cupredoxins such as azurin (Az), pseudoazurin (Paz) and plastocyanin (Pc) [1 - 17]. Az scaffold has been successfully applied in engineering of binuclear copper (Cu) site, Cu_A [18], mononuclear type zero Cu site [19 - 21] and nonheme Fe(II) site [22].

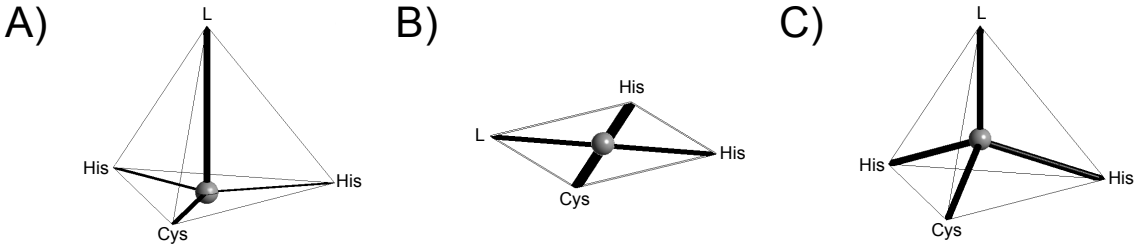

Figure 4.1 Variations in the geometry of four-coordinate Cu sites, with a His_2Cys ligand set and a variable fourth ligand depicted as **L**. The Cu ion is a gray sphere. (A) A trigonal pyramidal type 1 (T1) Cu site, (B) a planar, thiolate-containing type 2 (S(Cys)-T2) Cu site and (C) a tetrahedral type 1.5 (T1.5) Cu site. Image adapted from [23].

Historically, the Cu sites in proteins have been classified into three types, mononuclear type 1 (T1 Cu, so-called 'blue Cu site'), mononuclear type 2 (T2 Cu, so-called 'normal Cu site') and the binuclear type 3 (T3 Cu) [24 - 27] (Chapter 1.2). The T2 Cu and the T3 Cus form a trinuclear cluster (T2/T3 Cu site, Chapter 1.2.4). The T1 Cu sites of most cupredoxins, such as Paz [28], Pc [29] and amicyanin [30], are typically trigonal pyramidal (Figure 4.1.A) with the Cu ion slightly displaced from the N_2S equatorial plane in the direction of a Met ligand. The geometry of a T1 Cu site varies depending on the residue in the axial position. In stellacyanin (STC), the axial ligand is Gln leading to a distorted tetrahedral Cu site [31]. In plantocyanins from lily [32] and tomato [33] it is Leu and Val, respectively, thus the T1 Cu sites in those proteins are probably three-coordinate. The T1 Cu site of Az contains an additional ligand provided by a backbone carbonyl oxygen, resulting in a trigonal bipyramidal

active site [34]. The T1 Cu site is characterized by a dominant S(Cys)→Cu(II) ligand to metal charge transfer (LMCT) transition band at ~ 600 nm and a small hyperfine coupling in the parallel region, $A_{\|,} < 95 \times 10^4$ cm^{-1} [1, 27, 35, 36] (Chapter 1.2.1). Studies on engineered, four-coordinate T1 Cu sites with a single Cys ligand have shown two additional geometries [1, 23]. A thiolate-containing T2 (S(Cys)-T2) Cu site with a tetragonal planar geometry (Figure 4.1.B) is characterized by a S(Cys)→Cu(II) LMCT transition band at ~ 400 nm and a large $A_{\|,} > 130 \times 10^4$ cm^{-1} [1]. A type 1.5 (T1.5) Cu site is found when a strong axial ligand moves the Cu ion out of the N_2S trigonal plane giving a tetrahedral geometry (Figure 4.1.C). The UV-Vis (characterized by two S(Cys)→Cu(II) LMCT transition bands at 420 - 450 nm and 540 - 600 nm) and electron paramagnetic resonance (EPR) spectra of a T1.5 Cu site are intermediate between those of a T1 Cu and a S(Cys)-T2 Cu sites [1].

4.1.1 *Design studies of Cu-binding sites*

Binding of metal into a non-metalloprotein or a *de novo* synthesized protein requires creation of the optimal coordination environment by introduction of the ligating side chains at favorable positions. By protein redesign, Hellinga [23] and Lu *et al.* [37] created T1.5 Cu sites in thioredoxin and superoxide dismutase as scaffolds. A T1.5 Cu site was also created within a four helix-bundle systems, a very different tertiary structure compared to the β-barrel of cupredoxins [38]. By changing the environment of the coordination sphere of this T1.5 Cu site, structurally different Cu_A and S(Cys)-T2 Cu sites have been obtained [39]. Shiga *et al.* created a T1 Cu site within the hydrophobic core of a four-stranded α-helical coiled-coil protein that possesses a vacant cavity at the axial position of the Cu-binding site [40, 41]. Changing the axial interaction shifted the geometry of this site from trigonal planar towards a distorted tetrahedral. Similar, α-helical coiled-coil synthetic model has also been used to design a functional T2 Cu center that shows nitrite reductase activity [4].

Modeling biological Cu sites using copper complexes has been widely studied. Kitajama and co-workers reported the X-ray structure of the first model compounds, tetrahedral thiolato Cu(II) complexes, which had spectral properties similar to a T1 Cu site [42 - 44]. Tolman and co-workers synthesized Cu(II) models of the three-coordinate T1 Cu and four-coordinate T1.5 Cu sites [45 - 47]. The three-coordinate N_2S(thiolate) Cu(II) complex closely mimics the coordination sphere of the trigonal T1 Cu(II) sites of fungal laccases and ceruloplasmin. However the $A_{\|}$ value of this site was larger than

those for the proteins, whilst the reduction potential was considerably lower [45]. The length of (thiolate)S-Cu bond has been altered by addition of a thioether ligand (N_2S(thiolate)S(thioether) Cu(II) complex), leading to a flattened tetrahedral geometry of the site, similar to that observed in T1.5 Cu sites (Figure 4.1.C) [46]. Recently, new model complexes, characterized by an LMCT transition band at ~ 610- 630 nm, $A_{\|} < 100 \times 10^4$ cm^{-1} and an increased reduction potential (217 - 317 mV) similar to those of low-potential T1 Cu sites (for example Az), have been synthesized [48].

4.1.2 *Cupredoxin-like domains as a scaffold for design of Cu-binding centers*

The cupredoxin fold is a common motif in metalloproteins and is essential to several cellular processes such as respiration, catalysis and metal homeostasis [49, 50]. Cupredoxins can occur as either single-domain monomeric proteins [49 - 51] or as components of Cu-containing multi-domain proteins (Chapter 1.3). These cupredoxin-like, metal-binding domains (MBDs) are found in NiRs [52 - 54], MCOs and cytochrome *c* oxidase [55, 56]. The MCOs family includes among others two-domain and three-domain laccases [57 - 62], six-domain ceruloplasmin [63], three-domain ascorbate oxidase (AO) [64] and Fet3p [65], each containing T1, T2 and T3 Cu sites (Chapter 1.3 and 3).

Several models explaining the evolution of multiple domain Cu-binding proteins have been proposed [66 - 69], but most evidence favors that proposed by Nakamura *et al.* [67, 70] (for more details see Chapter 1.3). Trimeric MCOs, in which each monomer consists of two cupredoxin-like domains, are considered the key intermediates in this model [67]. The authors predicted three types (A, B and C) of the two-domain MCOs and classified them according to the location of a T1 Cu site [67]. Type A two-domain MCOs contain a T1 Cu site in each domain, whereas type B and type C house a T1 Cu site in second (MBD-2) or first (MBD-1) domain, respectively. The latter two types are postulated to originate from the type A two-domain MCOs. So far, 31 different two-domain MCOs have been identified in genome databases, including 3 of type A, 17 of type B and 11 of type C [70], from which only few have been isolated and characterised. Small laccase (SLAC) from *Streptomyces coelicolor* [57, 58] belongs to the type B MCOs (Figure 4.2.A and Figure 4.3.A.i), whereas mgLAC from metagenome [59], blue copper oxidase (BCO) from *Nitrosomonas europaea* [60] and the unpublished MCO, gdcLAC, from *Arthrobacter* sp. fb24 (pdb file: 3GDC) to the type C. Trimeric NiRs, which contain a T1 Cu site in the MBD-1

(Figure 4.2.B and Figure 4.3.A.i), are postulated to have descended either from the type C MCOs with concomitant loss of two, inter-domain Cu ions, or from the two-domain type Y ancestor (not identified in the genome database [67, 70]), which contains the inter-domain T2 Cu site and T1 Cu sites in each domain.

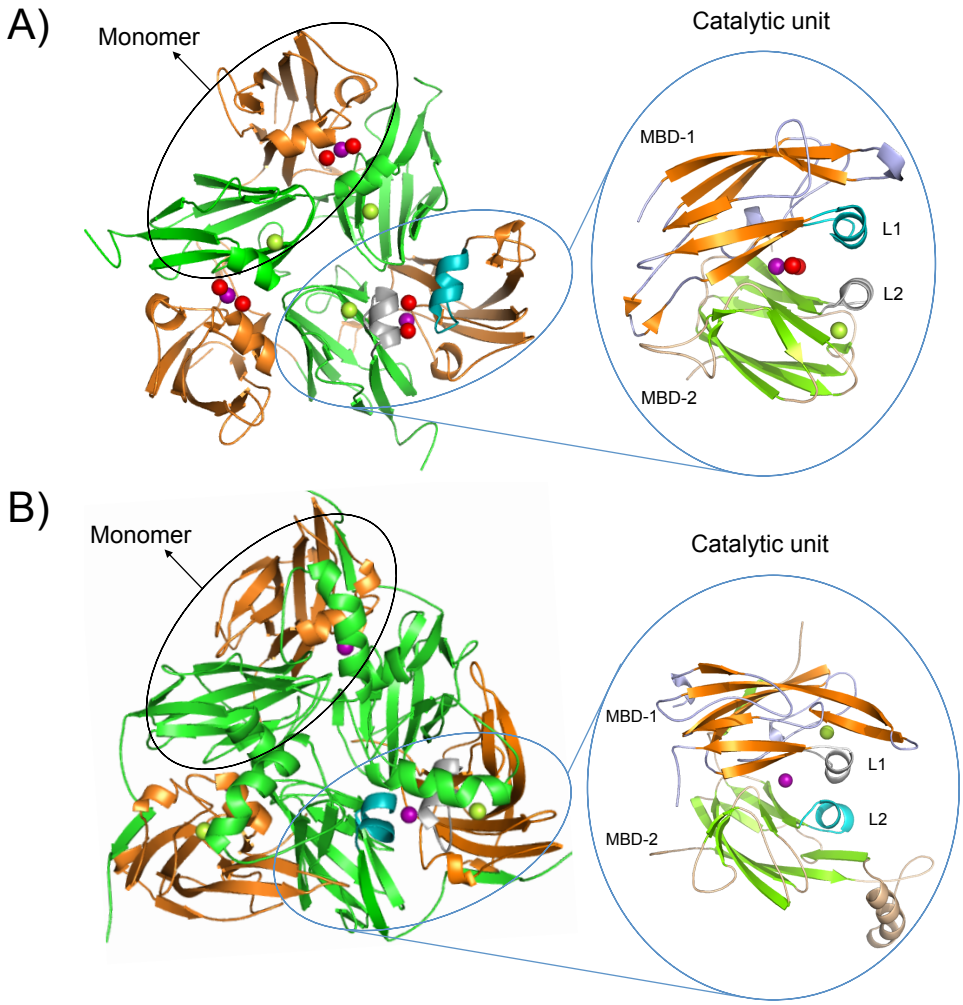

Figure 4.2 Representations of the homotrimeric structures of (A) SLAC [58] and (B) bNiR [52]. MBD-1 and MBD-2 are shown in orange and green, respectively. The insets show the location of the Cu ions in and between MBD-1 and MBD-2 of adjacent monomers. The β-sheets of MBD-1 are orange, whereas those of MBD-2 are green. The loops, L1 from MBD-1 and L2 from MBD-2 that are involved in T1 Cu binding are grey, whilst those that are not are cyan. The T1, T2 and T3 Cu ions are shown as green, purple and red spheres, respectively.

A)

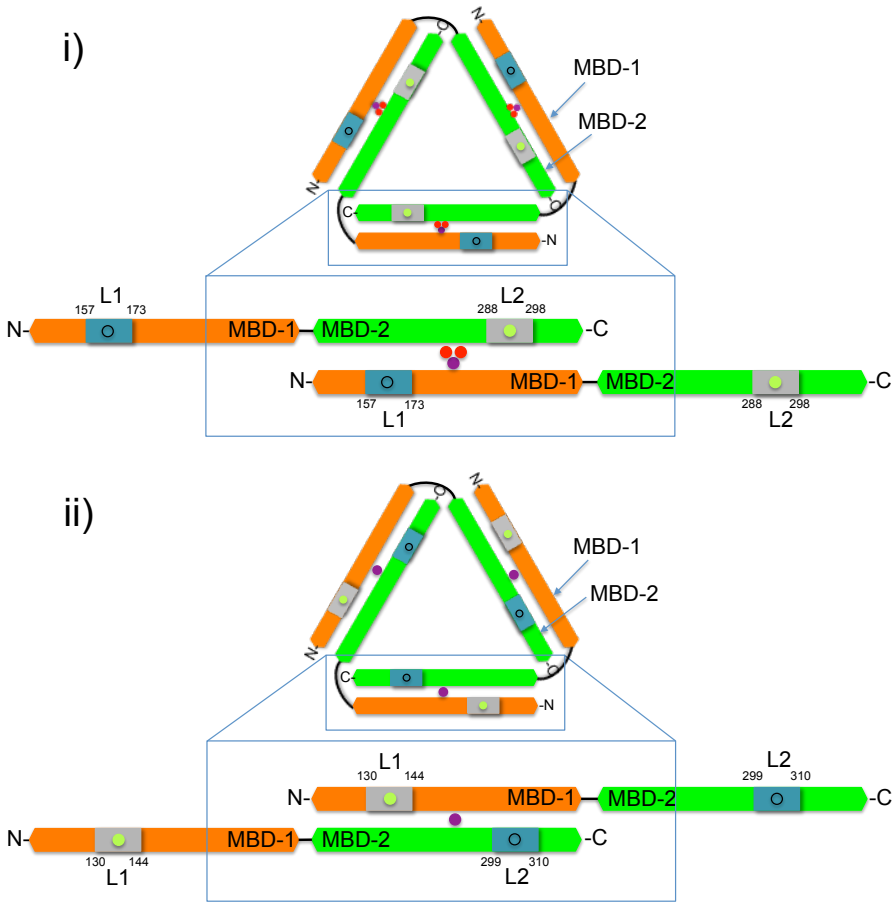

B)

i)

Protein	Sequence of the L1																		
SLAC	D^{157}	H	V	–	–	V	G	T	E	H	H	T	G	G^{168}	I	R	N	–	G	L^{173}
bNiR	**C^{130}**	A	P	E	G	–	M	V	–	–	–	P	W	**H^{139}**	V	V	S	–	G	**M^{144}**
mgLAC	**C^{105}**	H	V	–	–	–	N	V	–	–	–	N	E	**H^{112}**	V	G	V	R	G	**M^{118}**
gdcLAC	**C^{144}**	H	Q	S	–	–	P	L	–	–	–	A	P	**H^{152}**	I	A	K	–	G	**L^{157}**

ii)

Protein	Sequence of the L2																		
SLAC	**C^{288}**	H	V	Q	S	**H^{293}**	S	–	–	–	–	–	–	–	–	D	–	M	G	**M^{298}**
bNiR	N^{299}	H	N	L	I	E^{304}	A	–	–	–	–	–	–	–	–	F	E	L	G	A^{310}
mgLAC	D^{253}	H	V	D	T	H^{258}	V	T	A	G	G	K	H	P	G	–	–	–	G	P^{269}
gdcLAC	A^{281}	H	K	T	E	F^{286}	A	–	–	–	–	–	–	–	–	E	–	L	G	W^{298}

Figure 4.3 (A) Schematic representations of the homotrimers and the N- and C-terminal cupredoxin-like domains (MBD-1 orange and MBD-2 green) of adjacent monomers of SLAC (i) and bNiR (ii) using the same colour scheme as in Figure 4.2. L1 (MBD-1) and L2 (MDB-2), which are involved in T1 Cu-binding, are shown as gray boxes, whilst loops that are not are cyan. The T1 Cu site (green dot) is located within MBD-2 and MDB-1, whilst the potential Cu-binding site (black circle) within MBD-1 (i) and MBD-2 (ii) of SLAC and bNiR, respectively. The T2 (purple dot) and T2/T3 Cu (purple/red dots) sites of bNiR and SLAC are found at the interface of two adjacent monomers. (B) Structure-based sequence alignments of L1 (MBD-1, i) and L2 (MBD-2, ii) of bNiR, SLAC, mgLAC and gdcLAC with the coordinating residues bold and numbered.

The structure of two-domain trimeric SLAC [58] superposes on the structures of mgLAC [59], gdcLAC and bNiR [52] with root-mean-square deviation (RMSD) of 2.59 Å, 2.07 Å and 2.05 Å, respectively. Three of the four ligands of the T1 Cu site, Cys, one His and the axial ligand are situated on a single loop (L1 in mgLAC, gdcLAC and bNiR and L2 in SLAC) linking the β-strands (typically β7 - β8), whereas the second His ligand, is provided from the core of the protein [71]. The length and the composition of the Cu-containing loop varies (Figure 4.3). While in single-domain cupredoxins it is rather short (7 to 11 residues) [49], the corresponding loops in two-domain MCOs and NiRs are typically longer (11 to 15 residues) [52, 57 - 60, 72]. In cupredoxins, the structure of this loop is dictated by length and is independent of sequence [5]. Side-chain variations within the loop control surface properties and facilitate interaction with a particular protein partner. Comparison of the trimeric structures of SLAC, mgLAC (Figure 4.4.A) and bNiR (Figure 4.4.B), as well as the overlay of both domains of SLAC (Figure 4.4.C), shows that a T1 Cu site in MBD-1 of SLAC is missing, mainly due to the replacement of the potentially Cu-ligating Cys by an Asp157. Similarly, at the potential Cu-binding site in the MBD-2 of bNiR (Figure 4.4.D) and mgSLAC (Figure 4.4.E), a Cys ligand is substituted by Glu and Asp, respectively.

The T2/T3 Cu cluster and the T2 Cu site are placed at the interface between the MBD-1 and the MBD-2 of two adjacent monomers of SLAC (Figure 4.2.A and Figure 4.3.A.i) and bNiR (Figure 4.2.B and Figure 4.3.A.ii), respectively, contributing strongly to the stability of the trimer [52, 58]. The T1 and the T2 Cu sites (NiRs) or the T2/3 Cu cluster (two-domain MCOs) are 12 - 13 Å apart and are connected by a His(T2)-Cys(T1) and His(T3)-Cys(T1)-His(T3) motif, respectively, which enable electron transfer (ET) between both Cu centers [52, 57 - 60] (Chapter 1.3). The T2/T3 Cu cluster is ligated by eight His, which are donated by the two adjacent monomers. At the corresponding location, NiRs contain only four His residues, three of which ligate to the T2 Cu, whereas the fourth, His249, is not involved in metal ligation.

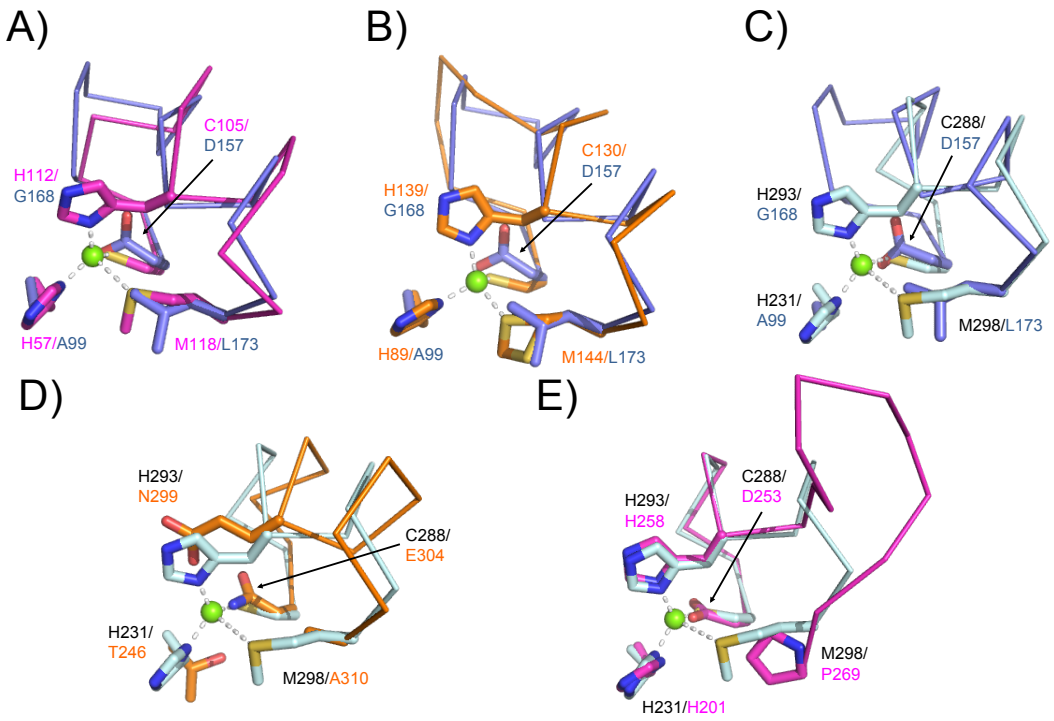

Figure 4.4 The potential Cu-binding site of SLAC (MBD-1, blue, [58]) superposed on a T1 Cu site of (A) mgLAC (MBD-1, magenta, [59]), (B) bNiR (MBD-1, orange, [52]) and (C) SLAC (MBD-1, pale cyan). The T1 Cu site of SLAC (MBD-2, pale cyan) overlaid on the potential Cu-binding sites of (D) bNiR (MBD-2, orange) and (E) mgLAC (MBD-2, magenta). The T1 Cu ions are depicted as green spheres.

4.2 Scope of the chapter

Research presented in this chapter focuses on the design of a T1 Cu site using the scaffold of cupredoxin-like domains, MBD-1 and MBD-2, of SLAC and bNiR, respectively. Additionally, the possibility of introducing T3 Cus into bNiR (in the LacNiR variant) has been investigated. Twenty variants of bNiR and SLAC have been prepared, from which fifteen have been isolated, purified and characterized in terms of metal content, spectral properties and activity.

4.3 Materials and methods

4.3.1 *Cloning of SLAC, bNiR and their variants*

The genes encoding for wild type (WT) SLAC from *S. coelicolor* [73] (Chapter 3.3.1.5, $SLAC_{truncated}$ referred to as SLAC in the following sections), and WT bNiR from

A. xylosoxidans [74] were used as previously described. The genes encoding for qSLAC, tSLAC, A99H_nirSLAC, qNiR and LacNiR were synthesized with Multi QuickChange Lightening Mutagenesis Kit (Stratagene), as described in Chapter 5.7.2, using templates and the primers listed in Table 4.1. The genes encoding for T1D qSLAC, T1D tSLAC, nirSLAC, mgSLAC, T1D nirSLAC, T1D A99H nirSLAC, T1D qNiR, T1D azNiR (prepared by Dr. Isabelle Salard), T1D T246H azNiR and Δ252G LacNiR were synthesized with QuickChange Mutagenesis Kit (Stratagene), as described in Chapter 5.7.2, using templates and the primers listed in Table 4.1. The gene encoding for A99H_mgSLAC was amplified by polymerase chain reaction (PCR), as described in Chapter 5.7.1, using template and the primers listed in Table 4.1. The genes were verified by sequencing both strands.

4.3.2 *Expression and purification of proteins*

The proteins were expressed in *Escherichia coli* BL21 (DE3) and purified, as described in Chapter 5.10.1 (WT SLAC), Chapter 5.10.2 (SLAC variants) and Chapter 5.10.3 (WT bNiR and its variants). T1D SLAC [75] was kindly provided by Prof. G.W. Canters. The concentrations of proteins were determined either by using extinction coefficients (ε) of 4400 $M^{-1}cm^{-1}$ at 590 nm (WT SLAC) [73] and 5200 $M^{-1}cm^{-1}$ at 594 nm (WT bNiR) [74] or Bradford assays (Comassie Plus protein assay; Thermo Scientific).

4.3.3 *Determination of the apparent molecular weight by gel-filtration*

The apparent molecular weight (MW^{app}) of proteins was determined, as described in Chapter 5.13.4 using a HiLoad Superdex 200 16/60 (GE Healthcare) gel-filtration column in 20 mM tris(hydroxymethyl)aminomethane (Tris) pH 7.5 containing 200 mM NaCl. When MW^{app} could not be determined, the trimeric state of the protein was determined from the elution volume (V_e) relative to V_e of the control, trimeric protein (for example WT SLAC or WT bNiR).

Cycle	Construct	Template	Primer sequence 5' to 3'	Function [a]
0	SLAC_pET22b	Genomic DNA form *S. coelicolor*	GTTGGAGTCTCATATGGGGGGCGAGGTGAGACACCTC AAG	Cloning, FP
			GTTGGCCATCTCGAGTCAGTGCTCGTGTTCGTGTG	Cloning, RP
	bNiR_pET22b [b]			
1	tSLAC_pET22b	SLAC_pET22b	CGGTGCCGACGACGTGGCAGTGGTAGTGCCAGTAG	D157C [c] mutation, RP
			ACCGGGCCGTACATGCCGTTGCGGATGTGTCCGGTG	G168H [c] and L173M [c] mutations, RP
	mgSLAC_pET22b	A99H_mgSLAC_pET22b	GATGGACGTGCGGCACAGCCTGCACGTGCA	H99A [c] mutation, FP
	nirSLAC_pET22b	A99H_nirSLAC_pET22b	TGCACGTGCAGGCTGTGCCGCACGTCCATC	H99A [c] mutation, RP
2	qSLAC_pET22b	SLAC_pET22b	CGGTGCCGACGACGTGGCAGTGGTAGTGCCAGTAG	D157C [c] mutation, RP
			ACCGGGCCGTACATGCCGTTGCGGATGTGTCCGGTG	G168H [c] and L173M [c] mutations. RP
	A99H_mgSLAC_ pET22b	qSLAC_pET22b	TGCACGTGCAGGCTGTGCCGCACGTCCATC	A99H [c] mutation, RP
			CTACTGGCACTACCACTGCCACGTCAACGTGAACGAA CACGTGGGCGTGCGTGGCATGTACGGCCCGGTGATC	Loop (mgLAC) mutation, FP
			GATCACCGGGCCGTACATGCCACGCACGCCCACGTGT TCGTTCACGTTGACGTGGCAGTGGTAGTGCCAGTAG	Loop (mgLAC) mutation, RP

[a] FP - forward primer, RP - reverse primer. [b] Used as in [74]. [c] The $SLAC_{long}$ gene numbering [73] (Chapter 3).

Table 4.1 List of constructs and primers used in this chapter.

Cycle	Construct	Template	Primer sequence 5' to 3'	Function [a]
2	A99H_nirSLAC_ pET22b	qSLAC_pET22b	CTACTGGCACTACCACTGCCACCCGGAAGGTATGGTGC CCTGGCACGTGGTGTCTGGTATGTACGGCCCGGTGATC	Loop (bNiR) mutation, FP
	qNiR_pET22b	bNiR_pET22b	GCCTACCTGTGCCACAACCTGATCCACGCCTTCGAAC	N299C and E304H mutations, FP
			TTCGAACTGGGCATGGCCGGCCACATCAAG	A310M mutation, FP
			CAATCGCGACCATCGCCCGCACCTG	T246H mutation, FP
3	T1D_tSLAC_pET22b	tSLAC_pET22b	GTACCACAGCCACGTCCAGAG CTCTGGACGTGGCTGTGGTAC	C288S [c] mutation, FP C288S [c] mutation, RP
	T1D_qSLAC_pET22b	qSLAC_pET22b		
	T1D_mgSLAC_ pET22b	mgSLAC_pET22b		
	T1D_nirSLAC_ pET22b	nirSLAC_pET22b		
	T1D_A99H_nirSLAC _pET22b	A99H_nirSLAC_ pET22b		

[a] FP - forward primer, RP - reverse primer. [c] The $SLAC_{long}$ gene numbering [73] (Chapter 3).

Table 4.1 List of constructs and primers used in this chapter - continued.

Cycle	Construct	Template	Primer sequence 5' to 3'	Function [a]
3	T1D_bNiR_pGEMT [d]	bNiR_pGEMT	CCTTCGTCTACCACAGCGCGCCCGAAGGC	C130S mutation, FP
	T1D_qNiR_pET22b	qNiR_pET22b	GCCTTCGGGCGCGCTGTGGTAGACGAAGG	C130S mutation, RP
	T1D_azNiR_pET22b [d]	T1D_bNiR_pGEMT	GGCGTGTATGCCTACCTGTGCACCTTCCCGGGCCATA	Loop (Az) mutation, FP
			GCGCGCTGATGGCCGGCCACATCAAGG	
			CCTTGATGTGGCCGGCCATCAGCGCGCTATGGCCCGG	Loop (Az) mutation, RP
			GAAGGTGCACAGGTAGGCATACACGCC	
	T1D_T246H_azNiR_ pET22b	T1D_azNiR_pET22b	CAATCGCGACCATCGCCCGCACCTG	T246H mutation, FP
			CAGGTGCGGGCGATGGTCGCGATTG	T246H mutation, RP
4	LacNiR_pET22b	bNiR_pET22b	GGCGCCGTGGAAGTGGACGTTGTGC	D92H mutation, RP
			CATGCCTTCGGGGTGGCAGTGGTAGAC	A131H mutation, RP
			CATGGCCGCCGTGCAGGTGCG	I251H mutation, RP
			CCTCGATCAGGTTGTGGTTGTGGTAGGCATAC	L298H mutation, RP
	Δ252G_LacNiR_ pET22b	LacNiR_pET22b	CACCTGCACGGCCATGGCGACTGGGTCTG	Depletion of G252, FP
			CAGACCCAGTCGCCATGGCCGTGCAGGTG	Depletion of G252, RP

[a] FP - forward primer, RP - reverse primer. [d] Designed by Dr. Isabelle Salard.

Table 4.1 List of constructs and primers used in this chapter - continued.

4.3.4 *Determination of the molecular weight by mass spectrometry*

The molecular weight (MW) of proteins was determined by matrix-assisted laser desorption ionization time-of-flight mass spectrometry, MALDI-TOF-MS, as described in Chapter 5.12.1.

4.3.5 *UV-Vis absorption spectroscopy*

UV-Vis spectra were acquired at room temperature (RT) on a Perkin Elmer λ 35 spectrophotometer equipped with a Parkin Elmer PTP-1 peltier, as described in Chapter 5.12.2. The ε values of the SLAC and bNiR variants have been estimated from the relative absorbance at 280 nm, ~ 360 nm and ~ 590 nm.

4.3.6 *Continuous wave electron paramagnetic resonance spectroscopy*

Continuous wave (cw) X-band (9.48 GHz) EPR spectra were acquired at ~ 80 K on a Bruker EMX EPR spectrometer equipped with an ESR900 cryostat (Oxford Instruments), as described in Chapter 5.12.5.

4.3.7 *Circular dichroism spectroscopy*

Far-UV (190 - 260 nm) and visible (300 - 700 nm) circular dichroism (CD) spectra were acquired at 25 °C with Jasco J-810 spectrometer, as described in Chapter 5.12.3. The protein concentration ranged from 0.56 to 1.09 mg/mL for the far-UV CD and 11, 25 and 34 mg/mL for the visible CD measurements of WT SLAC, nirSLAC and T1D nirSLAC, respectively.

4.3.8 *Metal content determination*

The Cu and zinc (Zn) content of purified proteins was determined with a Thermo Electron M Series Atomic Absorption Spectrometer (AAS), as described in Chapter 5.12.4.

4.3.9 *Activity measurements*

The activity of WT SLAC and its variants was determined spectrophotometrically by following the oxidation of 50 mM 2,6-dimethylphenol (2,6-DMP, Appendix A) at 468 nm (ε_{468} = 14800 $M^{-1}cm^{-1}$ [76]) at 21 °C in 0.1 M acetate (pH 5.3 - 5.9), 0.1 M phosphate (pH 6.0 - 8.0), 0.1 M Tris (pH 8.0 - 9.0) and 0.1 M carbonate (pH 9.0 - 10.0), as previously described [73]. The activity was calculated from the initial rates of product formation and expressed as nanomoles of substrate, which is oxidized by one mg of the enzyme in one second (10^{-9} $mol \times s^{-1} \times mg^{-1}$).

The nitrite reductase activity of WT bNiR and LacNiR was compared by measuring the fluorescence intensity changes of reduced N-terminally ATTO 550 labeled proteins in the presence of nitrite. The procedure for fluorescent labeling of proteins is described in Chapter 5.11. The reaction mixtures were prepared in an anaerobic chamber (Belle technology, $[O_2] << 2$ ppm) in sealed cuvettes (3 mL) and contained equal concentration (150 nM) of LacNiR and WT bNiR in 50 mM phosphate pH 7.5. ATTO 550 labeled bNiR and ATTO 550 labeled LacNiR were reduced either by sodium ascorbate and phenazine ethosulfate (PES) or 15 μM of dithionite-reduced Az from *Pseudomonas aeruginosa* as described in Chapter 2.3.10. Turnover was studied by the addition of anaerobic solution of $NaNO_2$ (66 μM - 5.3 mM). The fluorescence intensity of ATTO 550 for the oxidized labeled proteins was determined by the addition of an excess of $K_3[Fe(CN)_6]$. The emission of ATTO 550 was followed at 20 °C at 575 nm using an excitation wavelength of 540 nm.

4.3.10 *Crystallization and structure determination*

Numerous unsuccessful attempts to crystallize WT SLAC, tSLAC, qSLAC, mgSLAC and T1D azNiR were undertaken by using the sitting and/or hanging drop method of vapor diffusion at 20 °C. This included the use of buffer/precipitant combinations that had previously proven successful for WT SLAC [57], WT bNiR [77] and NIRAMI [77], and commercially available solutions.

Crystals of LacNiR were obtained, as previously described for WT bNiR [77], by using the hanging drop vapour diffusion method at 20 °C with a solution of protein (1.5 μL, 10 mg/mL) in 5 mM Tris buffer, pH 8.6 mixed with precipitant solution (1.5 μL) containing 100 mM Mes pH 6.5, 10 mM $ZnSO_4 \times 7H_2O$ and 25% PEG-MME 550, where MME corresponds to monomethyl ether. Crystals formed overnight and

were bright blue. Prior to being frozen in liquid nitrogen, a crystal was immersed (by Dr. Adriana Badarau) in N-paratone oil as a cryoprotectant. High-resolution diffraction data were collected at 100 K at DLS (I03 at 0.9763 Å) The data collection and processing, including preliminary structure solution and model building were performed by Dr. Arnaud Baslé. The structure was only partially solved using molecular replacement with bNiR structure (pdb file: 2VN3) as the search model. Secondary Structure Motif (SSM) algorithms implemented in COOT were used to generate all superimposed structures and determine the RMSDs for C^{α} atoms. PyMol software was used to visualize the crystal structure [78].

4.3.11 *Creation of structural models of the SLAC variants*

Structure modeling was performed using I-TASSER software [79]. The crystal structure of WT SLAC (pdb file: 3CG8, [57]) was used as the template for homology modeling of tSLAC and qSLAC, the crystal structure of mgLAC (pdb file: 2ZWN, [59]) was used as the template for homology modeling of mgSLAC, A99H mgSLAC and T1D mgSLAC, and the structure of WT bNIR (pdb file: 1OE1, [52]) as the template for modeling of nirSLAC, T1D nirSLAC and T1D A99H nirSLAC. The template modeling (TM) scores and RMSD between the main chain atoms of the modeled structure and the template of 0.77 ± 0.10 and 5.3 ± 3.4 Å for tSLAC, 0.74 ± 0.11 and 5.8 ± 3.6 Å for qSLAC, 0.74 ± 0.11 and 5.7 ± 3.6 Å for mgSLAC, 0.83 ± 0.08 and 4.4 ± 2.9 Å for A99H mgSLAC, 0.82 ± 0.08 and 4.5 ± 3.0 Å for T1D mgSLAC, 0.72 ± 0.11 and 6.1 ± 3.7 Å for nirSLAC, 0.71 ± 0.11 and 6.1 ± 3.8 Å for T1D nirSLAC and 0.83 ± 0.08 and 4.3 ± 2.9 Å for T1D A99H nirSLAC, respectively, were calculated. The TM-score indicates the difference between the modeled structure and the template by a score 0 to 1, where 1 indicates a perfect match between two structures. To create trimeric structures of variants, the monomeric models were overlaid onto the crystal structure of trimeric WT SLAC (pdb file: 3KW8) [58]. PyMol software was used to visualize the structural model [78].

4.3.12 *Pulsed electron-electron double resonance measurements*

X-band pulsed electron-electron double resonance (PELDOR) measurements were performed by Dr. Jessica H. van Wonderen (University of East Anglia). Spectra were acquired on a Bruker E680 spectrometer using a Bruker MD5-W1 EPR probehead

equipped with an Oxford helium (CF 935) cryostat, as previously described [80], with modifications. The microwave pulses were amplified using a 1 kW Traveling Wave Tube (TWT) amplifier (Applied Systems Engineering, USA). All EPR experiments were carried out at 10 K using 200 μM protein samples (final concentration). WT SLAC and mgSLAC were prepared in 10 mM Tris pH 7.5 containing 100 mM NaCl and 50% glycerol, whereas T1D mgSLAC in deutarated 10 mM Tris pH 7.5 containing 100 mM NaCl and 50% deuterated glycerol.

The pulse sequence for a four-pulse PELDOR is shown in Figure 4.5. Two microwave frequencies, $\nu_{detection}$ and ν_{pump}, ($\Delta\nu$ ($\nu_{detection}$ - ν_{pump}) of 84 MHz) are used to selectively excite two groups of spins, A and B, respectively. The first detection pulse ($\pi/2$), which is applied at a microwave frequency $\nu_{detection}$ and time t = 0, flips A spins to the x-y plane where the spin magnetic moments process around the z-axis with different angular frequencies. The second detection pulse (π) is applied at time $t = \tau_1$ and reverses the direction of all the magnetic moments. This two-pulse sequence ($\pi/2$-τ_1-π) creates a Hahn echo at time $t = 2\tau_1$. By integrating a Hahn echo signal as a function of the magnetic field, the field-swept spectrum is obtained. The third pulse (π, pump pulse) is applied at a microwave frequency ν_{pump} at $t = T$ and inverts the magnetic moments of B spins. The final detection pulse at time $t = 2\tau_1 + \tau_2$ refocuses A spins and creates a refocused echo at time $t = 2\tau_1 + 2\tau_2$. Upon inversion of the B spins (the pump pulse), the A spins that are coupled with the B spins through dipolar interaction are inverted and process in the opposite direction in the x-y plane influencing the intensity of the refocused echo [80, 81, 82].

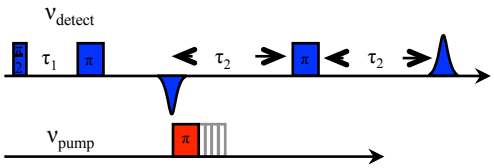

Figure 4.5 The four-pulse PELDOR experiments. The image is taken from [80]. ν_{detect} and ν_{pump} - microwave frequencies for selective excitation of two groups of spins; π - pulse; τ_1, τ_2 - pulse separations.

The pulse lengths in a four-pulse PELDOR were 16 ns for $\pi/2$ and 32 ns for π. The pump pulse lengths were 24 ns (WT SLAC), 30 ns (mgSLAC) and 28 ns (T1D mgSLAC) incremented by 16 ns for a total of 160 (WT SLAC), 147 (mgSLAC) and 142 (T1D mgSLAC) points in time *T*. The delays between pulses, τ_1, τ_2 and τ_3, were

196 ns, 2364 ns and 50 ns for WT SLAC, 200 ns, 2364 ns and 100 ns for mgSLAC and 140 ns, 2234 ns and 50 ns for T1D mgSLAC, respectively. 2020 (WT SLAC), 10240 (mgSLAC) and 1400 (T1D mgSLAC) scans with a repetition time of 500 μs, 500 μs and 20000 μs, respectively, were recorded.

4.4 Results

4.4.1 *Creation of the Cu-binding site using SLAC*

4.4.1.1 *Design cycles of the Cu-binding site within the MBD-1 of SLAC*

In the *first design cycle* (Figure 4.6.A) of a new metal-binding site (MBS), the L1 of SLAC (D^{157}HVVGTEHGTGGIRNGL^{173}) has been replaced with the loops involved in the T1 Cu-binding of mgLAC (Figure 4.4.A) and WT bNiR (Figure 4.4.B), resulting in mgSLAC and nirSLAC, respectively (Table 4.2). Based on the structural resemblance between the L1 and L2 of WT SLAC (Figure 4.4.C), the tSLAC variant carrying D157C, G168H and L173M point mutations in the L1 has been made (Table 4.2, $SLAC_{long}$ gene numbering [73]). All variants from this cycle contain the ligands for a T1 Cu site in MBD-2, a T2/T3 Cu cluster at the interface between the MBD-1 and the MBD-2, and an MBS in their MBD-1 (MBS-1). In the *second design cycle* (Figure 4.6.A), Ala99 ($SLAC_{long}$ gene numbering [73], Chapter 3) in the MBD-1 of tSLAC, mgSLAC and nirSLAC has been substituted with His, resulting in the qSLAC, A99H mgSLAC and A99H nirSLAC variants. This residue corresponds to the T1 Cu-coordinating His57 in the MBD-1 of mgLAC, His89 in the MBD-1 of WT bNiR and His231 in the MBD-2 of WT SLAC. In the *third design cycle* (Figure 4.6.A), the C288S variants ($SLAC_{long}$ gene numbering [73], Chapter 3) of the proteins from the previous cycles, which lack the T1 Cu site (T1D) in MBD-2, have been created, resulting in T1D tSLAC, T1D qSLAC, T1D mgSLAC, T1D nirSLAC and T1D A99H nirSLAC. The T1D A99H mgSLAC variant was not prepared.

4.4.1.2 *Expression and purification of SLAC variants*

tSLAC, qSLAC, mgSLAC and nirSLAC were isolated and purified at relatively high amounts (~ 20 - 50 mg/L), whilst the expression yield of A99H mgSLAC was significantly lower (~ 5 mg/L). A99H nirSLAC was not purified, due to the low

expression of the protein. The V_e of proteins (except for A99H mgSLAC) on the gel-filtration column correspond to MW^{app}s of 105.9 kDa, 103.8 kDa, 101.5 kDa and 105.8 kDa, respectively, which are close to the MW^{app} of WT SLAC (104.3 kDa) (Table 4.3). A99H mgSLAC elutes at a V_e lower to that of mgSLAC suggesting that the protein aggregates in solution (Table 4.3). The expression levels of proteins from the *third design cycle* were lower than those from the *first* and *second design cycles*, but the variants (except for T1D qSLAC) were purified in decent amounts (~ 5 - 20 mg/L). T1D mgSLAC and T1D nirSLAC elute at a V_e similar to those of mgSLAC and nirSLAC (Table 4.3), indicative of the proteins being stable trimers in solution, whereas T1D tSLAC and T1D A99H nirSLAC elute at a V_e significantly lower, suggesting that these SLAC variants aggregate in solution (Table 4.3). The MALDI-TOF-MS gives the MW for the monomer of each protein, which is close to the calculated value (Table 4.4).

4.4.1.3 *Activity of SLAC variants with 2,6-DMP*

WT SLAC shows typical for laccases, bell-shaped activity pattern with the maximal turnover of ~ 80 × 10^{-9} mol×s^{-1} of 2,6-DMP per mg of the protein at pH 8.0 (Table 4.5). tSLAC and qSLAC are the only variants, which show bell-shaped activity pattern, reaching the maximal turnover of ~ 2.0 and 1.0 × 10^{-9} mol×s^{-1} of 2,6-DMP, respectively, at pH of 5.3 to 5.9 (Table 4.5). mgSLAC, nirSLAC and their T1D variants show very little activity with no obvious pH pattern within pH range of 5.3 to 10.

4.4.1.4 *Determination of metal content in SLAC variants*

AAS quantifies 3.38 ± 0.16 equivalents of Cu per monomer of WT SLAC (Table 4.6), which is consistent with the reported values [73]. Low occupancy and absence of the T2 Cu has previously been observed in the crystal structure of WT SLAC [57] and other laccases [83] and is presumably the reason for having < 4 Cu ions per monomer. T1D SLAC contains 2.77 ± 0.08 equivalents of Cu and negligible Zn per monomer (Table 4.6), which is also consistent with previous findings [75].

tSLAC has been isolated with 3.36 ± 0.14 equivalents of Cu per monomer, whilst mgSLAC and nirSLAC have decreased Cu occupancy (2.68 ± 0.31 and 2.91 ± 0.34 equivalents per monomer, respectively) compared to WT protein (Table 4.6). The A99H mutation (*second design cycle*) resulted in qSLAC having decreased Cu occupancy compared to tSLAC, but similar to those of mgSLAC and

nirSLAC (Table 4.6). Dramatic loss of metal has been observed for A99H mgSLAC, which was purified with only 0.85 equivalents of Cu per monomer, and negligible Zn. The C288S mutation (*third design cycle*) resulted in 2.09 ± 0.02 and 2.10 ± 0.07 equivalents of Cu per monomer for T1D mgSLAC and T1D nirSLAC (Table 4.6) and significant increase of Zn content (0.58 ± 0.05 and 1.00 ± 0.12 per monomer respectively). T1D tSLAC and T1D A99H nirSLAC hardly bind any metal yielding as little as 0.87 and 0.53 equivalents of Cu per monomer, and a negligible amount of Zn (Table 4.6).

4.4.1.5 *Far -UV CD spectroscopy of SLAC variants*

The secondary structure composition of the purified SLAC variants have been estimated using far-UV CD spectroscopy and compared to that of WT SLAC (Figure 4.7.A and Table 4.7). The far-UV CD spectra of tSLAC (Figure 4.7.B), mgSLAC (Figure 4.7.C) and nirSLAC (Figure 4.7.D) resemble that of WT SLAC and consist of three bands at around 202 nm (+), 222 nm (−) and 232 nm (+). While the far-UV CD spectrum of qSLAC (Figure 4.7.B) is only slightly different to that of WT SLAC, the spectrum of A99H mgSLAC (Figure 4.7.C) exhibits a maximum at 192 nm (+) and a minimum at 218 nm (−) indicative of this protein not folding correctly. The C288S mutation does not affect the protein fold (T1D SLAC variant, Figure 4.7.A), which is also the case for T1D mgSLAC (Figure 4.7.C) and T1D nirSLAC (Figure 4.7.D). However, the far-UV CD spectra of T1D tSLAC (Figure 4.7.B) and T1D A99H nirSLAC (Figure 4.7.D) are similar to that of A99H mgSLAC, indicative of these proteins not folding correctly.

The obtained secondary structure compositions (Table 4.7) of WT SLAC, tSLAC, mgSLAC, nirSLAC, qSLAC, T1D SLAC, T1D mgSLAC and T1D nirSLAC are in relatively good agreement with those calculated from the crystal structure of WT SLAC [58]. T1D tSLAC, A99H mgSLAC and T1D A99H nirSLAC show an almost 10-fold increase in α-helical content and a lowered percentage of β-strands as compared to that of WT SLAC.

4.4.1.6 *UV-Vis absorption spectra of SLAC variants*

The UV-Vis spectra of WT SLAC (Figures 4.8.A), tSLAC (Figure 4.8.B), qSLAC (Figure 4.8.B) and mgSLAC (Figure 4.8.C) are dominated by the

S(Cys)π→Cu(II) $d_{x^2-y^2}$ LMCT transition band at 590 nm from the T1 Cu(II) site. The ratio of the absorbance at 280 nm (due to the presence of Trp, Tyr, Phe and disulfide bonds) and 590 nm (A_{280}/A_{590}) for WT SLAC and tSLAC is ~ 13, whilst for mgSLAC and qSLAC is ~ 20 - 23 and decreases in the presence of oxidant to ~ 15 - 17 (Table 4.8). The UV-Vis spectrum of nirSLAC (Figure 4.8.D) is decidedly different and does not exhibit an LMCT band at 590 nm. The protein absorbs weakly at 610 nm (with a shoulder at ~ 700 nm, Table 4.8) but in the presence of oxidant, this band is shifted from 610 nm to 590 nm. This shift and an increase in absorption intensity at ~ 590 nm suggest that the spectral features of the T1 Cu site become more dominant over those of the introduced MBS-1 (Figure 4.9.A). After removal of an oxidant, the absorbance at 590 nm of qSLAC, mgSLAC and nirSLAC returns to the value before oxidation. A99H mgSLAC hardly absorbs at 590 nm (even in the presence of oxidant), but the UV-Vis spectrum shows an intense band at ~ 360 nm, with an A_{280}/A_{360} ratio of ~ 13.

The binuclear T3 Cu site of WT SLAC and T1D SLAC gives rise to an intense LMCT transition at ~ 330 nm. The 330 nm band is also present in the UV-Vis spectrum of tSLAC but not mgSLAC, nirSLAC and qSLAC (Table 4.8). The latter SLAC variants exhibit an intense band at ~ 360 nm (an A_{280}/A_{360} ratio of ~ 23 - 25), presumably an LMCT transition from the thiolate (Cys) to the introduced Cu(II)-binding site. The T1D SLAC variants (except for T1D SLAC) absorb strongly at ~ 360 nm, with an A_{280}/A_{360} ratio of ~ 30 to 47 (Figure 4.8 and Table 4.8). Additionally the T1D mgSLAC (Figure 4.8.C) and T1D nirSLAC (Figure 4.8.D) variants weakly absorb at ~ 640 nm. The position and intensity of this band does not change in the presence of oxidant.

4.4.1.7 *Visible CD spectra of nirSLAC and T1D nirSLAC*

The visible CD spectrum of WT SLAC (Figure 4.9.B) is characterized by intense bands at 438 nm (22830 cm^{-1}; −) and 540 nm (18520 cm^{-1}; +) and resembles those of small blue copper proteins, Pc and STC [84 - 86], and also Fet3p [87] and laccases [84]. By comparison the bands at 540 and 438 nm can be assigned as S(Cys)pseudo-σ→Cu(II) $d_{x^2-y^2}$ and N(His)π→Cu(II) $d_{x^2-y^2}$ LMCT transitions, respectively.

The visible CD spectrum of nirSLAC (Figure 4.9.B) is different to that of WT SLAC, and is characterized by an intense band at 360 nm (27778 cm^{-1}, −) and weaker bands at 450 nm (22222 cm^{-1}, +), 570 nm (17544 cm^{-1}, +) and 650 nm (15385 cm^{-1}, −).

The intensity ratio for the 450 nm and 570 nm bands changes and the 650 nm band is shifted towards longer wavelength in the presence of oxidant (Figure 4.9.B), however, the spectrum lacks the spectral features typical of WT SLAC. The spectrum of T1D nirSLAC (Figure 4.9.B) exhibits only two bands, at 360 nm (−) and 450 nm (+).

4.4.1.8 *EPR spectra of SLAC variants*

The EPR spectra of tSLAC and WT SLAC are alike and originate from two distinct paramagnetic centers (Figure 4.10.A). The T1 and T2 Cu(II) sites demonstrate the axial EPR signals with A_z values of 77 and 107 × 10^{-4} cm^{-1}, respectively, which are consistent with the reported values for WT [73] and T1D SLAC [75]. The spectra of qSLAC (Figure 4.10.A) and mgSLAC (Figure 4.10.B) originate from multiple Cu(II) centers but the overlap between EPR signals does not allow for accurate deconvolution. The EPR spectrum of nirSLAC (Figure 4.10.C) is different to that of mgSLAC, and originates from a single paramagnetic center with an A_z of 189 × 10^{-4} cm^{-1} (Table 4.9). The EPR signal for the T1 Cu site is either absent or of very low intensity suggesting that the T1 Cu is either absent or in the Cu(I) form. This is consistent with the lack of the LMCT band at 590 nm in the UV-Vis spectrum of nirSLAC in the resting form.

The EPR spectra of T1D mgSLAC (Figure 4.10.B) and T1D nirSLAC (Figure 4.10.C) resemble that of nirSLAC giving the A_z values of 190 × 10^{-4} cm^{-1} and 188 × 10^{-4} cm^{-1} respectively (Table 4.9). The A_z values in the EPR spectra of T1D mgSLAC, T1D nirSLAC and nirSLAC are significantly higher then that of the T1 Cu sites (< 95 × 10^{-4} cm^{-1}, [1, 27, 35, 36]) and are similar to that observed for the tetragonal S(Cys)-T2 Cu sites (> 130 × 10^{-4} cm^{-1}, [1]). The EPR spectra of T1D tSLAC (Figure 4.10.A) and A99H mgSLAC (Figure 4.10.B) are very similar, but different to those of T1D mgSLAC and T1D nirSLAC, and originate from a single paramagnetic center with an A_z of 160 × 10^{-4} cm^{-1} (Table 4.9). The EPR spectrum of T1D A99H nirSLAC (Figure 4.10.C) originates from two signals: one with A_z of 160 × 10^{-4} cm^{-1} (similar to those of T1D tSLAC and A99H mgSLAC) and second of very low intensity with A_z of 189 × 10^{-4} cm^{-1} (similar to those of nirSLAC, T1D nirSLAC and T1D mgSLAC).

4.4.1.9 *Preliminary studies on the PELDOR of WT SLAC and T1D mgSLAC*

The field-swept electron-spin echo (FSE) spectrum of WT SLAC (Figure 4.11.A) is similar to that of WT bNiR [80] and is typical of the T1 Cu(II) and the T2 Cu(II) sites. The four-pulse ELDOR spectra of WT SLAC and T1D mgSLAC are depicted in Figure 4.11.B and Figure 4.12.B, respectively. These spectra are relatively noisy, however the time traces are typical of PELDOR spectra after background subtraction [80]. The curves were fitted using a distance-domain Tikhonov regularization (thick line). Figure 4.11.C and Figure 4.12.C show the frequency domain (thin line) and simulated (thick lines) spectra of WT SLAC and T1D mgSLAC, respectively. Figure 4.11.D and Figure 4.12.D depict the molecular distances, which were derived from weak dipolar interactions between pairs of paramagnetic species. The distances determined within WT SLAC are 1.8, 2.2, 2.8, 3.1, 3.4, 4.0 and 4.8 nm, whereas within T1D mgSLAC these are 2.1, 2.8, 3.2, 4.0 and 4.8 nm. For comparison, the distances obtained from the crystal structure of WT SLAC between the T1 Cu and the T2 Cu are shown in Figure 4.11.E. T1D mgSLAC could not be crystallized, therefore, the distances between the MBS-1 and the T2 Cu have been calculated from the structural model of the protein overlaid on the trimeric structure of WT SLAC (Figure 4.12.E). Despite several attempts, it was not possible to obtain the distance distribution between the paramagnetic centers in mgSLAC using the PELDOR technique.

The Cu-Cu distances of 1.8, 2.2, 2.8 and 3.1 nm for WT SLAC are very close to those obtained from the crystal structure [58] (1.67, 2.22, 2.88 and 3.22 nm, respectively, Figure 4.11.F). The shortest distance observed in crystal structure, 1.44 nm, could not be resolved using the PELDOR technique. Three longer distances resolved from PELDOR (3.4 nm, 4.0 nm and 4.8 nm) are not observed in the crystal structure. Their presence is likely an artifact caused by the very noisy PELDOR spectrum. The relative intensity between identified peaks varies, with the most intensive peak at 1.8 nm and the least at 3.1 nm. Given that the 1.67 nm peak corresponds to the (T1)Cu-(T1)Cu and 3.22 nm to the (T2)Cu-(T2)Cu distances, the intensity ratio directly reflects significantly lower occupancy of Cu(II) at the T2 Cu site compared to the T1 Cu site. Accordingly, the peaks corresponding to the (T1)Cu-(T2)Cu distances show intermediate intensity.

Preliminary PELDOR measurements on T1D mgSLAC are highly inconclusive. Five Cu-Cu distances have been resolved, from which only two (3.2 and 4.0 nm) are close to those estimated from the structure model of T1D mgSLAC (Figure 4.12.F).

Possibly, the two distances of 3.22 nm and 3.58 nm between the (T2)Cu-(T2)Cu and (MBS-1)Cu-(T2)Cu, respectively, in the structure model of T1D variant, are not resolved in PELDOR data and appear as a single peak at 3.2 nm. Likewise, the distances of 4.15 nm of (MBS-1)Cu-(T2)Cu and 4.31 nm of (MBS-1)Cu-(MBS-1)Cu possibly appear as a single peak at 4.0 nm. Similar lack of resolution has been previously reported for PELDOR measurements on WT bNiR (Figure 4.12.F) [80]. The short distance between the MBS-1 Cu and the T2 Cu sites within the monomer of T1D mgSLAC (1.29 nm) is not observed and the presence of remaining three distances (2.1, 2.8 and 4.8 nm) can possibly be an artifact, caused by too noisy data and low accuracy of data fitting.

4.4.2 *Design of the Cu-binding site and the T2/T3 Cu sites using bNiR*

4.4.2.1 *Design cycles of the Cu-binding sites in bNiR*

Attempts to introduce an MBS in the L2 of MBD-2 (N^{299}HNLIEAFELGA^{310}) in bNiR were undertaken in parallel with those within MBD-1 of SLAC. The first design cycle, which for consistency with the studies on SLAC variants is referred herein as the *second design cycle* (Figure 4.6.B), produced qNiR (Table 4.2), which contains all the ligands for the T1 and T2 Cu sites, and an MBS in MBD-2 (MBS-2). The variant carries N299C, E304H, A310M point mutations in the L2, and T246H mutations in the core of the protein. Thr246 residue corresponds to the T1 Cu-coordinating His89 in the MBD-1 of WT bNiR, His46 in Az and His231 in the MBD-2 of WT SLAC.

In the second design cycle (referred herein as the *third design cycle,* Figure 4.6.B) T1D qNiR, T1D azNiR and T1D T246H azNiR (T1D azNiR carrying the T246H point mutation) that lack the T1 Cu site (C130S mutation) in MBD-1 were prepared. In the T1D azNiR and T1D T246H azNiR variants, the L2 has been replaced with the T1 Cu-binding loop of Az (C^{299}TFPGH^{304}SALM^{308}) (Table 4.2). The T2 Cu site of T1D azNiR and T1D T246H azNiR is coordinated only by two His ligands, as His300, which is the third T2 Cu-coordinating ligand, is removed during the replacement of the L2.

Based on comparison of the T2 Cu site of bNiR and the T2/T3 Cu cluster of laccases, in the third cycle (referred herein as the *fourth design cycle,* Figure 4.6.B), an attempt was made to introduce a T2/T3 Cu site at the interface of the MBD-1 and MBD-2 of bNiR. The LacNiR variant of bNiR contains D92H, A131H, I251H and

L298H mutations that correspond to His102, His158, His236 and His287 of WT SLAC (Table 4.2).

4.4.2.2 *Expression and purification of bNiR variants*

The qNiR, T1D azNiR and T1D T246H azNiR variants were isolated at relatively large amounts (20 - 30 mg/L), whereas the expression level of T1D qNiR was too low to enable protein purification (results not shown). qNiR was very unstable and therefore, was not characterized. The V_e of T1D azNiR from the gel-filtration column corresponds to an MW^{app} of 111.5 kDa, which is similar to an MW^{app} of WT bNiR (115.2 kDa) (Table 4.3), and is indicative of the protein being a stable trimer in solution. MALDI-TOF-MS gives an MW of 36375.5 Da per monomer, which is close to the calculated value (Table 4.4). The T1D T246H azNiR variant elutes from the gel-filtration column as two peaks (Table 4.3). The peak eluting at a lower V_e corresponds to the trimeric form of the protein, whilst the oligomeric state of the protein eluting at a higher V_e, was not estimated. When both fractions were re-applied to the gel-filtration column, the heavier form elutes mainly as a trimer, whereas the lighter form as a mixture, with the relative amount of forms varying between preparations. The T1D T246H azNiR variant was therefore studied in two forms: purified trimer (T1D T246H azNiR trimer) and a mixture (T1D T246H azNiR mixture). LacNiR was isolated in large amounts (~ 50 mg/L), with a V_e from the gel-filtration column similar to that of WT bNiR (Table 4.3), indicative of a stable trimer in solution. MALDI-TOF-MS gives an MW of 36780.5 Da per monomer, which is similar to the calculated value (Table 4.4).

4.4.2.3 *Determination of metal content in bNiR variants*

WT bNiR contains 1.94 ± 0.02 of Cu per monomer (Table 4.6). The metal content in T1D azNiR varies between different preparations, yielding 1.52 ± 0.53 of Cu per monomer and negligible Zn (Table 4.6). The T1D T246H azNiR trimer and mixture were isolated with 1.44 ± 0.01 and 1.96 ± 0.09 of Cu per monomer, respectively, and negligible Zn (Table 4.6). For LacNiR, AAS quantifies 2.68 ± 0.15 of Cu per monomer and negligible Zn (Table 4.6). All attempts to reconstitute the T2/T3 Cu site of LacNiR with Cu(II) were unsuccessful.

4.4.2.4 *Far-UV CD spectroscopy of bNiR variants*

The far-UV CD spectrum of WT bNiR (Figure 4.13.A) consists of three bands at ~ 197 nm (+), 216 nm (−) and 226 nm (−). The spectra of T1D azNiR and T246H variants (Figure 4.13.A) differ, showing a maximum at 196 nm (+) and the two minima at ~ 210 nm (−) and 215 nm (−). The obtained secondary structure composition of WT bNiR is in relatively good agreement with that calculated from the structure [52], whilst the T1D azNiR and T1D T246H azNiR variants show a significant increase in random coil content and a lowered percentage of α-helical and β-strand secondary structure compared to the WT protein (Table 4.7). The far-UV CD spectrum of LacNiR is comparable to that of WT bNiR (Figure 4.14.A) and the obtained secondary structure composition (Table 4.7) is in good agreement with that calculated from the crystal structure of LacNiR (Section 4.4.2.7).

4.4.2.5 *UV-Vis absorption spectra of bNiR variants*

The UV-Vis spectrum of WT bNiR (Figure 4.13.B) is dominated by an intense S(Cys)π→Cu(II) $d_{x^2-y^2}$ LMCT, and a weak S(Cys)σ→Cu(II) $d_{x^2-y^2}$ LMCT transition bands at 594 and 470 nm respectively, from the T1 Cu(II) site. The UV-Vis spectrum of T1D azNiR (Figure 4.13.B) has an LMCT transition band at ~ 370 nm (A_{280}/A_{370} ratio of ~ 42) and a much weaker band at ~ 573 nm, which intensities do not change upon oxidation (Table 4.8). The addition of imidazole as a potential exogenous Cu ligand (data not shown), does not affect the intensity and position of the 370 and 573 nm bands, however high concentrations of imidazole destabilize T1D azNiR leading to precipitation. The UV-Vis spectra of both forms of T1D T246H azNiR (Figure 4.13.B) exhibit weak absorption bands at ~ 550 nm, which do not change upon oxidation. Only T1D T246H azNiR mixture shows an absorption band at 370 nm exhibiting the A_{280}/A_{370} ratio of ~ 49. The UV-Vis spectrum of LacNiR (Figure 4.14.B) shows an intense LMCT band, which is shifted to slightly longer wavelength (600 nm) compared to WT bNiR (594 nm) and WT SLAC (590 nm), and its intensity does not change upon oxidation. In contrary to WT SLAC, LacNiR hardly absorbs at 330 mm suggesting that a T3 Cu(II) site is not present.

4.4.2.6 *EPR spectra of bNiR variants*

The EPR spectrum of WT bNiR (Figure 4.13.C) consists of two EPR signals corresponding to the T1 and T2 Cu(II) centers (Table 4.10) [74]. The EPR spectra of the T1D azNiR and T1D T246H azNiR variants (Figure 4.13.C) also originate from two different EPR signals, one corresponding to the T2 Cu(II) and the other to MBS-2 Cu(II) (Table 4.10). Despite differences in oligomeric state and UV-Vis spectra, the EPR spectra of T1D T246H azNiR trimer and mixture are alike and only slightly different to that of T1D azNiR (Figure 4.13.C and Table 4.10). The g_z values for the T2 Cu(II) site of T1D azNiR and both T1D T246H azNiR variants decrease, whilst the A_z values increase compared to WT bNiR (Table 4.10). This indicates a major change in the coordination sphere of the T2 Cu(II) site of the bNiR variants. The MBS-2 Cu(II) sites of T1D azNiR and T1D T246H azNiR variants demonstrate EPR signals with higher A_z values (188 - 206 × 10^{-4} cm^{-1}) compared to that of the T1 Cu(II) site of WT protein (66 × 10^{-4} cm^{-1}). The EPR spectrum of LacNiR, similar to that of WT bNiR, consists of two EPR signals (Figure 4.14.C). The g_z and the A_z values of the T1 Cu(II) site of LacNiR are similar to those of the WT protein, whilst those of the T2 Cu(II) site are significantly different (Table 4.10), indicative of a major change in the coordination sphere of the T2 Cu site of LacNiR.

4.4.2.7 *Crystal structure of LacNiR*

LacNiR was crystallized in the presence of 10 mM $ZnSO_4$, using identical conditions to those reported for WT bNiR [77]. Soaking the crystals in an excess of $CuSO_4$ resulted in decrease in the quality of the diffraction data. The crystal structure of LacNiR was determined at 1.75 Å resolution from almost perfectly twinned crystals. Similar to WT bNiR, LacNiR crystallizes in space group H3, which, owing to the twinning of the crystal, gives the apparent symmetry of space group H32. LacNiR crystallizes as a trimer in identical oligomeric arrangement to WT bNiR, with a monomer in the asymmetric unit (the trimer is generated by rotational crystallographic symmetry). Partial refinement of almost perfectly twinned crystal of LacNiR possibly generates a certain inaccuracy in values of bond distances and angles. However, the overall structure of LacNiR does not deviate substantially from the structure of WT bNiR. Superposition of the C^{α} atoms of the complete trimer produces an RMSD of 0.65 Å.

The coordination environment of the T1 Cu in LacNiR is similar to that found in WT bNiR. The positions of His89, His139 and the axial ligand, Met144 are similar, however, a small displacement of the thiolate sulfur of Cys130 is observed. The most significant alteration in the structure of LacNiR compared to WT bNiR is observed at the T2 Cu site (Figure 4.15.A and Figure 4.15.B). The electron density and anomalous difference maps (Figure 4.15.A) of this region show a single peak that could be attributed to the T2 Cu. There are no other peaks that could be attributed to additional Cu ions. However, it is important to note, that diffraction data were collected at a wavelength of 0.98 instead of 1.33 Å. Therefore, an anomalous difference map to identify the location of any Cu ions in the crystal was generated at lower electron contribution to the anomalous signal than in experiment conducted at 1.33 Å. The superimposition of the structures of LacNiR and WT SLAC show small displacements of the imidazole rings of His92, His94 and His129 of LacNiR (Figure 4.15.C). However, a major structural alteration is observed for His251, which occupies a dramatically different position of the corresponding residue in WT SLAC (Figure 4.15.C). This results in the imidazole ring being shifted much more to the center of the active site, possibly preventing Cu from binding.

Cycle	Protein	Mutation	Expected metal binding sites
0	WT SLAC		T1 Cu, T2/T3 Cu
	WT bNiR		T1 Cu, T2 Cu
1	tSLAC	D^{157}HVVGTEHGTGG^{168}IRNGL^{173} to **C**^{157}HVVGTEHGTG**H**^{168}IRNG**M**^{173}	T1 Cu, T2/T3 Cu, MBS-2 Cu
	mgSLAC	D^{157}HVVGTEHGTGG^{168}IRNGL^{173} to **C**^{157}HVNVNE**H**^{164}VGVRG**M**^{170}	
	nirSLAC	D^{157}HVVGTEHGTGG^{168}IRNGL^{173} to **C**^{157}H̲PEGMVPW**H**^{166}VVSG**M**^{171}	
2	qSLAC	D^{157}HVVGTEHGTGG^{168}IRNGL^{173} to **C**^{157}HVVGTEHGTG**H**^{168}IRNG**M**^{173} and A99**H** [a]	T1 Cu, T2/T3 Cu, MBS-2 Cu
	A99H mgSLAC	D^{157}HVVGTEHGTGG^{168}IRNGL^{173} to **C**^{157}HVNVNE**H**^{164}VGVRG**M**^{170} and A99**H** [a]	
	A99H nirSLAC	D^{157}HVVGTEHGTGG^{168}IRNGL^{173} to **C**^{157}H̲PEGMVPW**H**^{166}VVSG**M**^{171} and A99**H** [a]	
	qNiR	N^{299}HNLIE^{304}AFELGA^{310} to **C**^{299}HNLI**H**^{304}AFELG**M**^{310} and T246**H**	T1 Cu, T2 Cu, MBS-1 Cu

[a] Numbering of the *SLAC$_{long}$* gene [73] (Chapter 3).

Table 4.2 Variants of SLAC and bNiR studied in this chapter.

Cycle	Protein	Mutation	Expected metal binding sites
3	T1D SLAC	C288S [b]	T2/T3 Cu
	T1D tSLAC	D^{157}HVVGTEHGTGG^{168}IRNGL^{173} to **C**^{157}HVVGTEHGTG**H**^{168}IRNG**M**^{173} and C288S [a]	T2/T3 Cu, MBS-2 Cu
	T1D qSLAC	D^{157}HVVGTEHGTGG^{168}IRNGL^{173} to C^{157}HVVGTEHGTGH^{168}IRNGM^{173}, A99**H** [a] and C288S [a]	
	T1D mgSLAC	D^{157}HVVGTEHGTGG^{168}IRNGL^{173} to **C**^{157}HVNVNE**H**^{164}VGVRG**M**^{170} and C288S [a]	
	T1D nirSLAC	D^{157}HVVGTEHGTGG^{168}IRNGL^{173} to **C**^{157}HPEGMVPW**H**^{166}VVSG**M**^{171} and C288S [a]	
	T1D A99H nirSLAC	D^{157}HVVGTEHGTGG^{168}IRNGL^{173} to C^{157}HPEGMVPWH^{166}VVSGM^{171}, A99**H** [a] and C288S [a]	
	T1D qNiR	N^{299}HNLIE^{304}AFELGA^{310} to **C**^{299}HNLI**H**^{304}AFELG**M**^{310}, C130S and T246**H**	T2 Cu, MBS-1 Cu
	T1D azNiR	N^{299}HNLIEAFELGA^{310} to **C**^{112}TFPG**H**^{117}SAL**M**^{121} and C130S	
	T1D T246H azNiR	N^{299}HNLIEAFELGA^{310} to **C**^{112}TFPG**H**^{117}SAL**M**^{121} and C130S and T246**H**	
4	LacNiR	Asp92, Ala131, Ile251 and Leu298	T1 Cu, T2/T3 Cu
	Δ252G LacNiR	Asp92, Ala131, Ile251, Leu298 and Δ252G	

[a] Numbering of the *SLAC$_{long}$* gene [73] (Chapter 3).

Table 4.2 Variants of SLAC and bNiR studied in this chapter - continued.

Cycle	Protein	Elution volume (V_e), mL		MW^{app}, kDa	Estimated oligomeric state
		Protein	Control protein		
0	WT SLAC			104.3	Trimer
	WT bNiR			115.2	Trimer
1	tSLAC			105.9	Trimer
	mgSLAC			101.5	Trimer
	nirSLAC			105.8	Trimer
2	qSLAC			103.8	Trimer
	A99H mgSLAC	69.9	72.2 (T1D nirSLAC)	[a]	[a]
3	T1D SLAC	[a]	[a]	[a]	Trimer [b]
	T1D tSLAC	70.1	72.2 (T1D nirSLAC)	[a]	[a]
	T1D mgSLAC	73.1	72.2 (T1D nirSLAC)	[a]	Trimer [c]
	T1D nirSLAC			100.6	Trimer
	T1D A99H nirSLAC	75.4	77.3 (T1D nirSLAC)	[a]	[a]
	T1D azNiR			111.5	Trimer
	T1D T146H	75.0	74.5 (LacNiR)	[a]	Trimer [c]
	azNiR	81.0		[a]	[a]
4	LacNiR	77.0	76.5 (WT bNiR)	[a]	Trimer [c]

[a] Not determined. [b] Taken from [75]. [c] Trimeric state was estimated from V_e value relative to the V_e of trimeric control protein (shown in brackets).

Table 4.3 Gel-filtration data for purified proteins and calculated apparent molecular weights (MW^{app}).

Cycle	Protein	Experimental mass (MW), Da	Theoretical mass ($MW^{theoretical}$), Da
0	WT SLAC	32591.6	32587.0 (− Met)
	WT bNiR	36652.3	36654.8 (+ Met)
1	tSLAC	32664.5	32673.2 (− Met)
	mgSLAC	32419.5	32419.0 (− Met)
	nirSLAC	32513.4	32534.2 (− Met)
2	qSLAC	32736.3	32739.3 (− Met)
	A99H mgSLAC	[a]	32485.0 (− Met)
3	T1D tSLAC	[a]	32657.2 (− Met)
	T1D mgSLAC	32400.5	32400.5 (− Met)
	T1D nirSLAC	32519.1	32518.1 (− Met)
	T1D A99H nirSLAC	[a]	32584.2 (− Met)
	T1D azNiR	36374.5	36374.5 (+ Met)
	T1D T146H azNiR	[a]	36410.6 (+ Met)
5	LacNiR	36780.5	36790.9 (+ Met)

[a] Not determined.

Table 4.4 MALDI-TOF-MS data and calculated theoretical masses of purified proteins.

Cycle	Protein	Optimal pH [a]	Activity (10^{-9} mol×s^{-1}×mg^{-1})
0	WT SLAC	8.0	77
1	tSLAC	5.9	1.9
	mgSLAC	5.3 - 9.5	0.0 - 0.4
	nirSLAC	5.3 - 9.5	0.0 - 0.8
2	qSLAC	5.3	1.0
	A99H mgSLAC	[b]	[b]
3	T1D SLAC	9.0	0.1
	T1D tSLAC	[b]	[b]
	T1D mgSLAC	5.3 - 9.5	0.0 - 0.4
	T1D nirSLAC	5.3 - 9.5	0.0 - 0.1
	T1D A99H nirSLAC	[b]	[b]

[a] pH range indicates no optimal pH. [b] Not determined.

Table 4.5 Activity of the SLAC variants with 50 mM of 2,6-DMP at RT.

Cycle	Protein	Theoretical Cu/monomer	Experimental	
			Cu/monomer	Zn/monomer
0	WT SLAC	4.00	3.38 ± 0.16	Negligible
	WT bNiR	2.00	1.94 ± 0.02	Negligible
1	tSLAC	5.00	3.36 ± 0.14	0.07 ± 0.02
	mgSLAC	5.00	2.68 ± 0.31	0.15 ± 0.05
	nirSLAC	5.00	2.91 ± 0.34	0.18 ± 0.14
2	qSLAC	5.00	2.24 ± 0.21	0.17 ± 0.04
	A99H mgSLAC	5.00	0.85 [a]	Negligible [a]
3	T1D SLAC	3.00	2.77 ± 0.08	Negligible
	T1D tSLAC [a]	4.00	0.87 [a]	Negligible [a]
	T1D mgSLAC	4.00	2.09 ± 0.02	0.58 ± 0.05
	T1D nirSLAC	4.00	2.10 ± 0.07	1.00 ± 0.12
	T1D A99H nirSLAC [a]	4.00	0.75 [a]	Negligible [a]
	T1D azNiR	2.00	1.52 ± 0.53	0.07 ± 0.04
	T1D T246H azNiR trimer	2.00	1.44 ± 0.01	0.08 ± 0.00
	T1D T246H azNiR mixture	2.00	1.96 ± 0.09	0.08 ± 0.01
4	LacNiR	4.00	2.68 ± 0.15	0.11 ± 0.02

[a] Single measurement.

Table 4.6 Cu and Zn quantifications for the purified proteins.

Cycle	Protein	Data analazyed [a]	Fitting NRMSD [b]	Secondary structure, %			
				Helix	β-sheet	Turn	Random coil
0	WT SLAC [c]	X-ray		6.6	46.5	27.5	19.4
		Far-UV CD	0.034	3.0	47.0	22.0	27.0
	WT bNiR [c]	X-ray		12.2	39.6	26.4	21.8
		Far-UV CD	0.040	7.0	41.0	21.0	29.0
1	tSLAC	Far-UV CD	0.041	3.0	45.0	23.0	30.0
	mgSLAC	Far-UV CD	0.039	4.0	44.0	22.0	29.0
	nirSLAC	Far-UV CD	0.051	3.0	44.0	22.0	29.0
2	qSLAC	Far-UV CD	0.041	3.0	43.0	24.0	30.0
	A99H mgSLAC	Far-UV CD	0.017	30.0	23.0	19.0	28.0
3	T1D SLAC	Far-UV CD	0.035	3.0	47.0	21.0	27.0
	T1D tSLAC	Far-UV CD	0.014	29.0	23.0	20.0	28.0
	T1D mgSLAC	Far-UV CD	0.049	3.0	44.0	22.0	30.0
	T1D nirSLAC	Far-UV CD	0.049	3.0	46.0	22.0	29.0
	T1D A99H nirSLAC	Far-UV CD	0.016	29.0	22.0	19.0	28.0
	T1D azNiR	Far-UV CD	0.039	4.0	33.0	17.0	44.0
	T1D T146H azNiR Trimer	Far-UV CD	0.045	4.0	35.0	18.0	41.0
	T1D T146H azNiR Mixture	Far-UV CD	0.54	4.0	33.0	18.0	44.0
4	LacNiR	X-ray		10.4	34.2	28.5	26.9
		Far-UV CD	0.030	11.0	36.0	20.0	31.0

[a] In 10 mM phosphate pH 7.0 at 25 °C. [b] Normalised to 1 root-mean square deviation [88] for fitting of the far-UV CD spectra in 190 - 240 nm range using CDSSTR analysis method [89], protein reference sets 4 or 7, as implemented by Dichroweb [90]. [c] The structures used were the crystal structures of WT bNiR (pdb code: 1OE1) [52] and WT SLAC (pdb code: 3KW8) [58].

Table 4.7 Comparison of the secondary structure contents determined from available structures using STRIDE [91] with those calculated from the far-UV CD spectra using Dichroweb [90].

Cycle	Protein	$\lambda_{max(1)}$, nm; ($\varepsilon_{max(1)}$, $M^{-1}cm^{-1}$)	$\lambda_{max(2)}$, nm; ($\varepsilon_{max(2)}$, $M^{-1}cm^{-1}$)	$\varepsilon_{280}/\varepsilon_{max(1)}$	$\varepsilon_{280}/\varepsilon_{max(2)}$
0	WT SLAC	~ 330; (3700)	590; (4400) [a]	15.2	12.5
	WT bNiR	470; (1040) [b]	594; (5200) [b]	53.0	10.8
1	tSLAC	330; (3200)	590; (4300)	17.0	12.9
	$tSLAC_{oxy}$ [c]	[d]	590; (4400)	N/A	12.4
	mgSLAC	360; (2250)	590; (2400)	24.7	22.9
	$mgSLAC_{oxy}$ [c]	[d]	590; (3600)	N/A	15.3
	nirSLAC	360; (2500)	610; (700)	22.7	76.4
	$nirSLAC_{oxy}$ [c]	[d]	590; (3000)	N/A	18.6
2	qSLAC	352; (2170)	590; (2400)	25.5	19.6
	$qSLAC_{oxy}$ [c]	[d]	590; (3200)	N/A	17.2
	A99H mgSLAC	360; (4400)	590; (190)	12.6	~ 290
	A99H $mgSLAC_{oxy}$ [c]	[d]	590; (190)	N/A	~ 290
3	T1D SLAC	330; (2270)	N/A	24.4	N/A
	T1D tSLAC	357; (1700)	590; (80)	33.1	N/A
	T1D mgSLAC	360; (1180)	590; (190)	46.9	~ 290
	T1D nirSLAC	365; (1850)	637; (200)	30.1	269
	T1D A99H nirSLAC	356; (1200)	N/A	45.3	N/A
	T1D azNiR	370; (1300)	573; (350)	42.4	~ 160
	T1D T146H azNiR Trimer	370; (790)	550; (230)	70.9	~ 239
	T1D T146H azNiR Mixture	~ 370; (1150)	550; (310)	48.5	~ 180
4	LacNiR	470; (1170)	600; (4400)	47.8	12.6

[a] Taken from [73]. [b] Taken from [77]. [c] In the presence of an excess of $[Fe(CN)_6]^{3-}$. [d] Not determined.

Table 4.8 Comparison of the UV-Vis parameters of purified proteins.

Parameters [b]	Protein [a]									
	WT SLAC	tSLAC	mgSLAC [c]	nirSLAC	qSLAC [c]	A99H mgSLAC	T1D tSLAC	T1D mgSLAC	T1D nirSLAC	T1D A99H nirSLAC [d]
g_x (T1 Cu)	2.032	2.032	2.032		2.032					
g_y (T1Cu)	2.049	2.049	2.049		2.049					
g_z (T1Cu)	2.233	2.233	2.233		2.233					
A_x (T1 Cu)	9.3	9.3	9.3		9.3					
A_y (T1 Cu)	9.6	9.6	9.6		9.6					
A_z (T1 Cu)	77	77	77		77					
g_x (T2 Cu)	2.048	2.034								
g_y (T2 Cu)	2.055	2.053								
g_z (T2 Cu)	2.362	2.352								
A_x (T2 Cu)	0.0	0.0								
A_y (T2 Cu)	0.0	0.0								
A_z (T2 Cu)	107	107								
g_x (MBS-2)				2.046		2.026	2.026	2.048	2.046	2.026
g_y (MBS-2)				2.064		2.079	2.079	2.065	2.061	2.079
g_z (MBS-2)				2.247		2.201	2.201	2.252	2.248	2.201
A_x (MBS-2)				0.0		0.0	0.0	0.0	0.0	0.0
A_y (MBS-2)				0.0		0.0	0.0	0.0	0.0	0.0
A_z (MBS-2)				189		160	160	190	188	160

[a] In 20 mM Tris pH 7.5 containing 200 mM NaCl at ~ 80 K. [b] The units of the hyperfine coupling constants are 10^{-4} cm^{-1}. [c] Signals overlap allows only for accurate simulation of the T1 Cu(II) site. [d] Second, low intensity signal present at $g_z = 2.252$ and $A_z = 189 \times 10^{-4}$ cm^{-1}.

Table 4.9 Comparison of the EPR parameters of WT SLAC and the variants made in this study.

Parameters [a]	Protein				
	WT bNiR [b]	LacNiR [b]	T1D azNiR [c]	T1D T246H azNiR trimer [c]	T1D T246H azNiR mixture [c]
g_x (T1 Cu)	2.038	2.038			
g_y (T1Cu)	2.058	2.058			
g_z (T1Cu)	2.221	2.227			
A_x (T1 Cu)	10.3	10.4			
A_y (T1 Cu)	8.3	8.4			
A_z (T1 Cu)	66	75			
g_x (T2 Cu)	2.017	2.049	2.048	2.058	2.048
g_y (T2 Cu)	2.122	2.127	2.058	2.068	2.058
g_z (T2 Cu)	2.372	2.253	2.266	2.255	2.266
A_x (T2 Cu)	0.0	0.0	1.0	1.0	1.0
A_y (T2 Cu)	0.0	0.0	1.0	1.0	1.0
A_z (T2 Cu)	110	142	177	180	177
g_x (MBS-1)			2.019	2.029	2.010
g_y (MBS-1)			2.074	2.063	2.084
g_z (MBS-1)			2.206	2.210	2.206
A_x (MBS-1)			0.0	0.0	0.0
A_y (MBS-1)			0.0	0.0	0.0
A_z (MBS-1)			206	188	206

[a] The units of the hyperfine coupling constants are 10^{-4} cm^{-1}. [b] In 24 mM Tris pH 7.5 plus 40 % glycerol at ~ 80 K. [c] In 20 mM Tris pH 7.5 containing 200 mM NaCl at ~ 80 K.

Table 4.10 Comparison of the EPR parameters of WT bNiR and the variants made in this study.

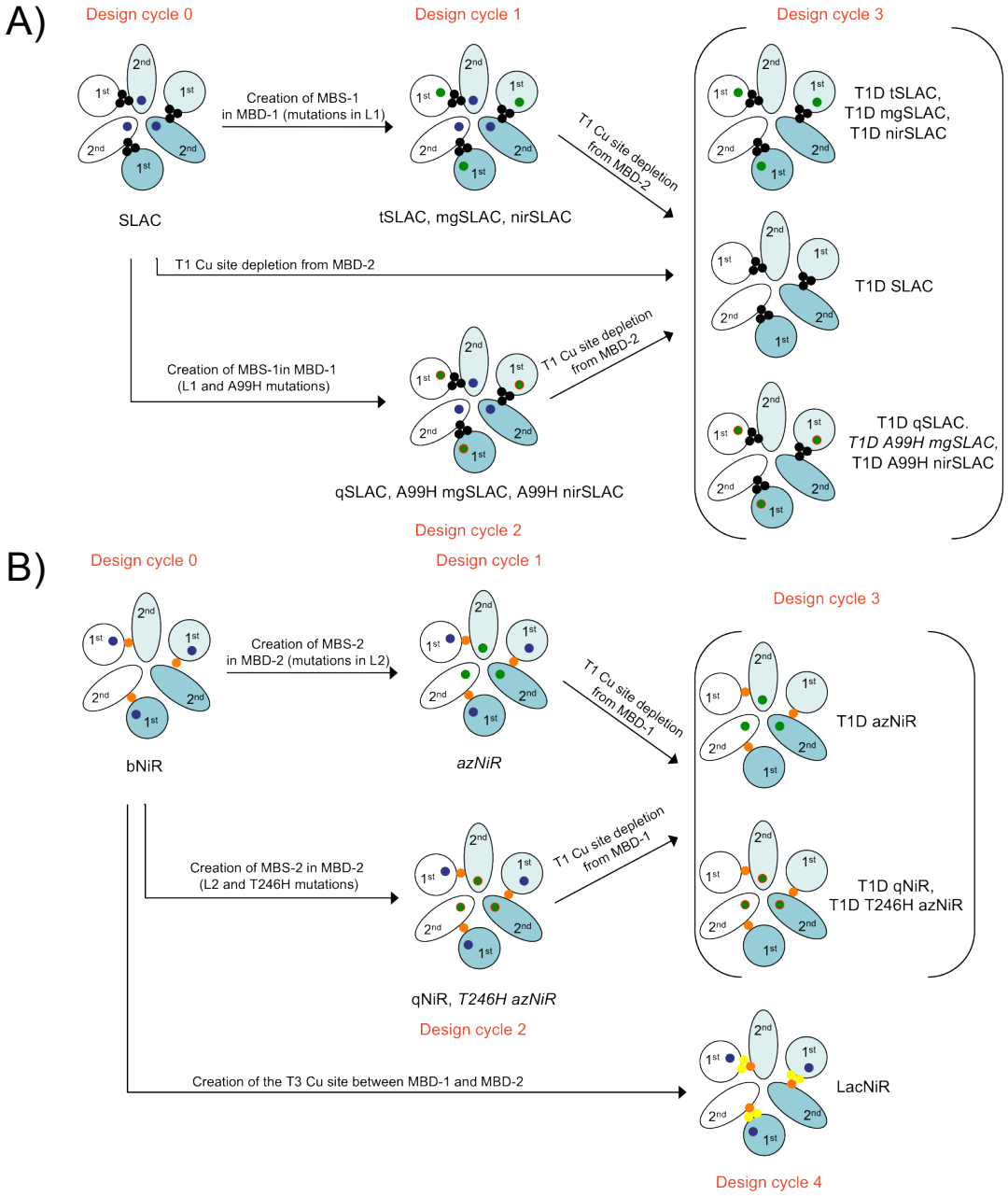

Figure 4.6 Schemes of the design cycles for the variants of (A) SLAC and (B) bNiR. Oval and circle shapes represent MBD-1 and MBD-2, respectively. Blue colours represent the two-domain monomer of trimeric proteins. T1, T2, T3, T2/T3 Cus are blue, orange, yellow and black dots respectively. MBS-1 and MBS-2 are green dots, whilst A99H and T246H mutations at the MBS-1 and MBS-2 are shown as red rings around these dots. The proteins that were not prepared are shown in italic.

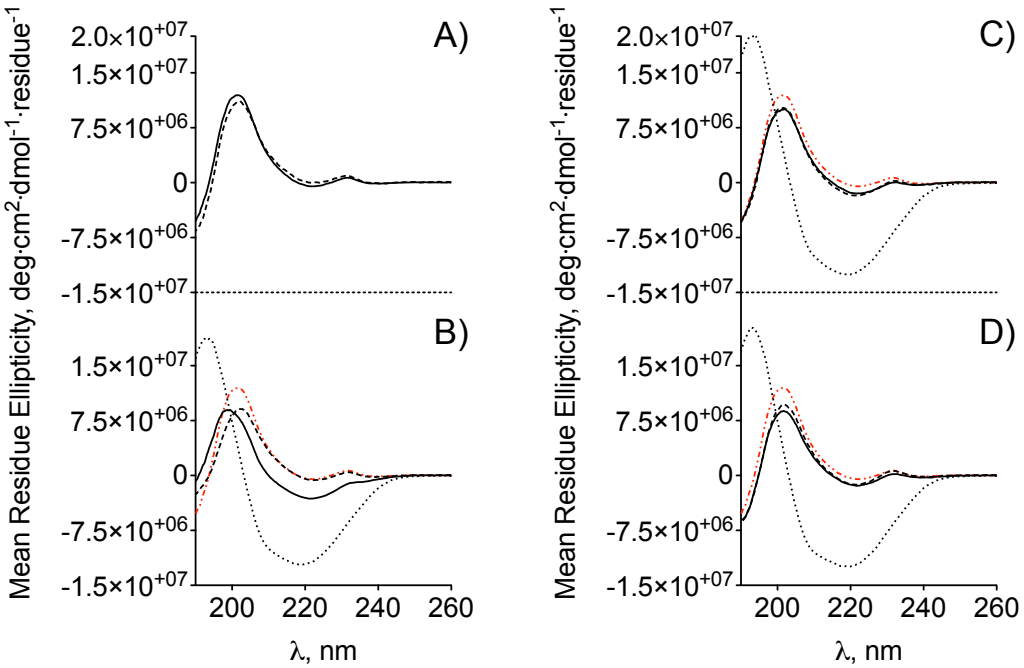

Figure 4.7 Far-UV CD spectra of (A) WT SLAC (——) and T1D SLAC (– – –); (B) WT SLAC (- - - -), tSLAC (– – –), T1D tSLAC (····) and qSLAC (——); (C) WT SLAC (- - - -), mgSLAC (——), T1D mgSLAC (– – –) and A99H mgSLAC (····); (D) WT SLAC (- - - -), nirSLAC (——), T1D nirSLAC (– – –) and T1D A99H nirSLAC (····). The spectra were acquired at 25 °C in 10 mM phosphate at pH 7.0.

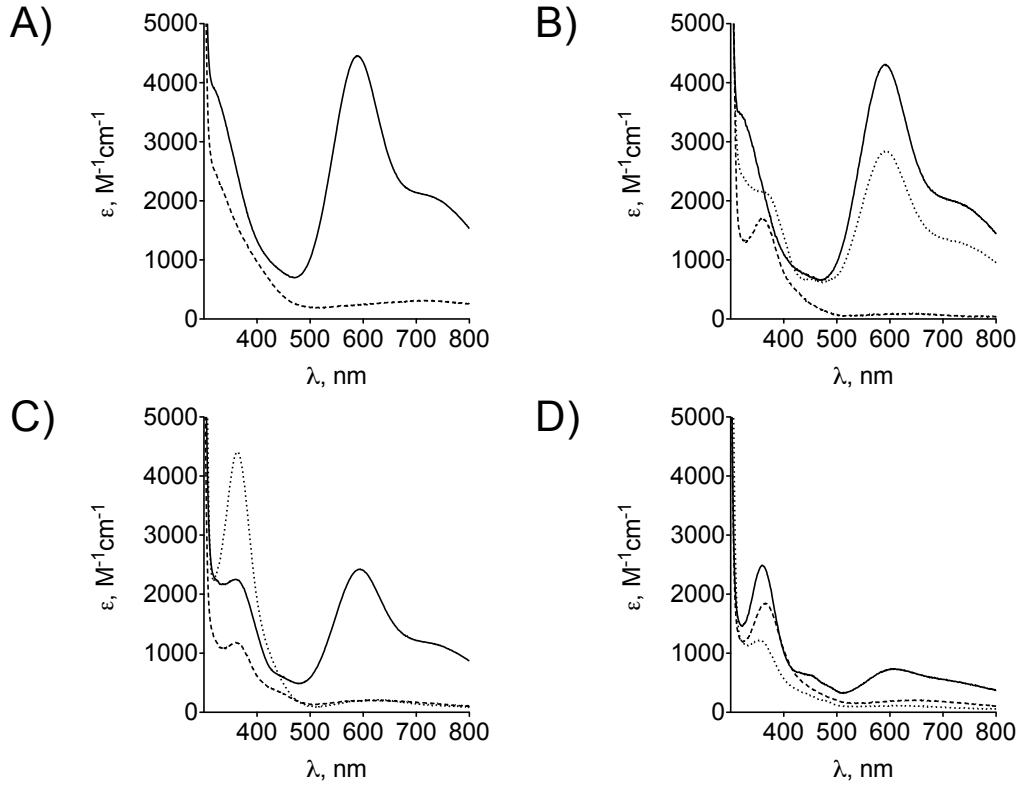

Figure 4.8 UV-Vis absorption spectra of (A) WT SLAC (——) and T1D SLAC (▪▪▪); (B) tSLAC (——), T1D tSLAC (▪▪▪) and qSLAC (▪▪▪▪); (C) mgSLAC (——), T1D mgSLAC (▪▪▪) and A99H mgSLAC (▪▪▪▪); (D) nirSLAC (——), T1D nirSLAC (▪▪▪) and T1D A99H nirSLAC (▪▪▪▪). Spectra were acquired at RT in 20 mM Tris pH 7.5 containing 200 mM NaCl.

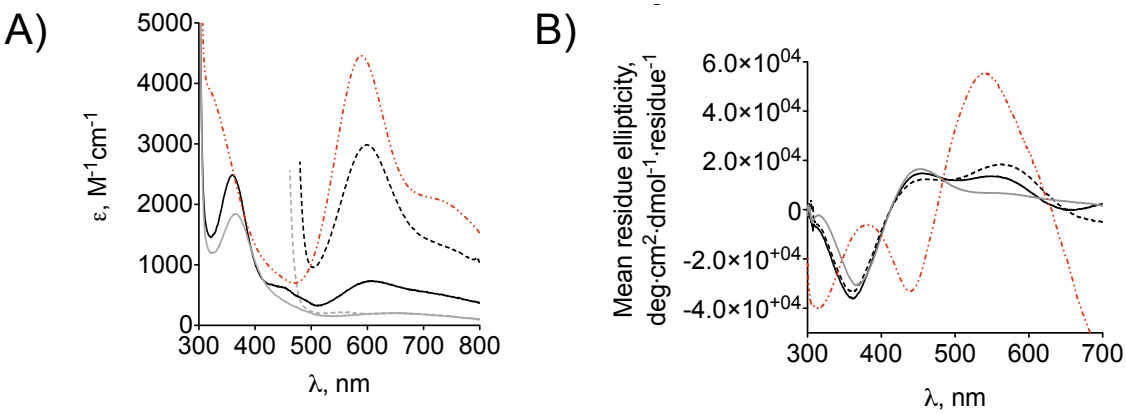

Figure 4.9 UV-Vis absorption (A) and visible CD (B) spectra of WT SLAC (▪▪▪▪), nirSLAC as isolated (——), nirSLAC in the presence of an excess of $[Fe(CN)_6]^{3-}$ (▪▪▪), T1D nirSLAC as isolated (——) and T1D nirSLAC in the presence of an excess of $[Fe(CN)_6]^{3-}$ (- - -). The spectra were acquired in 20 mM Tris pH 7.5 containing 200 mM NaCl.

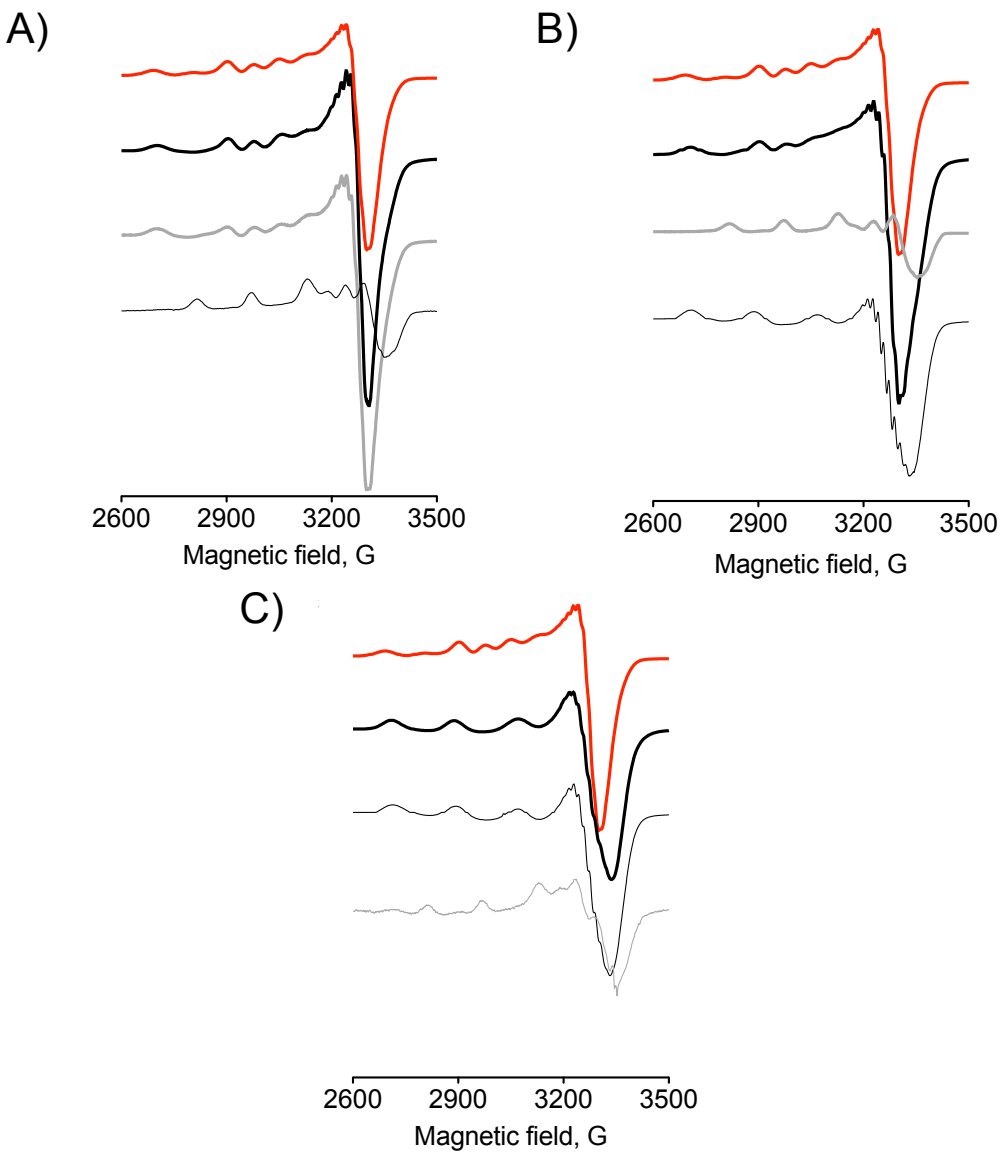

Figure 4.10 EPR spectra of (A) WT SLAC (—), tSLAC (—), qSLAC (—) and T1D tSLAC (—). (B) WT SLAC (—), mgSLAC (—), A99H mgSLAC (—) and T1D mgSLAC (—). (C) WT SLAC (—), nirSLAC (—) and T1D nirSLAC (—) and T1D A99H nirSLAC (—). The spectra were acquired at ~ 80 K in 20 mM Tris pH 7.5 containing 200 mM NaCl.

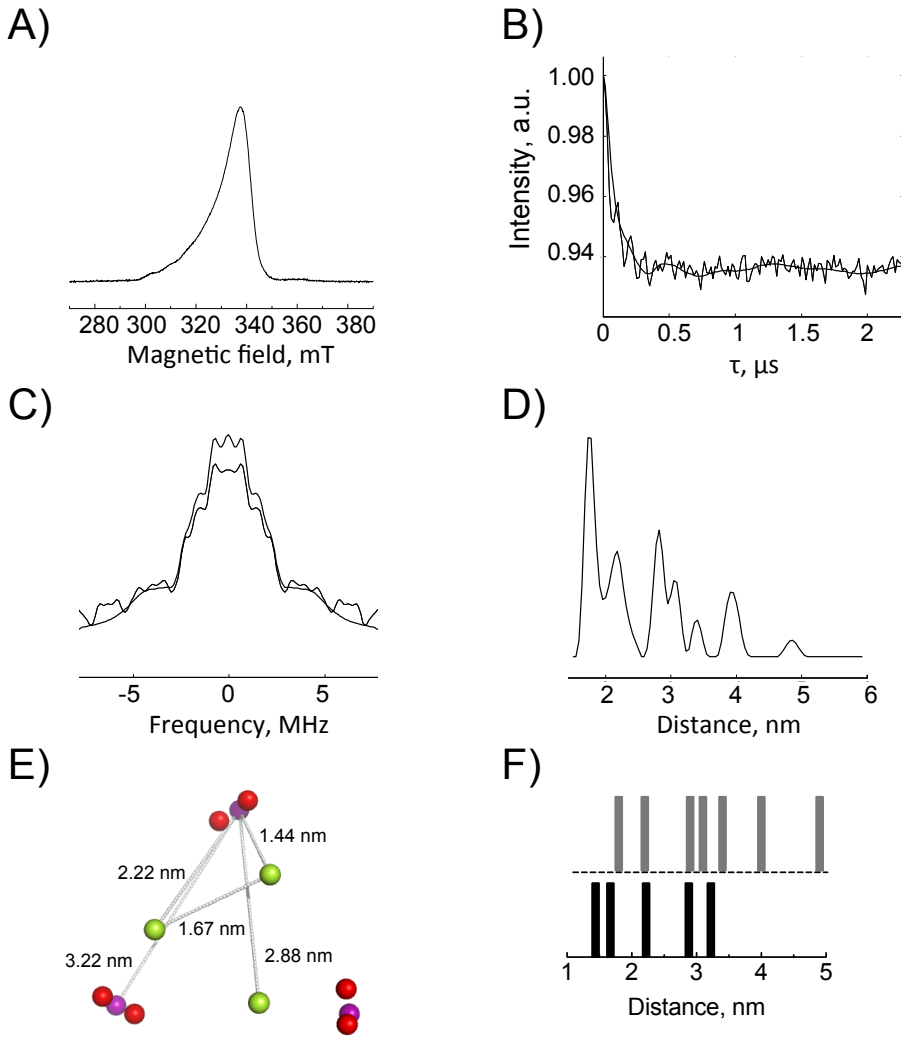

Figure 4.11 (A) The FSE spectrum of WT SLAC using a two-pulse echo sequence ($\pi/2$-τ_1-π, Figure 4.5) with a 16 ns 32 ns π-pulse and τ_1 = 196 ns. (B) A four-pulse PELDOR spectrum (—, after subtraction of an exponential decay) of WT SLAC at 9.687 GHz, 10 K and τ_2 = 2364 ns using the pulse sequence in Figure 4.5, and the fit (—) of the spectrum. (C) Frequency domain spectrum (—) with simulation (—). (D) Distance distribution with peaks at 1.8, 2.2, 2.9, 3.1, 3.4, 4.0 and 4.9 nm and (E) the Cu-Cu distances within the WT SLAC trimer [58]. T1, T2 and T3 Cus are green, purple and red spheres, respectively. (F) Comparison of the distances obtained from four-pulse PELDOR (gray bars) with those from the crystal structure (black bars). *Figures (A) - (D) prvided by Dr. Jessica H. van Wonderen.*

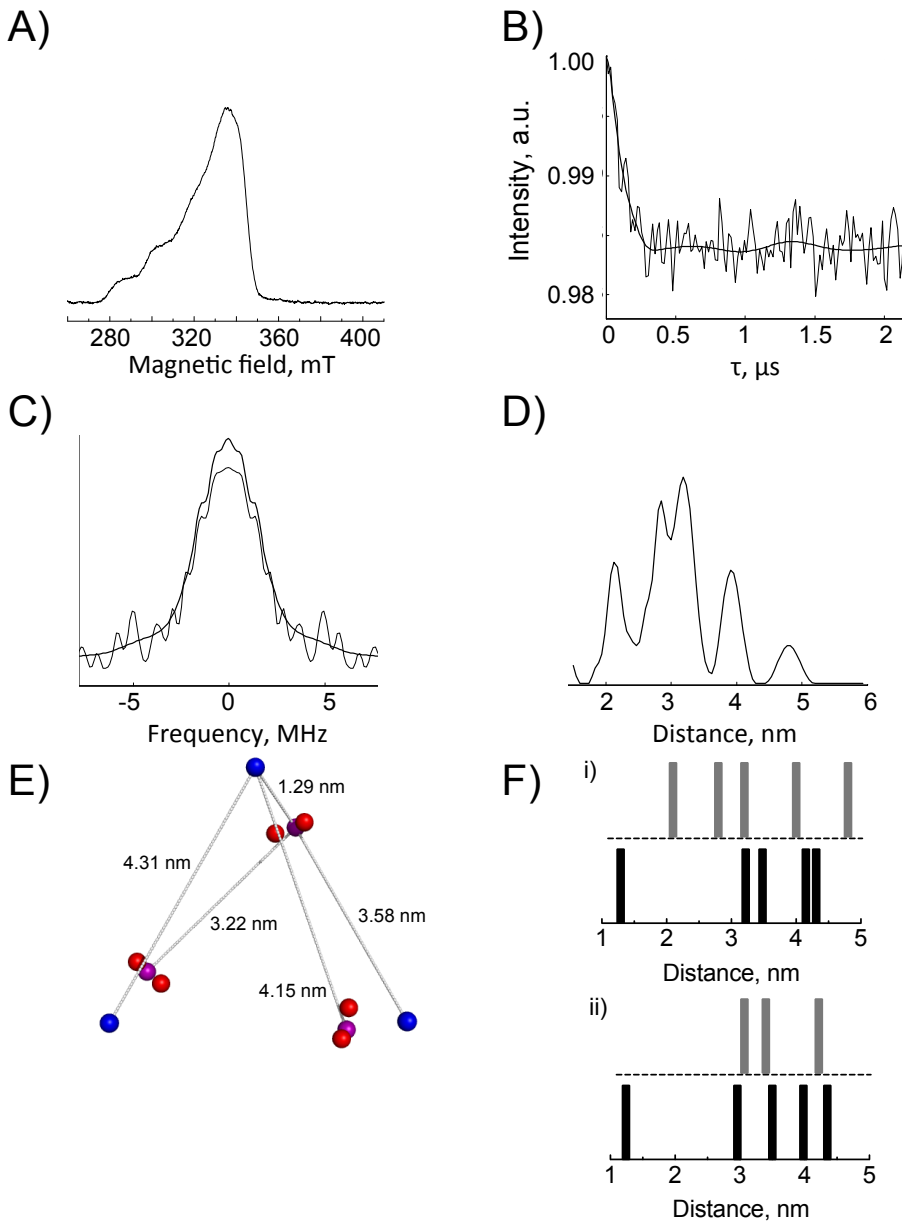

Figure 4.12 (A) The FSE spectrum of T1D mgSLAC using a two-pulse echo sequence ($\pi/2$-τ_1-π, Figure 4.5) with a 16 ns 32 ns π-pulse and τ_1 = 140 ns. (B) A four-pulse PELDOR spectrum (—, after subtraction of an exponential decay) of T1D mgSLAC at 9.668 GHz, 10 K and τ_2 = 2232 ns using the pulse sequence in Figure 4.5, and the fit (**—**) of the spectrum. (C) Frequency domain spectrum (—) with simulation (**—**). (D) Distance distribution with peaks at 2.1, 2.8, 3.2, 4.0 and 4.8 nm. (E) The Cu-Cu distances within the trimer of T1D mgSLAC structural model overlaid on the trimeric WT SLAC [58]. MBS-1, T2 and T3 Cus are green, purple and red spheres, respectively. (F) Comparison of the distances obtained for T1D mgSLAC (i) and WT bNiR (3.07, 3.40 and 4.22 nm, [80]) from four-pulse PELDOR (gray bars) with those from the structural model (T1D mgSLAC) and crystal structure (WT bNiR [52]) (black bars). *Figures (A) - (D) prvided by Dr. Jessica H. van Wonderen.*

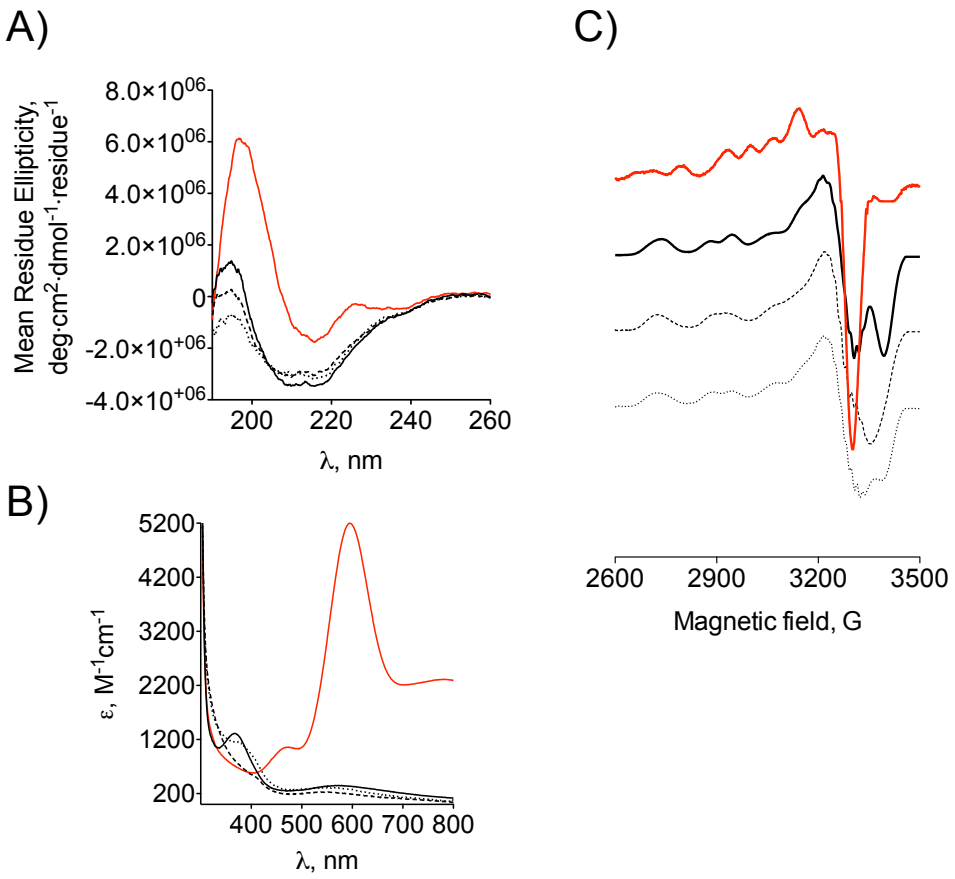

Figure 4.13 (A) Far-UV CD, (B) UV-Vis absorption and (C) EPR spectra of WT bNiR (—), T1D azNiR (—), T1D T246H azNiR trimer (- - -) and T1D azNiR mixture (····). The far-UV CD spectra were acquired at 25 °C in 20 mM Tris pH 7.5, the UV-Vis spectra at RT in 20 mM Tris pH 7.5 containing 200 mM NaCl and the EPR spectra at ~ 80 K in 20 mM Tris pH 7.5 containing 200 mM NaCl.

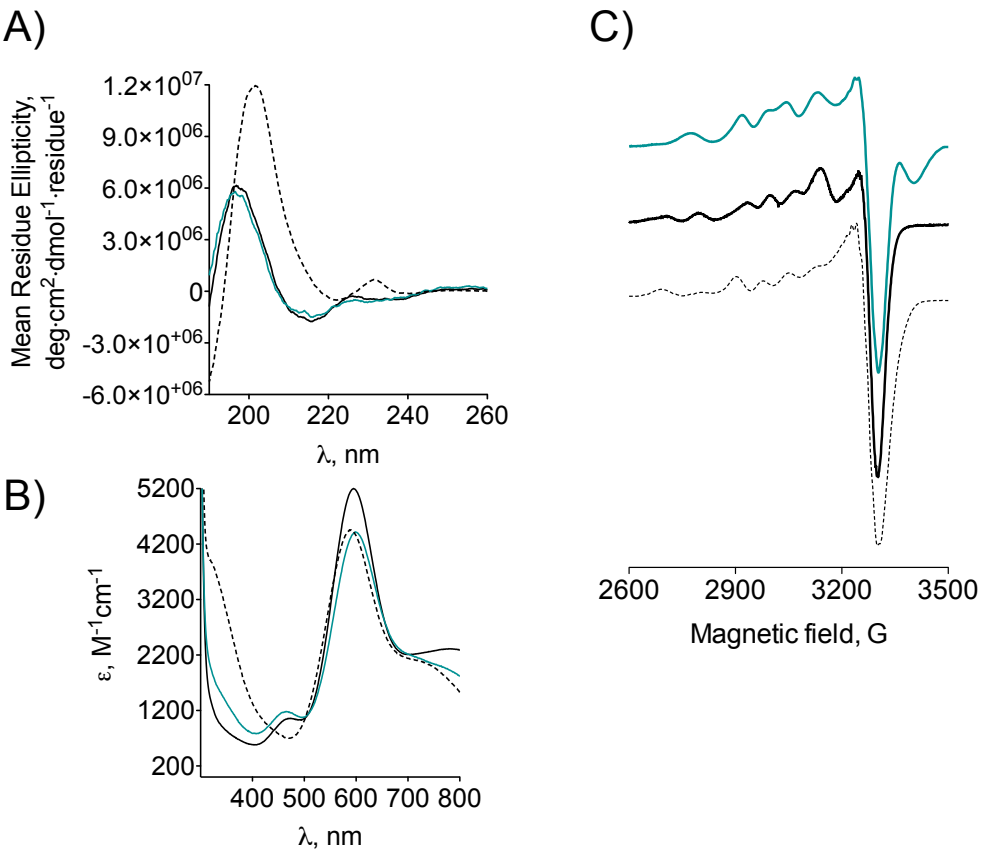

Figure 4.14 (A) Far-UV CD, (B) UV-Vis absorption and (C) EPR spectra of LacNiR ( ), WT bNiR ( ) and WT SLAC ( ). The far-UV CD spectra were acquired at at 25 °C in 10 mM phosphate pH 7.0, the UV-Vis spectra at RT in 20 mM Tris pH 7.5 and the EPR spectra at ~ 80 K in 24 mM Tris pH 7.5 plus 40 % glycerol (LacNiR and WT bNiR) or 20 mM Tris pH 7.5 containing 200 mM NaCl (WT SLAC).

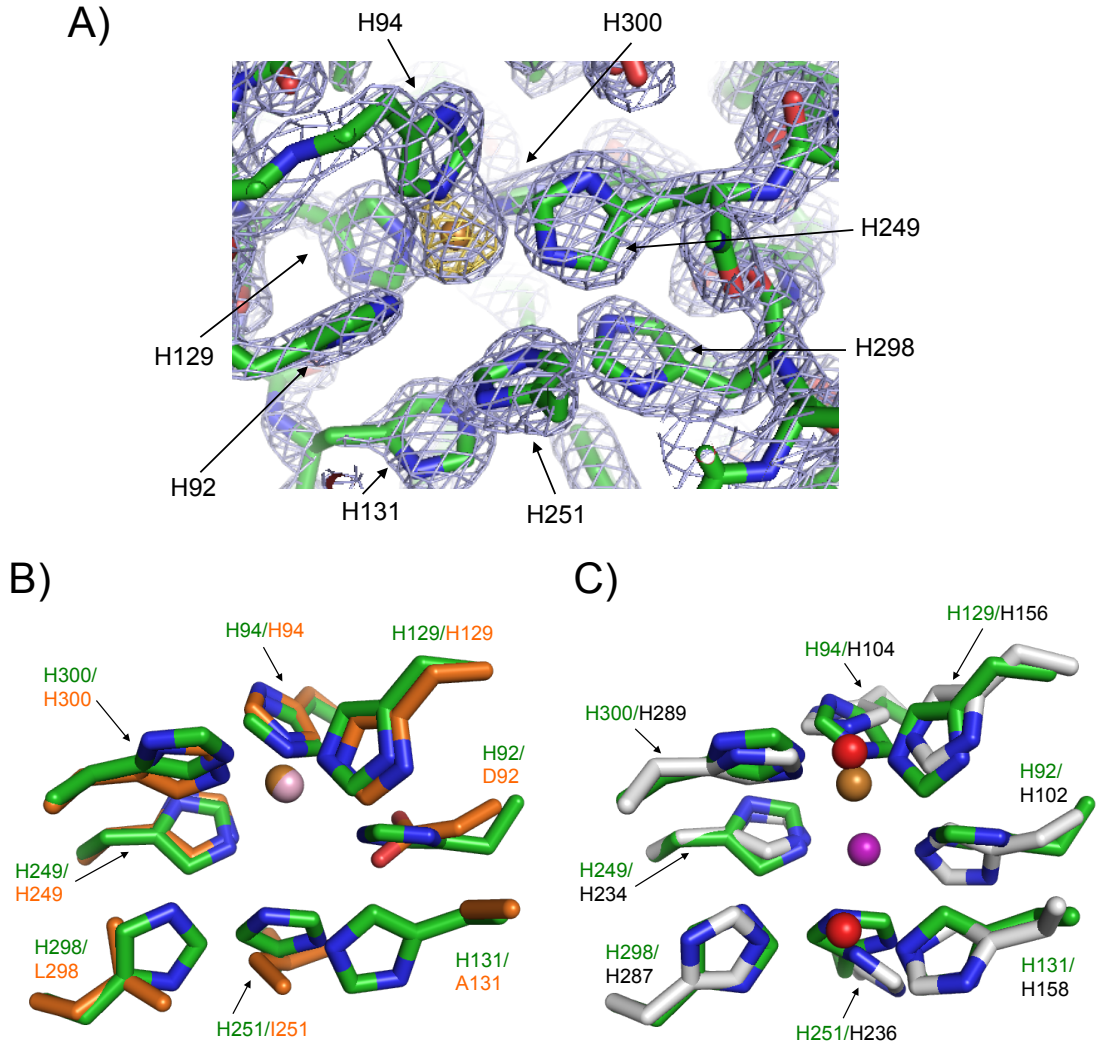

Figure 4.15 (A) The T2 Cu site of LacNiR superimposed on the $2F_o$ - F_c electron density map (blue) contoured at the 2σ and the anomalous difference map (orange) contoured at 5σ level. Overlays of the T2 Cu site of LacNiR (green) on (B) the T2 Cu site of WT bNiR (orange) [52] and (C) the T2/T3 Cu cluster of WT SLAC (gray) [58]. The T2 Cu is shown as gold, pink and purple spheres in LacNiR, WT bNiR and WT SLAC and the T3 Cus are red spheres.

4.5 Discussion

4.5.1 *Design of Cu sites*

Structural comparison between two-domain MCOs and bNiR reveals striking similarities suggesting close evolutionary links. However, several features, such as the location of the T1 Cu site and the structure of an active center (the T2/T3 Cu cluster in MCO and the T2 Cu site in bNiR) imply perhaps a more distant relationship [52, 57, 59, 60, 67, 69] (Chapter 1.3).

The SLAC variants (except for tSLAC), which carry mutations in the L1 of MBD-1 exhibit an intense LMCT transition band at ~ 360 nm, which is typical of a tetragonal S(Cys)-T2 Cu site [1, 18, 92 - 97]. Additionally, mgSLAC and nirSLAC variants contain the T1 Cu site, which is characterized by a typical LMCT transition band at ~ 590 nm (Chapter 1.2.1). However, this band in the UV-Vis spectrum of nirSLAC appears only in the presence of oxidant, indicative of the T1 Cu site in the resting state of nirSLAC being in the Cu(I) form. In the resting state, nirSLAC exhibits a weak band at ~ 610 nm, suggesting that the introduced MBS-1 site exists as a mixture of a tetragonal S(Cys)-T2 Cu and distorted T1 Cu sites. Similar heterogeneity has previously been reported for H46G Az, in which the equilibrium between these sites changes with the external ligand [15]. However, conversion of the two sites in nirSLAC upon addition of imidazole and Cl^- was not observed (data not shown). A preliminary study on gdcSLAC, with a $C^{157}HQSPLAPH^{165}IAKGL^{170}$ loop replacing the L1 of SLAC (Appendix D), implies the role of an axial Met in binding of S(Cys)-T2 Cu. Substitution of Met with Leu affects the spectral properties of the site, as indicated by the lowered intensity of the 360 nm band compared to those of mgSLAC and nirSLAC.

The C288S and C130S mutations in the SLAC and bNiR variants (*third design cycle*) led to the depletion of the T1 Cu sites in these proteins (judged from the disappearance of the LMCT transition band at 590 nm in the UV-Vis spectra and decrease in a total content of Cu). However, T1D tSLAC does not fold correctly what is surprising, as the C288S mutation did not affect the secondary structure composition of SLAC (in T1D SLAC) or other variants. The T1D azNiR variant is partially unfolded and is significantly less stable than the WT protein. This decreased stability is likely caused by the substitution of L2, as depletion of just the T1 Cu site (in C130A variant of WT bNiR) has previously shown not to affect the protein's fold [98]. The T1D variants of SLAC (except for T1D SLAC) and bNiR exhibit an intense LMCT band at ~ 360 nm

and weak bands at ~ 570 nm (T1D azNiR), ~ 590 nm (T1D tSLAC and T1D mgSLAC) or ~ 637 nm (T1D nirSLAC). Similar UV-Vis spectra consisting of ~ 360 nm ($\varepsilon \sim 2000\ M^{-1}cm^{-1}$) and weak ~ 550 nm ($\varepsilon \sim 300\ M^{-1}cm^{-1}$) bands have been observed for the ligand-containing loop peptides of Az [99] and Pc [100], which bind Cu(II) *via* Cys and His, but cannot stabilize a site with T1 Cu properties. Similar spectra have also been observed for nitrosocyanin [92], and H117G [11 - 13] and H46G [15] Az. The EPR spectra of T1D mgSLAC and T1D nirSLAC exhibit only one paramagnetic site, whilst two Cu(II) centers are present in the spectrum of T1D azNR. According to a Plumberg-Peisach-Vanngard plot extended for the T1.5 and S(Cys)-T2 Cu(II) sites [13, 101], which displays a linear relationship between $g_{\|}$ and $A_{\|}$ values for various Cu(II) sites, the relation between the g_z and A_z values for MBS-1 and MBS-2 indicate the characteristics of a S(Cys)-T2 Cu(II) site.

The *first design cycle*'s mutations in the SLAC and bNiR variants supply only the Cys, His and Met ligands on a single loop (L1 and L2) for coordination of the MBS-1 and MBS-2 Cus. In H46G [15] and H117G [11 - 13] Az water molecules enter the coordination shell of the Cu site to compensate for the loss of a His ligand. The resulting Cu site is distorted towards square planar, with a S(Cys) thiolate ligand and three nitrogen/oxygen (N/O) donors. Therefore it is possible that the vacant coordination position in T1D mgSLAC, T1D nirSLAC and T1D azNiR is occupied either by an exogenous ligand (e.g. H_2O, OH^-), or by N and O donors from the protein backbone or nearby side chains. A S(Cys)-T2 Cu site was formed in H117G Az when bidentate ligands such as histidine and histamine were added, whereas the addition of monodentate ligands such as imidazole and Cl^- restored characteristic T1 Cu site features [11 - 13]. Histidine does not bind to the Cu(II) in H46G Az, whereas in the presence of Cl^- and imidazole, the variant tends to form a S(Cys)-T2 Cu site or an equilibrium mixture of a T1 and a S(Cys)-T2 Cu species [15]. The addition of either imidazole or Cl^- did not affect the spectroscopic features of the S(Cys)-T2 Cu sites of mgSLAC, nirSLAC and T1D azNiR (data not shown), indicative of either saturation of the coordination sphere or no accessibility for external ligands.

The inclusion of the second His ligand situated in the core of the β-barrel of MBD-1 of SLAC and MBD-2 of bNiR (*second design cycle*) produced proteins, which except for qSLAC and T1D T246H azNiR, either did not express or failed to fold properly. Despite the additional ligand, the qSLAC and T1D T246H azNiR variants posses S(Cys)-T2 Cu sites. Different spectroscopic properties for the two forms of T1D T246H azNiR indicate possible flexibility at the S(Cys)-T2 Cu site, a property that

has been previously reported for the T1 Cu site of NIRAMI, in which the short amicyanin loop replaces L1 of WT bNiR [77]. The presence of two forms of T1D T246H azNiR indicates that the amino-acid replacement destabilizes the protein's quaternary structure. Similarly, two forms with different quaternary structure and spectral properties were reported for NIRAMI, and L1 was found to be important for stabilizing both a functional T1 Cu site and the trimeric arrangement of the enzyme [77]. Murphy *et al.* hypothesized that it is unlikely for the ancestral two-domain structures exist as monomers with the functional active sites at the interface of the two domains [68]. However, Sato *et al.* showed that the T1 Cu-binding loop in AZ3A3A (the Az variant with 3 introduced Ala residues between the coordinating Cys, His and Met in the T1 Cu-binding loop), which only differs in length by one residue to that of the WT protein, favors the formation of stable homodimers in solution and a strand swapped dimer in the crystal structure with a Cu site at the dimer interface [5].

Phylogenetic analyses performed by Nakamura *et al.* [67, 70] indicate that BCO [60] is the closest relative to the NiRs, leading to the hypothesis that NiRs might have descended from type C two-domain MCOs with concomitant loss of the T3 Cu site (see Chapter 1.3). However, the replacement of Asp92, Ala131, Ile251 and Leu298 by His residues in bNiR (*fourth design cycle*) did not result in the incorporation of a T3 Cu site, probably as a consequence of the conformation adapted by the side chain of the introduced His251. An attempt to enlarge the metal binding pocket by deleting Gly252 and thus altering the position of the imidazole ring of His251 was not successful, as the ΔG252 LacNiR variant expressed very poorly (results not shown). LacNiR shows hardly any activity with NO_2^-, which is not surprising, considering that Asp92, Ala131 and Ile251 are identified as being catalytically important [52, 102 - 104]. Although more detailed analysis is necessary, it is possible that the NiRs appeared before the creation of a T2/T3 Cu cluster, evolving from a type Y (containing two T1 Cu sites, one in each domain, and the T2 Cu site) rather than a type C ancestor (Chapter 1.3).

4.5.2 *Structural models of the Cu sites in SLAC variants*

Despite multiple attempts, SLAC and bNiR variants could not be crystallized. Assuming that, as in loop chimeras of cupredoxins, the loops replacing L1 and L2 adapt a conformation almost identical to those in the native proteins [3, 51], structural models of SLAC variants were built using WT SLAC, WT bNiR and mgLAC crystal structures as templates. None of the models predicts the tetragonal planar S(Cys)-T2 Cu geometry

of MBS-1, and in some cases, the distances between the ligands identified by the modeling software (I-TASSER) and the Cu site are too long (~ 5 Å) for these residues to be considered as ligands.

In the structural model of mgSLAC (Figure 4.16.A), the Cu ion is coordinated by Cys157, His164, Met170 and a backbone amide N from Ala99. In T1D mgSLAC (Figure 4.16.B), the latter is replaced by the backbone amide N from Ser100. The modeled site in the A99H variant has the same ligands as in T1D mgSLAC. Therefore, the reasons for incorrect folding of A99H mgSLAC remain unclear. The structural model of nirSLAC (Figure 4.16.C) shows that MBS-1 Cu is coordinated by Cys157, His164, Met171 and the backbone amide N of Ser100. This model predicts a steric hindrance between His164 and Met171, which possibly alters the actual structure of the MBS-1 and even T1 Cu sites. The model of T1D nirSLAC (Figure 4.16.D) exhibits a different overall structure compared to that of nirSLAC. The C-terminal loop (residues 304 - 341) rearranges and Ser100 does not participate in binding of Cu ion. Instead, His102 and His104, which are normally ligands to the T2 and T3 Cus, respectively, and a backbone carbonyl O from Val103 seem to coordinate the Cu site. However, this modeled structure seems unlikely, as such coordination would require a significant rearrangement of the protein fold, which does not occur (the far-UV CD spectrum is very similar to that of the WT protein).

The EPR spectrum of T1D mgSLAC indicates the presence of only one paramagnetic center (the EPR signal from the T2 Cu(II) was not observed), however, preliminary PELDOR experiments predict several Cu(II)-Cu(II) distances (2.1, 2.8, 3.2, 4.0 and 4.8 nm). This method yields reliably very precise distances in the range of ~ 1.5 to 8 nm [81, 82] and has successfully been applied in the study of the Fe(III)-binding proteins transferrin and lactoferrin [105], a dimeric form of Az [106], and WT bNiR [80]. Although the distances between the T1 and the T2 Cus in the structural model of T1D mgSLAC and the crystal structure of WT bNiR are similar, those estimated using PELDOR differ (Figure 4.12.F, [80]). The creation of a S(Cys)-T2 Cu site in all of the SLAC variants results in a concomitant loss of total Cu and incorporation of Zn ions. The disappearance of the LMCT band at 330 nm (characteristic for the T3 Cu site) from the UV-Vis spectra, suggests that the T2/T3 Cu cluster is disrupted in these variants, and therefore the T3 Cu ions are no longer antiferromagnetically coupled to give a diamagnetic ground state. Consequently, multiple (T3)Cu-(T3)Cu, (T2)Cu-(T3)Cu and (MBS-1)Cu-(T3)Cu distances within a trimer ranging from 2.88 to 3.31 nm, 2.92 to 3.35 nm and 3.45 to 4.20 nm

(T1D mgSLAC structural model, Figure 4.12.E), respectively, could be observed. Further investigations are necessary to extract more accurate distance distributions between the Cu(II) ions, possibly by using a combination of the inversion-recovery filter (IRf) technique with PELDOR (IRf PELDOR). This method was successfully applied to suppress distances between pairs of like sites in WT bNiR to simplify and the distance distributions [80].

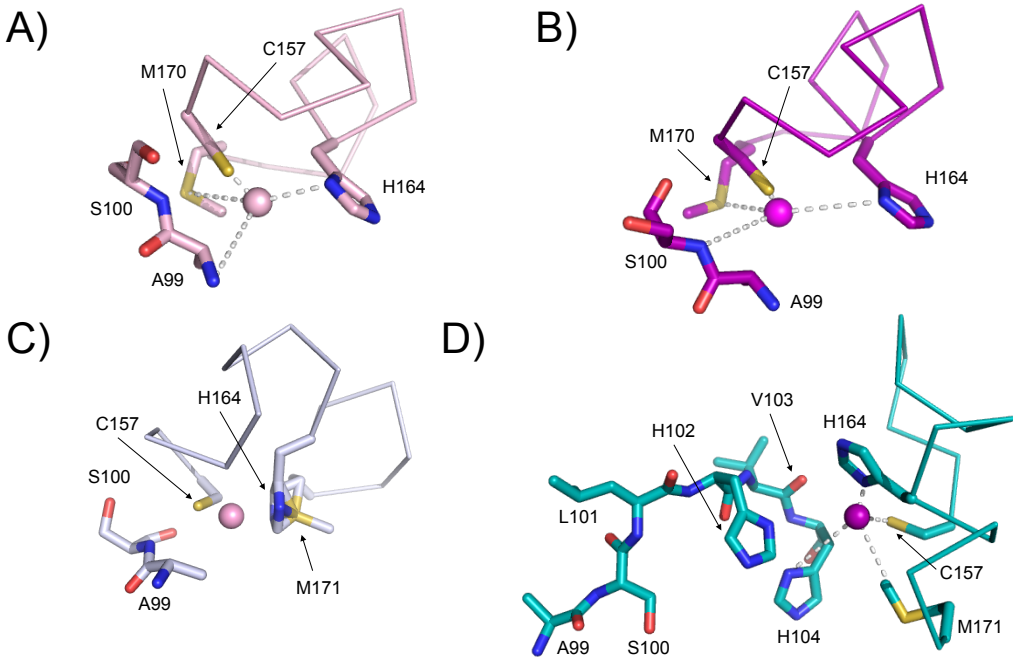

Figure 4.16 Structure models of the introduced Cu sites in (A) mgSLAC, (B) T1D mgSLAC, (C) nirSLAC and (D) T1D nirSLAC. Gray dashed lines connect ligands to the S(Cys)-T2 Cu site that were identified by I-TASSER software. The Cu of mgSLAC and nirSLAC are pink, whilst the Cus in T1D mgSLAC and T1D nirSLAC are magenta spheres.

4.5.3 *Activity of SLAC variants*

The tSLAC variant shows similar to the WT protein spectral features but a significant, almost 40-fold, decrease in activity with 2,6-DMP (Table 4.5). Substitution of the L1 in SLAC variants creates proteins that are almost inactive. Although WT SLAC has not been crystallized in the presence of substrate, the center of the trimer has been suggested to contain a shallow substrate-binding pocket [57]. Redesign of this putative site in the M198G and M198G/M266A variants resulted in enhanced activity towards phenolic substrates [107, 108]. On the other hand, MCO from *Streptomyces*

viridosporus T7A (type B two-domain MCO, Chapter 1.3) was crystallized with acetovanillone at the interface of the MBD-1 and MBD-2 within a monomer (pdb file: 3TBC). MCO from *Amycolatopsis* sp. ATCC 39116 (type B two-domain MCO, Chapter 1.3) was crystallized with 1-(3,4-dimethoxyphenyl)-2-(2-methoxyphenoxy)-1,3-dihydroxypropane at the interface of MBD-1 and MBD-2 of each neighboring chains of the trimer, above the T2/T3 Cu cluster (pdb file: 3TA4). The L1 is located relatively far (~ 7 - 10 Å) from the binding site of acetovanillone (Figure 4.17.A) but close to the binding site of 1-(3,4-dimethoxyphenyl)-2-(2-methoxyphenoxy)-1,3-dihydroxypropane (Figure 4.17.B) in these structures. Considering that all the SLAC variants that contain the S(Cys)-T2 Cu site (except for qSLAC) showed decreased occupancy of Cu (Table 4.6) and almost no activity with 2,6-DMP (Table 4.5), it is probable that the L1 of WT SLAC is important for stabilizing a functional T2/T3 Cu site and interactions with phenolic substrates.

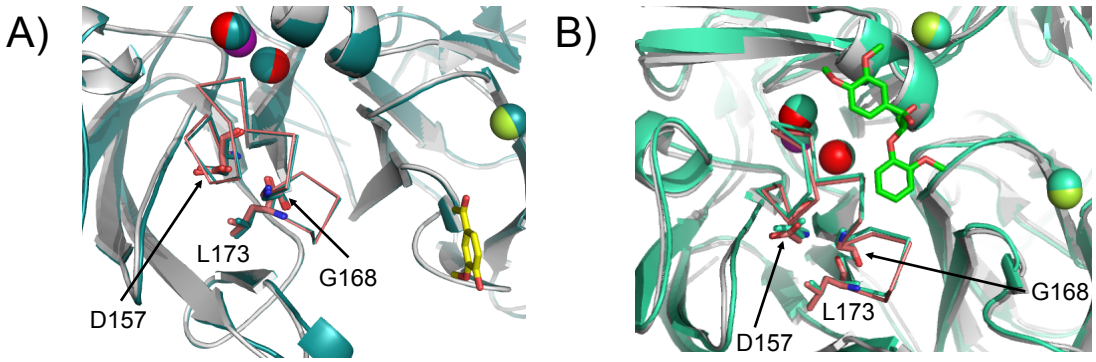

Figure 4.17 Cartoon representation of WT SLAC (gray, [58]) overlaid on two-domain MCOs from (A) *S. viridosporus* T7A (teal, pdb file: 3TBC) and (B) *Amycolatopsis* sp. ATCC 39116 (limegreen, pdb file: 3TA4) binding acetovanillone (yellow sticks) and 1-(3,4-dimethoxyphenyl)-2-(2-methoxyphenoxy)-1,3-dihydroxypropane (green sticks), respectively. The L1 of WT SLAC is shown as pink C^{α} trace. The T1, T2 and T3 Cus of WT SLAC are green, purple and red spheres, respectively. The Cus of MCOs from *S. viridosporus* T7A and *Amycolatopsis* sp. ATCC 39116 are teal and limegreen spheres.

4.6 Conclusions

De novo design of Cu-binding sites in proteins or modification of existing sites is of special interest for understanding the important features of Cu sites in proteins, but also for biotechnological and industrial applications. In the first part of this chapter attempts

were made to create a T1 Cu site within the cupredoxin-like domains of WT SLAC and WT bNiR that naturally lack a Cu-binding site. This resulted in the introduction of a Cu site in MBD-1 and MBD-2 of WT SLAC and WT bNiR, respectively. Spectroscopic studies indicate that the Cu in these engineered sites adopts a (distorted) tetragonal S(Cys)-T2 Cu site rather than a T1 Cu site. Construction of a geometrically correct primary coordination is not sufficient, as the introduced Cu is ligated by Cys, His, Met, and the coordination environment is most likely completed by a backbone carbonyls O or amides N, solvent components and side chains of neighboring amino acids. Further experiments, particularly resonance Raman spectroscopy measurements are underway to establish the coordination and electronic structure of these sites. Design strategy that constrain primary and secondary coordination sphere is an objective for future experiments.

The second part of the work focused on attempts to introduce a T2/T3 Cu cluster as found at the monomer-monomer interface in SLAC into the corresponding location in bNiR in place of the catalytic T2 Cu site. The electron density of the X-ray high-resolution data set of LacNiR shows no evidence that the T3 Cu site, and therefore T2/T3 cluster has been introduced.

4.7 References

1) Canters G.W., Gilardi G., 1993, FEBS Lett., 325(1-2), 39-48

2) Dennison C., 2008, Nat. Prod. Rep., 25, 15-24

3) Li C., Banfield M.J., Dennison C., 2007, J. Am. Chem. Soc., 129, 709-718

4) Tegoni M., Yu F., Bersellini M., Penner-Hahn J.E., Pecoraro V.L., 2012, Proc. Natl. Acad. Sci. USA, 109, 21234-21239

5) Sato K., Li C., Sallard I., Thompson A.J., Banfield M.J., Dennison C., 2009, Proc. Natl. Acad. Sci. USA, 106, 5616-5621

6) Velarde M., Huber R., Yanagisawa S., Dennison C., Messerschmidt A., 2007, Biochemistry, 46, 9981-9991

7) Yanagisawa S., Dennison C., 2004, J. Am. Chem. Soc., 126, 15711-15719

8) Li C., Yanagisawa S., Martins B.M., Messerschmidt A., Banfield M.J., Dennison C., 2006, Proc. Natl. Acad. Sci. USA, 103, 7258-7263

9) Yanagisawa S., Crowley P.B., Firbank S.J., Lawler A.T., Hunter D.M., McFarlane W., Li C., Kohzuma T., Banfield M.J., Dennison C., 2008, J. Am. Chem. Soc., 130, 15420-15428

10) Yanagisawa S., Banfield M.J., Dennison C., 2006, Biochemistry, 45, 8812-8822

11) Den Blaauwen T., van de Kamp M., Canters G.W., 1991, J. Am. Chem. Soc., 113, 5050-5052

12) Den Blaauwen T., Hoitink C.W.G., Canters G.W., Han J., Loehr T.M., Sanders-Loehr J., 1993, Biochemistry, 32, 12455-12464

13) Den Blaauwen T., Canters G.W., 1993, J. Am. Chem. Soc., 115, 1121-1129

14) Gorren A.C., Den Blaauwen T., Canters G.W., Hopper D.J., Duine J.A., 1996, FEBS Lett., 381, 140-142

15) van Pouderoyen G., Andrew C.R., Loehr T.M., Sanders-Loehr J., Mazumdar S., Hill H.A.O., Canters G.W., 1996, Biochemistry, 35, 1397-1407

16) Messerschmidt A., Prade L., Kroes S.J., Sanders-Loehr J., Huber R., Canters G.W., 1998, Proc. Natl. Acad. Sci. USA, 95, 3443-3448

17) Hall J.F., Kanbi L.D., Strange R.W., Hasnain S.S., 1999, Biochemistry, 38, 12675-12680

18) Wilson T.D., Savelieff M.G., Nigels M.J., Marschall N.M., Lu Y., 2011, J. Am. Chem. Soc., 133, 20778-20792

19) Lancaster K.M., Yokoyama K., Richards J.H., Winkler J.R., Gray H.B., 2009, Inorg. Chem. 48, 1278-1280

20) Lancaster K.M., DeBeer George .S., Yokoyama K., Richards J.H., Gray H.B., 2009, Nat. Chem., 1, 711-715

21) Lancaster K.M., Farver O., Wherland S., Crane E.J. 3rd, Richards J.H., Pecht I., Gray H.B., 2011, J. Am. Chem. Soc., 133, 4865-4873

22) McLaughlin M.P., Retegan M., Bill E., Payne T.M., Shafaat H.S., Pena S., Sudhamusu J., Ensign A.A., Crane B.R., Neese F., Holland P.L., 2012, J. Am. Chem. Soc., 134, 19746-19757

23) Hellinga H.W., 1998, J. Am. Chem. Soc., 120, 10055-10066

24) Malkin R., Malmstrom B.G., 1970, Adv. Enzymol., 33, 177-244

25) Fee J.A., 1975, Struct. Bonding, 23, 1-60

26) Gray H.B., Malmstrom B.G., Williams R.J.P., 2000, J. Biol. Inorg. Chem., 5, 551-559

27) Solomon E.I., Szylagyi R.K., DeBeer George S., Basumallick L., 2004, Chem. Rev., 104, 419-458

28) Inoue T., Nishio N., Suzuki S., Kataoka K., Kohzuma T., Kai Y., 1999, J. Biol. Chem., 274, 17845-17852

29) Xue Y., Okvist M., Hansson O., Young S., 1998, Protein Sci., 7, 2099-2105

30) Romero A., Nar H., Huber R., Messerschmidt A., Kalverda A.P., Canters G.W., Durley R., Mathews F.S., 1994, J. Mol. Biol., 236, 1196-1211
31) Hart P.J., Nersissian A.M., Herrmann R.G., Nalbansyan R.M., Valentine J.S., Eisenberg D., 1996, Protein Sci., 5, 2175-2183
32) Kim S., Mollet J.C., Dong J., Zhang K., Park S.Y., Lord E.M., 2003, Proc. Natl. Acad. Sci. USA, 100, 16125-16130
33) Dennison C., Harrison M.D., Lawle A.T., 2003, Biochem. J., 371, 377-383
34) Nar H., Messerschmidt A., Huber R., van de Kmap M., Canters G.W., 1991, J. Mol. Biol., 221, 765-772
35) Solomon E.I., Randall D.W., Glaser T., 2000, Coord. Chem. Rev., 200-202, 595-632
36) Solomon E.I., 2006, Inorg. Chem., 45, 8012-8025
37) Lu Y., LaCroix L.B., Lowery M.D., Solomon E.I., Bender C.J., Peisach J., Roe J.A., Gralla E.B., Valentine J.S., 1993, J. Am. Chem. Soc., 115, 5907-5918
38) Schnepf R., Horth P., Bill E., Wieghardt K., Hildebrandt P., Haehnel W., 2001, J. Am. Chem. Soc., 123, 2186-2195
39) Schnepf R., Haehnel W., Wieghardt K., Hildebrandt P., 2004, J. Am. Chem. Soc., 126, 14389-14399
40) Shiga D., Nakane D., Inomata T., Funahashi Y., Masuda H., Kikuchi A., Oda M., Noda M., Uchiyama S., Fukui K., Kanaori K., Tajima K., Takano Y., Nakamura H., Tanaka T., 2010, J. Am. Chem. Soc., 132, 18191-18198
41) Shiga D., Hamano Y., Kamei M., Funahashi Y., Masuda H., Sakaguchi M., Ogura T., Tanaka T., 2012, J. Biol. Inorg. Chem., 17, 1025-1031
42) Kitajima N., Fujisawa K., Moro-oka Y., 1990, J. Am. Chem. Soc., 112, 3210-3212
43) Kitajima N., Fujisawa K., Moro-oka Y., 1992, J. Am. Chem. Soc., 114, 9232-9233
44) Kitajima N., 1992, Adv. Inorg. Chem., 39, 1-77
45) Holland P.L., Tolman W.B., 1999, J. Am. Chem. Soc., 121, 7270-7271
46) Holland P.L., Tolman W.B., 2000, J. Am. Chem. Soc., 122, 6331-6332
47) Tolman W.B., 2006, J. Biol. Inorg. Chem.., 11, 261-271
48) Yang L., Tolman W.B., 2012, J. Biol. Inorg. Chem., 17, 285-291
49) Dennison C., 2005, Coord. Chem. Rev., 249, 3025-3054
50) Choi M., Davidson V.L., 2011, Metallomics, 3, 140-151
51) Dennison C., 2005, Dalton Trans., 3436-3442
52) Ellis M.J., Dodd F.E., Sawers G., Eady R.R., Hasnain S.S., 2002, J. Mol. Biol., 328, 429-438

53) Yamaguchi K., Kobayashi M., Kataoka K., Suzuki S., 2003, Biochem. Biophys. Res. Commun., 300, 36-40

54) Adman E.T., Jensen L.H., 1981, Isr. J. Chem., 21, 8-12

55) Iwata S., Ostermeier C., Ludwig B., Michel H., 1995, Nature, 376, 660-669

56) Iwata S., 1998, J. Biochem, 123, 369-375

57) Skálová T., Dohnálek J., Østergaard L.H., Østergaard P.R., Kolenko P., Dusková J., Stepánková A., Hasek J., 2009, J Mol Biol., 385, 1165-1178

58) Skálová T., Dušková J., Hašek J., Stěpánková A., Koval T., Østergaard L.H., Dohnálek J., 2011, Acta Crystallogr Sect F Struct Biol Cryst Commun., 67, 27-32

59) Komori H., Miyazaki K., Higuchi Y., 2009, FEBS Lett., 583, 1189-1195

60) Lawton T.J., Sayavedra-Soto L.A., Arp D.J., Rosenzweig A.C., 2009, J. Biol. Chem., 284, 10174-10180

61) Piontek K., Antorini M., Choinowski T., 2002, J. Biol. Chem., 277, 37663-37669

62) Hakulinen N., Andeberg M., Kallio J., Koivula A., Rouvinen J., 2008, J. Struct. Biol., 162, 29-39

63) Zaitseva I., Zaitsev V., Card G., Moshkov K., Bax B., Ralph A., Lindley P., 1996, J. Biol. Inorg. Chem., 1, 15-23

64) Messerschmidt A., Ladenstein R., Huber R., Bolognesi M., Avigliano L., Petruzzelli R., Rossi A., Finazzi-Agró A., 1992, J. Mol. Biol., 224, 179-205

65) Taylor A.B., Stoj C.S., Ziegler L., Kosman D.J., Hart P.J., 2005, Proc. Natl. Acad. Sci. USA, 102, 15459-15464

66) Ryden L.G., Hunt L.T., 1993, J. Mol. Evol., 36, 41-66

67) Nakamura K., Kawabata T., Yura K., Go N., 2003, FEBS Lett., 553, 239-244

68) Murphy M.E., Lindley P.F., Adman E.T., 1997, Protein Sci., 6, 761-770

69) Lindley P., Card G., Zaitseva I., Zaitsev V., 1999, Perspect. Bioinorg. Chem., 4, 51-89

70) Nakamura K., Go N., 2005, Cell. Mol. Life Sci., 62, 2050-2066

71) Adman E.T., 1991, Adv. Protein Chem., 42, 145-197

72) Kukimoto M., Nishiyama M., Murphy M. E. P., Turley S., Adman E. T., Horinouchi S., Beppu T., 1995, Biochemistry, 33, 5246-5252

73) Machczynski M.C., Vijgenboom E., Samyn B., Canters G.W., 2004, Protein Sci., 13, 2388-2397

74) Sato K., Dennison C., 2006, Chem. Eur. J., 12, 6647-6659

75) Tepper A.W., Milikisyants S., Sottini S., Vijgenboom E., Groenen E.J., Canters G.W., 2009, J. Am. Chem. Soc., 131, 11680-11682

76) Solano F., Lucas-Elío P., López-Serrano D., Fernández E., Sanchez-Amat A., 2001, FEMS Microbiol Lett., 204, 175-181

77) Sato K., Firbank S.J., Li C., Banfield M.J., Dennison C., 2008, Chem. Eur. J., 14, 5820-5828

78) The PyMOL Molecular Graphics System, Version 1.6.0.0 Schrödinger, LLC.

79) Roy A., Kucukural A., Zhang Y., 2010, Nat Protoc., 5, 725-738

80) van Wonderen J.H., Kostrz D.N., Dennison C., MacMillan F., 2013, Angew. Chem. Int. Ed. Engl., 52, 1990-1993

81) Reginsson G.W., Schiemann O., 2011, Biochem. J., 434, 353-363

82) Jeschke G., 2002, ChemPhysChem, 3, 927-932

83) Li X., Wei Z., Zhang M., Peng X., Yu G., Teng M., Gong W., 2007, Biochem. Biophys. Res. Commun., 354, 21-26

84) Palmer A.E., Randall D.W., Xu F., Solomon E.I., 1999, J. Am. Chem. Soc., 121, 7138-7149

85) LaCroix L.B., Shadle S.E., Wang Y., Averill B.A., Hedman B., Hodgson K.O., Solomon E.I., 1996, J. Am. Chem. Soc., 118, 7775-7768

86) Zhekova H.R., Seth M., Zigler T., 2010, J. Phys. Chem. A., 114, 6308-6321

87) Machonkin T.E., Quintanar L., Palmer A.E., Hasset R., Severance S., Kosman D.J., Solomon E.I., 2001, J. Am. Chem. Soc., 123, 5507-5517

88) Mao D., Wechter E., Wallace B.A., 1982, Biochemistry, 21, 4960-4968

89) Johnson W.C., 1999, Proteins, 35, 307-312

90) Whitmore L., Wallace B.A., 2004, Nucleic Acids Res., 32, W668-73

91) Heinig M., Frishman D., 2004, Nucl. Acids Res., 32, W500-2

92) Basumallick L., Sarangi R., DeBeer G.S., Elmore B., Hooper A.B., Hedman B., Hodgson K.O., Solomon E.I., 2005, J. Am. Chem. Soc., 127, 3531-3544

93) Lu Y., Roe J.A., Bender C.J., Peisach J., Banci L., Bertini I., Gralla E.B., Valentine J.S., 1996, Inorg. Chem., 35, 1692-1700

94) Lu Y., Gralla E.B., Roe J.A., Valentibe J.S., 1992, J. Am. Chem. Soc., 114, 3560-3562

95) van Amsterdam I.M., Ubbink M., van den Bosch M., Rotsaert F., Sanders-Loehr J., Canters G.W., 2002, J. Biol. Chem., 277, 44121-44130

96) Mandal S., Das G., Singh R., Shukla R., Bharadwaj P.K., 1997, Coord. Chem. Rev., 160, 191-235

97) Savelieff M.G., Wilsom T.D., Elias Y., Nilges M.J., Garner D.K., Lu Y., 2008, Proc. Natl. Acad. Sci. USA, 105, 7919-7924

98) Hough M.A., Ellis M.J., Antonyuk S., Strange R.W., Sawers G., Eady R.R., Hasnain S.S., 2005, J. Mol. Biol., 350, 300-309

99) Pozdnyakova I., Guidry J., Wittung-Stafshede P., 2000, J. Am. Chem. Soc., 122, 6337-6338

100) Daugherty R.G., Wasowicz T., Gibney B.R., DeRose V.J., 2002, Inorg. Chem., 41, 2623-2632

101) Andrew C.R., Yeom H., Valentibe J.S., Karlsson B.G., Bonander N., van Pouderoyen G., Canters G.W., Loehr T.M., Sanders-Loehr J., 1994, J. Am. Chem. Soc., 116, 11489-11498

102) Ellis M.J., Dodd F.E., Strange R.W., Prudencio M., Sawers G., Eady R.R., Hasnain S.S., 2001, Acta Crystallogr D57, 1110-1118

103) Hough M.A., Eady, R.R., Hasnain S.S., 2008, Biochemistry, 47, 13547-13553

104) Dodd F.E., Van Beeumen, J., Eady R.R., Hasnain S.S., 1998, J. Mol. Biol., 282, 369-382

105) Kay C.W.M., El Mkami H., Cammack R., Evans R.W., 2007, J. Am. Chem. Soc., 129, 4868-4869

106) Finiguerra M.G., Prudencio M., Ubbink M., Huber M., 2008, Magn. Reson. Chem., 46, 1096-1101

107) Sherif M., Waung D., Korbeci B., Mavisakalyan V., Flick R., Brown G., Abou-Zaid M., Yakunin A.F., Master E.R., 2013, Microb. Biotechnol., 6, 588-597

108) Toscano M.D., De Maria L., Lobedanz S., Ostergaard L.H., 2013, Chembiochem., 14, 1209-1211

CHAPTER 5

Experimental methods

5.1 Buffer solutions

All buffer solutions were prepared using Milli-Q grade water obtained with a Millipore Simplicity water purification system with a rated resistivity ≥ 18 MΩcm at room temperature (RT).

Sodium acetate (BDH) was used to buffer protein solutions in the pH range of 5.2 to 6.0, 2-(N-morpholino)ethanesulphonic (Mes) (Sigma) in the pH range of 6.0 to 6.5, Tris(hydroxymethyl)aminomethane (Tris) (Sigma) in the pH range of 7.4 to 9.0, 4-(2-hydroxyethyl)piperazine-1-ethanesulfonic acid (Hepes) (VWR) in the pH range of 7.0 to 8.3 and sodium carbonate (Fisher Scientific) in the range of 9.0 to 10.0. The pH was adjusted by addition of either HCl (BDH), NaOH (BDH) or acetic acid (Aldrich), in case of sodium acetate buffer.

Citrate/phosphate (McIlvaine) buffer was used to buffer solutions within the pH range of 2.2 to 7.0. Buffers were prepared by mixing stock solutions of 0.2 M dibasic sodium phosphate (Na_2HPO_4, Fluka), and 0.1 M citric acid (BDH) (Table 5.1), and diluted as required.

pH	Na_2HPO_4 (mL)	Citric acid (mL)
2.2	1.8	98.2
2.6	10.8	89.2
3.0	20.4	79.6
3.4	28.2	71.8
3.8	35.4	64.6
4.0	38.6	61.4
4.2	41.2	58.8
4.6	46.6	53.4
5.0	51.4	48.6
5.4	55.6	44.4
5.8	60.6	39.4
6.2	66.2	33.8
6.6	72.8	27.2
7.0	87.2	13.0

Table 5.1 Volumes of 0.2 M Na_2HPO_4 and 0.1 M citric acid required for preparation of 100 mL of McIlvaine buffer in the pH range of 2.2 - 7.0 [1].

Phosphate buffer was used to buffer solutions within the pH range of 6.0 to 8.0. Buffers were prepared by mixing stock solutions (Table 5.2) of 1 M dibasic and monobasic potassium phosphate K_2HPO_4 (BDH) and KH_2PO_4 (Fluka), respectively, and diluted as required.

pH	K_2HPO_4 (mL)	KH_2PO_4 (mL)
6.0	13.2	86.8
6.2	19.2	80.8
6.4	27.8	72.2
6.6	38.1	61.9
6.8	49.7	50.3
7.0	61.5	38.5
7.2	71.7	28.3
7.4	80.2	19.8
7.6	86.6	13.4
7.8	90.8	9.2
8.0	94.0	6.0

Table 5.2 Volumes of 1 M stocks of K_2HPO_4 and KH_2PO_4 required for preparation of 100 mL of 1 M phosphate buffer solutions in the pH range of 6.0 - 8.0 [1].

5.2 Growth media

All growth media were prepared in deionized water and sterilized by autoclaving at 121 °C for 30 min.

5.2.1 *Luria-Bertani medium*

Luria-Bertani (LB) medium consists of 10 g/L tryptone (Melford), 10 g/L NaCl (Sigma) and 5 g/L yeast extract (Melford), whilst Low Salt LB medium of 10 g/L tryptone, 5 g/L NaCl and 5 g/L yeast extract. The LB-agar and Low Salt LB-agar solid media consist of LB and Low Salt LB supplemented with 15 g/L agar (Melford). The media were used to grow *Escherichia coli* strains for molecular cloning and protein expression, typically in the presence of an appropriate antibiotic (100 μg/mL ampicillin, 50 μg/mL kanamycin, 25 μg/mL tetracycline, 34 μg/mL chloramphenicol and 25 μg/mL zeocin)

5.2.2 *2×Yeast Extract and Tryptone medium*

2×Yeast Extract and Tryptone (2×YT) medium consists of 16 g/L tryptone, 5 g/L NaCl and 10 g/L yeast extract. The medium was used for expression of proteins in *E. coli* BL21(DE3) strain in the presence of an appropriate antibiotic.

5.2.3 *Terrific Broth medium*

Terrific Broth (TB) medium consists of 12 g/L Bacto peptone (BD Biosciences), 24 g/L yeast extract, 0.4 % (v/v) glycerol (Sigma), 17 mM KH_2PO_4 and 72 mM K_2HPO_4. The medium was used for high-yield over-expression of proteins in *E. coli* BL21(DE3) in the presence of an appropriate antibiotic.

5.2.4 *Yeast Extract Peptone Dextrose, Yeast Extract Peptone Dextrose Sorbitol and Yeast Extract Peptone Dextrose Adenine media*

Yeast Extract Peptone Dextrose (YPD) medium consists of 10 g/L yeast extract, 20 g/L Bacto peptone, 20 g/L dextrose (Melford), and an appropriate antibiotic (100 μg/mL zeocin), if necessary. Yeast Extract Peptone Dextrose Sorbitol (YPDS) medium is additionally supplemented with 182.2 g/L sorbitol (Melford), whilst Yeast Extract Peptone Dextrose Adenine (YPAD) with 0.1 g/L adenine. The YPD-agar, YPDS-agar and YPAD-agar solid media are supplemented with 20 g/L agar and 100 μg/mL zeocin, if necessary. The media were used for over-expression of Lcc1 in *Pichia pastoris* X-33 and *Pichia methanolica* PMAD11 strains.

5.2.5 *Buffered Dextrose Complex and Buffered Methanol Complex media*

Buffered Complex (BM-Y) medium consists of 10 g/L yeast extract, 20 g/L Bacto peptone, 100 mM phosphate buffer, pH 6.0 (or pH 6.5), 13.4 g/L Yeast Nitrogen Base (YNB, Melford) and 400 μg/L biotin (Sigma). Buffered Dextrose Complex (BMDY) medium is additionally supplemented with 20 g/L dextrose, whilst Buffered Methanol Complex (BMMY) medium with 5 g/L methanol. The media were used for over-expression of secreted Lcc1 in *P. methanolica* PMAD11.

5.2.6 *Minimal Dextrose and Minimal Methanol media*

Minimal dextrose (MD) and methanol (MtM) solid medium consists of 13.4 g/L YNB, 400 μg/L biotin and 20 g/L dextrose (MD-agar) or 5 g/L methanol (MtM-agar) supplemented with 15 g/L agar. The media were used for growth of *P. pastoris* X-33 and *P. methanolica* PMAD11 strains and selection of Lcc1-expressing transformants.

5.2.7 *Minimal medium*

Minimal medium (MM) consists of 22 g/L dextrose, 1.5 g/L L-asparagin, 0.12 mg/L thiamine, 0.06 mg/L HBO_3, 0.5 g/L $MgSO_4 \times 7H_2O$, 5 mg/L $FeCl_3 \times 6H_2O$, 0.2 mg/L $CuSO_4 \times 5H_2O$, 2.0 mg/L $ZnSO_4 \times 7H_2O$, 0.1 mg/L $MnSO_4 \times 4H_2O$, 0.04 mg/L $(NH_4)_6Mo_7O_{24} \times 4H_2O$, 1.2 mg/L $Ca(NO_3)_2 \times 4H_2O$, 0.4 mg/L $CoCl_2 \times 6H_2O$, 0.46 g/L KH_2PO_4 and 1.31 g/L $K_2HPO_4 \times 3H_2O$ [2]. The MM-agar consists of MM supplemented with 15 g/L agar. The MM and MM-agar were used for growth of *Schizophyllum commune* WT and KS8 strains and over-expression of Lcc1.

5.2.8 *Complete medium*

Complete medium (CM) consists of 22 g/L dextrose, 2.0 g/L Bacto peptone, 2.0 g/L yeast extract, 0.5 g/L $MgSO_4 \times 7H_2O$, 0.46 g/L KH_2PO_4 and 1.31 g/L $K_2HPO_4 \times 3H_2O$. The CM was used for over-expression of Lcc1 in *S. commune* WT and KS8 strains.

5.2.9 *Production medium*

Complete medium (PM) consists of 22 g/L dextrose, 1 % ethanol (v/v), 0.12 mg/L thiamine, 1.32 g/L $(NH_4)_2SO_4$, 0.5 g/L $MgSO_4 \times 7H_2O$, 5 mg/L $FeCl_3 \times 6H_2O$, 0.2 mg/L $CuSO_4 \times 5H_2O$, 2.0 mg/L $ZnSO_4 \times 7H_2O$, 0.1 mg/L $MnSO_4 \times 4H_2O$, 0.04 mg/L $(NH_4)_6Mo_7O_{24} \times 4H_2O$, 1.2 mg/L $Ca(NO_3)_2 \times 4H_2O$ and 0.4 mg/L $CoCl_2 \times 6H_2O$. The PM was used for studies on expression of Lcc1 in *S. commune* WT and KS8 strains.

5.2.10 *Regeneration medium*

Regeneration medium (RM) consists of 20 g/L dextrose, 123 g/L $MgSO_4 \times 7H_2O$, 2 g/L peptone, 2 g/L of yeast extract, 1.85 g/L KH_2PO_4 and 5.24 g/L $K_2HPO_4 \times 3H_2O$. The RM was used for DNA transformation of *S. commune* WT and KS8 protoplasts.

5.3 Manipulation of *Escherichia coli* strains

5.3.1 *Strains*

E. coli strains (JM101, BL21 (DE3), Rosetta (DE3), BL21 Tuner (DE3), XL1-Blue and

XL10-Gold) were maintained either in liquid LB, Low Salt LB, LB-agar and Low Salt LB-agar media with an appropriate antibiotic at 4 °C. For long-term storage, the strains were maintained as cryo-stocks (at - 80 °C) containing 1.5 mL of pelleted saturated culture resuspended in 250 µL of 1 % (w/v) Bacto peptone and 250 µL of 50 % glycerol.

5.3.2 *Preparation of Escherichia coli competent cells*

An isolated colony of *E. coli* was inoculated in 5 mL of LB media and grown overnight at 37 °C with shaking at 200 rpm in an orbital shaker. The overnight culture was diluted 100-fold into fresh 10 mL of LB and grown for approximately 2 h under the same conditions. The cells were centrifuged at 1500 g at 4 °C for 10 min and the pellet was resuspended in 1 mL ice-cold sterile buffer containing 85 % (v/v) LB, 10 % (w/v) polyethylene glycol (PEG) 8000, 5 % (v/v) dimethyl sulfoxide (Sigma) and 50 mM $MgCl_2$, pH 6.5, frozen in liquid nitrogen and stored at - 80 °C [3].

5.3.3 *Transformation in Escherichia coli*

Typically 100 µL of competent *E. coli* cells were incubated with 200 ng of plasmid DNA and stored on ice for 20 min. The cells were heat-shocked by incubating them at 42 °C for 1 min, followed by 2 min incubation on ice. 0.9 mL of LB medium was added and the cells were incubated at 37 °C with rotary shaking for ~ 60 min. Typically 100 µL of the transformed cells was spread on LB-agar (or Low Salt LB-agar) with the appropriate antibiotics and incubated overnight at 37 °C. Alternatively, prior to deposition, 1 mL of transformed cells was centrifuged at 1500 g at RT for 3 min and the cell pellet was resuspended in 100 µL of fresh LB [3].

5.4 Manipulation of *Pichia methanolica* and *Pichia pastoris*

5.4.1 *Strains*

Pichia methanolica PMAD11 and *Pichia pastoris* X33 strains were kindly provided by Dr. Karin Scholtmeijer. For short-time storage, the strains were maintained at 4 °C on YPAD-agar (*P. methanolica* PMAD11) and YPD-agar (*P. pastoris* X33), respectively, whilst for long-term storage, as cryo-stocks (at - 80 °C) containing 1 mL of pelleted

overnight culture resuspended in 250 µL of YPAD (*P. methanolica* PMAD11) or YPD (*P. pastoris* X33) and 250 µL of 30 % sterile glycerol.

5.4.2 *Preparation of Pichia methanolica electrocompetent cells*

The *P. methanolica* PMAD11 electrocompetent cells were prepared according to the manufacturer's protocol (Invitrogen). 200 mL of YPAD media was inoculated with the overnight culture of PMAD11 strain (starting $OD_{600} \approx 0.3$) and grown for 4 h at 30 °C until an OD_{600} of 0.6 - 1.0 was reached. The cells were centrifuged at RT for 5 min at 1500 g and the pellet was resuspended in 40 mL of sterile 50 mM phosphate pH 7.5 containing 25 mM dithiothreitol (DTT). The cell suspension was incubated for 15 min at 30 °C, centrifuged for 5 min at 1500 g at 4 °C and washed (three times) with 50 mL of ice-cold sterile STM buffer containing 270 mM sucrose, 10 mM Tris pH 7.6 and 1 mM $MgCl_2$. After pelleting cells for the third time, the cells were resuspended in 1 mL of ice-cold sterile STM buffer.

5.4.3 *Transformation of Pichia methanolica electrocompetent cells*

Transformation of Lcc1_pMETαA into *P. methanolica* PMAD11 strain was conducted as previously described [4], with some modifications. Typically 100 µL of competent cells were incubated with linearized Lcc1_pMETαA (3 µg) and stored on ice for 2 min in the ice-cold sterile 0.2 cm electroporation cuvette (Bio-Rad GenePulser). After electroporation, 1 mL of YPAD media (at RT) was added and the mixture was incubated for 1 h at 30 °C without shaking. Cells were centrifuged for 3 min at 1500 g at RT and resuspended in 100 µL of YNB. 50 µL of cells were spread on MD-agar and incubated for 3 - 4 days at 30 °C.

5.4.4 *Preparation of Pichia pastoris electrocompetent cells*

Electrocompetent *P. pastoris* X33 cells were prepared according to the manufacturer's protocol (Invitrogen). 500 mL of YPD media was inoculated with 0.5 mL of the overnight culture and grown at 30 °C until an OD_{600} of 1.5 was reached. The cells were centrifuged at 1500 g for 5 min at 4 °C and resuspended in 500 mL of ice-cold sterile Milli-Q water. The cells were centrifuged again, resuspended in 250 mL of ice-cold sterile Milli-Q water, centrifuged again and resuspended in 20 mL of an ice-cold sterile

1 M sorbitol. Cells were centrifuged again and the pellet was resuspended in ~ 1 mL of ice-cold sterile 1 M sorbitol to the final volume of 1.5 mL.

5.4.5 *Transformation of Pichia pastoris electrocompetent cells*

Typically, 80 µL of electrocompetent *P. pastoris* X33 cells were incubated with linearized lcc1_pPICZαA (10 µg) and stored on ice for 5 min in the ice-cold sterile 0.2 cm electroporation cuvette (Bio-Rad GenePulser). After the pulse, 1 mL of ice-cold sterile 1 M sorbitol was added. After 2 h of incubation at 30 °C (without shaking), the cells were spread on YPDS-agar containing of 100 µg/mL zeocin and incubated for 3 days at 30 °C.

5.5 Manipulation of *Schizophyllum commune*

5.5.1 *Strains*

The *S. commune* wild type (WT) strain 4-8 [5, 6] and the KS8 *thn* mutant strain [7, 8] were kindly provided by Dr. Karin Scholtmeijer. For short-term storage, the strains were maintained on MM-agar at 4 °C. For long-term storage, the strains were maintained as cryo-stocks containing 5×5 mm squares of MM-agar grown fungi and stored at - 80 °C.

5.5.2 *Preparation of protoplasts of Schizophyllum commune*

Protoplasts of *S. commune* WT and KS8 were prepared from mycelial homogenate as previously described [9]. The strains were grown on MM-agar for 7 days at 30 °C. A quarter of a colony (petri dish, 92 mm diameter×16 mm height) was homogenized with a blender (Waring Products, Inc.) in 50 mL of MM, diluted with 100 mL of MM, and grown for 24 h at 24 °C with shaking in an orbital shaker at 200 rpm. Cultures were homogenized again and grown with additional 50 mL of fresh MM for 16 h at 24 °C with shaking in an orbital shaker at 200 rpm. Mycelium was centrifuged for 10 min at 3500 rpm in a swing rotor and the pellet was washed with 40 mL of sterile 1 M $MgSO_4$. The mycelium was centrifuged for additional 15 min at 3500 rpm and the pellet was incubated for 4 h at 30 °C at 30 rpm with filter-sterile 50 mL of lysing enzymes mixture containing 1.0 mg/mL of *Trichoderma harzianum* enzymes (Horst) dissolved in 30 mM

maleic acid pH 5.8 and 1 M $MgSO_4$. The culture was 2-fold diluted with sterile Milli-Q water, incubated for 10 min, and harvested by filtration over nylon miracloth (200 µm mesh size, Calbiochem). The flow through was incubated for 10 min with 100 mL of sterile 1 M sorbitol and centrifuged for 10 min at 2500 rpm. The pellets were pooled and washed twice with 50 mL of sterile 1 M sorbitol and centrifuged for additional 10 min at 2500 rpm. The pellet was resuspended in 50 mL of sterile 1 M sorbitol, the protoplasts were counted and diluted to the number of (2 - 10)×10^7 protoplasts in 1 mL of sterile 1 M sorbitol. 100 µL of sterile 0.5 M $CaCl_2$ was added to each 900 µL aliquot of protoplasts. Aliquots of protoplasts were frozen at a cooling rate of 1 °C/min using a freezing container Mr. Frosty (Nalagene), and stored at -80 °C.

5.5.3 *Transformation of Schizophyllum commune protoplasts*

Typically 100 µL of *S. commune* WT and KS8 protoplasts (fresh or thawed on ice) were incubated with ~ 5 µg of purified DNA for 15 min on ice. Subsequently the mixture was incubated for 5 min at RT with one volume of freshly prepared 40 % (w/v) PEG4000 in 10 mM Tris pH 7.0, diluted with 2.5 mL of RM supplemented with 10 µg/mL (WT strain) or 25 µg/mL (KS8 strain) of phleomycin and incubated overnight at 25 °C. The next day, 7.5 mL of 1 % low-melting point (at 37 °C) agarose in MM containing 50 µg/mL penicillin, 50 µg/mL streptomycin sulfate, and 8 µg/mL (WT strain) or 20 µg/mL (KS8 strain) nourseothricin (final concentrations) were added to the regenerated protoplasts. The mixture was poured onto MM-agar containing 8 µg/mL nourseothricin, and when solidified, the selection plates were incubated at 30 °C for 3 - 4 days [9]. For a selection of stable transformants, the strains were transferred to a MM-agar (without nourseothricin) and incubated at 30 °C for 3 - 4 days.

5.6 *Trametes versicolor* genomic DNA isolation

Trametes versicolor was grown at RT in 100 mL for 8 days in media containing 10 g/L dextrose, 20 g/L KH_2PO_4, 1.6 g/L Na_2HPO_4, 264 mg/L $CaCl_2×H_2O$, 200 mg/L $FeSO_4×7H_2O$, 15 mg/L $MnSO_4×H_2O$, 20 mg/L $ZnSO_4×7H_2O$, 10.0 g/L $MgSO_4×7H_2O$, 40 mg/L $CuSO_4×5H_2O$, 550 mg/L adenine, 3.0 g/L α-phenylalanine, 1.0 mg/L thiamine and 50.0 g/L asparagine until the surface was fully covered.

The fungus was frozen in liquid nitrogen and ground to a homogenous paste. The ground material was incubated for 1 h at 60 °C with 800 µL of preheated

0.1 M Tris pH 8.0 containing 2 % (w/v) hexadecyltrimethylammonium bromide (Sigma), 0.2 % (v/v) β-mercaptoethanol (Aldrich) and 1.4 M NaCl. The material was mixed with 400 μL of phenol/chloroform/isoamyl alcohol (25:24:1) and spun down at 18500 g for 15 min. 600 μL of the water phase was incubated with 10 μL of RNAse (Sigma, final concentration 0.3 mg/mL) at 37 °C for 45 min, mixed with 400 μL of phenol/chloroform/isoamyl alcohol and spun down at 18500 g for 15 min. Subsequently, 600 μL of the water phase was incubated with 400 μL of isopropanol for 1 h on ice, after which the precipitated DNA was spun down at 18500 g for 5 min. The pellet was washed for 45 min in 80 % ethanol, after which the solvent was removed and the pellet was left to dry on air for 10 min. The DNA pellet was dissolved in Milli-Q water, diluted to the final concentration of 1.0 mg/mL and incubated for 1 h at 37 °C with 2.5 μL of RNAse.

5.7 Molecular cloning

5.7.1 *Polymerase chain reaction*

Polymerase chain reactions (PCR) were typically prepared in 0.5 mL eppendorf tubes containing around 20 - 50 ng of template DNA, 0.4 mM deoxyribonucleotide triphosphates (dNTPs) mix (Promega), 125 ng of forward and reverse DNA primers (Sigma-Genosys), 1 μL (2.5 units) of *Pfu* polymerase (Agilent Technologies), 5 μL of 10×*Pfu* buffer made up to 50 μL volume by addition of sterile Milli-Q water. The PCR conditions were modified according to the manufacturer's instructions.

Alternatively, PCR reactions were carried out using Platinum *Pfx* DNA Polymerase (Invitrogen) according to the manufacturer's instructions. The reaction mixture consisted of 10 - 50 ng of template DNA, 0.3 mM dNTP mixture, 1 mM $MgSO_4$, 300 nM of each DNA primer, 0.4 μL (1 unit) of Platinum *Pfx* polymerase, 5 μL of 10×*Pfx* buffer made up to 50 μL volume by addition of sterile Milli-Q water.

5.7.2 *Site-directed mutagenesis*

Mutations in plasmid DNA were introduced using a QuickChange Site-Directed Mutagenesis Kit (Agilent Technologies), if not stated otherwise. The reaction mixture (50 μL) consisted of around 10 - 50 ng template DNA, 0.5 mM dNTP mixture, 125 ng of each DNA primer, 1 μL (2.5 units) of *Pfu* polymerase, 5 μL of 10×*Pfu* buffer in

sterile Milli-Q water. Alternatively, multiple point mutations in plasmid DNA were introduced using a QuickChange Lightening Multi Site-Directed Mutagenesis Kit (Agilent Technologies). The reaction mixture (25 µL) consisted of ~ 100 ng template DNA, 1 µM dNTP mixture, 100 ng of each DNA primer, 1 µL of QuickChange Lightening Multi enzyme blend, 0.75 µL QuickSolution, 2.5 µL of 10×QuickChange Lightening Multi buffer in sterile Milli-Q water. The conditions for mutant strand synthesis reaction were modified according to the manufacturer's protocol. Prior to transformation into XL1-Blue or XL10-Gold competent cells, 1 µL of DpnI restriction enzyme (New England BioLabs or Agilent Technologies) was added to digest template plasmid DNA.

5.7.3 *Extraction of DNA from Escherichia coli*

Plasmid DNA was isolated from bacterial cultures using a GenElute Plasmid Mini- and Midiprep kit (Sigma) according to the manufacturer's instructions. DNA for transformation in *S. commune* was isolated using a NucleoBond Xtra Maxi kit (Macherey-Nagel) according to the manufacturer's instructions. The purity of DNA was judged by from the relative absorption at 260 nm and 280 nm, where the A_{260}/A_{280} ratio in the range of 1.5 to 1.8 usually indicated a suitably pure DNA with little protein contamination.

5.7.4 *Digestion of DNA using restriction endonucleases*

Plasmid and PCR-amplified DNA was digested using restriction enzymes (New England BioLabs) according to the manufacturer's instructions. Typically, 1 - 3 µg of DNA was incubated at 37 °C with the appropriate endonucleases for 1 - 3 h. Prior to ligation reaction (Section 5.7.6), the digested DNA was analyzed by agarose gel electrophoresis (Section 5.8.1) and purified (Section 5.7.5).

5.7.5 *Isolation of DNA from agarose gel*

The target bands were excised from the agarose gel using a scalpel and isolated from the gel using a GenElute Gel Extraction Kit (Sigma) according to the manufacturer's instructions.

5.7.6 *DNA ligation*

Ligation of the digested with restriction endonucleases vector and insert DNA was achieved using a rapid T4 DNA ligase (Fermentas) according to the manufacturer's instructions. Typically, 50 - 100 ng of digested and purified vector was mixed with digested and purified DNA insert (using a molar vector to insert ratio of 1:5) in a rapid T4 DNA ligase buffer and incubated at RT with a rapid T4 DNA ligase for 30 - 60 min. 5 - 20 µL of ligation mixture was used for subsequent transformation in *E. coli* JM101 competent cells. Successful ligation was verified by the digestion of the ligated plasmid with the appropriate restriction endonuclease followed by agarose gel electrophoresis (Section 5.8.1) and sequencing of the DNA insert (Section 5.7.7).

5.7.7 *DNA sequencing*

DNA sequence of amplified and mutated genes in plasmid DNA was verified using DNA sequencing service of Backman-Coulter Genomics or GATC Biotech.

5.7.8 *Determination of DNA concentration*

Concentration of plasmid DNA was determined by measuring the absorption intensity at 260 nm and using the relationship that one intensity unit at 260 nm is equal to 50 µg/mL of double stranded DNA.

5.8 Electrophoresis

5.8.1 *Agarose gel electrophoresis*

Agarose (1.0 - 2.0 % (w/v), Melford) was dissolved in 50 mL of Tris-Acetate-EDTA (TAE) buffer (40 mM Tris pH 8.0, 40 mM acetate and 1 mM ethylenediaminetetraacetic acid (EDTA, BDH) by boiling in a microwave. The molten agarose was cooled to 50 - 55 °C, poured into a gel cast (BioRad) with 0.1 % (v/v) of 1 µg/mL ethidium bromide and left to set at RT. Once set, the gel was transferred into a gel tank containing TAE buffer and loaded with DNA samples containing DNA loading buffer (0.4 % (w/v) bromophenol blue (BDH), 5 % glycerol). A voltage of 120 V was applied and electrophoresis was carried out for 30 - 45 min. Lambda DNA (Promega)

digested with PstI endonuclease (New England BioLabs) was used as molecular weight (MW) marker. Typically, DNA fragments were visualized under UV irradiation (BioRad Gel Doc 1000). However, when DNA fragments were required for further experiments (e.g. DNA ligation), the agarose gel was illuminated using UV transilluminator (UV Tec).

5.8.2 *Sodium dodecyl sulfate-polyacrylamide gel electrophoresis*

The expression of proteins was visualized using sodium dodecyl sulfate-polyacrylamide gel electrophoresis (SDS-PAGE). The gels consisted of a 5 % acrylamide/bis-acrylamide stacking gel poured above a layer of 10, 12 and 20 % acrylamide/bis-acrylamide separation gel with a plastic comb to produce the ridges in the gel. The stacking gel consists of 5 % (v/v) acrylamide/bis-acrylamide (BioRad), 125 mM Tris pH 6.8, 0.1 % (w/v) sodium dodecyl sulfate (SDS, Sigma), 0.05 % (w/v) ammonium persulfate (APS, Aldrich) and 0.1 % (v/v) N,N,N',N'-tetramethylene diamine (TEMED, Aldrich) in dionised water. The separation gel consists of 10 - 20 % acrylamide/bis-acrylamide, 375 mM Tris pH 8.8, 0.1 % SDS, 10 % glycerol, 0.05 % APS and 0.05 % TEMED in dionised water. Once polymerized, the gel was transferred into a Mini-Protein II Cell tank (BioRad) containing SDS-PAGE buffer (25 mM Tris pH 8.8, 200 mM glycine (Aldrich) and 0.1 % SDS.

Protein samples for SDS-PAGE were prepared in cracking buffer containing 50 mM Tris pH 6.8, 1 % SDS, 15 % glycerol, 2 % β-mercaptoethanol and 0.025 % (w/v) bromophenol blue in water. The samples were heated at 100 °C for 5 min. Typically 20 μL of protein sample was loaded onto the gel, along with a broad range MW marker (6.5 kDa - 200 kDa, BioRad) in cracking buffer or pre-stained Dual Color MW marker (10 kDa - 250 kDa, BioRad).

Electrophoresis was carried out at a constant voltage of 200 V and current of ~ 60 mA for 60 - 90 min until the dye front reached the bottom of the separation gel. Protein bands were visualized by incubating the separation gel in a solution of Instant Blue (Expedian).

5.8.3 *Western blotting*

The expression of Lcc1_cMYC and C452S_Lcc1_cMYC in *S. commune* KS8 strain was verified by immunoblotting. The protein samples were prepared in SDS cracking

buffer and loaded (20 µL) onto 20 % SDS PAGE gels or gradient, 4 - 20 % pre-cast SDS-PAGE gels (BioRad) along with 5 µL of pre-stained Dual Color MW marker. The proteins were electrophoresed at a constant voltage of 200 V until the dye front reached the bottom of the gel (Section 5.8.2). Subsequently, the gel was transferred into a plastic cast (BioRad), onto a wet blotting card (Sigma) with a foam pad underneath. The gel was covered with a pre-wetted Hybond ECL nitrocellulose membrane (GE Healthcare), followed by another piece of wet blotting card and a foam pad. Prior to assembling, the blotting cards, foam pads and the nitrocellulose membrane were thoroughly soaked in transfer buffer (12.5 mM Tris pH 8.8, 100 mM glycine and 20 % (v/v) methanol). The cast was sealed and placed inside a Mini-Protean II Cell (BioRad) containing transfer buffer. The proteins were transferred onto nitrocellulose membrane by applying a constant current at 270 mA until all proteins from the pre-stained Dual Color MW marker were transferred.

When protein transfer was completed, the membrane was removed from plastic cast and rinsed with TBS buffer (10 mM Tris pH 7.4 and 150 mM NaCl) with 0.05 % (v/v) Tween 20. The membrane was blocked in 8 % (w/v) skimmed milk in TBS and 0.05 % Tween 20 buffer for 60 min with gentle rocking. Subsequently, the blocking solution was discarded and the membrane was incubated overnight in 1:1000 diluted mouse anti-cMYC primary antibody (Sigma) in 8 % skimmed milk in TBS and 0.05 % Tween 20 buffer at 4 °C with gentle rocking.

The next day the membrane was washed three times with TBS and 0.05 % Tween 20 buffer and incubated with 1:5000 diluted rabbit anti-mouse IgG conjugated with alkaline phosphatase (AP) secondary antibody (Promega) in 8 % skimmed milk solution in TBS and 0.05 % Tween buffer 20 for 60 min at RT with gentle rocking. The blocking solution was discarded and the membrane was washed with TBS with 0.05 % Tween 20, followed by TBS and AP (100 mM Tris, pH 9.5 containing 100 mM NaCl and 5 mM $MgCl_2$) buffers. To visualise protein bands, the membrane was incubated overnight with 20 mL of AP buffer containing 88 µL of nitroblue tetrazolium (NBT, 75 mg/mL in 70 % dimethylformamide, Promega) and 66 µL of 5-bromo-4-chloro-3-indyl phosphate (BCIP, 50 mg/mL in 100 % dimethylformamide, Promega).

5.8.4 *Sandwich immunodetection of the Lcc1_cMYC and C452S_Lcc1_cMYC variants*

S. commune KS8 strains secreting Lcc1_cMYC and C452S_Lcc1_cMYC were selected by sandwich immunodetection by Dr. Karin Scholtmeijer. *S. commune* KS8 strains transformed with glcc1_cMYC_pESCT and C452S_glcc1_cMYC_pESCT were grown for 3 days at 30 °C on the sterile perforated polycarbonate (PC) membranes (diameter ~ 7.5 cm, pore size 0.1 μm, Poretics USA) placed on top of MM-agar. The PC membranes with colonies were removed from the MM-agar and placed onto polyvinylidene difluoride (PVDF) membranes (pre-wetted with methanol and rinsed with water) and placed on top of fresh, pre-warmed MM-agar. After incubation for 2 - 3 h at 30 °C, the PC membranes with colonies were removed and the PVDF membranes were allow to dry. The PVDF membrane was wetted with methanol, rinsed with water and blocked for 30 min with 5 % (w/v) skimmed milk in PBS (12 mM NaH_2PO_4, 1.76 mM KH_2PO_4, 2.68 mM KCl and 137 mM NaCl) with 0.1 % (v/v) TritonX-100. The blocking solution was discarded and the PVDF membranes were incubated with freshly prepared 1:5000 diluted anti-cMYC antibody conjugated with AP (Acris SM1863AP) in 5 % skimmed milk solution in PBS, 0.1 % TritonX-100 for 2 h at RT. The membranes were washed for 5 min with PBS, 0.1 % TritonX-100 changing the solution twice and then washed once in the AP buffer. The membrane was developed by subsequent incubation with 44 μL of NBT and 33 μL of BCIP in 10 mL of AP buffer.

5.9 Small scale protein over-expression

5.9.1 *Over-expression in Escherichia coli*

In order to determine the growing period optimal for protein over-expression, small-scale expression trials were carried out. Typically, 10 mL of LB containing an appropriate antibiotic was inoculated with a single colony of *E. coli* transformed with the expression plasmid and grown overnight at 37 °C, with shaking at 200 rpm in an orbital shaker. The next day a 100-fold dilution into 50 mL of LB containing an appropriate antibiotic was made and incubated for approximately 2 h, until the OD_{600} had reached the required value (typically 0.5 - 1.5). The temperature of the cultures was lowered if necessary, the protein expression was induced by the addition of isopropyl

β-D-1-thiogalactopyranoside (IPTG). Several growing parameters were optimized, including type of *E. coli* host (BL21 (DE3), BL21 Tuner (DE3) or Rosetta (DE3)), duration (6 - 48 h), temperature (4 - 37 °C) of growth, IPTG concentration (0.05 - 1.0 mM), media type (LB, 2×YT and TB), and concentration of $Cu(NO_3)_2$ (0 - 0.2 mM) and proline (0 or 25 mM) (Fluka) in the media.

Routinely, 4 mL samples of the cultures were collected every few hours (typically: 0, 2, 4, 6, 8, 20 h), sonicated and centrifuged for 10 minutes at 5000 g. 50 µL samples of sonicated cultures (representing all expressed proteins) and 50 µL of supernatant from the spun-down cultures (representing soluble proteins) were taken and lysed in SDS-PAGE cracking buffer.

Proteins from periplasm of *E. coli* were isolated using an osmotic shock-based method. Pellets from 3 mL *E. coli* cultures were resuspended in 500 µL of the 30 mM Tris pH 8.0 containing 1.2 mM EDTA and 20 % (w/v) sucrose, gently shaken for 10 min at 4 °C and centrifuged at 13000 g for 5 minutes. The pellets were resuspended in the ice-cold deionised water, gently shaken at 4 °C for 10 minutes and spun down at 13000 g for 5 minutes. The pellets were re-suspended in 500 µL of 20 mM Tris pH 8.0, sonicated and centrifuged at 4000 g for 15 minutes. The supernatant was subsequently centrifuged at 21000 g for 20 minutes and pellets resuspended in 500 µL of 20 mM Tris pH 8.0. 50 µL were taken, lysed in SDS-PAGE cracking buffer and analyzed by SDS-PAGE electrophoresis to identify the expression level of soluble protein.

5.9.2 *Over-expression in Schizophyllum commune*

The *S. commune* WT and KS8 strains containing clcc1_pESCT or glcc1_pESCT were grown at 30 °C on the MM-agar for ~ 7 days until the whole surface of perti dish (92 mm diameter × 16 mm height) was fully covered. A quarter of the colony was homogenized for 15 s with a blender in 50 mL of MM pH 7.0. The liquid standing cultures were prepared in the petri dishes (92 mm diameter × 16 mm height) by diluting 2.5 mL of homogenized colony with 22.5 mL of appropriate media (CM/MM/PM) to the final volume of 25 mL. The pH of MM was adjusted to 6.6, 7.0, 7.4 or 8.0. After overnight incubation at 30 °C or 23 °C, 0, 1, 2, 3 and 4 mM of $Cu(NO_3)_2$ was added (1^{st} day of growth). After 6, 9, 12 and 15 days 5 mL of fresh media with an appropriate $Cu(NO_3)_2$ concentration was added. Samples (1 mL) were taken every 1 - 3 days for measurements of Lcc1 activity with 2,2'-azino-bis(3-ethylbenzothiazoline-6-sulphonic acid (ABTS).

5.10 Large scale protein over-expression and purification

5.10.1 *Over-expression and purification of WT SLAC and WT $SLAC_{long}$ in Escherichia coli*

WT $SLAC_{long}$ and WT SLAC from *Streptomyces coelicolor* were over-expressed in *E. coli* BL21 (DE3), isolated and purified as previously described [10], with modifications. *E. coli* BL21 (DE3) cells transformed with either SLAC(long)_pET29a or SLAC_pET29a were grown in LB containing 100 μg/mL ampicillin at 37 °C with shaking at 200 rpm in an orbital shaker until an OD_{600} of ~ 1.5 was reached. The cells were cooled to ~ 20 °C and the protein expression was induced by the addition of 0.4 mM IPTG. Cells were incubated at 25 °C for a further 20 h before harvesting by centrifugation. The cell pellet from 2 L culture was resuspended in 10 mM phosphate pH 7.4, sonicated and centrifuged at 35000 g for 30 min. The supernatant was incubated overnight at 4 °C with 1 mM $Cu(NO_3)_2$ and centrifuged again at 35000 g for 30 min prior to loading onto a Diethylaminoethyl (DEAE) Fast Flow Sepharose (GE Healthcare) column (~ 20 cm length, ~ 2.6 cm diameter) equilibrated with 10 mM phosphate pH 7.4. Bound proteins were eluted with a linear NaCl gradient (0 - 0.4 M) in the same buffer. The SLAC-containing fractions (identified by SDS-PAGE) were combined and exchanged into 20 mM Tris pH 7.5 containing 200 mM NaCl *via* ultrafiltration (Amicon stirred cell, 30 kDa molecular weight cut off (MWCO) membrane). Concentrated protein was further purified on a HiLoad Superdex 200 16/60 gel filtration column (GE Healthcare) in the same buffer.

5.10.2 *Over-expression and purification of SLAC variants*

E. coli BL21 (DE3) cells transformed with tSLAC_pET22b, qSLAC_pET22b, mgSLAC_pET22b, nirSLAC_pET22b or gdcSLAC_pET22b were grown in 2×YT media containing 100 μg/mL ampicillin and 0.2 mM $Cu(NO_3)_2$. *E. coli* BL21 (DE3) cells transformed with T1D_tSLAC_pET22b, T1D_qSLAC_pET22b, T1D_mgSLAC_pET22b, A99H_mgSLAC_pET22b, T1D_nirSLAC_pET22b, A99H_nirSLAC_pET22b, T1D_A99H_nirSLAC_pET22b or A99H_gdcSLAC_pET22b were grown in TB media containing 100 μg/mL ampicillin. In each case, transformed cells were grown at 37 °C with shaking at 200 rpm in an orbital shaker until an OD_{600} of ~ 1.5 - 2.0 was reached. The cultures were cooled to

~ 10 °C, 25 mM proline was added and the protein expression was induced by the addition of 1.0 mM IPTG. Cells were incubated at 16 °C for a further 22 h before harvesting by centrifugation.

The cell pellet from 4 L culture was resuspended in 10 mM phosphate pH 7.5, sonicated and centrifuged at 35000 g for 30 min. The supernatant was incubated overnight at 4 °C with 1 mM $Cu(NO_3)_2$ and centrifuged again at 35000 g for 30 min prior to loading onto a DEAE Fast Flow Sepharose column (~ 30 cm length, ~ 2.6 cm diameter) equilibrated with 10 mM phosphate pH 7.5. Bound protein was eluted with a linear NaCl gradient (0 - 0.25 M) in the same buffer. The protein-containing fractions (identified by SDS-PAGE) were combined and dialyzed against 20 mM phosphate pH 6.8, changing the buffer at least three times. The protein was centrifuged at 35000 g for 30 min prior to loading onto a 5 mL HiTrap Q High Performance (HP) column (GE Healthcare) equilibrated with 20 mM phosphate pH 6.8. Bound protein was eluted with a linear gradient of NaCl (0 - 0.2 M) in the same buffer. The purest, protein-containing fractions (identified by SDS-PAGE) were combined, concentrated *via* ultrafiltration (Amicon ultra 15, 30 kDa MWCO membrane) and exchanged into 20 mM Tris pH 7.5 containing 200 mM NaCl. Protein was further purified on a HiLoad Superdex 200 16/60 gel filtration column in the same buffer.

5.10.3 *Over-expression and purification of WT bNiR, M87C bNiR, K329C bNiR LacNiR, Δ252G LacNiR, T1D azNiR and T1D T246H azNiR*

WT bNiR from *Alcaligenes xylosoxidans* and its variants were over-expressed in *E. coli* BL21 (DE3) as previously described [11], except for LacNiR, Δ252G LacNiR and qNiR, which were grown in the presence of 0.2 mM $Cu(NO_3)_2$.

WT, M87C and K329C bNiR were isolated and purified as previously described [11]. For K329C bNiR the only modification to this method was that the amount of streptomycin sulfate used for the precipitation of DNA during purification was lowered to 0.3 % (w/v). The cell pellet from 2 L culture of LacNiR, Δ252G LacNiR, T1D azNiR, T1D T246H azNiR and qNiR was resuspended in 20 mM Mes pH 6.0, sonicated and centrifuged at 35000 g for 30 min. The supernatant was incubated for 4 h at 4 °C with 1 mM (T1D azNiR, T1D T246H azNiR and qNiR) or 2 mM (LacNiR and Δ252G LacNiR) $Cu(NO_3)_2$. The protein mixture was incubated for additional 2 h at 4 °C with 0.2 % (T1D azNiR, T1D T246H azNiR and qNiR) or 0.1 % (LacNiR and Δ252G LacNiR) of streptomycin sulfate, after which the precipitated DNA was spun

down at 35000 g for 30 min prior to loading onto a Sulfopropyl (SP) Fast Flow Sepharose column (~ 25 cm length, ~ 2.6 cm diameter) equilibrated with 20 mM Mes pH 6.0 (T1D azNiR, T1D T246H azNiR and qNiR) or 10 mM phosphate pH 6.0 (LacNiR and Δ252G LacNiR). Bound proteins were eluted with a linear gradient of NaCl (0 - 0.4 M) in the same buffers. The protein-containing fractions (identified by SDS-PAGE) were combined, concentrated *via* ultrafiltration (Amicon ultra 4, 10 kDa MWCO membrane) and exchanged into 20 mM Tris pH 7.5 containing 200 mM NaCl. Proteins were further purified on a HiLoad Superdex 200 16/60 gel filtration column in the same buffer.

5.10.4 *Purification of Laccase A from crude acetone powder from Trametes versicolor*

Typically 5 g of crude acetone powder from *T. versicolor* (Fluka, UK) was mixed with 150 mL of 100 mM phosphate pH 6.0 and stirred at 4 °C for 5 h until all the powder was dissolved. The solution was centrifuged at 10000 rpm for 20 min prior to loading onto a DEAE Fast Flow Sepharose column (~ 5 cm length, ~ 2.6 cm diameter) equilibrated with 100 mM phosphate pH 6.0 containing 100 mM NaCl. The unbound greenish-blue fraction was collected and dialyzed against 10 mM phosphate pH 6.0 changing the buffer at least three times. The solution was centrifuged at 15000 rpm for 20 min prior to loading onto a DEAE Fast Flow Sepharose column (~ 15 cm length, ~ 2.6 cm diameter) equilibrated with 10 mM phosphate pH 6.0. The unbound flow through was collected (Laccase B) and the bound protein (Laccase A) was eluted with a 0 - 0.35 M NaCl linear gradient in the same buffer. Fractions from the main peak were pooled and exchanged into 10 mM phosphate pH 6.5 (Amicon stirred cell, 30 kDa MWCO membrane). The protein was further purified on a DEAE Fast Flow Sepharose column (~ 15 cm length, ~ 2.6 cm diameter) equilibrated with 10 mM phosphate pH 6.5. The loaded protein was eluted with a 0 - 0.2 M NaCl gradient in the same buffer. Fractions with A_{278}/A_{250} ratios ranging from 11 to 12.8 and A_{278}/A_{610} ratios of 16.5 to 18 were combined and the salt was removed by ultrafiltration (Amicon stirred cell, 30 kDa MWCO membrane).

5.10.5 *Bacterial over-expression and purification of Lcc1*

5.10.5.1 *Refolding of Lcc1 from Escherichia coli BL21 (DE3) inclusion bodies*

The Lcc1 protein was slowly refolded from inclusion bodies (IB) using previously published procedure [12], with modifications. Two denaturing agents, urea and guanidine hydrochloride (Gdn), were used for resolubilization of IB. Typically, ~ 0.4 g of IB were incubated at RT in an anaerobic chamber (Belle Technology, $[O_2] << 2$ ppm) for ~ 40 min in 20 mL of 6 M urea (or Gdn), 10 mM EDTA and 10 mM DTT in 25 mM Tris pH 7.5. Lcc1 was refolded at 4 °C by a 10-fold slow dilution (~ 3.5 mL/h flow rate) with 25 mM Tris pH 7.5 supplemented with 0.5 mM EDTA. The protein solution was subsequently 10-fold rapidly diluted with 10 mM Tris pH 7.5 and incubated overnight with 1.0 mM $CuSO_4$. The proteins were captured using a DEAE Fast Flow Sepharose material equilibrated with 25 mM Tris pH 7.5 and eluted with 0.5 M NaCl in the same buffer. The protein solution was concentrated and the excess of $CuSO_4$ was removed by ultrafiltration (Amicon stirred cell, 30 kDa MWCO membrane). The protein solution was further incubated overnight with 2 mM $CuSO_4$ and excess of metal was removed by ultrafiltration.

Lcc1 was fast refolded from IB using previously published procedure [13], with modifications. Typically, ~ 0.4 g of IB were incubated at RT in an anaerobic chamber for ~ 60 min with 5 mL of 6 M urea (or Gdn), 2 mM DTT and 10, 30 or 50 mM EDTA in 10 mM Hepes pH 8.0. Lcc1 was refolded at 4 °C by 50-fold rapid dilution in 10 mM Hepes pH 8.0 supplemented with 2 or 5 mM DTT. The protein mixture was dialysed against 250 mM ammonium acetate pH 8.0 and further dialysed against the same buffer containing different concentrations of $CuSO_4$ (1 - 5 mM). Excess of metal was removed by dialysis.

5.10.5.2 *Over-expression and purification of soluble Lcc1*

E. coli BL21 (DE3) cells transformed with Lcc1_pET29a were grown at 37 °C in LB containing 50 μg/mL kanamycin and 0.1 mM $Cu(NO_3)_2$ until an OD_{600} of ~ 1.0 was reached. The cells were cooled to ~ 10 °C and 25 mM proline was added. Protein expression was induced by the addition of 0.5 mM IPTG and cells were incubated at 10 °C for an additional 42 h before harvesting by centrifugation. Alternatively, *E. coli* BL21 (DE3) cells transformed with Lcc1_pET22b were grown at 37 °C in LB

containing 100 µg/mL ampicillin and 0.1 mM $Cu(NO_3)_2$ until an OD_{600} of ~ 0.8 was reached. The cells were cooled to ~ 30 °C and the protein expression was induced by the addition of 0.5 mM IPTG. The cells were incubated at 30 °C for an additional 20 h before harvesting by centrifugation.

The cell pellet was resuspended in 20 mM Mes pH 6.0, sonicated and centrifuged at 35000 g for 30 min. The supernatant was incubated overnight with 2.5 mM $Cu(NO_3)_2$ at 4 °C. The protein mixture was centrifuged at 35000 g for 30 min prior to loading onto a DEAE Fast Flow Sepharose column (~ 15 cm length and ~ 2.6 cm diameter) equilibrated with 50 mM phosphate pH 6.0 and eluted with a linear NaCl gradient (0 - 500 mM) in the same buffer. Fractions containing Lcc1 (identified by SDS-PAGE) were combined, exchanged *via* ultrafiltration (Amicon stirred cell, 30 kDa MWCO membrane) into 50 mM phosphate pH 6.0 and incubated overnight with 1 mM $Cu(NO_3)_2$.

5.10.5.3 *Over-expression and purification of N-terminally fused NusA_Lcc1*

E. coli BL21 (DE3) cells transformed with Lcc1_pET44a were grown at 37 °C in LB containing 100 µg/mL ampicillin and 0.5 mM $Cu(NO_3)_2$ until an OD_{600} of 1.3 was reached. Protein expression was induced by the addition of 0.5 mM IPTG and cells were incubated for additional 6 h before harvesting by centrifugation. The cell pellet was resuspended in 20 mM phosphate pH 7.4 containing 500 mM NaCl and 30 mM imidazole, sonicated and centrifuged at 35000 g for 30 min. The supernatant was loaded onto a $NiSO_4$-charged Immobilized Metal Ion Affinity Chromatography (IMAC) HiTrap Sepharose HP column (5 mL, GE Healthcare) and eluted with a linear imidazole gradient (30 - 225 mM) in 20 mM phosphate pH 7.4 containing 500 mM NaCl. Fractions containing NusA_Lcc1 (identified by SDS-PAGE) were combined and exchanged *via* ultrafiltration (Amicon ultra 4, 30 kDa MWCO membrane) into 20 mM Tris pH 8.4 containing 150 mM NaCl and 2.5 mM $CaCl_2$. The protein mixture was incubated for 7 h at 4 °C with thrombin (1:100 dilution, Sigma) and the enzymatic digestion was inhibited with 1 mM 4-(2-aminoethyl)benzenesulfonyl fluoride hydrochloride. The protein mixture was exchanged *via* ultrafiltration (Amicon ultra 4, 10 kDa MWCO membrane) into 50 mM phosphate pH 6.0 prior to loading onto a 1 mL HiTrap SP HP column. The flow through was collected and exchanged into 20 mM Mes pH 6.0, and incubated overnight with 1 mM $Cu(NO_3)_2$ at 4 °C.

5.10.6 *Over-expression in Pichia methanolica and purification of Lcc1*

Expression of recombinant Lcc1 in *P. methanolica* PMAD11 strain was performed as previously described [14]. The Lcc1 secreting PMAD11 transformant was incubated in BMDY media at 30 °C with shaking (300 rpm) until an OD_{600} of ~ 3.5 was reached. Cells were centrifuged at 3000 g for 5 min and the cell pellet was resuspended in a BMMY media, pH 6.5 supplemented with 0.2 mM $CuSO_4$. The cultures (500 mL each) were incubated at 19 °C with shaking (300 rpm) and 0.8 % (v/v) methanol was added daily. After five days of incubation, the cells were harvested by centrifugation at 10000 g for 10 min and the supernatant was passed through a 0.45 μm filter.

The supernatant was concentrated (Amicon stirred cell, 30 kDa MWCO membrane) and diluted with 20 mM phosphate pH 6.5. The sample was applied onto a DEAE Fast Flow Sepharose column (~ 30 cm length, ~ 2.6 cm diameter) equilibrated with 20 mM phosphate pH 6.5 and protein was eluted with a 0 - 1.0 M NaCl linear gradient in the same buffer. Fractions showing laccase activity with ABTS were pooled and exchanged into 20 mM phosphate pH 6.5 containing 200 mM NaCl (Amicon stirred cell, 30 kDa MWCO membrane). The concentrated sample (1 mL) was further purified on a HiLoad Superdex 75 16/60 column (GE Healthcare) in the same buffer.

5.10.7 *Over-expression in Schizophyllum commune and purification of Lcc1*

S. commune KS8 strain transformed with gLcc1_pESCT was grown at 30 °C on MM-agar (petri dish, 92 mm diameter × 16 mm height) for ~ 7 days until the whole surface was covered. A quarter of the colony was blended for 15 s with 50 mL of CM pH 7.0. The liquid standing cultures were prepared in the tissue culture flasks with a filter cap (Greiner Bio One) by diluting 10 mL of macerated colony with 90 ml of CM pH 7.0 to a final volume of 100 mL. After overnight incubation at 30 °C, 2 mM of $Cu(NO_3)_2$ was added (day 1). After 6 and 9 days of growth 20 mL of fresh CM, pH 7.0 was added and after 12 days of growth the supernatant was collected and filtered using miracloth filters (200 μm mesh size).

The supernatant was incubated overnight at 4 °C with a DEAE Fast Flow Sepharose material equilibrated in 20 mM phosphate pH.7.0. Bound protein was eluted with a 0 - 0.4 M NaCl gradient in the same buffer and fractions showing laccase activity with ABTS were pooled and dialyzed against 20 mM phosphate pH 6.0 changing buffer at least three times. The protein was loaded onto a 5 mL HiTrap Q HP column

equilibrated with 20 mM phosphate pH 6.0 and eluted in the linear salt gradient (0 - 0.3 M NaCl) in the same buffer. The purest (judged by SDS-PAGE) and the most active (with ABTS) fractions were pooled, concentrated by ultrafiltration (Amicon ultra 4, 30 kDa MWCO membrane) and NaCl was added to the final concentration of 200 mM. The protein was further purified using a HiLoad Superdex 75 16/60 column in 20 mM phosphate pH 6.0 containing 200 mM NaCl.

5.11 Fluorescent labeling of proteins

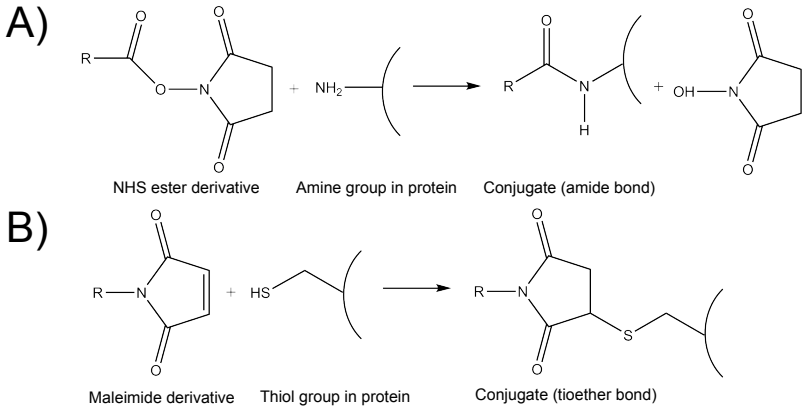

Figure 5.1 Schematic reactions for labeling of (A) amine groups in proteins with an N-hydroxysuccinimide (NHS) ester and (B) thiol groups of Cys residues with a maleimide derivative of fluorescent dyes (depicted as R).

The proteins were labeled with ATTO fluorescent dyes (ATTO-TEC GmbH, Appendix A) at surface-exposed amine groups (including an N-terminus) or at a free thiol group of a surface-exposed Cys residue (Figure 5.1) using modified versions of published protocols [15, 16] and manufacturer's recommendation. Conditions, such as labeling buffer, label to protein molar ratio, and incubation time and temperature were adjusted for each protein.

For labeling of amine groups, a protein (typically ~ 100 μM) was incubated with an N-hydroxysuccinimide (NHS) ester-modified label (0.25 to 10-fold of label to protein molar excess) in 100 mM Hepes pH 8.3 or 100 mM phosphate pH 6.0 (Laccase A and Lcc1) for 30 min to 2 h. For labeling of thiol groups, a protein was incubated with a maleimide-modified label (0.5 to 50-fold of label to protein molar excess) in 100 mM phosphate pH 7.5 for 30 min to 60 min. Labeling was typically performed on ice, except for anaerobic experiments, which were conducted at RT in an anaerobic chamber. Unbound dye was removed by single step size-exclusion

chromatography using a desalting PD10 column (GE Healthcare). The dye to protein labeling ratios (DOL) was determined according to the manufacturer's protocol using Equation 5.1. Depending on experiment, DOL was kept in the range of 7 to 80 % per monomer.

$$DOL = \frac{A_{\max} / \varepsilon_{\max}}{A_{prot} / \varepsilon_{prot}} \cdot 100\% = \frac{A_{\max} \cdot \varepsilon_{prot}}{\left(A_{prot} - A_{\max} \cdot CF_{280}\right) \cdot \varepsilon_{\max}} \cdot 100\% \qquad \text{(Equation 5.1),}$$

where A_{max} is absorbance intensity at the absorption maximum of a dye, ε_{max} - the extinction coefficient of a dye at the absorption maximum A_{prot} - protein absorbance intensity at 280 nm, ε_{prot} - the extinction coefficient of the protein at 280 nm and CF_{280} is a correction factor.

5.12 Spectroscopy

5.12.1 *Determination of the molecular weight of proteins by mass spectrometry*

The MWs of proteins were determined by matrix-assisted laser desorption ionization time-of-flight mass spectrometry (MALDI-TOF-MS, Voyager - DE STR, Applied Biosystems). Spectra were recorded in the positive ion linear mode using a *m/z* range of 10000 to 40000 (bNiR and SLAC) or 20000 to 80000 (Lcc1) by Bob Liddell (Pinnacle Service, Newcastle University).

5.12.2 *UV-Vis absorption spectroscopy*

UV-Vis spectra of proteins were acquired on a Parkin-Elmer λ 35 spectrophotometer equipped with a Parkin Elmer PTP-1 peltier or on a Varian Cary 50 (Varian Inc., Agilent Technologies) spectrophotometer in a range of 200 - 900 nm using a slitwidth equivalent to a bandwidth of 1 nm, unless stated otherwise. Measurements were conducted using 2 mm or 10 mm path length quartz cuvettes. Activity measurements were conducted using a time drive method in which absorption intensity at fixed wavelength can be measured over time of experiment.

For the anaerobic measurements typically the protein samples were prepared in septum sealed gas tight 3 mL cuvette in anaerobic chamber. Alternatively, the buffer

solution was deoxygenated in the cuvette prior to measurements by equilibrating with O_2-free Ar ([O_2] << 1 ppm) for 45 min before the protein was added. A gentle flow of Ar was passed through the head of the cuvette for an additional 15 min.

5.12.3 *Circular dichroism spectroscopy*

Far-UV (190 - 260 nm) and visible (300 - 700 nm) circular dichroism (CD) spectra of proteins were obtained on a Jasco J-810 spectrometer using 2 mm and 10 mm path length quartz cuvettes, respectively. The cuvette compartment was maintained at a temperature of 25 °C during measurements. 5 (Vis CD) and 10 (Far-UV CD) scans were accumulated per sample for both blank and protein spectra.

5.12.4 *Atomic absorption spectroscopy*

Atomic absorption spectroscopy (AAS) was performed on the M Series Atomic Absorption Spectrometer (Thermo Electron Corp.) to determine the Cu and Zn ion content of proteins by comparison to a set of calibration standards (Fluka) of known concentrations of Cu^{2+} and Zn^{2+}. Calibration standards of Cu^{2+} and Zn^{2+} (0 - 1 ppm) were prepared from stock solutions of atomic absorption standards of 987 and 1005 ppm in 1.2 % (v/v) nitric and 1 % (v/v) hydrochloride acids respectively. The intensity of copper absorption was measured at 325.8 nm, whilst of Zn at 213.9 nm.

5.12.5 *Electron paramagnetic resonance spectroscopy*

Continuous wave (cw) electron paramagnetic resonance (EPR) spectra were acquired at the X-band (9.42 GHz) and at temperature between 20 - 80 K using a Bruker EMX EPR spectrometer equipped with a TE_{102} cavity and an ESR900 Cryostat (Oxford Instruments) or liquid nitrogen finger dewar. A gentle flow of N_2 was passes through to avoid condensation in the cavity. Typically, 1 to 8 scans were accumulated per spectrum under the conditions of 0.2 mW - 20 mM microwave power, 100 kHz modulation frequency and 3 - 5 G modulation amplitude with sweep width of 1000 G or 1200 G and points resolution of 512, 1024 or 2048, depending on the sample. Diphenylpicrylhydrazyl (DPPH) and α,γ-bis-diphenylene-β-phenyl allyl (BDPA) were used as external reference compounds. EPR spectra were simulated using either SimFonia software (Bruker) or EasySpin [17].

5.12.6 *Fluorescence spectroscopy*

Fluorescence spectra and time course measurements were performed on a Cary Eclipse Fluorescence Spectrophotometer (Varian Inc., Agilent Technologies). Excitation and emission band-pass slits were routinely set to 5 nm spectral width and suitable optical filters were used both in the excitation and emission paths. The cuvette compartment was maintained at a temperature of 20 °C during all measurements. Measurements were conducted using 10 mm path length quartz cuvettes, and excitation and emission wavelengths appropriate for each fluorescent label. Intrinsic Trp residues were excited at 285 nm, whilst emission was monitored at 334 nm.

For the anaerobic measurements, the protein samples were typically prepared in septum sealed gas tight 3 mL cuvette in the anaerobic chamber. Alternatively, the buffer solution was deoxygenated in the cuvette prior to measurements by equilibrating with O_2-free Ar for 45 min before the protein was added. A gentle flow of Ar was passed through the head of the cuvette for an additional 15 min.

The protein's switching ratio (*SR*) is defined as the difference between the maximum (F_{red}, fully reduced protein) and the minimum (F_{oxy}, fully oxidized sample) fluorescence intensity divided by the maximum value (Equation 5.2).

$$SR = \frac{F_{red} - F_{oxy}}{F_{red}} \qquad \text{(Equation 5.2)}$$

5.13 Chromatography

Ion-exchange, affinity and gel filtration chromatography were used for purification of proteins. Gel filtration chromatography was additionally used for analytical purposes to determine the apparent MW and oligomeric states of proteins.

5.13.1 *Ion-exchange Fast Flow Sepharose columns*

DEAE Fast Flow Sepharose column material was used for preparation of anion-exchange columns for the purification of Laccase A, Lcc1, WT SLAC and their variants. SP Fast Flow Sepharose column material was used for preparation of cation-exchange columns for purification of WT bNiR and its variants.

Prior to use of column, DEAE or SP Fast Flow Sepharose column material was washed with at least 2 L of buffer solution. The pH of the flow-through was checked to ensure the equilibration of the material. Proteins were loaded onto DEAE or SP Fast Flow Sepharose columns in the same buffer as that used for equilibration of the column material. Elution of proteins was achieved by increasing the ionic strength of the buffer by providing a linear salt gradient, typically, between 0 and 500 mM NaCl in the same buffer as that used for equilibration.

DEAE and SP Fast Flow Sepharose materials were regenerated according to manufacturer's instructions (GE Healthcare). The column material was washed with 2 M NaCl (providing contact time of ~ 30 min) to remove bound proteins, followed by an excess of Milli-Q water. Subsequently the column material was washed with 0.5 M NaOH (providing contact time of ~ 60 min) followed by an excess of Milli-Q water until the pH was close to neutral. Columns were run and short-term stored at 4 °C. For long-term storage at 4 °C, column material was exchanged into 20 % (v/v) ethanol.

5.13.2 *Ion-Exchange HiTrap High Performance columns*

HiTrap Q HP and HiTrap SP HP (5 mL) columns attached to an AKTA purifier (GE Healthcare) were used in second or final step of purification process. The protein was loaded onto the columns in the same buffer as that used for equilibration of the column and eluted with an optimized linear salt gradient.

The columns were typically regenerated by washing with five column volumes (CV) of 1 M NaCl, followed by at least five CV of Milli-Q water. Subsequently the columns were passed with five CV of 0.5 M NaCl, followed by an excess of Milli-Q water until pH was neutral. The columns were stored in 20 % ethanol at RT.

5.13.3 *Immobilized metal ion affinity HiTrap Sepharose HP columns*

HiTrap IMAC Sepharose HP (5 mL) column attached to an AKTA purifier was used for purification of His-tagged proteins (NusA_Lcc1). The column was charged with 0.1 M $NiSO_4$ in Milli-Q water following the manufacturer's instructions. The column was equilibrated with a buffer of choice (typically 20 mM phosphate pH 7.4, 0.5 M NaCl and 30 mM imidazole) with at least 5 CV prior to protein loading. Elution of proteins was achieved by providing a linear imidazole gradient, typically, between 30 and 500 mM in the same buffer as that used for equilibration.

The immobilized metal ions were stripped off with 20 mM phosphate pH 7.4 containing 0.5 M NaCl and 50 mM EDTA, washed with 10 CV of 20 mM phosphate pH 7.4 containing 0.5 M NaCl and 30 mM imidazole, and 10 CV of Milli-Q water prior to recharging a column. The column was typically regenerated with 10 CV of 1.5 M NaCl, followed by at least 3 CV of Milli-Q water. Subsequently the column was washed with 20 CV of 1 M NaOH followed by 10 CV of Milli-Q water until pH of the flow through was neutral. Alternatively, the column was washed with 10 CV of 30 % (v/v) of isopropanol followed by 10 CV of Milli-Q water. The columns were stored in 20 % ethanol at RT.

5.13.4 *Gel-filtration*

HiLoad Superdex 75 16/60 and HiLoad Superdex 200 16/60 gel-filtration columns attached to an AKTA purifier were used for protein purification, typically in 50 mM phosphate pH 6.0 containing 200 mM NaCl or 20 mM Tris pH 7.5 containing 200 mM NaCl. Protein injection volumes were less than 2 % of the column volume. Elution of proteins (flow rate of 1 mL/min) was typically monitored at 280 nm, 420 nm and ~ 600 nm at RT.

The columns were calibrated using a low MW and high MW calibration kits (GE Healthcare). HiLoad Superdex 200 16/60 column was calibrated with blue dextran (2000 kDa), ferritin (440 kDa), catalase (232 kDa), aldolase (158 kDa), albumin (67 kDa), ovalbumin (43 kDa), chymotrypsinogen A (25 kDa) and ribonuclease A (13.7 kDa). HiLoad Superdex 75 16/60 column was calibrated with blue dextran (2000 kDa), conalbumin (75 kDa), ovalbumin (43 kDa), carbonic anhydrase (29 kDa), ribonuclease A (13.7 kDa) and aprotinin (6.5 kDa).

The columns were typically washed with almost 2 CV of 0.5 M NaOH, followed by at least 5 CV of Milli-Q water until pH of the flow through was neutral. The columns were stored in 20 % ethanol at RT.

5.14 Ultrafiltration

5.14.1 *Amicon Stirred Cell ultrafiltration*

An Amicon stirred cell (10 and 200 mL, Amicon) fitted with an appropriate cellulose membrane (10 to 30 kDa MWCO, Millipore) was used to concentrate and remove

chemicals during the purification of proteins at 4 °C. Exchanging buffer involved concentrating the protein solution and then diluting the sample 10-fold in the concentrator and repeating this process at least 3 times. A pressure of approximately 3 - 4 bars supplied from a compressed N_2 cylinder (O_2-free) was applied during operation of the stirred cell.

5.14.2 *Centrifugal ultrafiltration*

Amicon ultra 4 (4 mL) and 15 (15 mL) (10 kDa and 30 kDa MWCO, Millipore) and Vivaspin 500 (5 kDa MWCO, Sartorius) centrifugal concentrators were used to concentrate the proteins and remove chemicals through buffer exchange. Exchanging buffer and removal of chemicals involved concentrating the protein solution and then diluting the sample 5 to 10-fold in the concentrator and repeating this process at least 5 times. Buffers were typically exchanged at 4 °C, except for experiments conducted at RT in the anaerobic chamber.

5.15 Dialysis

5.15.1 *Preparation of dialysis tubing*

Dialysis tubing (8 kDa and 14 kDa MWCO, Sigma) was prepared by soaking the tubing for ~ 60 min in an aqueous solution of 1 % (v/v) acetic acid followed by exchange into Milli-Q water. The tubing was soaked in a solution containing 1 mM EDTA and 1 % (w/v) sodium carbonate and stirred for around 5 minutes. The solution was refreshed and the tubing heated up to around 60 °C. The heating process was repeated once more with a fresh solution and the dialysis tubing was allowed to cool down to RT over a period of 30 min. The dialysis tubing was exchanged into Milli-Q water, heated again to around 60 °C, and allowed to cool before storing at 4 °C in Milli-Q water [18].

5.15.2 *Dialysis of protein solution*

Prior to use, dialysis tubing was washed in an appropriate buffer. Protein solutions were sealed in tubing and dialyzed against buffer solution at 4 °C for at least 3 h, with stirring. The buffer solution (volume of at least 50-fold sample volume) was typically exchanged three times.

5.16 Bioinformatics

The alignment of DNA sequences was performed using LALIGN tool from ExPasy Bioinformatics Resource Portal using default settings. The theoretical MWs of proteins were estimated using Compute pI/Mw tool from ExPasy Bioinformatics Resource Portal. Clone Manager (Sci-Ed Software) software was used for design of DNA primers and analysis of DNA sequences. The ClustalX software [19] was used to align amino acid sequences of proteins using the default settings. Secondary structure composition was estimated from crystal structures using STRIDE software [20] and from the far-UV CD spectra using Dichroweb software [21]. Structural models were prepared using I-TASSER software [22]. The figures of crystal structures of proteins were created using PyMol 1.6.0.0 (Schrödinger) [23], whilst structural alignment of proteins was performed using Secondary Structure Motif (SSM) algorithms implemented in COOT [24]. Figures and data fitting were typically prepared using GraphPad Prism 5 Software.

5.17 References

1) Gomori, G., 1955, Methods Enzymol., 1, 138-146

2) Dons J.J., de Vries O.M., Wessels J.G., 1979, Biochim. Biophys. Acta, 563, 100-112

3) Chung C.T., Niemela S.L., Miller R.H., 1989, Proc. Natl. Acad. Sci. USA, 86, 2172-2175

4) Guo M., Lu F., Pu J., Bai D., Du L., 2005, Appl. Microbiol. Biotechnol., 69, 178-183

5) Fowler T.J., Mitton M.F., 2000, Genetics, 156, 1585-1594

6) Ohm R.A., de Jong J.F., Lugones L.G., Aerts A., Kothe E., Stajich J.E., de Vries R.P., Record E., Levasseur A., Baker S.E., Bartholomew K.A., Coutinho P.M., Erdmann S., Fowler T.J., Gathman A.C., Lombard V., Henrissat B., Knabe N., Kües U., Lilly W.W., Lindquist E., Lucas S., Magnuson J.K., Piumi F., Raudaskoski M., Salamov A., Schmutz J., Schwarze F.W., van Kuyk P.A., Horton J.S., Grigoriev I.V., Wösten H.A., 2010, Nature Biotechnol., 28, 957-963

7) Wösten H.A., Schuren F.H., Wessels J.G., 1994, EMBO J., 13, 5848-5854

8) van Wetter M.A., Schuren F.H.J., Schuurs T.A., Wessels J.G.H., 1996, FEMS Microbiol. Lett., 140, 265-269

9) van Peer A.F., de Bekker C., Vinck A., Wösten H.A., Lugones L.G., 2009, Appl. Environ. Microbiol., 75, 1243-1247

10) Machczynski M.C., Vijgenboom E., Samyn B., Canters G.W., 2004, Protein Sci.,

13, 2388-2397

11) Sato K., Dennison C., 2006, Chem. Eur. J., 12, 6647-6659

12) Harrison M.D., Dennison C., 2004, Proteins, 155, 426-435

13) Diederix RE, Canters GW, Dennison C., 2000, Biochemistry, 9551-9560

14) Guo M., Lu F., Liu M., Li T., Pu J., Wang N., Liang P., Zhang C., 2008, Biotechnol. Lett., 30, 2091-2096

15) Schmauder R., Alagaratnam S., Chan C., Schmidt T., Canters G.W., Aartsma T.J., 2005, J. Biol. Chem., 10, 683-687

16) Kuznetsova S., Zauner G., Schmauder R., Mayboroda O.A., Deelder A.M., Aartsma T.J., Canters G.W., 2006, Anal. Biochem., 350, 52-60

17) Stoll S., Schweiger A., 2006, J. Magn. Reson., 178, 42-55

18) Sato K., PhD Thesis, 2004, Newcastle University

19) Larkin M.A., Blackshields G., Brown N.P., Chenna R., McGettigan P.A., McWilliam H., Valentin F., Wallace I.M., Wilm A., Lopez R., Thompson J.D., Gibson T.J., Higgins D.G., 2007, Bioinformatics, 23, 2947-2948.

20) Heinig M., Frishman D., 2004, Nucl. Acids Res., 32, W500-2

21) Whitmore L., Wallace B.A., 2004, Nucleic Acids Res., 32, W668-73

22) Roy A., Kucukural A., Zhang Y., 2010, Nat Protoc., 5, 725-738

23) The PyMOL Molecular Graphics System, Version 1.6.0.0 Schrödinger, LLC.

24) Emsley P., Lohkamp B., Scott W.G., Cowtan K., 2010, Acta Crystallogr. D Biol. Crystallogr., 66, 486-501

APPENDIX A

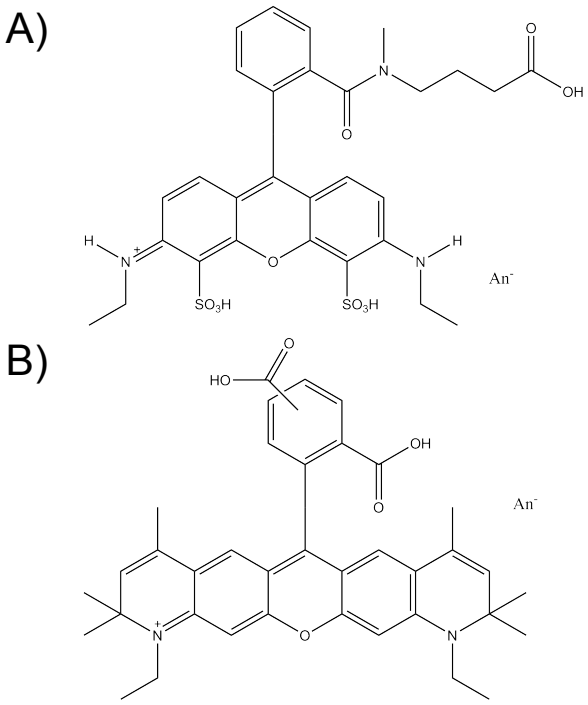

Figure A.1 The structures of (A) ATTO 532 and (B) ATTO 590. Structure of ATTO 647N is not available.

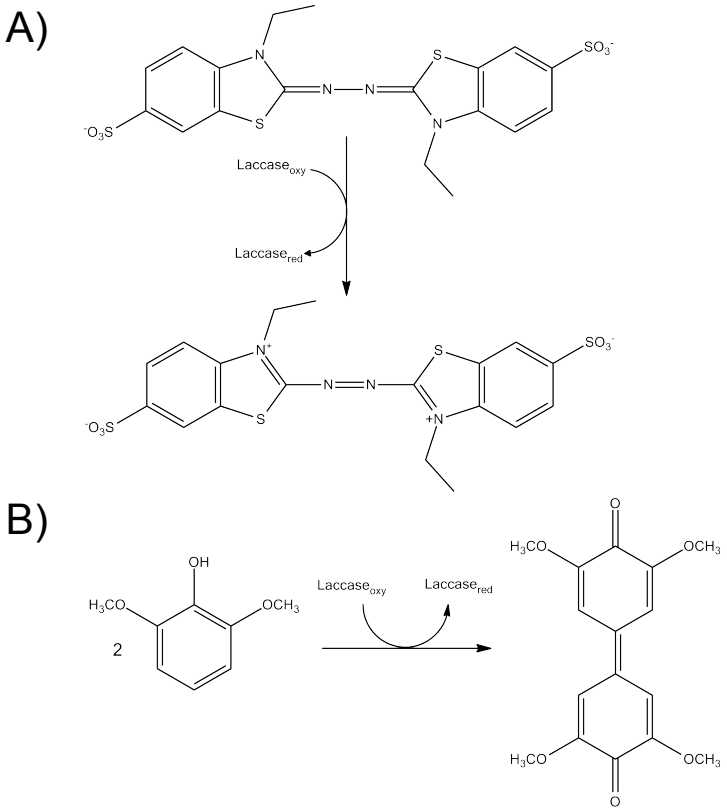

Figure A.2 The reaction scheme of (A) 2,2'-azinobis-3-ethylthiazoline-6-sulfonat (ABTS) and (B) 2,6-dimethylphenol (2,6-DMP).

APPENDIX B

To investigate the influence of a) dwell time per pixel (bin size), b) time resolution and c) the accuracy of τ_{on} and τ_{off} determinations on the final result, a series of simulated ON/OFF time traces (where "ON" and "OFF" periods correspond to the T1 Cu reduced and oxidize, respectively) were constructed and analyzed by Dr. Leandro C. Tabares. The simulated time traces were constructed by generating a row of 6×10^6 data-points *y(x)* in which *x* is the time and *y* has a value of 1 or 0. The *x*-axis was divided into increments of 1×10^{-5} s mimicking a 60 s long trajectory with a resolution of 0.01 ms. At the $x = 0$, *y* was arbitrarily set to "ON" ($y = 1$), followed by one "OFF" period ($y = 0$) before another "ON" period was started. While "OFF" periods were fixed to 1000 points (τ_{off} = 10 ms), the "ON" periods were allowed to last for a time $\tau_{on} = -1\times\ln(rand)\times\tau_{red}$, where *rand* is a computer generated evenly-distributed random number between 0 and 1. In this way the "ON" periods lasted for a random time τ_{on}, the cumulative distribution of which obeys an exponential decay with a time constant τ_{red} [1]. Traces were generated in this way for τ_{red} = 0.5, 1.0, 3.0, 5.0, 10, 25, 50, 100 and 200 ms. Subsequently a 60 s, 4 ms-binned simulated trace was treated as in the spot measurements, i.e., blocks were extracted and separated by intervals of 800 ms. The extracted blocks had subsequent lengths of 20, 36, 44, 52, 52, 52, 52, 52, 44, 36 and 20 ms. This pattern corresponds with a circular spot with a 12 pixel diameter. The extracted blocks were placed one behind the other to form a continuous time trace. For each τ_{red}, 100 independent traces were generated to mimic 100 spots. The simulated data were used to construct "ON"-time histograms as presented in Figure B.1.A. These were fit with single exponentials, the exponential decay constants proving estimates of τ_{red}. Apart from the procedure described above the full 60 s trajectories with 1 ms binning were analyzed. The less extensive simulation mimicking only 50 spots of 5 pixels diameter with 4 ms binning was also performed (Figure B.1.B). The experimental τ_{red} values deviate appreciably from the theoretical τ_{red} only when the latter is much shorter then the observed experimentally dwell time per pixel (1 or 4 ms) or much larger than the time windows used for the analysis (20 to 60 ms). The latter requirement can be fulfilled as the enzyme rates for NiR are expected to be in the ms range [2 - 4].

To investigate the effect of shape of the spots on the results (P_{ox} distribution and τ_{oxy} and τ_{red} values) the same analysis as presented in Chapter 2 was performed by Dr. Leandro C. Tabares but using different shapes for the selected area. Figure B.2 shows that the use of a whole spot, a rectangular (5×15 pixels) or a square (7×7 pixels) area produced similar trends in τ_{oxy} and τ_{red} values.

A)

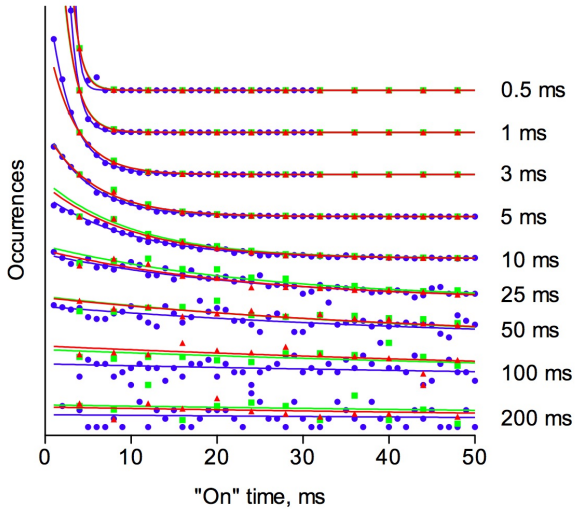

B)

τ_{red} (ms) [a]	Fit τ_{red} (ms) [b]	Fit τ_{red} (ms) [c]	Fit τ_{red} (ms) [d]
0.5	0.5	1.0	0.9
1.0	1.0	1.5	1.5
2.5	2.6	3.2	3.2
5.0	5.0	5.6	5.7
10	10.2	10.5	10.3
25	25	27	24
50	52	47	50
100	112	108	102
200	198	178	137

[a] τ_{red} values used to construct the time traces. [b] 100 traces, 12 pixels diameter of a spot, 1 ms bin time. [c] 100 traces, 12 pixels diameter of a spot, 4 ms bin time. [d] 50 traces, 5 pixels diameter of a spot, 4 ms bin time.

Figure B.1 (A) Time histograms for "ON" periods (T1 Cu reduced) extracted from the simulated time traces using τ_{red} values as specified on the right side of the figure. Lines show the fits to single exponential decays. ***Blue circles:*** data obtained from 100 simulated traces, each 60 s long, 1 ms binned, 12 pixel diameter spots; ***green squares:*** data obtained from 50 simulated traces, each 60 s long, 4 ms binned trace, 12 pixel diameter spots; ***red triangles:*** 100 spots of 12 pixels diameter. (B) The fitting parameters of the "ON"-times histograms extracted from simulated time traces to single exponential decays. The dwell time histograms were obtained from 60 s long time traces simulated with τ_{red} values of 0.5, 1.0, 5.0, 10, 25, 50, 100 and 200 ms.

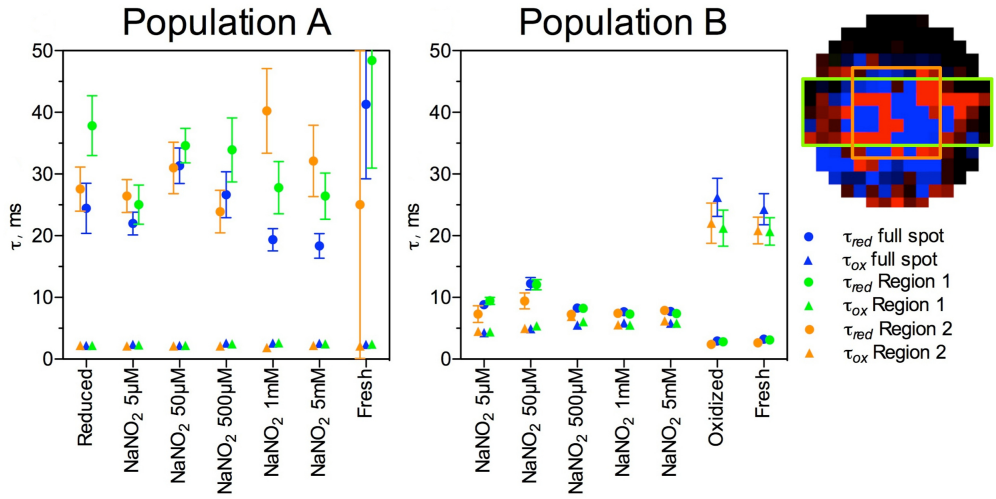

Figure B.2 Effect of the selected spot area on the τ_{on} and τ_{off} values for the population **A** (left) and **B** (right). ***Blue points:*** data obtained by analyzing all the pixels within a spot with a diameter of 15 pixels. ***Green points:*** data obtained by analyzing all the pixels within the area of 5×15 pixels around the center of the spot (region 1 on the spot at the right, marked with green rectangle). ***Orange points:*** data obtained by analyzing all the pixels within the area of 7×7 pixels around the center of the spot (region 2, marked with orange square).

References:

1) Luo G., Wang M., Konigsberg W.H., Xie X.S., 2007, Proc. Natl. Acad. Sci. USA, 104, 12610-12615

2) Kuznetsova S., Zauner G., Aartsma T.J., Engelkamp H., Hatzakis N., Rowan A.E., Nolte R.J.M., Christianen P.C.M., Canters G.W., 2008, Proc. Natl. Acad. Sci. USA, 105, 3250-3255

3) Farver O., Eady R.R., Abraham Z.H.L., Pecht I., 1998, FEBS Letters., 436, 239-242

4) Wijma H. J., Canters G. W., de Vries S., Verbeet M. P., 2004, Biochemistry, 43, 10467-10474

APPENDIX C

Figure C.1 The comparison of *clcc1* and *glcc1* sequences. Introns are highlighted in red and single nucleotide mutations in teal.

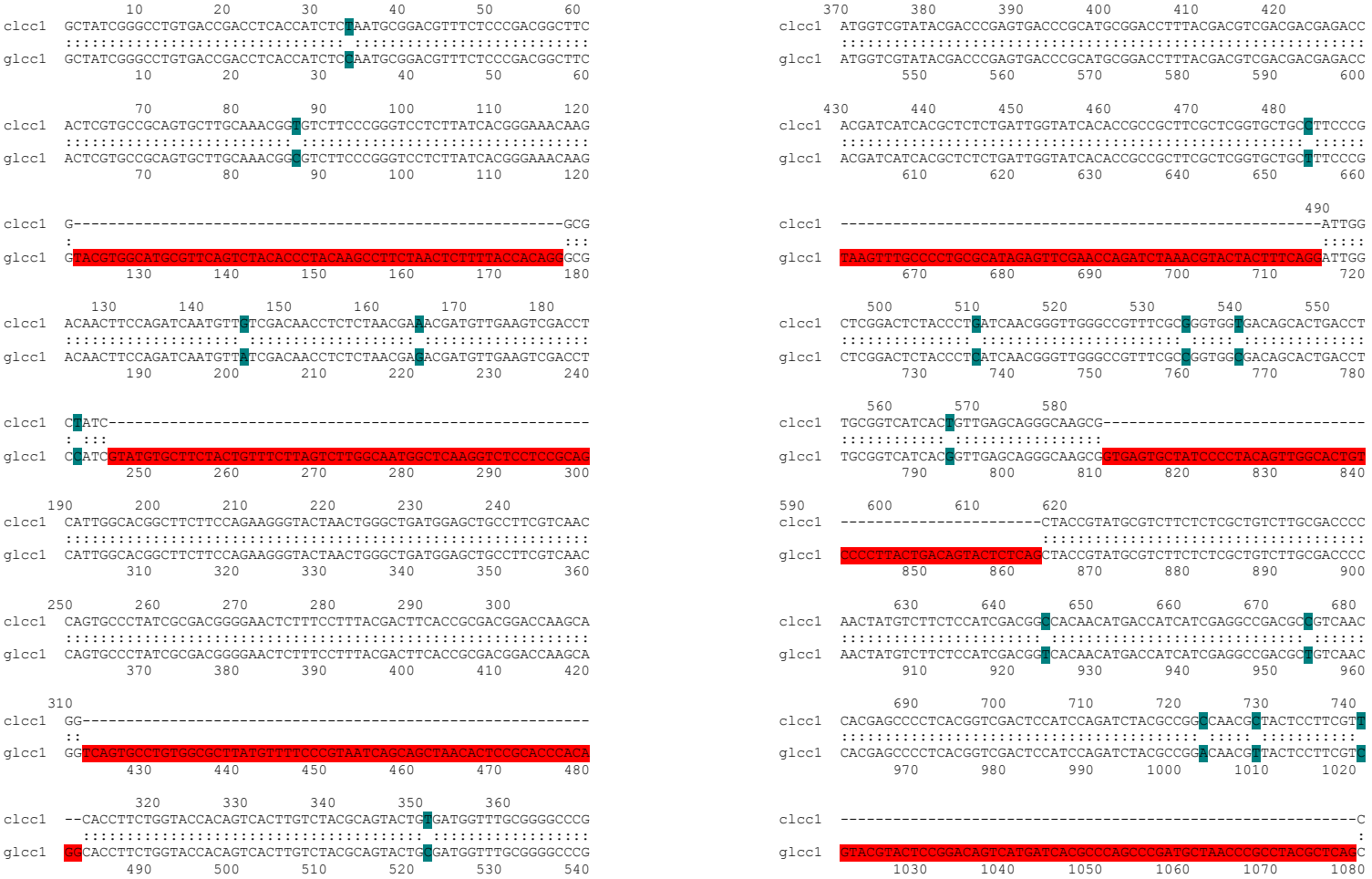

Figure C.1 The comparison of *clcc1* and *glcc1* sequences. Introns are highlighted in red and single nucleotide mutations in teal - continued.

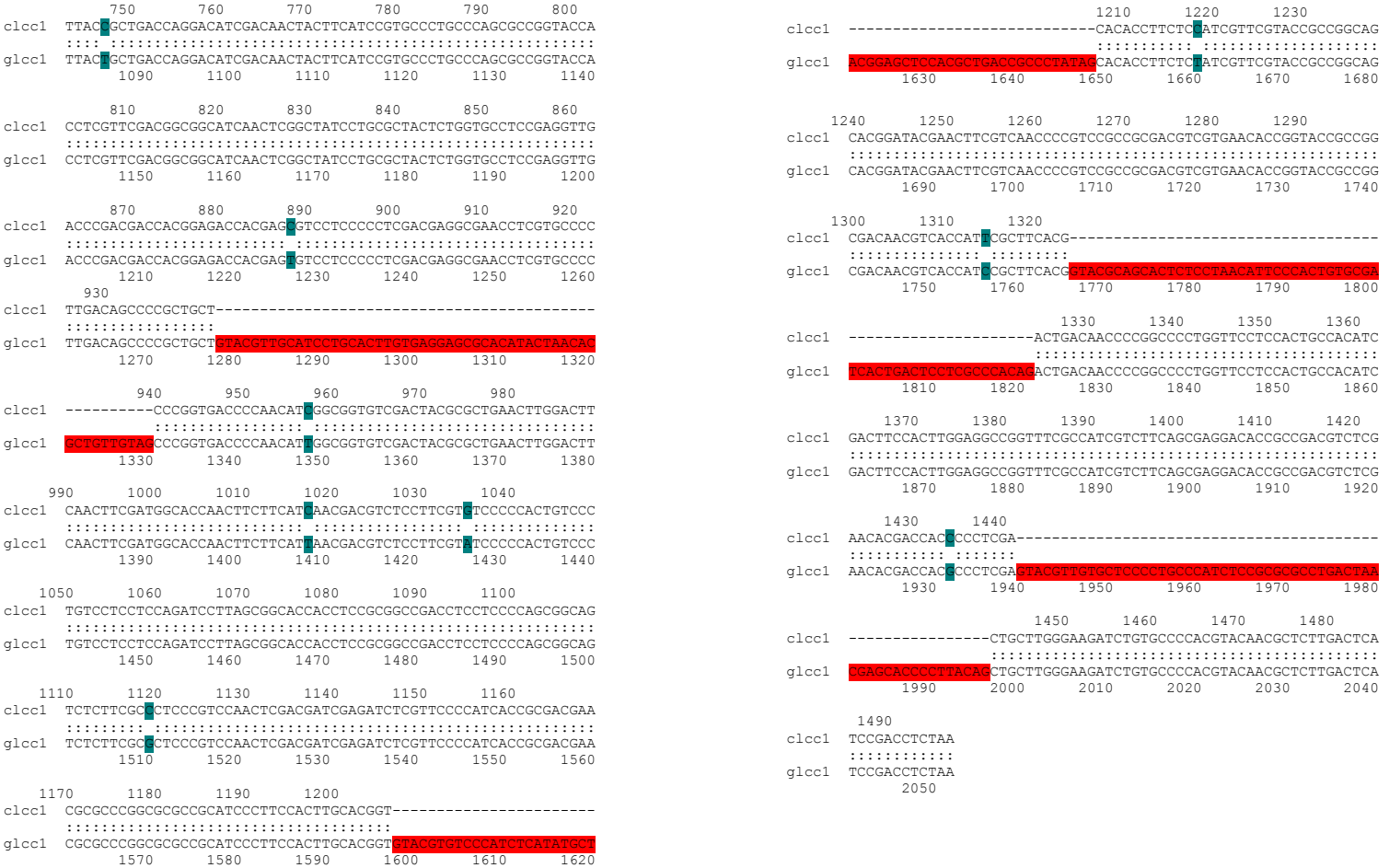

APPENDIX D

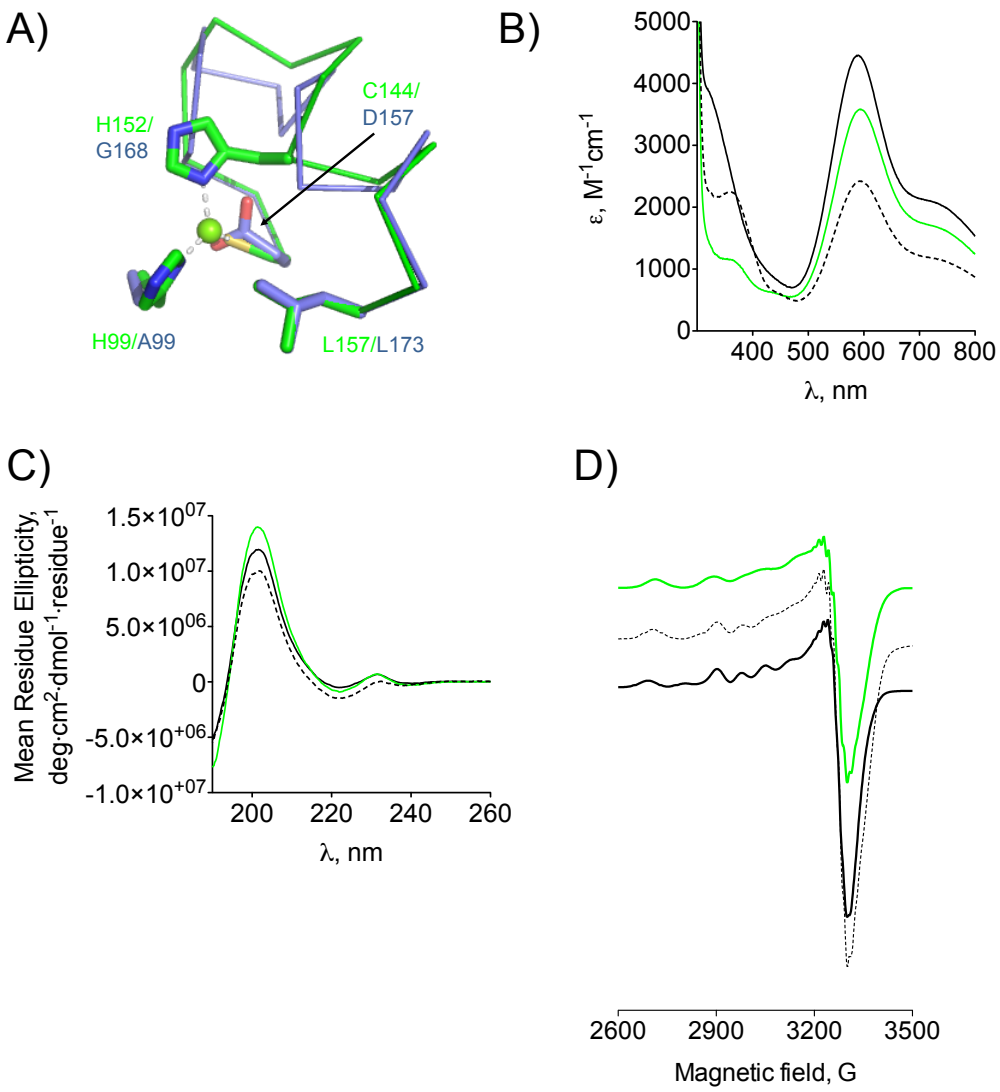

Figure D.1 (A) Superposition of the T1 Cu site of gdcLAC (green) on the potential MBS-1 site of WT SLAC (blue). The T1 Cu is a green sphere. UV-Vis absorption (B), far-UV CD (C) and EPR (D) spectra of gdcSLAC (—), mgSLAC (- - -) and WT SLAC (—). The UV-Vis spectra were acquired at RT in 20 mM Tris pH 7.5 containing 200 mM NaCl, far-UV CD spectra at 25 °C in 20 mM Tris pH 7.5 and EPR spectra at ~ 80 K in 20 mM Tris pH 7.5 containing 200 mM NaCl.